Solar Wind-Magnetosphere-Ionosphere Interactions During Passage at Earth of Interplanetary CMEs

by

Yngvild Linnea Andalsvik

Thesis submitted for the degree of
Philosophiae Doctor

Department of Physics
University of Oslo

July 2012

Series of dissertations submitted to the
Faculty of Mathematics and Natural Sciences, University of Oslo
No. 1253

ISSN 1501-7710

Cover: Inger Sandved Anfinsen.
Printed in Norway: AIT Oslo AS.

Produced in co-operation with Akademika publishing.
The thesis is produced by Akademika publishing merely in connection with the thesis defence. Kindly direct all inquiries regarding the thesis to the copyright holder or the unit which grants the doctorate.

Abstract

In a series of case studies we investigate the ionospheric convection response to enhanced magnetopause reconnection rate driven by interplanetary (IP) CMEs. In this response we distinguish between two stages of evolution, i.e., an initial transient phase, and a persistent phase, and different convection regimes in different sectors of the polar cap (center versus periphery). Plasma convection in these two regimes may have different boundary layer sources, i.e., the high-latitude boundary layer (HBL) versus the low-latitude boundary layer (LLBL). The temporal evolution of flows in the center and periphery of the PC is monitored by the ground magnetic signatures in the form of the PCN - index and magnetograms from the IMAGE chain of magnetometers in Svalbard - Scandinavia - Finland, respectively. In order to determine the temporal structure of the boundary flow channels we study during steady IP conditions and a south-west ($B_y < 0$) directed magnetic field in ICMEs we selected the observation interval from 1200 to 1800 UT, when the IMAGE chain of magnetometers traverses the post-noon and dusk sectors. Flow channels (FCs) along the periphery of the PC and in the dusk-sector of the auroral oval are placed in the context of the Dungey flux circulation cycle which includes the following stages of field line evolution: newly open (NOFL; FC 1 flow) and old open field lines (OOFLs; FC 2 flow) and field lines connected to the tail lobe (FC 3 flow) and plasma sheet (FC 4 flow). We find that the polar cap (PC) boundary flow in the postnoon sector is characterized by the persistence of flux tubes excited by magnetopause reconnection events (see prediction by Southwood (1987)) and enhanced flow speeds associated with conductivity gradients at the boundary against the auroral oval, particularly during winter conditions (our FC 2 flows). The temporal variability of the cross-polar cap potential (CPCP) is estimated by a combination of the direct, but low-resolution measurements of the CPCP from satellite ion drift data with high-resolution (continuous) ground observations of equivalent convection in the central polar cap (PCN - index). The inferred CPCP variability is explained in terms of the expansion - contraction model of polar cap convection. This is summarized in the following empirical formula where we split the CPCP in contributions from (i) enhanced flows at the PC boundary, mapping to the LLBL (first term), and (ii), the potential in the rest of the PC, with contributions from the HBL dynamo source and the magnetotail source (second term): CPCP (V) = P_{LLBL} (V) + kPCN(mV/m)L_{PC} (km). k is an empirical constant which is conductivity (season) - dependent and L_{PC} (km) is the cross-polar cap distance. We find that the persistent phase of solar wind - magnetosphere coupling (steady, strong IP driving) is characterized by a repetitive substorm activity and as-

sociated convection enhancements in the contracting ($\Delta L_{PC} < 0$) phases of the polar cap oscillations.

Acknowledgements

This has truly been a great four years. Not the least due to all the amazing people I have met during this time.

Many people deserves thanks, first of all my supervisor Per Even Sandholt and co-supervisors Charlie Farrugia and Hans Pécseli for invaluable guidance and patience along the way. Per Even, you have always been there when I needed help and without you I would never have made it. Charlie, you have been a great source of enthusiasm, inspiration and guidance both at UNH and via e-mail. I want to thank Charlie Farrugia and Mary Farrugia for a very nice stay in New Hampshire and wonderful trips around the area. I always felt welcome and will remember the time there forever. I also want to thank Hans Pécseli for discussions and collaboration on the teaching of the Quantum Physics course. The technical support from Bjørn Lybekk and Espen Trondsen is also greatly appreciated.

My trip to the University of New Hampshire was financed by the Kristine Bonnevie travel scholarship from the Faculty of mathematics and natural science, University of Oslo. I have also been fortunate enough to participate in several rocket campaigns and optical campaigns from Svalbard. Thanks to Jøran Moen and Bjørn Lybekk for making this possible and everybody present there for making it a fantastic time.

I want to thank my office mates Vegard and Hiro for making the days at the office more enjoyable, Espen for many nice times both on Svalbard and in Oslo, Tore André and Anja for nice trips and a lot of fun. And all the rest of students and employees at the space physics group for a great work environment, it would not have been the same without all the lunches, coffee breaks and seminars. I'm going to miss you all!

I have also gotten to know many colleagues and friends around the world which I really appreciate. At the Optical network, the ISR/EISCAT radar school, the International Space University and many other places.

Thanks to the Physics department I feel very fortunate to have gotten to know you all. The theory group where I took my master's degree, the administration where I worked for a while, my fellow students at LilleFy and later, to mention some.

I also want to thank my family and last, but not least, my mother for believing in me.

Oslo, Norway, August 2012
Yngvild Linnea Andalsvik

List of Papers

Paper I:
Sandholt, P. E., Y. L. Andalsvik and C. J. Farrugia,
Polar cap convection/precipitation states during Earth passage of two ICMEs at solar minimum,
Ann. Geophys., 28, 1023-1042, 2010.

Paper II:
Andalsvik, Y. L., P. E. Sandholt and C. J. Farrugia,
Dayside and nightside contributions to cross-polar cap potential variations: the 20 March 2001 ICME case,
Ann. Geophys., 29, 2189-2201, 2011.

Paper III:
Andalsvik, Y. L., P. E. Sandholt and C. J. Farrugia,
Substorms and polar cap convection: the 10 January 2004 interplanetary CME case,
Ann. Geophys., 30, 67-80, 2012.

Paper IV:
Sandholt, P. E., Y. L. Andalsvik and C. J. Farrugia,
The pulsed nature of the nightside contribution to polar cap convection: Repetitive substorm activity under steady interplanetary driving,
Ann. Geophys., 30, 1539-1553, 2012.

Paper V:
Andalsvik, Y. L., P. E. Sandholt and C. J. Farrugia,
Temporal - spatial structure of polar cap convection during strong forcing of the magnetosphere by interplanetary CMEs: The 20 Nov. 2003 Superstorm case,
Solar Atm. Terr. Phys., submitted 2012.

Contents

Part I

Introduction

Chapter 1

Background

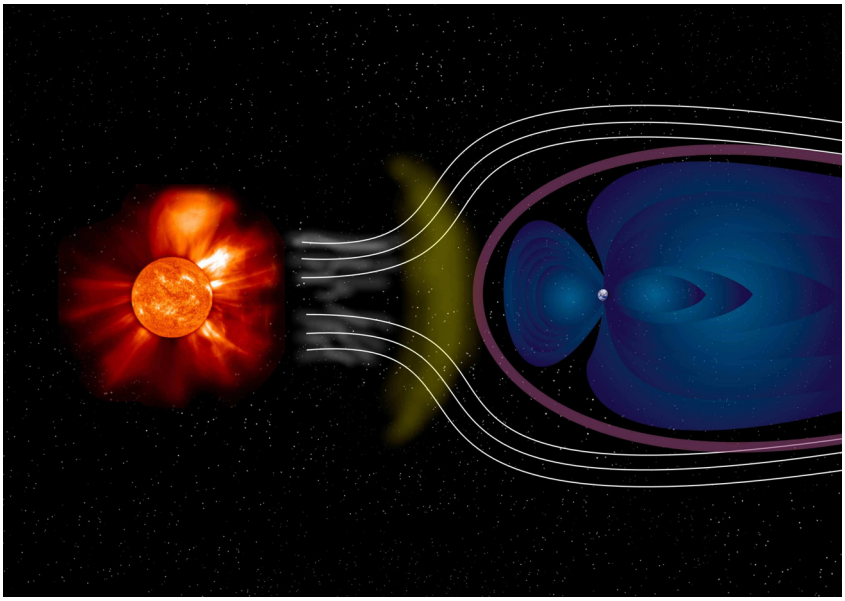

Figure 1.1: Illustration of the Sun-Earth connection concept. An eruption from the Sun propagates in the solar wind and interacts with the Earth's magnetosphere. Credits: ESA

The Sun, the Earth and the planets in our solar system are located inside a bubble called the Heliosphere where we are influenced by solar activity

transmitted by the solar wind, and where we have protection from most of the galactic radiation from the interstellar medium.

The activity on the Sun, our local star, affects the Earth's plasma environment in many ways. An artist rendition of the Eun-Earth connection is shown in Figure 1.1. In this thesis we study some of the effects on the coupled magnetosphere-ionosphere (M-I) system during passages of coronal mass ejections (CMEs) propagating from the Sun. This M-I response will be studied using both ground–based instruments such as radars and magnetometers, and in situ measurements by satellites (ACE, WIND, DMSP). The principal aim is to evaluate contributions to the plasma convection in the polar cap from both dayside and nightside magnetospheric sources. The continuous ground observations in combination with satellite data allow us to study the detailed temporal response of the ionospheric plasma convection during Earth passage of CMEs.

This thesis is organized as follows: The first part consists of Chapters 2-5 which introduce the scientific context of concepts and physical processes discussed in the scientific papers: An introduction to solar wind - magnetosphere interactions (Ch. 2), the process of magnetic reconnection (Ch. 3) and substorms (Ch. 4). After this we go through the subject of magnetosphere-ionosphere coupling (Ch. 5) and Ionospheric convection (Ch. 6). Following this, the second part consists of the papers included in the thesis.

Chapter 2

Solar activity

Solar activity varies with an 11-year cycle during which the sunspot number, which is low at solar activity minimum and rises to a maximum as the solar activity peaks. (see Figure 2.1) The origin of this systematic variation is the sun's gradual reversal of its magnetic field.

One of the ways the sun sends out magnetic flux and plasma is through coronal mass ejections (CMEs). Observed at 1 AU the CMEs are called interplanetary coronal mass ejections (ICMEs) A subset of ICMEs is called magnetic clouds (MCs), which have defined by clear properties (Burlaga et al. (1981)): configurations with higher-than-average magnetic field, a smooth rotation of the magnetic field vector and a low proton temperature.

2.1 Solar wind

The solar wind streams continuously from the sun with a bulk speed between 200 km/s and 800 km/s. It consists of primarily of electrons and protons. The solar wind also drags the solar magnetic field outwards to what is called the interplanetary magnetic field (IMF). Due to the rotation of the sun the IMF gets a spiral shape. The solar wind is usually divided in slow and fast winds. The former originates from streamers on closed field lines while the latter from coronal holes. The fast solar wind has a velocity of > 400 km/s and a temperature $T \simeq 8 \cdot 10^5$ K while the slow solar wind has a velocity of $250 - 400$ km/s, a temperature $T \simeq 1.5 \cdot 10^5$ K and a density two times the one for fast solar wind (Lepping et al. (2003)).

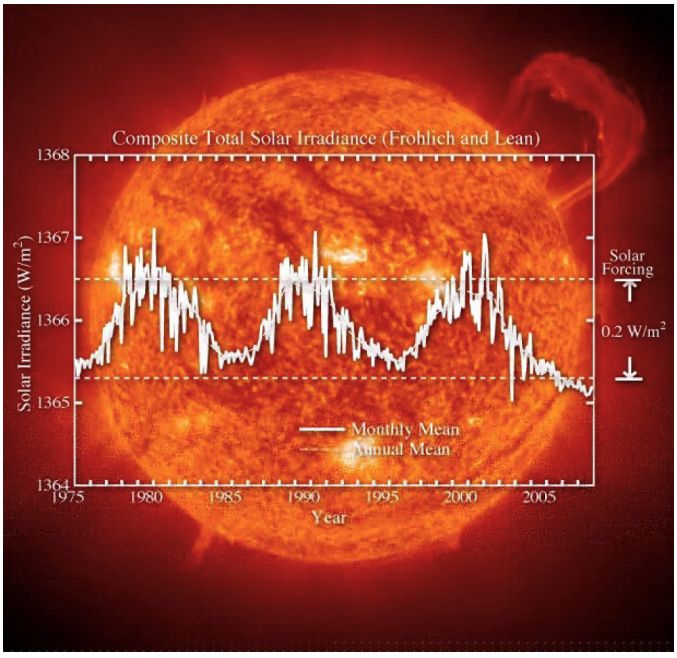

Figure 2.1: Illustration of solar activity by total solar irradiance over the past three solar cycles (between 1975 and 2008). Credits: NASA.

2.1.1 CIRs

As opposed to transients like the ICMEs, the Earth is also affected by flow and field configurations which co-rotate with the Sun, such as co-rotating interaction regions. Co-rotating interaction regions (CIRs) are regions of compressed field and plasma created when a fast-speed stream from coronal holes overtakes the slower solar wind ahead. CIRs lead to recurrent storms on Earth. These CIRs can be distinguished from the transient ejecta such as ICMEs by the high proton temperature, T_P, in the compressed plasma of CIRs compared to the low T_P in the expanding ejecta from a CME (Vennerstroem (2001)). The velocity profile also differs. Expanding ICMEs/magnetic clouds have a decreasing velocity profile due to radial expansion, while for CIRs it goes from slow to fast.

2.2 CMEs

The CMEs contribute to a mass loss of about 10% of the mass loss rate from the solar wind. On average 1-3 CMEs are ejected from the sun each day (Low (2001)). Below we give a brief description of CME structure and temporal evolution according to Low (2001). CMEs have a three-part structure consisting of (i) a bright front with high density (helmet dome), (ii) a dark cavity with low density, and (iii) a bright core with relatively high density (prominence). According to Low (2001) the process starts with a coronal helmet eruption followed by current sheet formation and reconnection. The latter gives rise to flares. The three forces acting on the CME are magnetic field and plasma pressure gradient and gravity. Initially the force-balance keeps the CME in place, but drainage of prominence material makes the CME lighter so that force imbalance results and it can break free and move away from the sun. The outward expansion is driven by the magnetic curvature force and plasma pressure gradient exceeding the gravitational force.

2.3 ICMEs and MCs

ICMEs and MCs are ideal for studying ionospheric response, as the flux rope magnetic field is strong, with smoothly changing orientation over a long time interval during it's Earth passage. Extreme values of physical parameters are reached and these are retained for long times. They vary slowly, slower than typical response times of the magnetosphere-ionosphere system so that the Earth goes through a long sequence of quasi-steady states (for more details

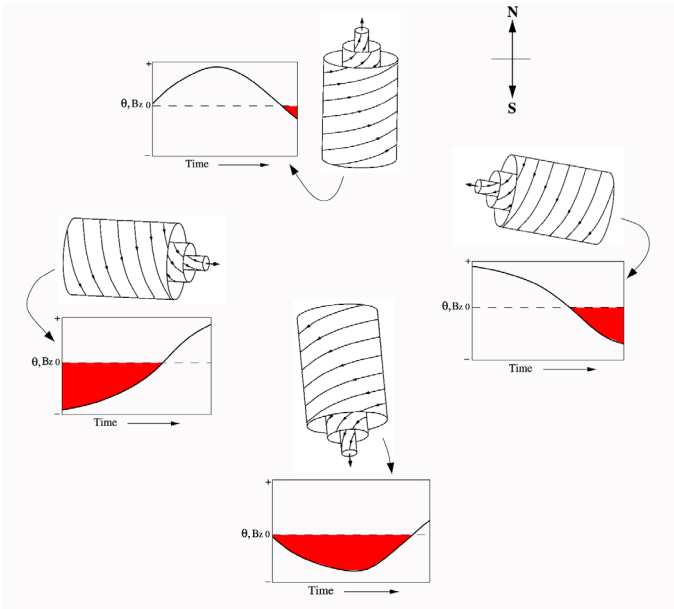

Figure 2.2: Sketch of flux rope structures with different inclinations of the axial field and their corresponding B_z or the polar angle in the GSM Y - Z plane, which is often referred to as the the IMF clock angle $\theta = \sin^{-1}(B_z/|B|)$ (where $|B|$ is the magnetic field magnitude) profiles from Lepping and Wu (2007). Shaded regions are the intervals where B_z is negative. All profiles show an enhanced field strength and a smoothly varying field orientation across the flux rope.

see Farrugia et al. (1993), Farrugia et al. (1993), Freeman et al. (1993) and Farrugia et al. (1997)).

MCs have a helical flux rope structure with any possible axial inclination (Lepping et al. (2003)). They are large structures with a typical duration of 7-48 hours at 1 AU Lepping and Wu (2007). Figure 2.2 shows flux rope orientations and corresponding B_z profiles for four different orientations for the whole MC from the leading (front) region to the trailing (end) region. This orientation is used to divide MCs into different types (B_z-profiles) to the various inclinations of the axial field. The figure shows the following B_z-profiles: S-N and N-S (bi-polar) and N and S (uni-polar).

The geoeffectiveness of magnetic clouds have been studied by many people

e.g. Gonzalez and Tsurutani (1987), Farrugia et al. (1993), Farrugia et al. (1993), Farrugia et al. (1997), Farrugia et al. (1998) and Burke et al. (2007).

Chapter 3

Magnetic reconnection

The Earths magnetic field has a roughly dipolar configuration, but is stretched out in a long tail on the nightside as it is dragged by the solar wind flow. The solar wind is hindered from penetrating the geomagnetic field by the frozen–in condition. The solar wind magnetic field is separated from the magnetospheric field by a current sheet at the outer boundary of the magnetosphere called the *magnetopause* (see Fig. 3.1). The central part of the tail is called the *plasma sheet* surrounded by the two low density *tail lobes* with oppositely directed magnetic fields. The lobe-current sheet boundary is called the *plasma sheet boundary layer*. The inner magnetosphere is the *plasmasphere* with only closed field lines, i.e. magnetic field lines with both ends on Earth. When the interplanetary magnetic field interacts with the magnetic field of the Earth we can, depending on the direction of the field lines, get a recombination of the magnetic field lines known as magnetic reconnection whereby two topologically different field lines forms. Open field lines are created: the field lines that are attached to earth with both ends are closed field lines, while the field lines with only one footpoint attached are open field lines.

The magnetic reconnection process as a main driver of magnetospheric dynamics was first proposed by Dungey (1961). In Dungey's open model of the magnetosphere the interplanetary field lines during southward IMF conditions will reconnect with northward-pointing terrestrial field lines at the dayside magnetopause and the newly opened field lines will be dragged by the solar wind over the polar cap to the nightside where reconnection takes place in the magnetotail (see Fig. 3.2). In addition to the reconnection in the distant magnetotail intermittent reconnection can take place in the near-Earth magnetotail ($<$30 R_E). This reconnection process is believed to be associated with substorms Zou et al. (2010). During substorms open field lines are closed and returned to the dayside (Baker et al. (1996), McPherron

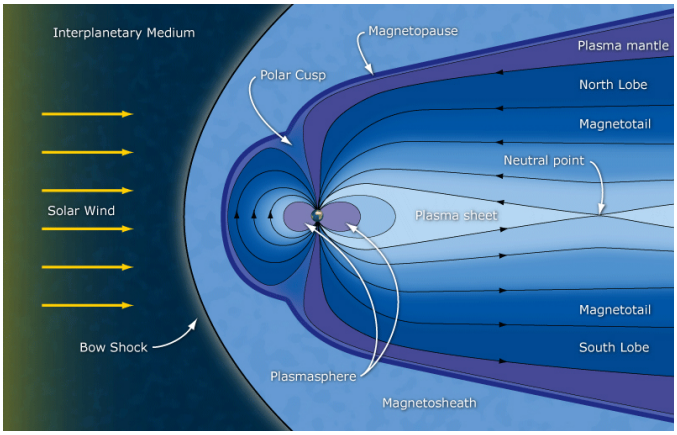

Figure 3.1: Earths magnetosphere with the different plasma populations/regions indicated. (Credits: ESA/C. T. Russel)

et al. (1973)). Reconnection can also occur when the field lines are not exactly antiparallel. For northward IMF the reconnection on the dayside will be between the solar wind field lines and the magnetospheric lobes (Dungey (1963)) poleward of the cusp.

In magnetic reconnection magnetic energy is converted into particle energy and thus it is the major contributor to the transfer of momentum and energy from the solar wind to the magnetosphere.

3.1 Theory

The actual reconnection process happens in a small region called the diffusion region. Here the frozen-in field condition breaks down allowing plasma mixing across boundaries. It is a 2-stage process leading to two length scales. First the ions are demagnetized in the so-called “ion diffusion region”. Later the electrons are demagnetized in a smaller region called the “electron diffusion region” (Figure 3.3). This happens when the scale size in the current sheet between antiparallel field lines becomes smaller than the ion inertial length and the terms on the right side of the generalized Ohm’s law becomes

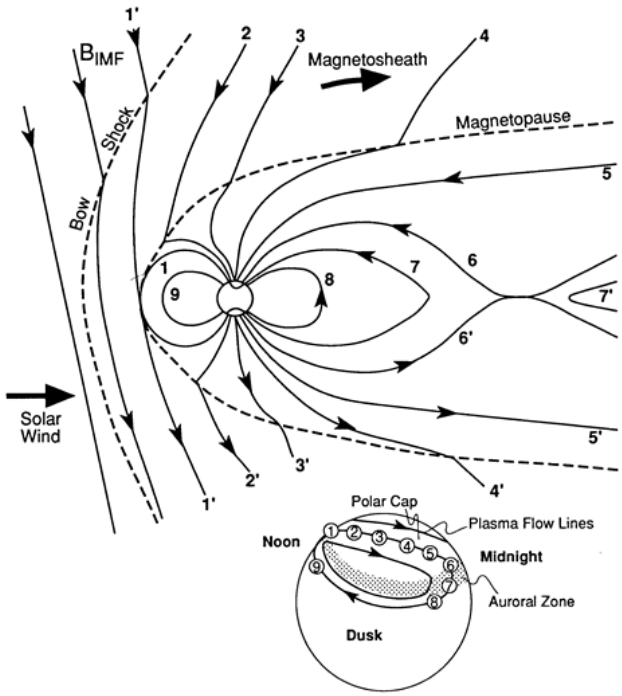

Figure 3.2: Dungey magnetic flux circulation cycle illustration field lines reconnecting (1 with 1' and so on) and the corresponding ionospheric footpoints of the same (numbered) field lines (from Hughes (1995))

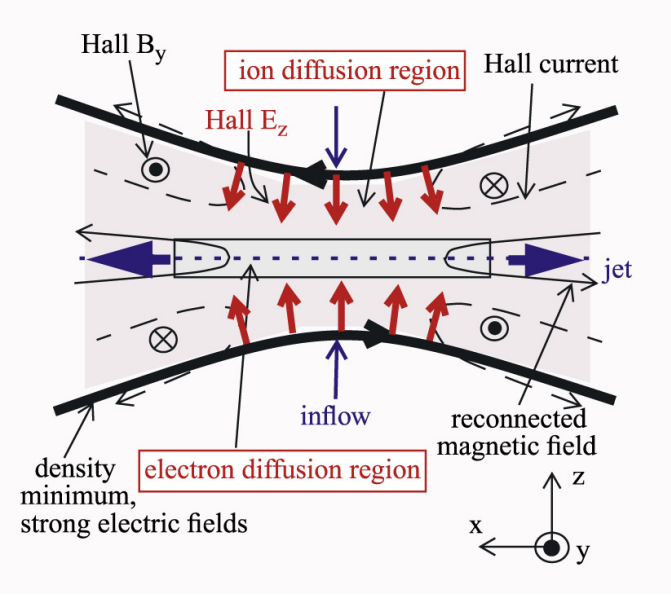

Figure 3.3: Illustration of the reconnection diffusion region from Borg et al. (2005)

non-negligible:

$$\vec{E} + \vec{u} \times \vec{B} = \frac{\vec{j}}{\sigma} + \frac{1}{ne}\left[\vec{j} \times \vec{B} - \nabla P_e\right] + \frac{m_e}{ne^2}\left[\frac{\partial \vec{j}}{\partial t} + \nabla \cdot (\vec{j}\vec{u})\right]$$

where $\vec{u}$ is the plasma velocity, $\vec{E}$ is the electric field, $\vec{B}$ is the magnetic field, σ is the conductivity, $\vec{j}$ is the current density, n is the density, P_e is the electron pressure tensor, m_e is the electron mass, and t is time. The first term is a resistive term and can be neglected in collisionless plasma. The Hall term (second term) becomes important around spatial scales comparable to the ion inertial scale λ_i. The third term, pressure gradient, becomes important at length scales $\lambda_i \beta^{1/2}$ where β is the ratio of the plasma pressure to the magnetic pressure. The fourth and fifth terms are inertial terms and contribute only at legthscales comparable to the electron inertial length. So if the current sheet scale size is of the order of the ion inertial length the Hall term and the pressure gradient term becomes important, this is the ion diffusion region. In the electron diffusion region the last two terms (inertial effects) become important.

Figure 3.3 shows a sketch of the diffusion region. The outer parts is the ion diffusion region and the square in the middle is the electron diffusion region. On the top and bottom the inflow regions are indicated where the plasma flows towards the central current sheet with velocities $\sim 0.1 V_A$. Perpendicular to this the outflow regions are indicated by jets of accelerated plasma with a velocity of $\sim V_A$. If there is no background magnetic field (guide field) the point where the field lines reconnect is a magnetic null point. In the direction perpendicular to the image plane this region forms a line called an x-line or neutral line (separator). In the ion diffusion region the ions can move freely while the electrons are frozen in. This leads to Hall currents and Hall electric field. In the figure the corresponding Hall magnetic field is indicated as going in or out of the four quadrants. That is they form a quadrupolar system (in symmetric reconnection) pointing in the out-of-plane direction Y. The Hall electric fields (red arrows) form an in-plane bipolar system, see review by Vaivads et al. (2006) and references therein.

3.2 Magnetopause reconnection

Reconnection is a major transfer mechanism for the magnetosphere (in addition to viscous transfer). Around 10% of the IMF flux reaching the magnetopause reconnects and this reconnection changes the magnetopause from a tangential to a rotational discontinuity (nonzero B_n, V_n and E_t) (Pashmann

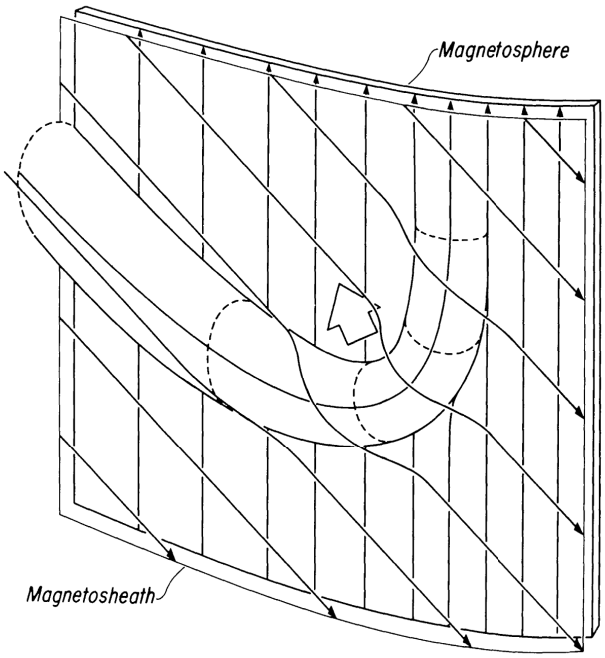

Figure 3.4: Illustration of a flux transfer event from Russell and Elphic (1978). A reconnected flux tube moving northward from the X-line in the direction of the arrow. Slanted arrows are magnetosheath field lines and vertical arrows are magnetospheric field lines.

(1991)). The plasma is accelerated at the magnetopause by the maxwell stress caused by tension in the reconnected field lines ($\vec{I} \times \vec{B}_n$-force) corresponding to the outflow region. The reconnection can be steady or more transient. The transient phase, gives rise to "flux transfer events" (FTEs; Russell and Elphic (1978)). FTEs have signatures that are interpreted as single twisted reconnected flux tubes that crosses the magnetopause and are being pulled through and deflecting the medium around (see Figure 3.4). Among the ionospheric signatures of pulsed reconnection at the magnetopause are a so-called stepped cusp where the ion energy in the precipitation flux decreases with increasing latitude in a stepwise fashion and repetitive, poleward moving electron precipitation/temperature features and auroral enhancements

are observed (Sandholt et al. (1990) and Lockwood et al. (1993)).

In the presence of a substantial IMF B_y component the tension on the reconnected field lines will drag them in the dawn or dusk direction if B_y is positive or negative, respectively, for the northern hemisphere and opposite for the southern hemisphere (Gosling et al. (1990)) (see also Fig. 3.5).

3.3 Lobe reconnection

For the case of northward interplanetary magnetic field we will not get subsolar magnetopause reconnection because the magnetic field are pointing in the same direction there. But poleward of the cusp the lobes have antiparallel field to a northward IMF. The so-called Cowley's catalog (see Fig. 3.6) shows physically possible magnetic topologies for northward IMF. a) displays symmetric, dual reconnection where closed nightside flux is transferred to closed dayside flux in both hemispheres. In b) IMF B_x or the dipole tilt is nonzero leading to a sequential lobe reconnection, involving closed-to-open flux transfer in the north and open-to-closed in the south. Figure c) we have symmetric, dual reconnection with open-closed transfer in both hemispheres while d) is single lobe reconnection in the B_x preferred hemisphere and closed-open transfer. Finally e) shows single lobe reconnection in B_x preferred hemisphere with open-open transfer.

Crooker (1992) developed this further with her idea of "overdraped lobe flux" where the reconnected open lobe flux is draped over the dayside magnetopause by the magnetosheath flow. Following this, the overdraped lobe flux reconnects with the Earths field inside the magnetopause in the winter hemisphere after diffusion across the magnetopause. Crooker (1992) then introduces a catalog shown in Figure 3.7 with reconnection topologies and corresponding ionospheric convection patterns. The first case (1) shows single lobe reconnection in the B_x-favored hemisphere giving lobe cells in the ionosphere in one hemisphere. The next case (2) is sequential dual merging with merging in the B_x-favored hemisphere followed by internal reconnection in the opposite hemisphere giving merging cells in both hemispheres. The last three cases are transitional states of decreasing tilt/B_x (3), increasing tilt/B_x (4) and transition from southward IMF (5).

Building on this Watanabe et al. (2006) showed observational evidence of two different sequential reconnection cycles. In Figure 3.8 the two cycles are A-B and C-D where A and C are the first stage on the magnetopause and B and D are internal reconnection (inside the magnetopause) between an overdraped summer lobe field line and either a winter lobe field line (B) or a closed field line (D).

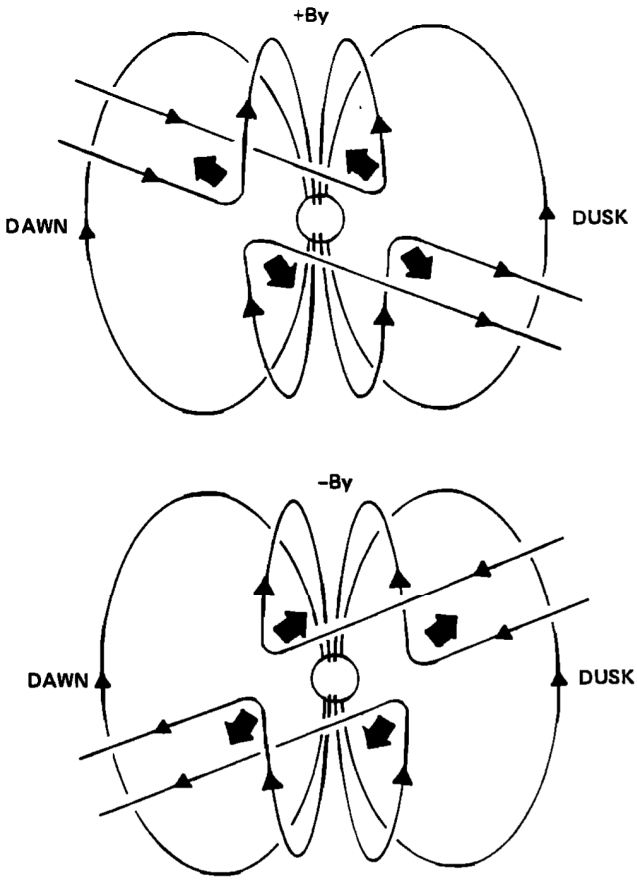

Figure 3.5: Newly reconnected field lines on the dayside magnetopause as viewed from the sun. B_y is positive in the top figure and negative in the bottom figure. The thick arrows indicate the direction of the magnetic field tension. Figure 1 in Gosling et al. (1990).

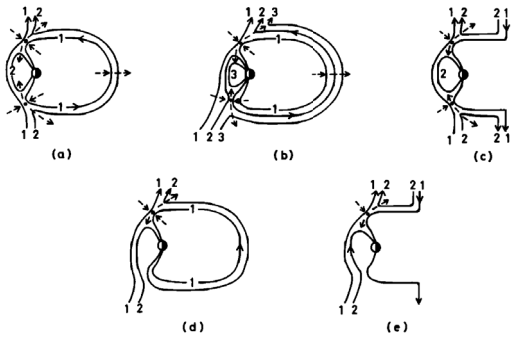

Figure 3.6: Cowley's catalog of possible reconnection topologies for northward IMF. Numbers indicate field line sequence, dashed arrows mark flow in the merging region and the dot marks the x-line. Figure 1 in Cowley (1981)

Watanabe et al. (2004) developed this further for $|B_y| \sim B_z$ conditions with a sequence of three reconnection processes (i) front side MP reconnection, (ii) internal reconnection, and (iii) magnetotail reconnection.

3.4 Magnetotail reconnection

Some of the best observational evidence of near-Earth magnetotail reconnection is fast flows/jets and signatures of tailward moving plasmoids. The two jets go tailward and earthward and the tailward jet flows quite easily as it moves along open field lines but the earthward jet encounters closed field lines and is ultimately slowed down by this. Other reconnection signatures are current sheet thinning followed by dipolarization of the magnetotail magnetic field.

3.4.1 Bursty Bulk Flows

The high speed plasma jets are often called Bursty Bulk Flows (BBFs) consisting of many short lived flow bursts with velocities of ≥ 400 km/s. Each burst is ≤ 1 min in duration with several bursts during a ~ 10 min period. The cross-tail extent is probably around 2-3 R_E. The earthward BBFs are responsible for 60-100% of the earthward transport of mass, energy and magnetic flux (Angelopoulos et al. (1994)). The most accepted model for BBFs

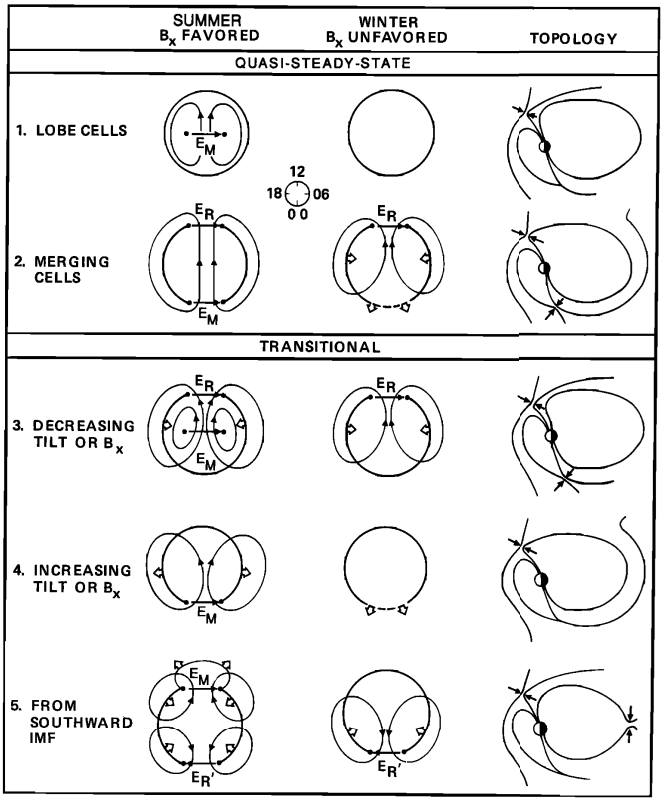

Figure 3.7: Crooker's catalog of northward IMF reconnection topologies and reverse-cell ionospheric convection. Figure 6 in Crooker (1992).

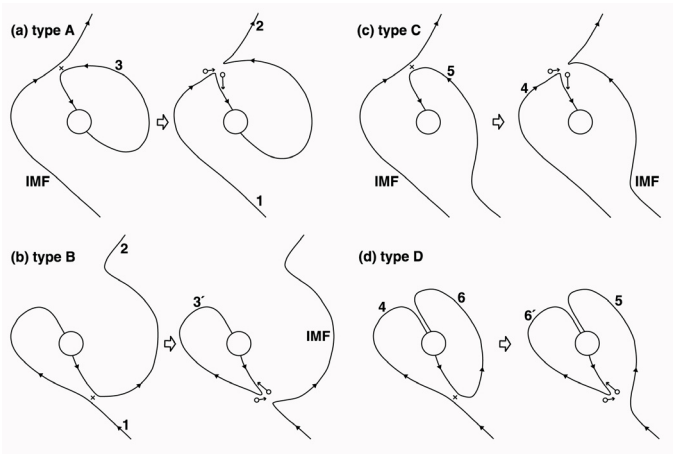

Figure 3.8: Northward IMF reconnection topologies from Watanabe et al. (2006), their Fig. 1.

is the bubble model (Chen and Wolf (1993) and Yang et al. (2012)) where the BBF is a channel of lower plasma density and pressure but higher magnetic pressure. This leads to accumulation of charge on the dawnward and duskward sides of the bubble. This gives a double vortex convection pattern with earthward flow inside and tailward flow at the flanks of the bubble. A pair of FACs goes from the center of the vorticies (the bubble boundaries) to the ionosphere creating an azimutally separated double convection vortex.

Chapter 4

Substorms

4.1 Auroral substorms

Akasofu's model of auroral substorms from 1964 (Akasofu (1964)) is even today widely used, although with some modifications. He divides the substorm into 2 phases and describes the auroral signatures: (i) expansion phase (10-30 min), and (ii) recovery phase (30 min-3 hours). In the expansion phase we have a sudden brightening, poleward motion, formation of an auroral bulge and westward traveling surge. The recovery phase exhibits an equatorward contraction of the nightside oval and return to more quiet conditions. Today it is common to use three phases, a growth phase with loading of magnetotail lobe flux and equatorward expansion of the oval in addition to Akasofu's two phases (expansion and recovery).

4.2 Substorm phases

A southward turning of the IMF gives rise to the growth phase. Magnetic flux is opened on the dayside and transported to the nightside. The lobe flux increases to a critical value of ~ 1 GWb before the substorm onset is triggered (Huang (2012)). Approximately 25% of this lobe flux is closed during the subsequent substorm expansion phase. In the growth phase the magnetic field in the near-Earth tail is stretched. We get plasma sheet thinning (Nakamura et al. (2002)) and increased tail cross section. In the ionosphere the polar caps expand and we get an enhancement of the auroral electrojets. During the expansion phase we get dipolarization of the magnetic field in the near-Earth tail followed by decreased tail lobe flux and impulsive electric fields (Sauvaud et al. (2012)). In mid-tail large fluctuating E-fields are observed, in addition to impulsive plasma flows (BBFs). Expansion phase

signatures in the ionosphere are sudden brightening of auroral arcs and enhancements of auroral electrojet followed by westward traveling surge (WTS) and the auroral bulge (Marghitu et al. (2009)). In the recovery phase drift echoes of energetic electrons and ions are observed in the near-Earth tail. In the midtail we get a plasma sheet thickening in addition to field-aligned plasma flows at the plasma sheet boundary layer. In the far tail electrons are streaming tailward and we have B_z fluctuations (northward, then southward). In the ionosphere the intensity of the aurora decreases as does the auroral bulge.

4.3 Substorm models

The processes responsible for the substorm are still debated (Lui (1991)), but the two main theories are: (i) Reconnection in the region $X \simeq 20 - 30R_E$ leading to the beginning of the expansion phase (the near-earth neutral line (NENL) model (Baker et al. (1996))), and, (ii) M-I coupling processes in the near-Earth tail (6-10 R_E) causing current disruption. The latter model may also lead to subsequent reconnection. Models (i) and (ii) are often referred to as outside-in and inside-out models respectively.

Zou et al. (2010) described the substorm onset and pre-onset sequence as starting with a plasma sheet thinning giving an auroral equatorward expansion followed by poleward boundary intensifications (PBIs) and streamers.

4.3.1 Substorms during strong solar wind forcing

Fast CMEs are observed to be the most geoeffective interplanetary conditions. Recurrent substorms are often observed during such events when magnetic storms are present. The series of quasi-periodic substorms often observed in these cases is referred to as sawtooth events (Henderson et al. (2006), Huang (2012), and ref. therein).

Sawtooth events are recurrent substorm-related injections of plasma particle fluxes at geostationary orbit which have a most probable period of 2.7 hours. According to Huang (2012) these events can be triggered by moderate solar wind dynamic pressure variations when the lobe magnetic flux is at a critical level of appr. 1 GWb.

4.4 Substorm Current Wedge

The increased westward electrojet (WEJ) in the expansion phase is due to the formation of the substorm current wedge (SCW) Belehaki et al. (1998).

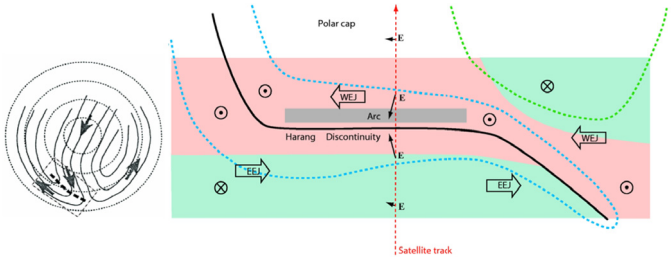

Figure 4.1: Large-scale convection (left) and FAC/electrojet configurations in the Harang region (right). Blue and green dashed lines represent the evening and morning convection cells, respectively. Pink and green background indicates regimes of upward and downward FACs. Figure 7 in Marghitu et al. (2009).

See figure 4.1 from Marghitu et al. (2009) for a sketch of the WEJ, EEJ and corresponding FACs in the Harang region. The current wedge is closing through the electrojet in the ionosphere and the cross tail current in the magnetosphere. SCW forms after a current disruption in a current sheet which is enhanced during the growth phase. For more details on current generators and M-I coupling see Haerendel (2011).

The BBFs and corresponding auroral streamers in the ionosphere are part of the substorm substructure (see Figure 4.2) and are described in more detail in Lyons et al. (2012), Yang et al. (2012) and Amm et al. (2011). Figure 4.2 shows a sketch of the Earthward injection of plasma (bulk flows) in the plasma bubble model and the associated current system (cross-tail current and FACs) in the bottom panel. Ionospheric signatures are shown in the top panel, i. e., channel of equatorward-directed convection, auroral form (streamer) on its western side and the Pedersen current (green) closure of FACs.

4.5 Magnetic indices

The westward electrojet signatures in magnetometers and the magnetic indices (AU, AL and AE) are often used to identify substorms. These indices are obtained from magnetograms located in the northern hemisphere auroral zone. They reflect the north-south magnetic perturbation as a function of time. Kristian Birkeland identified the same disturbance already in 1908 and called it the polar elementary storm. The AL index gives a lower bound of all

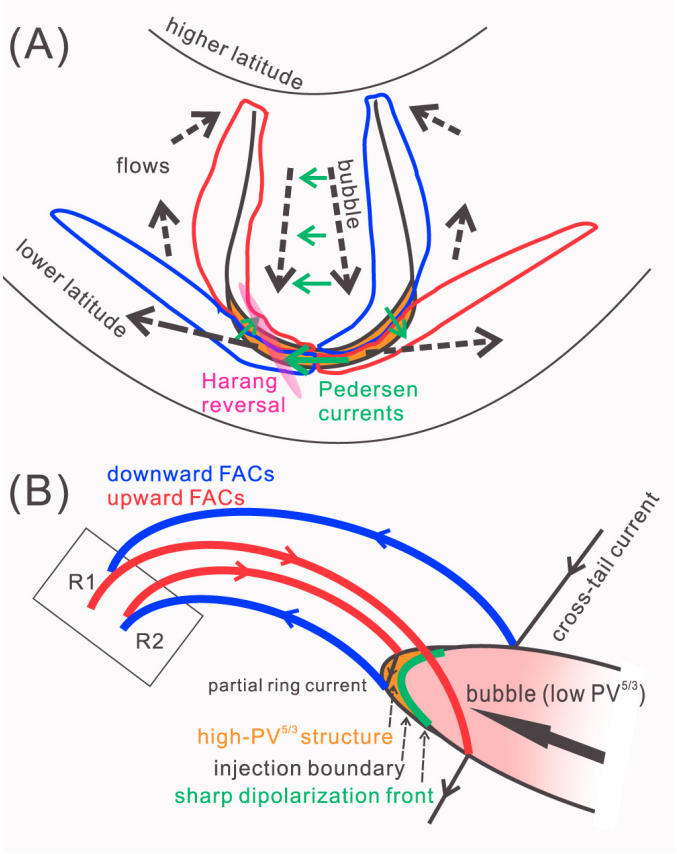

Figure 4.2: Ionospheric signatures of bubble injection (A) and magnetospheric dynamics (B) from Yang et al. (2012)

the negative H-component excursions as a measure of the westward electrojet and similarly the AU index is associated with the upper envelope of the positive deflections as a measure of the eastward electrojet. The difference AU-AL between the upper and lower envelope gives the AE index (Tomita et al. (2011); Davis and Sugiura (1966)).

The Dst index on the other hand uses mid-latitude magnetometer stations to monitor the storm level. The magnetic deflections are in this case caused by the equatorial ring current.

Chapter 5

M-I coupling

There is a close coupling between the magnetosphere and the ionosphere through the magnetic field lines and field-aligned currents (FACs). Magnetospheric electric fields map down to the ionosphere. Magnetospheric particles and FACs cause auroral particle precipitation (Knight (1973)).

5.1 SW-Magnetosphere coupling

The Akasofu ϵ function gives an empirical formula for the energy coupling between the solar wind and the magnetosphere

$$\epsilon(t) = VB^2 l_0^2 \sin^4(\theta/2),$$

where V is the solar wind speed, B is the interplanetary magnetic field, l_0 is an empirical scaling parameter (the effective magnetosphere radius) $l_0 = 7R_E$ and θ is the IMF clock angle. This is an empirical expression for the magnitude of the amount of electromagnetic power input from the solar wind integrated over the relevant magnetopause area, i.e., the rotational discontinuity of the open magnetosphere (see e.g. Lee and Roederer (1982) Vasyliunas et al. (1982)).

Kan and Lee (1979) (Sonnerup (1974)) introduced the following MP reconnection E-field dependence on solar wind parameters:

$$E_{KL} = VB_T \sin^2\left(\frac{\theta}{2}\right)$$

where $B_T = \sqrt{B_y^2 + B_z^2}$ and $\theta = \tan^{-1}(B_y/B_z)$. Eriksson et al. (2000) found that a version with $VB\sin^3(\theta/2)$ gave the best correlation with the polar cap potential drop. The cross polar cap potential (CPCP) is defined as the maximum potential difference across the polar region and characterizes the total strength of the convection.

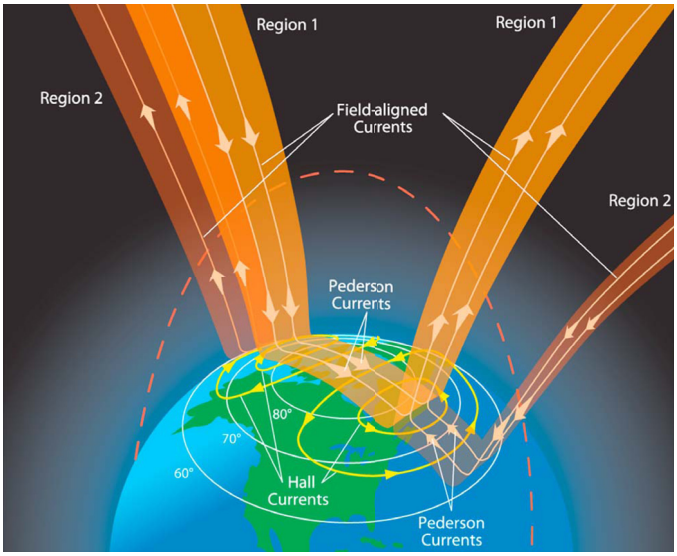

Figure 5.1: Sketch of FACs from Le et al. (2010)

5.2 Birkeland currents

Birkeland currents or field aligned currents (FACs) are the main coupling mechanism. The two major large scale current systems are called Region 1 (R1) and 2 (R2), where Region 1 are poleward of Region 2 (see Figure 5.1) (Iijima and Potemra (1976)). The FACs are mainly carried by electrons. For more details on FACs see Zmuda et al. (1966)

An additional third FAC-system poleward of R1 is also present, cusp currents (C1). The R1 current is downward on the dawn side and upward on the dusk side while the R2 direction is the opposite. The FACs form part of a current circuit closed by Pedersen currents in the ionosphere and magnetopause currents in the magnetosphere. The magnetopause currents corresponds to the generator in the circuit where $\vec{j} \cdot \vec{E} < 0$ and the Pedersen currents corresponds to the load with $\vec{j} \cdot \vec{E} > 0$ (Cowley (2000)). The circuit gives a perturbation, $\Delta \vec{B}_p = \mu_0 \Sigma_P \vec{E}$, in the magnetic field directed opposite of the ionospheric flow in the northern hemisphere and giving rise to a net downward Poynting flux

$$S_z = \vec{E} \Delta \vec{B}_p / \mu_0 = \Sigma_P \vec{E}^2$$

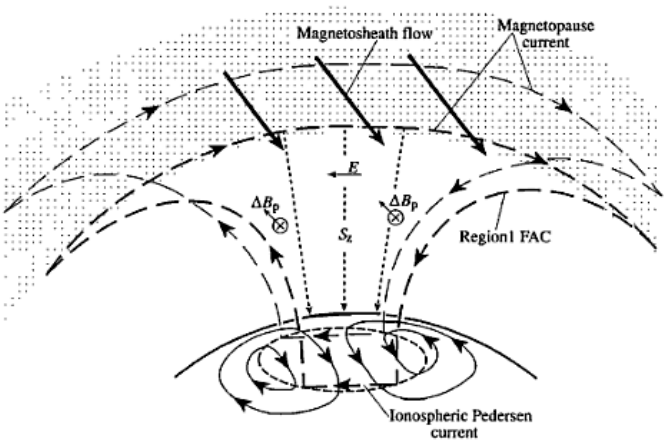

Figure 5.2: Sketch of polar cap convection and the dayside R1 current circuit from Cowley (2000). Dawn is to the right.

(see also Fig. 5.2). The Poynting flux is the source of Joule heating in the ionosphere. This energy is extracted from the solar wind by the $\vec{j} \times \vec{B}$ force in the high-latitude boundary layer (HBL) dynamo region ($\vec{j} \cdot \vec{E} < 0$) providing energy to the electromagnetic field.

Temporal response of the R1 current system to enhanced MP reconnection is discussed by Siscoe et al. (2011). They make the comparison between the region 1 current system and an LR circuit which is a coupled induction resistance circuit (Sanchez et al. (1991)). Analogous to an LR-circuit the current system has two phases, a transient start up phase and a steady-state persistent phase. During the transient phase the current builds up to a steady-state value and the voltage across the resistor (the ionosphere) rises from zero. The voltage (EMF) around the inductor, corresponding to the R1 current loop, decreases to zero and the inductor transforms the energy into magnetic flux. In the persistent phase the solar wind motional electric field strength, the reconnection efficiency and the ionospheric conductance are the factors determining the strength of the R1 current system.

Observational evidence of FACs spatial structure from satellite data are documented by e.g. Papitashvili et al. (2002) where R1 and R2 currents are clearly shown (their Fig. 3). An additional study using data from the Iridium satellites were done by Anderson et al. (2008).

5.2.1 Cusp currents

A specific set of FACs is present in the cusp region. The cusp currents for $B_z < 0$ have a strong B_y dependence due to the stresses in the newly opened field lines. For $B_y > 0$ the current is predominantly upward (downward) in the northern (southern) hemisphere and the other way around for $B_y < 0$.

Some of the first to describe two separate sheets of cusp currents were (Taguchi et al. (1993)) who referred to them as LCC and HCC (see Figure 5.3). The LCC and HCC currents are both on open field lines and the two field aligned current sheets with opposite polarity has a strong dependence on the direction of IMF B_y (see Figure 5.4)

We also have cusp currents when IMF B_z is positive. In this case we get an additional reversed twin vortex flow associated with lobe reconnection. The FACs are in this case called NBZ currents and go downward in dusk and upward in the dawn convection cell. For a more extensive treatment of cusp currents we refer to Potemra (1994) and Sandholt and Farrugia (2012).

5.3 Travelling Convection Vorticies

Travelling convection vorticies (TCVs) are accompanied by smaller scale transient FACs (Friis-Christensen et al. (1988)). They originate from a propagating magnetopause deformation due to a pressure front. In the ionosphere they are manifested as twin vortices at high latitudes moving east or west away from noon along the line between the centers of the vortices. The two vortices are associated with one upward and one downward directed FAC flowing from the center of each cell. The flow current is upward for the clockwise vortex and downward for the anticlockwise vortex in the northern hemisphere and the opposite in the southern hemisphere. The current closes in the ionosphere via Pedersen current between the two flow vorticies. The cell with downward current is slightly positive and the cell with upward FAC is slightly negative giving the electric field that drives the Pedersen current. The Hall current flows opp in the direction opposite of the $\vec{E} \times \vec{B}$ drift (Cowley (2000)). The magnetic disturbance on ground is mainly from the Hall currents, as the FAC effects and Pedersen current cancel under the ionosphere (Fukushima's theorem).

5.4 Boundary layers

In the model by Siscoe et al. (1991) for the Region 1 FAC system, the high-latitude boundary layer (HLBL) and low-latitude boundary layer (LLBL)

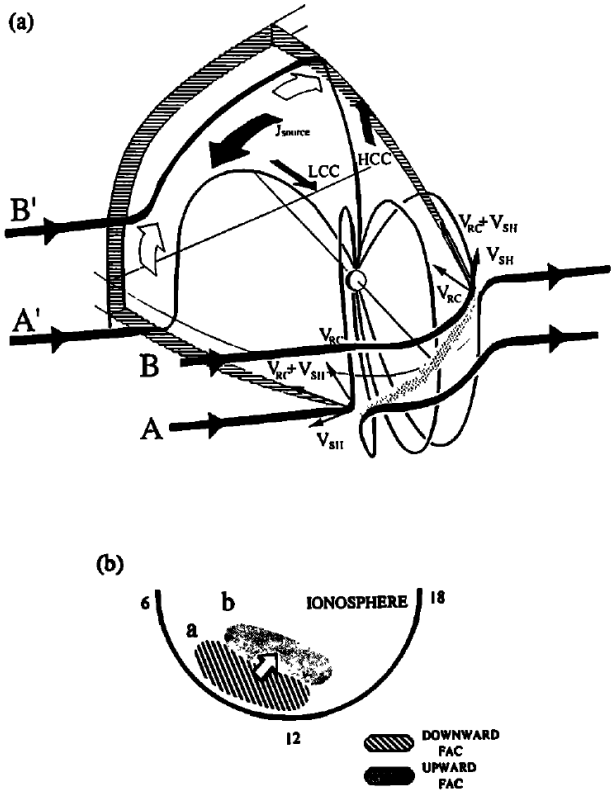

Figure 5.3: Model of the field aligned current (here denoted HCC and LCC) generation mechanism from Taguchi et al. (1993). a) Shows field lines A and B pulled by magnetic tension (V_{RC}) and carried downstream by the magnetosheath plasma (V_{SH}). The reconnection takes place in the dotted area. A' and B' is the location of the same field lines at a later time. The electric field is indicated by open arrows. b) Shows the ionospheric projection of the electric field (arrow) and FAC signatures.

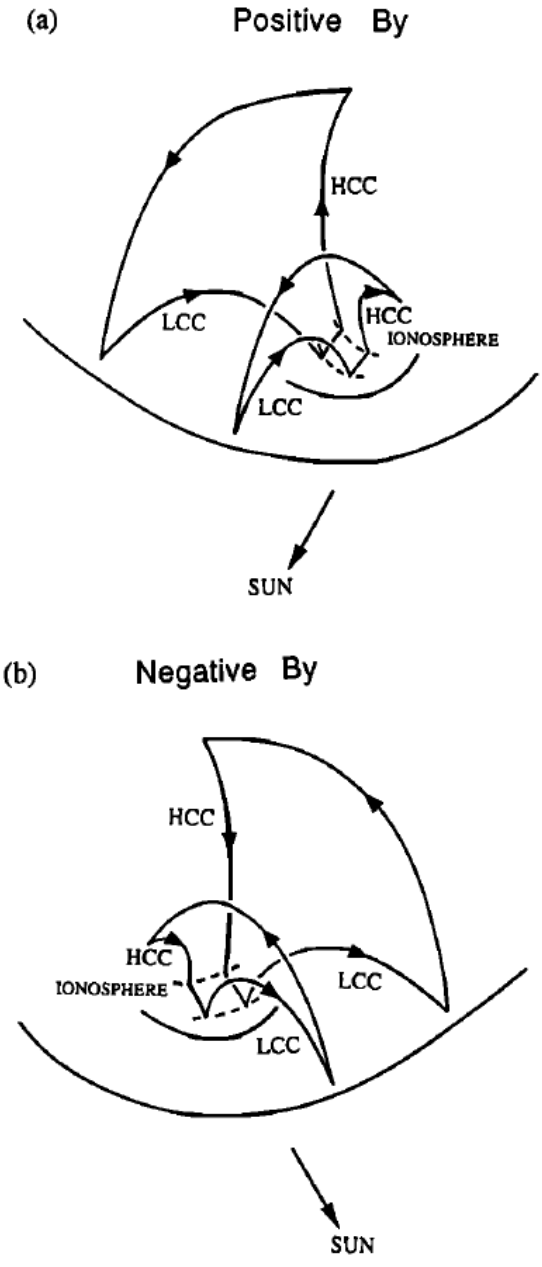

Figure 5.4: The northern hemisphere cusp current circuits for a) IMF B_y positive and b)IMF B_y negative conditions. Figure from Taguchi et al. (1993)

generate the voltage and the current respectively for the circuit that closes through the ionosphere. The current is here assumed to be generated by a vorticity in the LLBL through a solar wind viscous coupling. The voltage comes from the solar wind motional electric field penetrating the HLBL. This E-field maps to the ionosphere and thereby it gives rise to the cross-polar cap potential (CPCP). The current system is shown in Figure 5.5 without the region 2 currents. The current originating in the LLBL forms a complete loop by closing through the ionosphere and HLBL. On the dusk side on the cut trough the LLBL the plasma flow velocity profile is indicated. The shear in the plasma flow leads to a divergence in the current.

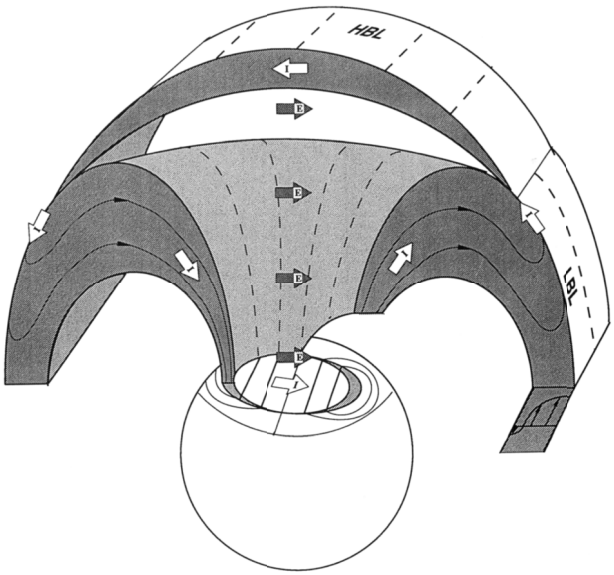

Figure 5.5: R1 Birkeland currents in relation to boundary layers at high (HBL) and low latitudes (LBL). Seen from the northern hemisphere at a post-noon local time (after Siscoe et al. (1991)).

A study by Newell et al. (1996) shows maps of statistical ionospheric precipitation patterns and which magnetospheric regions they map to. Figure 5.6 shows the maps according to source region for IMF B_z negative conditions. White means lack of significant precipitation, although the whole polar cap has polar rain precipitation only intense polar rain signal is indi-

cated in the figure. The cusp (red in the figure) is recently opened flux and represent the most direct entry of plasma from the magnetosheath into the magnetosphere. It extends 2.5-3 hours in local time and about one degree in latitude. The BPS (dark blue) and CPS (blue-green) precipitation are the nightside precipitation regions from the plasma sheet, that also extends to the dayside. The low-latitude boundary layer (LLBL) (yellow) has higher particle energies than the cusp and consists of a mixture of magnetosheath and magnetospheric plasma. The mantle (green) or high-latitude boundary layer (HLBL) has lower average energies than the cusp. They are on old open field lines and consists of de-energized magnetosheath plasma. Polar rain is homogeneous electron precipitation up to a few hundred eV in the polar cap on open field lines.

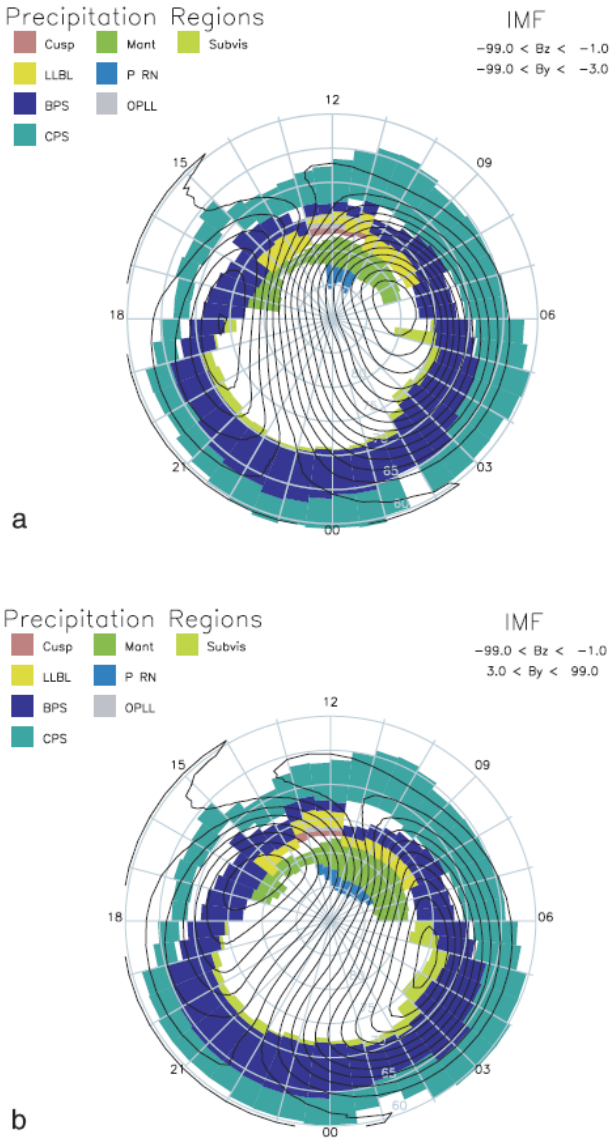

Figure 5.6: Maps of particle precipitation regimes in MLT/MLAT coordinates for a) B_z negative; B_y negative and b) B_z negative; B_y positive conditions from Newell et al. (1996).

Chapter 6

Ionospheric convection

In the high-latitude ionosphere the $\vec{E} \times \vec{B}$ plasma drift leads to convection by the E-field mapped from the solar wind. During due southward IMF we get the classical symmetrical twin cell convection pattern with antisunward flow over the polar cap and return flow at lower latitudes. Magnetopause reconnection will open more flux lines leading to an expansion of the polar cap and corresponding flow (Siscoe and Huang (1985) and Cowley et al. (1992)) (see Fig. 6.1). A similar process takes place for tail reconnection only this

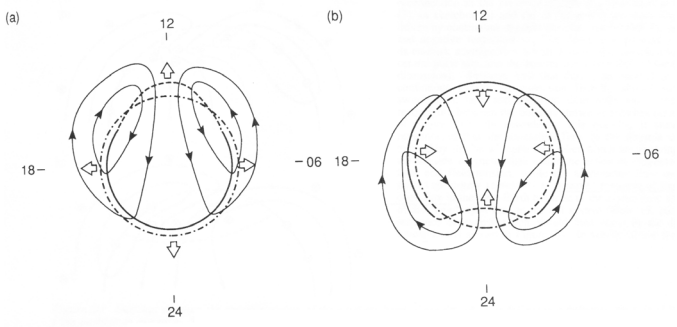

Figure 6.1: Steady unbalanced dayside (a) and steady unbalanced nightside reconnection (b). The dashed line is the merging region and the solid line is the part of the polar cap boundary that moves with the flow. The dot-dashed circle represents the equilibrium conditions after dayside (a) and nightside(b) reconnection events. From Fig. 6 in Cowley et al. (1992)

time flux is being closed and the polar cap contracts. The merging gap is the only place that flux crosses the open-closed field line boundary. Convec-

tion dominated by MP-reconnection/tail reconnection gives an unbalanced dayside/nightside convection pattern.

Cowley et al. (1992) also discusses the case of a nonzero IMF B_y component and the response to a change in the sign of B_y. For B_y positive and negative the reconnection region in the northern hemisphere shifts duskward and dawnward, respectively. This gives a flow pattern as shown in Fig. 6.2 for unbalanced dayside reconnection. With unbalanced reconnection we mean dayside reconnection which is not fully compensated by nightside reconnection or vice versa.

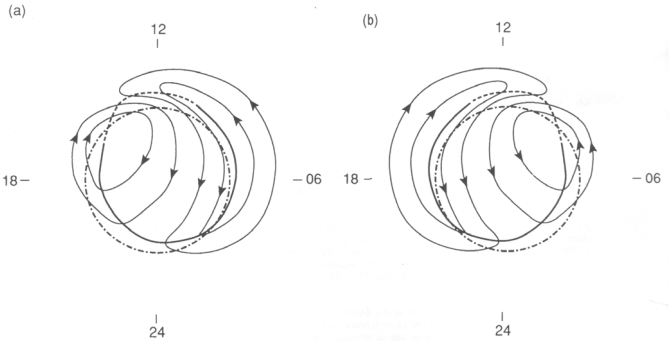

Figure 6.2: Steady unbalanced dayside reconnection for B_y positive (a) and negative (b) from Fig. 6 in Cowley et al. (1992)

The cross polar cap potential (CPCP) as measured by satellites in polar orbit consists of contributions from the dayside and nightside reconnection processes (see e.g. Provan et al. (2004)):

$$\Phi_{PC} = \Phi_D + \Phi_N$$

As the IMF rotates from a due southward the convection cells get distorted. If IMF has a considerable B_y component one cell will become more round and the other more crescent shaped. As B_z becomes more northward the convection evolves into a four cell pattern with two lobe cells and sunward convection in the middle of the polar cap. Weimer (1995) shows electric potential patterns from spherical harmonic fits to satellite data. Where the potential lines are closest together the gradient is greater and the convection is stronger. The electric potential satisfies the same equation as the stream function. Figure 6.3 shows statistical convection patterns in MLAT/MLT coordinates for B_T range of 5-10 nT from Ruohoniemi and Greenwald (2005) derived from SuperDARN data. Seasonal variations are found by both Weimer

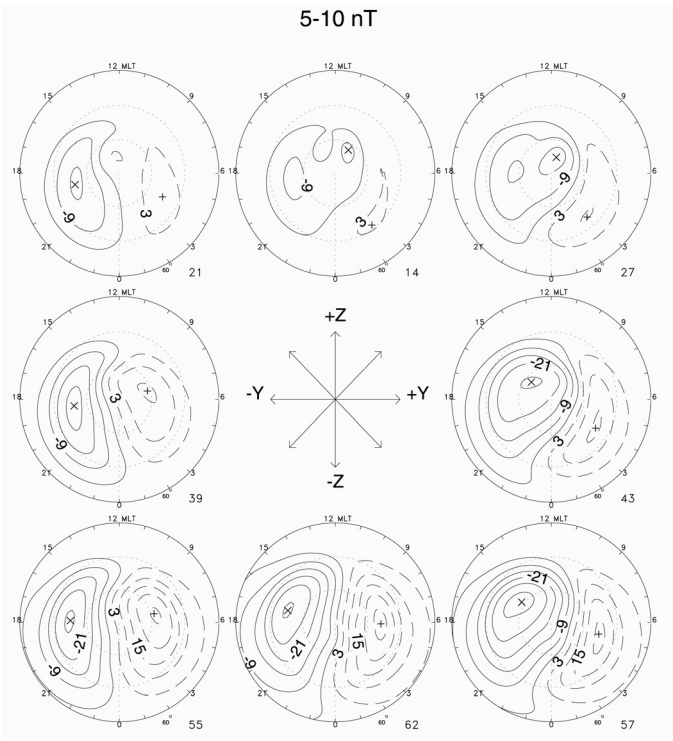

Figure 6.3: Statistical convection patterns ordered by clock angle for IMF magnitudes between 5 and 10 nT. Figure 7 in Ruohoniemi and Greenwald (2005)

(1995) and Ruohoniemi and Greenwald (2005). Weimer (1995) emphasizes an enhanced dawn-dusk asymmetry during summmer/$B_y > 0$ conditions and Ruohoniemi and Greenwald (2005) find that the summer season reinforces the B_y positive effect and the winter season the B_y negative effect.

6.1 Pedersen and Hall currents

The FACs are closed in the ionosphere by (Hall and) Pedersen currents. The Hall current is carried by electrons and is perpendicular to both $\vec{B}$ and $\vec{E_\perp}$ thus flowing in the opposite direction of the convection. The Pedersen current

is primarily carried by ions and is in the same direction as $\vec{E_\perp}$.

6.2 Convection signatures of Flux Transfer Events

Time-dependent MP reconnection gives rise to polar cap convection channels. Southwood (1987) describes the convection signature of flux transfer events (FTE's). The reconnected flux tubes forms an equatorward excursion in the polar cap boundary. Alfvén waves carries the information of the reconnection, and with it the redistribution of stresses, to the ionosphere. To move the footpoint of the flux tube in the ionosphere (and counter the ionospheric drag) the solar wind transfers momentum through field aligned current flow along the flanks of the flux tube. The flow around the flux tube is depicted in figure 6.4. The flux tube forms a channel of enhanced convection applicable to newly open and old open field lines with return flow on the two sides. The motion of the flux is in the $\vec{J_P} \times \vec{B}$ direction where J_P is the ionospheric closure current of $J_{||}$.

6.2.1 Auroral Electrojets

Figure 6.5 shows the ionospheric Pedersen current closure of the R1 and R2 FACs and associated electrojet currents. The convection return flow is established and maintained by the electrojets or currents flowing in the ionosphere, within a narrow latitudinal range of enhanced conductivity. Both the eastward and westward electrojet are Hall currents (see figure 6.5).

6.3 Flow channels

Sandholt and Farrugia (2009) introduced channels of enhanced antisunward convection on the dawn/dusk side of the polar cap on old open field lines, i.e. field lines that have been open for $\sim$ 10-20 min. The flow channels on old open field lines (>10 min. since reconnection) are called FC 2, distinguishing them from the noonward FC 1 flows on newly open field lines. These FC 2 channels are driven by Pedersen current closure of the C1-C2 Birkeland currents in the polar cap close to the polar cap boundary and maximises at the interface between C1 and C2. C1 is connected to HBL/magnetopause current ($j_{||}(C1) = -\nabla \cdot \vec{J}_{MP}$) and C2 to the inner LLBL at high latitudes (see Fig. 6.6). For B_y positive (negative) the flow channel appears on the dawn (dusk) side of the polar cap in the northern hemisphere and opposite

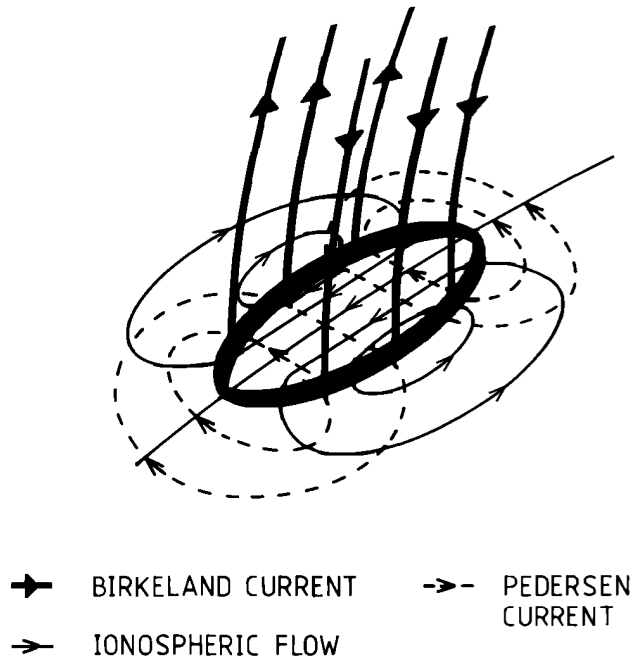

Figure 6.4: Convection-signature of FTEs after Southwood (1987).

for the southern hemisphere. With this current system they introduced a IMF B_y-related dawn-dusk asymmetry associated with old open field lines in addition to newly open field lines.

The R1 and C2 FACs are next to each other and have the same direction, but can be distinguished by that R1 is associated with newly opened field lines while C2 is on old open field lines. This distinction manifests itself in the stepped ion cusp dispersion signature seen in Figure 6.7. C1 is distributed in a wider latitudinal range in the polar cap where polar rain precipitation is observed. Since the time since reconnection is $t \propto \frac{\Delta s}{\sqrt{E_{co}}}$, where Δs is the distance to MP entry and E_{co} is the ion cutoff energy, the ion energies are higher for C2 than for R1. In addition the border between R1 and C2 marks the convection reversal (marked CR in Figure 6.7). According to Le et al. (2010) C2, flowing into (out of) the ionosphere in the dawnside (duskside), is approximately 5% of the total R1 FAC.

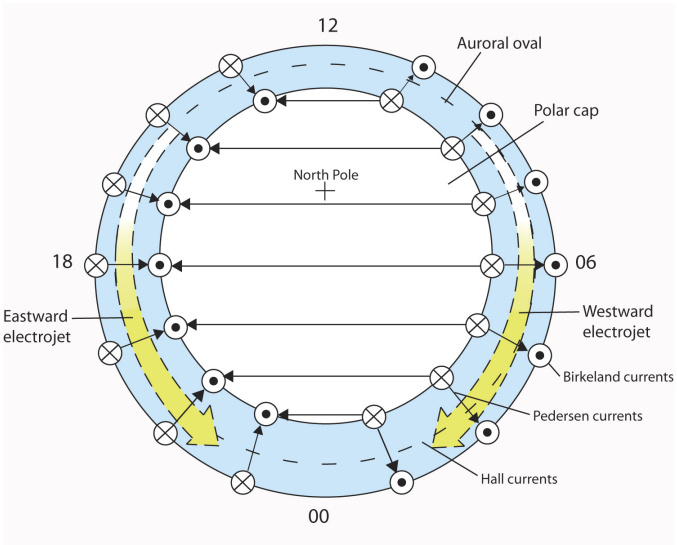

Figure 6.5: Configuration of Birkeland currents and auroral electrojet currents from Dahlgren (2010)

The conductivity difference between the polar cap and the auroral oval leads to a polarization electric field that contributes to the flow channel FC2. Since the conductivity Σ in the polar cap is lower for the winter hemisphere we get a larger gradient giving more pronounced flow channels compared to the summer hemisphere. The ground magnetometer signatures on the other hand can be given as

$$\Delta B_{gr} \propto \Sigma_H \frac{\vec{B} \times \vec{E}}{B}$$

where Σ_H is the Hall conductivity which is higher in the summer hemisphere compensating for the lower $\vec{E}$ leaving us with a good ground signature also in the summer hemisphere.

In Anderson et al. (2008) (their Figure 7) they show statistical Birkeland current distribution for varying IMF orientation (see Fig. 6.8). The FC 2 magnetic signatures are clearly visible in all the panels representing east/west and south-east/west IMF conditions.

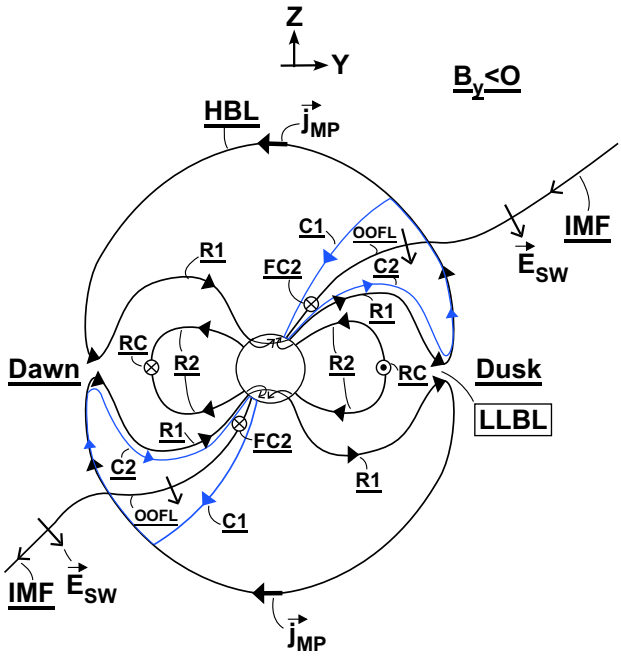

Figure 6.6: Sketch of the geometry of high-latitude field-aligned currents and flow channels FC 2 seen from the dayside after Sandholt and Farrugia (2012). The IMF orientation is south-west.

6.4 The Cross Polar Cap Potential (CPCP) and its saturation

Early satellite measurements of CPCP and its relationship with IMF B_z conditions are summarized by ESA (1984). Figure 3 (ESA (1984)) shows a

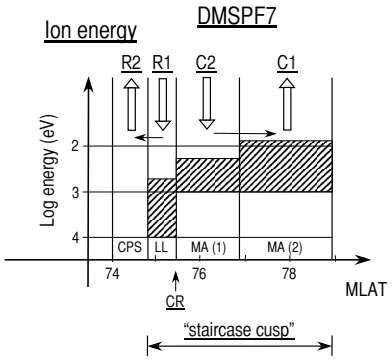

Figure 6.7: Illustration of the R1/R2 and C1/C2 FAC system related to ion precipitation regimes and convection reversal for a DMSP F7 pass trough the pre-noon sector 12 Dec. 1983 (see Sandholt and Newell (1992)). The direction of the Birkeland currents are marked with the big arrows. The horizontal arrows below them indicates the Pedersen current closure.

wide scatter of Φ_{PC} values for a given IMF B_z-value. This is as expected for a two-source model of polar cap convection (Siscoe and Huang (1985)) since the satellite observations of CPCP are made during different phases of substorm activity.

The coupling function E_{KL} introduced by Kan and Lee (1979)

$$E_{KL} = V B_T \sin^2\left(\frac{\theta}{2}\right),$$

where $B_T = \sqrt{B_y + B_z}$ and θ is the clock angle, is the geo-effective interplanetary electric field where for moderate values there is a linear relationship between CPCP and E_{KL}. However, the linearity of the response of CPCP to the interplanetary electric field is no longer valid for strong forcing of the magnetosphere, it saturates (see Figure 6.9), i.e. it does not grow any further with increasing interplanetary electric field. Several studies have identified this saturation of the CPCP: Reiff et al. (1981); Russell et al. (2001). Mühlbachler et al. (2005) did a statistical study and found that the day-side erosion starts to saturate when B_z is between -12 and -16 nT corresponding,

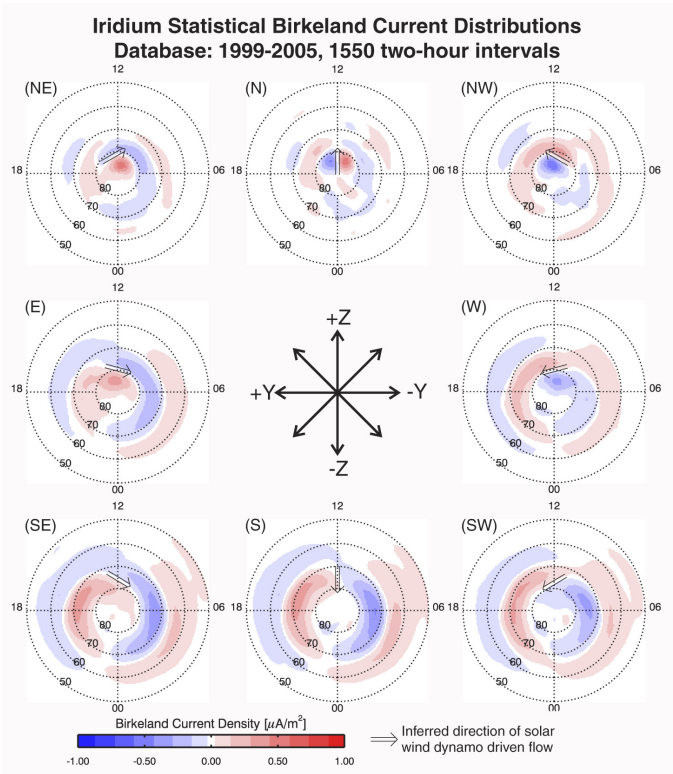

Figure 6.8: Iridium observations of statistical Birkeland currents under different IMF directions from Anderson et al. (2008), red is up and blue is down. The FC2 channel is indicated in each of the plots.

in this case, to an interplanetary electric field of $6.2 \pm 1.6\text{mVm}^{-1}$. Typical CPCP voltages at saturation is around 200 kV.

Boyle et al. (1997) derived the following formulae to calculate the CPCP in the linear regime, i.e. when no saturation has set in:

$$\Phi_{PC} = 10^{-4} V_{SW}^2 + 11.7 B \sin^3(\theta/2)\text{kV}.$$

where B is in nT, V_{SW} in km/s and θ is the IMF clock angle. Taking into account the effect of the variations in the solar wind ram pressure P_{SW} and

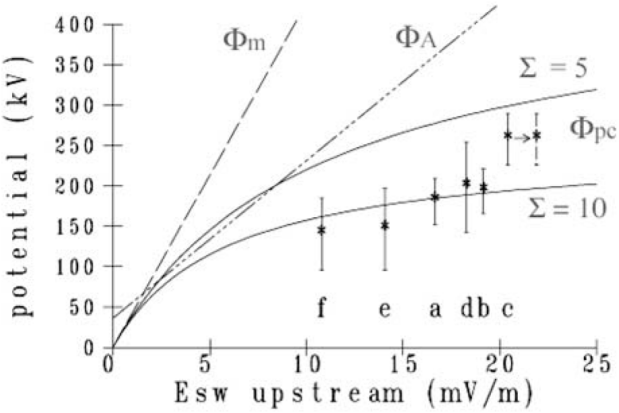

Figure 6.9: DMSP potential data from 31 March 2001 plotted against the solar wind electric field. Th Φ_{PC} curves are from the Hill-Siscoe model using $\Sigma = 5$ (upper curve) and $\Sigma = 10$ (lower curve). The Φ_A line is the Boyle potential and the Φ_m is the calculated potential at the magnetopause from reconnection in without the saturation effect. The figure is taken from Hairston et al. (2003).

the saturation effect Siscoe et al. (2002) introduces the relation

$$\Phi_{PC}(\text{kV}) = \frac{57.6 E_{SW} P_{SW}^{1/3} D^{4/3} F(\theta)}{P_{SW}^{1/2} D + 0.0125 \xi \Sigma_P E_{SW} F(\theta)} \tag{6.1}$$

where D is the Earth's dipole strength, $F(\theta) = \sin^2(\theta/2)$ is the IMF clock angle dependence of the MP reconnection, E_{SW} is the electric field in the upstream solar wind (in mV/m), ξ is a dimensionless coefficient between 3 and 4 that depends on the geometry of the currents in the ionosphere, Σ_p is the height integrated Pedersen conductivity in the ionosphere (in mho (S)) and $P_{SW} = \rho_{SW} v_{SW}^2$ is the ram pressure exerted by the solar wind (in nPa). From this we see that there is a dependence on pressure meaning that for high P_{SW} CPCP saturates at very high values of $E_{KL} = E_{SW} \cdot \sin^2 \frac{\theta}{2} F(\theta)$. A similar expression were found by Kivelson and Ridley (2008). The Siscoe-Hill model proposes that the polar cap saturation is caused by a transition from a Chapman-Ferraro closed magnetosphere to a Dungey-Alfvén open magnetosphere. Saturation occurs when the second term in the denominator

dominates over the first term (independence of E_{SW}). When P_{SW} is high this happens only at large E_{SW} values. As we said at the beginning extreme values of interplanetary parameters are typically reached in ICMEs and MCs. So we expect to see saturation of CPCP during passage of some ICMEs/MCs.

Peng et al. (2009) suggests that the cross polar cap potential depends on the Pedersen conductance Σ_P and a parameter f as follows:

$$\Phi_{PC}(\mathrm{kV}) = \frac{2.3 \times 10^3 (f + 0.8)(\Sigma_P + 2)^{-1}}{f + 8.2}$$

where $f = E_{SW}(\mathrm{mV/m}) P_{SW}(\mathrm{nPa}) M^{-1/2}$ is a function of the solar wind electric field E_{SW}, the ram pressure P_{SW} and the Alfven Mach number M_A. Saturation can thus be due to increase of E_{SW} or P_{SW} or decrease of M_A (that is variations in f) or equivalently, as f also is proportional to $n_{SW}^{3/4} v_{SW}^{5/2} B_S^{3/2}$, increase of these factors. They use the following values for the Pedersen conductivity: Σ_p = 1, 5, 10 S where 1S is a typical value for winter and in the summer 10S is more typical (sunlit ionosphere).

Burke et al. (2007) use the polar cap potential to estimate the unshielded Volland-Stern (V-S) electric field in the inner magnetosphere and the Dst-index during storm main phases:

$$I_{VS} = \int E_{VS} dt\,; \qquad E_{VS} \simeq \Phi_{PC}/2R_E L_Y;$$

$2L_Y$ is a cross magnetosphere distance and

$$Dst(nT) = -a \cdot I_{VS}.$$

6.4.1 Polar Cap Index

The polar cap (PC) index, an expression for geomagnetic activity over the polar cap, can be used as an instantaneous monitor of plasma convection (Troshichev et al. (2000)). The magnetometer stations used is Thule in the northern hemisphere (PCN) and Vostok in the southern hemisphere (PCS). It has been assumed that the PC index is related to the solar wind merging electric field, that is dependent on magnetopause reconnection. Gao et al. (2012) suggested PCN to be a combination of driven (E_{KR}) and unloading (AL_U) processes formulated as:

$$\mathrm{PCN} = \alpha_0 + \alpha_1 E_{KR} + \alpha_2 \mathrm{AL}_U + \epsilon$$

where α_0 is the intercept, α_1 and α_2 are regression coefficients, AL_U is unloading component of the AL index $\mathrm{AL}_U = \mathrm{AL} - \mathrm{AL}_D = \mathrm{AL} - \beta_0 - \beta_1 E_{KR}$.

E_{KR} is a modified merging electric field (Kivelson and Ridley (2008)) where $E_{KR} = E_{KL} \cdot f(v_A)$, where the transmission coefficient $f(v_A) = \frac{2\Sigma_A}{\Sigma_A+\Sigma_P} < 1$, Σ_P is the ionospheric Pedersen conductance, $\Sigma_A = 1/\mu_0 v_A$ is the Alfvén conductance, $v_A = B/(\mu_0\rho_{sw})^{1/2}$ is the Alfvén velocity, and ϵ is the error (with zero expectation and constant variance) incorporating all other contributing processes. Gao et al. (2012) found that the driven-to-unloading ratio has both a seasonal variation and a systematically variation over the solar cycle. Troshichev et al. (2000) showed that the Polar Cap (PC) index saturates at a value ~ 10 mho. From equation 6.1 we see a dependence on the conductivity Σ_p. When the last term in the denominator, containing $\Sigma_p E_{KL}$, dominates over the other terms the fraction can be simplified so that the E_{KL} factors disappear. This is what happens when we get saturation. Saturation is normally reached when $E_{KL} > 5$ mV/m, but the higher the conductivity is the earlier saturation can appear. This is also illustrated in Figure 6.9 for two different conductivity values.

Chapter 7

7.1 Summary

In five papers we distinguish between different stages of polar cap convection response to intervals of enhanced interplanetary driving during Earth passage of interplanetary CMEs. The interplanetary driving of the magnetosphere in these cases, as measured by the geoeffective interplanetary electric field (E_{KL}), typically show an abrupt increase followed by a long interval of steady external driving. The magnetospheric response consists of two basic stages. An initial transient phase is characterized by the build-up of the dayside R1 FAC system and the transfer of the magnetopause reconnection potential to the ionosphere. This is followed by the persistent phase characterized repetitive substorm activity under steady interplanetary driving.

We distinguish between convection sub-structure (flow channels) on newly open and old open magnetic field lines, and flow channels specifically related to substorm activity. We refer to these three types of flow channel as FC 1 (NOFLs), FC 2 (OOFLs), and FC 3 (substorm - related). The FC 2 flow channel is related to the ionospheric Pedersen current closure of Birkeland currents located poleward of the Region 1/2 current system.

By combining ground and satellite observations we are able to make estimates of the detailed temporal variability of the cross-polar cap potential (CPCP) in terms of the PCN - index and the cross-polar cap distance (L_{PC}): CPCP (V) = k_1 + k_2PCN(mV/m)L_{PC} (km). k_1 is a background potential not related to PCN-index. k_2 is a constant which differ from case to case (conductivity dependent).

We emphasize the CPCP variations observed in response to substorm activity in the persistent phase of solar wind - magnetosphere coupling: ΔCPCP/CPCP = ΔPCN/PCN + $\Delta L_{PC}/L_{PC}$. ΔL_{PC} estimates can be obtained from satellite crossings of the dusk-side polar cap boundary in different stages of the substorm evolution. We discuss the observations of CPCP variability in the context of the expansion-contraction model of polar cap

convection (Cowley and Lockwood, 1992). CPCP enhancements during substorm expansions are associated with polar cap contractions ($\Delta L_{PC} < 0$) as inferred from DMSP satellite data and/or auroral observations (e.g. poleward expansions at substorm onset). By this technique we identify a mode of pulsed polar cap convection and oscillating (expanding - contracting) polar caps during intervals of repetitive substorm activity.

In Paper 1 flow channels at the polar cap boundary are documented in ground and satellite data in a case study. In the DMSP F13 data the flow channel appears as a further enhancement of antisunward convection on the side of the polar cap where the flow is already strong due to the IMF B_y - related dawn - dusk convection asymmetry.

A combination of ground-based radar (SuperDARN) observations of plasma flow and the associated ground magnetometer deflections on the ground demonstrates the presence of a series of 5-10 min long FC 2 flow enhancements (pulsed antisunward convection) at polar cap latitudes. The FC 2 flow channel is described in relation to particle precipitation (DMSP satellite data) and the ionospheric Pedersen current closure of FACs located poleward of the R1/R2 FAC system. A conceptual model of the IMF - magnetosphere - ionosphere interconnection topology for this case is presented. This case demonstrates the presence of channels of FTE - related plasma flows along the periphery of the polar cap, as predicted by Southwood (1987).

In the next papers we investigate more carefully the distinction between dayside and nightside sources of the polar cap convection phenomena. All cases are characterized by a long interval of strong and steady interplanetary driving as demonstrated in Figure 7.1.

In Paper 2 (20 March 2001) we selected a case with strong forcing ($E_{KL} = 5 - 8$ mV/m) during ICME passage. The polar cap convection is inferred by looking at CPCP variations. Substorms lead to WEJ intensifications, poleward expansion, PC contraction and streamers. Double oval and auroral streamer forms (configuration) are identified at dusk in the UV images and the auroral streamer events are also identified in local magntograms from dusk sector of auroral oval. FC 3 flow activation is identified in DMSP F13 data and the CPCP enhancement measured by F13 from pre-substorm interval to substorm interval is: $\sim$55 kV.

In Papers 3, 4, and 5 we investigate the PC flow phenomena further, in the context of the Dungey cell flow circulation cycle, and discuss the responses to (i) enhanced MP reconnection rate (E_{KL}) and (ii) substorm activities under steady IP driving. FC 1 - FC 2 - FC 3 flows are identified in ground magnetometer data from the Svalbard IMAGE stations. An example of this (10 Jan. 2004 case) is shown in Figure 7.2 The marked FC 1 - FC 2 PC flows are directly driven by enhanced magnetopause reconnection rate

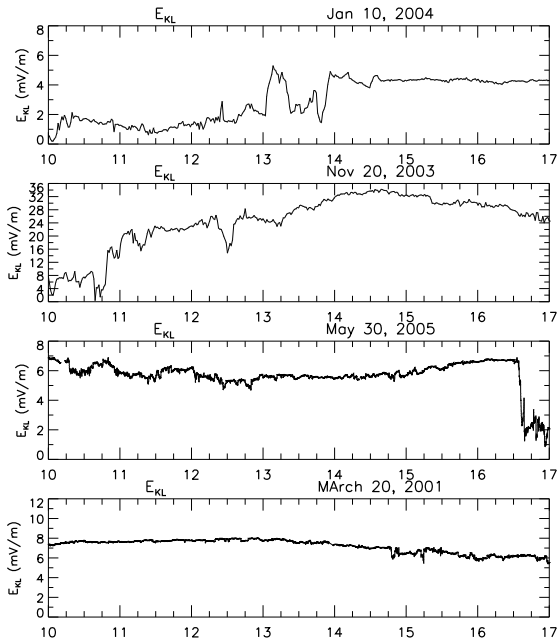

Figure 7.1: E_{KL} for the four events on January 10, 2004; November 20, 2003; May 30, 2005 and March 20, 2001.

as estimated by E_{KL} (see abrupt jumps from 2 to 5 mV/m in the top panel in Figure 7.1).

FC 3 flows, occurring under steady IP driving conditions, are related to substorm activities (the nightside source of PC convection), as inferred from the correlation with enhancements in the westward electrojet (WEJ) monitored by stations located at auroral oval latitudes. Onsets of two consecutive substorms are marked S1 and S2 in the Figure.

A plot of CPCP versus PCN for 10 Jan. 2004 (Paper 3) is shown in Figure 7.3. The figure illustrates the PCN response during the transient and persistent phases of polar cap convection. The persistent phase consists of an interval of steady convection (SMC) followed by convection enhancements related to substorms marked S1 and S2.

In paper 3 we study spatial-temporal convection structure from nightside (substorm) sources during moderate forcing for the event on 10 January 2004. IMAGE magnetometer data combined with DMSP F13 passes enables determination of the temporal flow structure over the whole interval. We compare the relative contributions from nightside and dayside sources to the CPCP and find an increase associated with nightside processes corresponding well with Kullen et al. (2010). The case has a non-traditional dawn-dusk convection asymmetry which we attribute to temporal variations in the flow strength due to substorm activity. The observations also include enhanced flow at the boundary of the polar cap in terms of flow channels FC 2 and FC 3.

In paper 4 we consider a 10-hour interval of strong and steady forcing during an ICME passage on 30 May 2005. This interval is initiated by enhanced magnetopause reconnection triggered by the southward turning of the ICME magnetic field. Substorms lead to electrojet intensifications with a $\sim$50 min. recurrence interval. We use DMSP F13 and F15 data to observe polar cap contraction events during the substorms. Additionally we observe CPCP enhancements, plasma flows in the central part of the polar cap and enhanced flows along the borders of the polar cap. Higher resolution is obtained by combining the low resolution DMSP satellite data with continuous ground observations using IMAGE magnetometer data and the PCN index. PCN substructure is also found to correspond well with AL minima. CPCP - PCN evolution for 30 May 2005 is shown in Figure 7.4. We note the PCN enhancement during a PC contraction event taking place in the interval between the F15 and F13 passes of the PC boundary at dusk. The relationship with the AL-index is shown in the bottom panel.

Paper 5 describes a case of extreme forcing on 20 November 2003. We look at the ionospheric response during an 8-hour interval. FC 1 and FC 2 flows are identified as a southward turning response studied by magnetometer

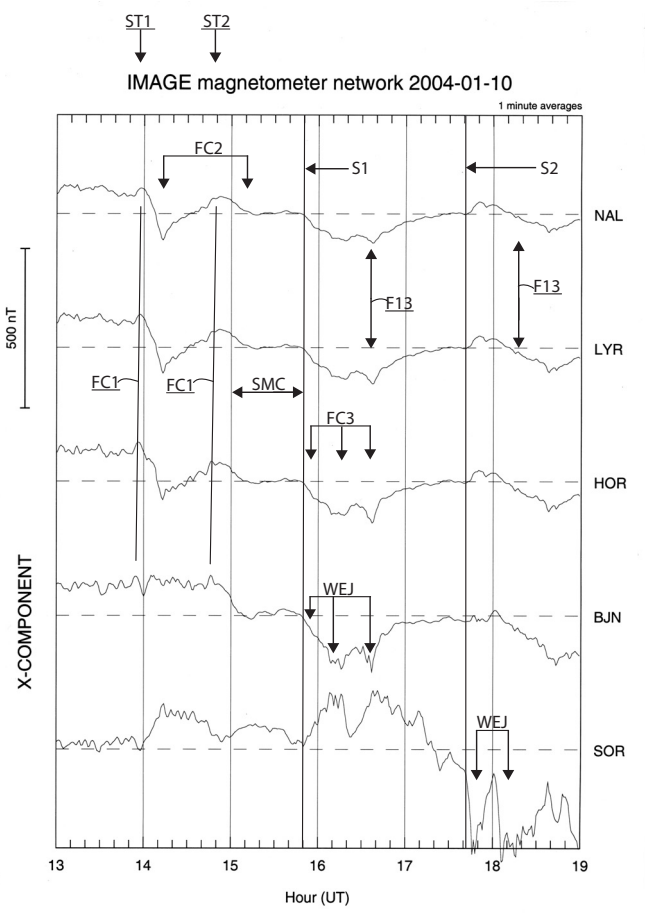

Figure 7.2: IMAGE magnetometer data from the stations NAL, LYR, HOR, BJN and SOR. The southward turnings of the IMF are marked by arrows (ST1 and ST2) as are FC1 and FC2, the WEJ and the DMSP F13 passes.

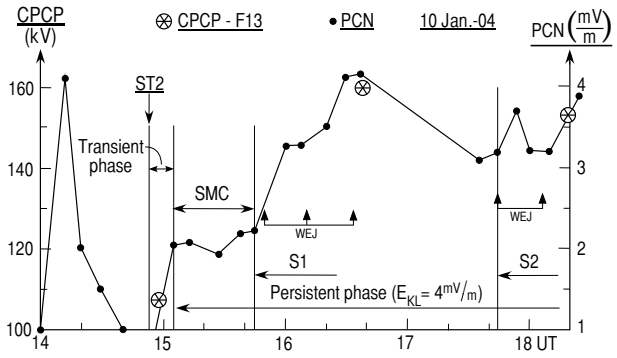

Figure 7.3: CPCP and PCN shown for the 10 January 2004 event.

x-deflections. We also observed the ground magnetic signature of FC 3 flows during substorms. We look at two substorms, the first (11:50 UT) triggered by the southward turning. The second substorm (14:50 UT) is identified in all-sky image data and IMAGE magnetometers. Both susbstorms lead to a PCN (and CPCP) increase. In addition smaller PCN enhancements due to substorm substructure like streamers are also shown to be present. The CPCP - PCN evolution for 20 November 2003 is shown in figure 7.5. We note the major PCN (CPCP) enhancements after onset of the substorms marked S1, S2 and S3. These are clear polar cap contraction events associated with substorm expansion. One of these PC contractions is directly observed by ASC data from Muonio, Finland during the interval 14:50-15:01 UT. Additional PCN (CPCP) fine-structure is observed during auroral streamer events documented in the interval of substorm S2.

7.2 Conclusions

Spatial-temporal structure of plasma flow in the polar cap (PC)

We distinguish between plasma flows (forward convection) appearing in different sectors of the polar cap (center versus periphery) and in different stages of field line evolution in the Dungey cycle. We studied the responses in PC

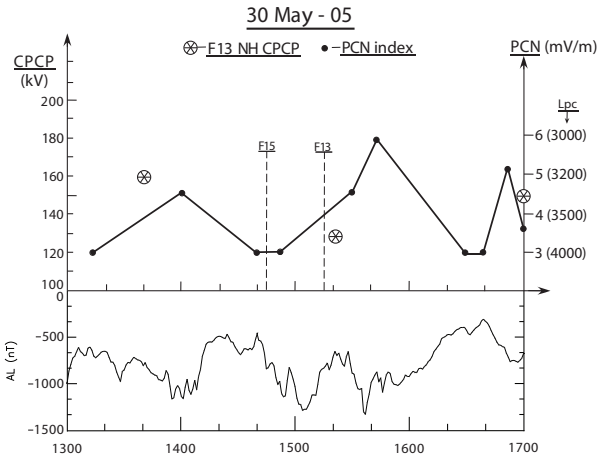

Figure 7.4: CPCP and PCN shown for the 30 May 2005 event (top panel) and AL-index for the same interval (bottom panel).

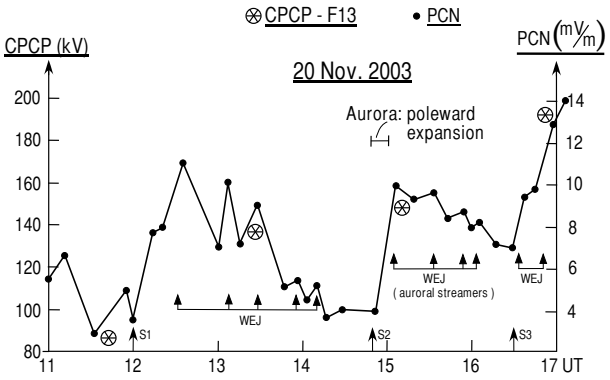

Figure 7.5: CPCP and PCN shown for the 20 November 2003 event.

flows to (i) enhanced magnetopause reconnection rate (southward turnings of the IMF or ICME magnetic field) and (ii) substorm activity (AL - index) as continuously monitored by the ground magnetic deflections excited underneath the ionospheric flows (IMAGE chain data and the PC - index). The different flow channels along the periphery of the polar cap are referred to as FC 1, FC 2, and FC 3. The magnetic field coupling of these flow channels to the magnetosphere is indicated in Paper 1. FC 1 and FC 2 flows are signatures of the dayside (magnetopause) source of plasma convection (in consecutive stages of open field line evolution), while FC 3 flows are related to the nightside (magnetotail reconnection) source.

FC 2 characteristics and interpretation

(i) This channel of enhanced antisunward plasma flow along the periphery of the polar cap (polar rain precipitation) appears most pronounced in the winter hemisphere. This is an effect of larger conductivity gradients at the PC boundary in the winter hemisphere. (ii) The stage of open field line evolution is referred to as old open field lines (OOFLs) and polar rain precipitation, i.e., the interval appr. 10 - 20 min. after the first signature of southward turning (ST) of the IMF (ICME magnetic field) (enhanced MP reconnection rate) arrives in the dayside ionosphere (Paper 3). (iii) The relationship with Pedersen current closure of high-latitude FACs poleward of R1/R2 system is

investigated in Papers 1 and 2. (iv) A conceptual model of IMF - magnetosphere - ionosphere interconnection topology is presented (Paper 1). (v) A pulsed mode of FC 2 flows (5-10 min. long events of antisunward convection) is documented by combined convection (SuperDARN spatial plots) and ground magnetograms (Svalbard IMAGE chain) in Paper 1. This observed flow behaviour along the periphery of the polar cap confirms a prediction by Southwood (1987) in relation to flux transfer events on the magnetopause.

FC 3 characteristics and interpretation

(i) Enhanced (> 1 km/s) antisunward convection along the polar cap boundary is observed in DMSP ion drift data at dusk and dawn (Papers 3 and 4). (ii) A relationship with substorm activity in the form of AL-excursions (WEJ intensifications) is documented.

Polar cap flow response to abrupt enhancement of the magnetopause reconnection rate

A two - stage convection response to enhanced IP driving (magnetopause reconnection rate) by ICMEs, as measured by E_{KL}, is documented in Papers 3, 4 and 5: (i) an initial transient phase (build-up of dayside convection cells and PC expansion) after E_{KL} enhancement, followed by (ii) a persistent phase characterized by repetitive substorms and PC flow events under steady, strong IP driving ($E_{KL} = 4$ - 30 mV/m in different cases).

Mode of pulsed flows (series of 10-15. min long plasma flow enhancements) in the central polar cap (PCN - index) during intervals of steady IP driving (persistent phase of solar wind - magnetosphere coupling)

(i) Relationship with AL-index excursions (repetitive substorm activity) is established (Papers 4 and 5). (ii) Relationship with polar cap contractions (substorm expansions) is estimated by satellite passes (at dusk PC boundary) in different stages of substorm evolution and by all-sky camera observations of substorm expansions (Papers 4 and 5). (iii) Mode of pulsed polar cap convection and oscillating polar caps (series of PC expansions - contractions) is explained in terms of the expansion - contraction model of PC convection which is characterized by two types of convection cells (accompanied by PC expansions and contractions) (Papers 4 and 5). (iv) Temporal variability of CPCP is estimated from the following empirical relationship: CPCP (V) $\sim$ kPCN (mV/m)xL_{PC} (km). ΔCPCP/CPCP = ΔPCN/PCN + $\Delta L_{PC}/L_{PC}$.

(v) Typical CPCP response to the individual major AL-events in the series: 25-30 percent enhancement.

PC flow response (fine-structure of PC convection) to substructure of substorm - activity

(i) Series of minor PC flow enhancements (PC - index) are observed during intervals of auroral streamer events (Papers 4 and 5). (ii) This substorm structure appears as equatorward-moving ground magnetic deflections (westward electrojet; WEJ) at auroral oval latitudes. The WEJ events are interpreted in terms of a channel of equatorward-directed flows (called FC 4 flows/streamer channel in Paper 1) associated with auroral streamer events. On the association with magnetotail dynamics (bursty bulk flows) we refer to previous studies reported in the literature (e.g. Sergeev et al. (2004)).

The substorm-related PC convection events may be explained by the mapping to the ionosphere of enhancements in the tail lobe **E** - field (E_{TL}) related to magnetic field dipolarizations - enhanced Earthward - directed bulk flows and associated increases in the rate of plasma sheet magnetic flux transfer ($\Phi_{Earth} \sim V_x B_z$) (see schematic illustration in Paper 1 and e.g., Sauvaud et al. (2012)).

7.3 Future work

Here we list a few points of natural extensions of the present work that should be pursued in the near future.

Further documentation of the mode of oscillating polar caps (series of expansion - contraction events) in the persistent phase of solar wind - magnetosphere coupling is recommended. One aim is to obtain a more precise determination of the CPCP variability in such cases by using planned ground radars with good coverage in the central polar cap in combination with data from polar orbiting satellites. The direct PC plasma flow monitoring by high - latitude radars can then be combined with more extensive use of global images of the UV aurora from space (see example in Paper 2) to obtain a high-resolution determination of the variability of the cross-polar cap distance (polar cap area). The global images can beneficially be combined with observations from the existing network of all-sky imagers on the ground (see example in Paper 5).

Investigation of magnetosphere - ionosphere coupling processes giving rise to convection fine-structure in the PC during substorms is recommended. Central to this issue is the monitoring of dynamical phenomena in the magne-

totail such as magnetic field dipolarizations, BBFs, and **E** - field-enhancements in the plasma sheet and tail lobes. This can be obtained by application of data from existing multiple spacecraft projects such as THEMIS and Cluster.

Bibliography

Akasofu, S. I. (1964). The development of the auroral substorm. *Planet Space Sci.*.

Amm, O., R. Fujii, K. Kauristie, A. Aikio, A. Yoshikawa, A. Ieda, and H. Vanhamki (2011). A statistical investigation of the Cowling channel efficiency in the auroral zone. *J. Geophys. Res. 116*(A02304).

Anderson, B. J., H. Korth, C. L. Waters, D. L. Green, and P. Stauning (2008). Statistical Birkeland current distributions from magnetic field observations by the Iridium constellation. *Ann. Geophys. 26*, 671–687.

Angelopoulos, V., C. F. Kennel, F. V. Coroniti, R. Pellat, M. G. Kivelson, R. J. Walker, C. T. Russell, W. Baumjohann, W. C. Feldman, and J. T. Gosling (1994). Statistical Characteristics of Bursty Bulk Flow Events. *J. Geophys. Res. 99*(A11), 21257–21280.

Baker, D. N., T. I. Pulkkinen, V. Angelopoulos, W. Baumjohann, and R. L. McPherron (1996). Neutral line model of substorms: Past results and present view. *J. Geophys. Res.*.

Belehaki, A., I. Tsagouri, and H. Mavromichalaki (1998). Study of the longitudinal expansion velocity of the substorm current wedge. *Ann. Geophysicae*.

Borg, A. L., M. ieroset, T. D. Phan, F. S. Mozer, A. Pedersen, C. Mouikis, J. P. McFadden, C. Twitty, A. Balogh, and H. Rme (2005). Cluster encounter of a magnetic reconnection diffusion region in the near-Earth magnetotail on September 19, 2003. *Geophys. Res. Lett. 32*(L19105).

Boyle, C. B., P. H. Reiff, and M. R. Hairston (1997). Empirical polar cap potentials. *J. Geophys. Res. 102*(A1), 111–125.

Burke, W. J., L. C. Gentile, and C. Y. Huang (2007). Penetration electric fields driving main phase Dst. *J. Geophys. Res. 112*(A07208).

Burlaga, L., E. Sittler, F. Mariani, and R. Schwenn (1981). Magnetic loop behind an interplanetary shock: Voyager, Helios, and IMP-8 observations. *J. Geophys. Res. 86*, 6673–6684.

Chen, C. X. and R. A. Wolf (1993). Interpretation of high-speed flows in the plasma sheet. *J. Geophys. Res. 98*(A12), 21409–21419.

Cowley, S. W. H. (1981). Magnetospheric and ionospheric flow and the interplanetary magnetic field. In *The Physical Basis of the Ionosphere in the Solar-Terrestrial System*, Number 295 in Advisory Group for Aerospace Research & Developement, 7 Rue Ancelle 92200 Neuilly Sur Seine, France. NATO.

Cowley, S. W. H. (2000). Magnetosphere-Ionosphere Interactions: A Tutorial Review. In *Magnetospheric Current Systems*, Volume 118 of *Geophysical Monograph*. American Geophysical Union.

Cowley, S. W. H., J. P. Morelli, M. P. Freeman, M. Lockwood, and M. F. Smith (1992, May). Excitation and decay of flows in the magnetosphere-ionosphere system due to magnetic reconnection at the dayside magnetopause and in the geomagnetic tail. In *Proceedings of the Internationla Conference on Substorms (ICS-1)*, Kiruna, Sweeden. ESA SP-335.

Crooker, N. (1992). Reverse Convection. *J. Geophys. Res. 97*(A12).

Dahlgren, H. (2010). *Multi-spetral analysis of fine scale aurora*. Ph. D. thesis, Alfvén Laboratory, KTH School of Electrical Engineering.

Davis, T. N. and M. Sugiura (1966). Auroral electrojet activity index ae and its universal time variations. *J. Geophys. Res. 71*, 785–.

Dungey, J. W. (1961). Interplanetary magnetic field and the auroral zones. *Phys. Rev. Lett. 6*(2), 47–48.

Dungey, J. W. (1963). *Geophysics, The Earth's Environment*, Chapter The structure of the exosphere or adventures in velocity space., pp. 503. Gordon and Breach Science Pub., New York.

Eriksson, S., R. E. Ergun, C. W. Carlson, and W. Peria (2000). The cross-polar potential drop and its correlation to the solar wind. *J. Geophys. Res. 105*(A8), 18639–18653.

ESA (1984). *Solar wind control of magnetospheric convection*. ESA.

Farrugia, C., L. Burlaga, V. Osherovich, I. Richardson, M. Freeman, R. Lepping, and A. Lazarus (1993). A Study of an Expanding Interplanetary Magnetic Cloud and Its Interaction with the Earth's Magnetosphere: The Interplanetary Aspect. *J. Geophys. Res. 98*(A5), 7621–7632.

Farrugia, C., M. Freeman, L. Burlaga, R. Lepping, and K. Takahashi (1993). The Earth's Magnetosphere Under Continued Forcing: Substorm Activity During the Passage of an Interplanetary Magnetic Cloud. *J. Geophys. Res. 98*(A5), 7657–7671.

Farrugia, C. J., L. Burlaga, and R. P. Lepping (1997). Magnetic Clouds and the Quiet/storm effect at Earth: A review. In B. T. Tsurutani, W. D. Gonzalez, Y. Kamide, and J. K. Arballo (Eds.), *Magnetic Storms*, Volume 98 of *Geophysical Monogr. Ser.*, pp. 91. AGU, Washington, D. C.

Farrugia, C. J., J. D. Scudder, M. P. Freeman, L. Janoo, G. Lu, J. M. Quinn, R. L. Arnoldy, R. B. Torbert, L. F. Burlaga, K. W. Ogilvie, R. P. Lepping, A. J. Lazarus, J. T. Steinberg, F. T. Gratton, and G. Rostoker (1998). Geoeffectiveness of three Wind magnetic clouds: A comparative study. *J. Geophys. Res. 103*(A8), 17261–17278.

Freeman, M., C. Farrugia, L. Burlaga, M. Hairston, M. Greenspan, J. Ruohoniemi, and R. Lepping (1993). The Interaction of a Magnetic Cloud with the Earth: Ionospheric Convection in the Northern and Southern Hemispheres for a Wide Range of Quasi-Steady Interplanetary Magnetic Field Conditions. *J. Geophys. Res. 98*(A5), 7633–7655.

Friis-Christensen, E., M. A. McHenry, C. R. Clauer, and S. Vennerstrm (1988). Ionospheric traveling convection vortices observed near the polar cleft: A triggered response to sudden changes in the solar wind. *Geophys. Res. Lett. 15*(3), 253256.

Gao, Y., M. G. Kivelson, R. J. Walker, and J. M. Weygand (2012). Long-term variation of driven and unloading effects on polar cap dynamics. *J. Geophys. Res. 117*(A2).

Gonzalez, W. D. and B. T. Tsurutani (1987). Criteria of interplanetary parameters causing intense magnetic storms (Dst¡100nT). *Planet. Space Sci. 35*, 1101.

Gosling, J., M. Thomsen, S. Bame, R. Elphic, and C. Russell (1990). Plasma Flow Reversals at the Dayside Magnetopause and the Origin of Asymmetric Polar Cap Convection. *J. Geophys. Res. 95*(A6).

Haerendel, G. (2011). Six auroral generators: A review. *J. Geophys. Res. 116*(A00K05).

Hairston, M. R., T. W. Hill, and R. A. Heelis (2003). Observed saturation of the ionospheric polar cap potential during the 31 March 2001 storm. *Geophys. Res. Lett. 30*(6).

Henderson, M. G., R. Skoug, E. Donovan, M. F. Thomsen, G. D. Reeves, M. H. Denton, H. J. Singer, R. L. McPherron, S. Mende, T. J. Immel, J. B. Sigwarth, and L. A. Frank (2006). Substorms during the 10-11 august 2000 sawtooth event. *J. Geophys. Res. 111*(A06206).

Huang, C.-S. (2012). Statistical analysis of dayside equatorial ionospheric electric fields and electrojet currents produced by magnetospheric substorms during sawtooth events. *J. Geophys. Res. 117*(A2).

Hughes, W. J. (1995). *Introduction to space physics*, Chapter The magnetopause, magnetotail and magnetic reconnection., pp. 227–287. Cambridge University Press.

Iijima, T. and T. A. Potemra (1976). The amplitude distribution of field-aligned currents at northern high latitudes observed by Triad. *J. Geophys. Res. 81*, 2165.

Kan, J. R. and L. C. Lee (1979). Energy coupling function and solar wind-magnetosphere dynamo. *Geophys. Res. Lett. 6(7)*, 577–580.

Kivelson, M. G. and A. J. Ridley (2008). Saturation of the polar cap potential: Inference from Alfvén wing arguments. *J. Geophys. Res. 113*(A05214).

Knight, S. (1973). Parallel electric fields. *lanet. Space Sci. 21*, 741.

Kullen, A., T. Karlsson, J. A. Cumnock, and T. Sundberg. (2010). Occurrence and properties of substorms associated with pseudobreakups. *J. Geophys. Res. 115*(A12310).

Le, G., J. A. Slavin, and R. J. Strangeway (2010). Space Technology 5 observations of the imbalance of regions 1 and 2 field-aligned currents and its implication to the cross-polar cap Pedersen currents. *J. Geophys. Res. 115*(A07202).

Lee, L. C. and J. G. Roederer (1982). Solar wind energy transfer through the magnetopause of an open magnetosphere. *J. Geophys. Res. 87*(A3), 1439.

Lepping, R. P., D. B. Berdichevsky, and C. C. Wu (2003). Sun-earth electrodynamics: The solar wind connection. *Recent Res. Devel. Astrophys. 1*, 139–171.

Lepping, R. P. and C.-C. Wu (2007). On the variation of interplanetary magnetic cloud type through solar cycle 23: Wind events. *J. Geophys. Res. 112*(A10103).

Lockwood, M., W. F. Denig, A. D. Farmer, V. N. Davda, S. W. H. Cowley, and H. Lhr (1993). Ionospheric signatures of pulsed reconnection at the Earth's magnetopause. *Nature 361*, 424–428.

Low, B. C. (2001). Coronal mass ejections, magnetic flux ropes, and solar magnetism. *J. Geophys. Res. 106*(A11), 25141–25163.

Lui, A. T. Y. (1991). A Synthesis of Magnetospheric Substorm Models. *J. Geophys. Res. 96*(A2), 1849–1856.

Lyons, R. L., Y. Nishimura, X. Xing, A. Runov, V. Angelopoulos, E. Donovan, and T. Kikuchi (2012). Coupling of dipolarization front flow bursts to substorm expansion phase phenomena within the magnetosphere. *J. Geophys. Res. 117*(A02212).

Marghitu, O., T. Karlsson, B. Klecker, G. Haerendel, , and J. McFadden (2009). Auroral arc and oval electrodynamics in the Harang region. *J. Geophys. Res. 114*(A03214).

McPherron, R. L., C. T. Russel, and M. P. Aubry (1973). Satellite studies of magnetospheric substorms on August 5, 1968, 9, Phenomenological model for substorms. *J. Geophys. Res. 78*, 3131.

Mühlbachler, S., C. J. Farrugia, J. Raeder, H. K. Biernat, and R. Torbert (2005). A statisitcal investigation of dayside magnetosphere erosion showing saturation of response. *J. Geophys. Res. 110*(A11207).

Nakamura, R., W. Baumjohann, A. Runov, M. Volwerk, T. L. Zhang, B. Klecker, Y. Bogdanova, A. Roux, A. Balogh, H. Reme, J. A. Sauvaud, and H. U. Frey (2002). Fast flow during current sheet thinning. *Geophys. Res. Lett. 29*(23).

Newell, P. T., Y. I. Feldstein, Y. Galperin, and C. I. Meng (1996). Morphology of nightside precipitation. *J. Geophys. Res. 101*(A01206), 10737–10748.

Papitashvili, V. O., F. Christiansen, and T. Neubert (2002). A new model of field aligned currents derived from high-precision satellite magnetic field data. *Geophys. Res. Lett. 29*(A2).

Pashmann, G. (1991). The earth's magnetopause. In Jacobs (Ed.), *Geomagnetism*, Volume 4.

Peng, Z., H. R. Lai, and Y. Q. Hu (2009). Transpolar potential and recconection voltage of the earth from global MHD simulations. *J. Geophys. Res. 114*(A04203).

Potemra, T. A. (1994). Sources of large-scale Birkeland currents. In *Physical Signatures of Magnetospheric Boundary Layer Processes*, Volume 425 of *NATO ASI Series C*, pp. 3–27. Dordrecht, Holland: Kluwer Academic Publishers.

Provan, G., M. Lester, S. B. Mende, and S. E. Milan (2004). Statistical study of high-latitude plasma flow during magnetospheric substorms. *Ann. Geophys. 22*, 3607–3624.

Reiff, P. H., R. Spiro, and T. Hill (1981). Dependence of Polar Cap Potential Drop on Interplanetary Parameters. *J. Geophys. Res. 86*(A9), 7639–7648.

Ruohoniemi, J. M. and R. A. Greenwald (2005). Dependencies of high-latitude plasma convection: Consideration of interplanetary magnetic field, seasonal, and universal time factors in statistical patterns. *J. Geophys. Res. 110*(A09204).

Russell, C., J. Luhmann, and G. Lu (2001). Nonlinear response of the polar ionosphere to large values of the interplanetary electric field. *J. Geophys. Res 106*(A9), 18,495–18,504.

Russell, C. T. and R. C. Elphic (1978). Initial ISEE magnetometer results: Magnetopause observations. *Space Sci. Rev.*.

Sanchez, E. R., G. L. Siscoe, and C.-I. Meng (1991). Inductive attenuation of the transpolar voltage. *Geophys. Res. Lett. 18*, 1173–1176.

Sandholt, P., M. Lockwood, T. Oguti, S. Cowley, K. Freeman, B. Lybekk, A. Egeland, and D. Willis (1990). Midday auroral breakup events and related energy and momentum transfer from the magnetosheath. *J. Geophys. Res. 95*(A2), 1039–1060.

Sandholt, P. E. and C. J. Farrugia (2009). Plasma flow channel at dawn/dusk polar cap boundaries: Momentum transfer on old open field lines and the roles of IMF By and conductivity gradients. *Ann. Geophys. 27*, 1527–1554.

Sandholt, P. E. and C. J. Farrugia (2012). Plasma flows, Birkeland currents and auroral forms in relation to the Svalgaard-Mansurov effect. *Ann. Geophys. 30*, 817–830.

Sandholt, P. E. and P. T. Newell (1992). Ground and satellite observations of an auroral event at the cusp/cleft equatorward boundary. *J. Geophys. Res. 97*, 8685–8691.

Sauvaud, J.-A., C. Jacquey, M. Oka, L. Palin, G. Fruit, L. M. Kistler, A. Balogh, J. B. Cao, G. Reeves, T. Mukai, I. Shinohara, and E. Grigorenko (2012). A study of the changes of the near-Earth plasma sheet and lobe driven by multiple substorms: Comparison with a full particle simulation of reconnection. *J. Geophys. Res. 117*(A1).

Sergeev, V. A., K. Liou, P. T. Newell, S.-I. Ohtani, M. R. Hairston, and F. Rich (2004). Auroral streamers: characteristics of associated precipitation,convection and field-aligned currents. *Ann. Geophys. 22*, 537 – 548.

Siscoe, G. and T. Huang (1985). Polar cap inflation and deflation. *J. Geophys. Res. 90*(A1), 543547. doi:10.1029/JA090iA01p00543.

Siscoe, G., W. Lotko, and B. Sonnerup (1991). A High-Latitude, Low-Latitude Boundary Layer Model of the Convection Current System. *J. Geophys. Res. 96*(A3), 3487–3495.

Siscoe, G. L., G. M. Erickson, B. Sonnerup, N. C. Maynard, J. A. Schoendorf, K. D. Siebert, D. R. Weimer, W. W. White, and G. R. Wilson (2002). Hill model of transpolar potential saturation: Comparisons with MHD simulations. *J. Geophys. Res. 107*(A6).

Siscoe, G. L., C. J. Farrugia, and P. E. Sandholt (2011). Comparison between the two basic modes of magnetospheric convection. *J. Geophys. Res. 116*(A05210).

Sonnerup, B. U. O. (1974). Magnetopause reconnection rate. *J. Geophys. Res. 79*, 1546.

Southwood, D. (1987). The ionospheric signature of flux transfer events. *J. Geophys. Res. 92*(A4), 3207–3213.

Taguchi, S., M. Sugiura, J. Winningham, and J. Slavin (1993). Characterization of the IMF - Dependent Field-Aligned Currents in the Cleft Region Based on DE 2 Observations. *J. Geophys. Res. 98*(A2), 13931407.

Tomita, S., M. Nos, T. Iyemori, H. Toh, M. Takeda, J. Matzka, G. Bjornsson, T. Saemundsson, A. Janzhura, O. Troshichev, and G. Schwarz (2011). Magnetic local time dependence of geomagnetic disturbances contributing to the AU and AL indices. *Ann. Geophys. 29*, 673–678.

Troshichev, O. A., R. Y. Lukianova, V. O. Papitashvili, F. J. Rich, and O. Rasmussen (2000). Polar cap index (PC) as a proxy for ionospheric electric field in the near-pole region. *Geophys. Res. Lett. 27*(23).

Vaivads, A., A. Retinò, and M. André (2006). Microphysics of magnetic reconnection. *Space Sci. Rev. 122*(19-2).

Vasyliunas, V. M., J. R. Kan, G. L. Siscoe, and S.-I. Akasofu (1982). Scaling relations governing magnetospheric energy transfer. *Planet. Space Sci. 30*, 359–365.

Vennerstroem, S. (2001). Interplanetary sources of magnetic storms: A statistical study. *J. Geophys. Res. 106*(A12), 29175–29184.

Watanabe, M., G. J. Sofko, D. A. André, T. Tanaka, and M. R. Hairston (2004). Polar cap bifurcation during steady-state northward interplanetary magnetic field with $|b_y| \sim b_z$. *J. Geophys. Res. 109*(A01215).

Watanabe, M., G. J. Sofko, D. A. Andr, J. M. Ruohoniemi, M. R. Hairston, and K. Kabin (2006). Ionospheric signatures of internal reconnection for northward interplanetary magnetic field: Observation of "reciprocal cells" and magnetosheath ion precipitation. *J. Geophys. Res. 111*(A06201).

Weimer, D. R. (1995). Models of high-latitude electric potentials derived with a least error fit of spherical harmonic coefficients. *J. Geophys. Res. 100*(A10), 19595–19607.

Yang, J., F. R. Toffoletto, R. A. Wolf, S. Sazykin, P. A. Ontiveros, and J. M. Weygand (2012). Large-scale current systems and ground magnetic disturbance during deep substorm injections. *J. Geophys. Res. 117*(A1).

Zmuda, A. J., J. H. Martin, and F. T. Heuring (1966). Transverse magnetic disturbances at 1100 km in the auroral region. *J. Geophys. Res. 71*, 5033.

Zou, S., M. B. Moldwin, L. R. Lyons, Y. Nishimura, M. Hirahara, T. Sakanoi, K. Asamura, M. J. Nicolls, Y. Miyashita, S. B. Mende, and C. J. Heinselman (2010). Identification of substorm onset location and preonset sequence using Reimei, THEMIS GBO, PFISR, and Geotail. *J. Geophys. Res. 115*(A12309).

Part II

Papers

I

Ann. Geophys., 28, 1023–1042, 2010
www.ann-geophys.net/28/1023/2010/
doi:10.5194/angeo-28-1023-2010

Annales Geophysicae

Polar cap convection/precipitation states during Earth passage of two ICMEs at solar minimum

P. E. Sandholt[1], **Y. Andalsvik**[1], **and C. J. Farrugia**[2]

[1]Department of Physics, University of Oslo, Oslo, Norway
[2]Space Science Center, University of New Hampshire, Durham, USA

Received: 30 September 2009 – Revised: 26 March 2010 – Accepted: 22 April 2010 – Published: 30 April 2010

Abstract. We report important new aspects of polar cap convection and precipitation (dawn-dusk and inter-hemisphere asymmetries) associated with the different levels of forcing of the magnetosphere by two interplanetary (IP) magnetic clouds on 20 November 2007 and 17 December 2008 during solar minimum. Focus is placed on two intervals of southward magnetic cloud field with large negative B_y components (B_x=−5 versus 0 nT) and with high and low plasma densities, respectively, as detected by spacecraft Wind. The convection/precipitation states are documented by DMSP spacecraft (Southern Hemisphere) and SuperDARN radars (Northern Hemisphere). The (negative) B_y component of the cloud field is accompanied by a newly-discovered flow channel (called here FC 2) threaded by old open field lines (in polar rain precipitation) at the dusk and dawn sides of the polar cap in the Northern and Southern Hemispheres, respectively, and a corresponding Svalgaard-Mansurov (S-M) effect in ground magnetic deflections. On 20 November 2007 the latter S-M effect in the Northern winter Hemisphere appears in the form of a sequence of six 5–10 min long magnetic deflection events in the 71–74° MLAT/14:30–16:00 MLT sector. The X-deflections are consistent with the flow direction in FC 2 (i.e. caused by Hall currents) in both IP cloud cases. The presence of a lobe cell and associated polar arcs in the Southern (summer) Hemisphere in the low density (1–2 cm^{-3}) and B_x=0 ICME case is accompanied by the dropout of polar rain precipitation in the dusk-side regime of sunward polar cap convection and inward-directed Birkeland current. The low-altitude observations are discussed in terms of momentum transfer via dynamo processes in the high- and low-latitude boundary layers and Birkeland currents located poleward of the traditional R1-R2 system.

Keywords. Ionosphere (Plasma convection) – Magnetospheric physics (Current systems; Polar cap phenomena)

Correspondence to: P. E. Sandholt
(p.e.sandholt@fys.uio.no)

1 Introduction

We present a study of certain aspects of the spatial and temporal structure of the reconnecting magnetosphere associated with dawn-dusk and inter-hemisphere asymmetries in polar cap convection and precipitation. This fine-structure in the convection/precipitation states is considered to be essential for an adequate understanding of solar wind-magnetosphere coupling. It includes the temporal evolution of plasma convection, involving stages of newly-open (LLBL/cusp precipitations) and old-open (mantle/polar rain precipitations) magnetic field lines, as well as spatial convection structure, i.e., the issue of cell structure (merging and lobe cells) in the Northern and Southern Hemispheres. A third, related aspect is the question of inter-hemisphere symmetry/asymmetry in polar cap precipitation including polar rain and polar cap arcs. It is our opinion that an approach through case studies is the most appropriate one for resolving these convection/precipitation features.

In recent investigations we argued that it is reasonable to distinguish between different types of plasma flow channels corresponding to two different stages of the evolution of field lines opened by dayside reconnection; i.e., newly open and old open field lines, respectively (Farrugia et al., 2003; Sandholt et al., 2004; Farrugia et al., 2004; Lund et al., 2008; Sandholt and Farrugia, 2009). Each of the two stages drives a characteristic flow channel, called hereunder FC 1 and FC 2. Our effort has been to establish the importance of FC 2 as a signature of efficient momentum transfer on old open field lines and its different source compared to FC 1, namely, through its coupling to the solar wind dynamo in the high-latitude boundary layer (HBL). We demonstrated that flow channel FC 2, which typically consists of a 200–300 km wide band of enhanced (1–3 km/s) antisunward convection situated at the dusk- or dawn-side polar cap boundary, enhances and extends the IMF B_y-related dawn-dusk asymmetry of polar cap convection. In Sandholt and Farrugia (2009) we distinguished between four categories of the flow channel

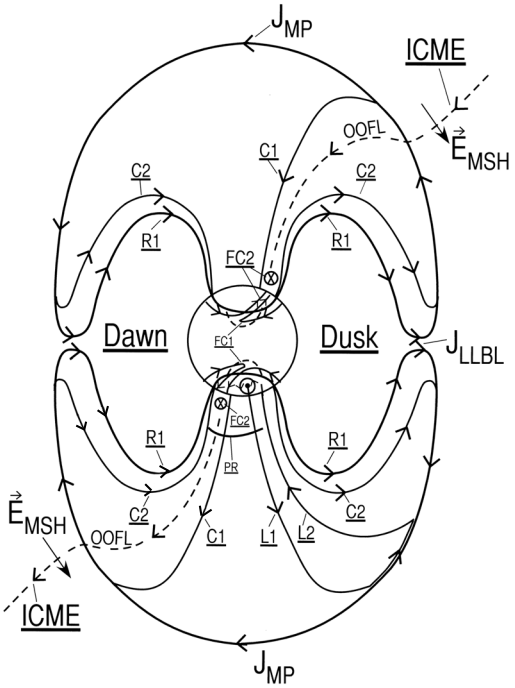

Fig. 1. A schematic illustration of the ICME-magnetosphere interconnection topology for $B_y < 0$ conditions and Birkeland currents current systems in the Northern (NH) and Southern (SH) Hemispheres relating to flow channels FC 2 ($\boldsymbol{E} \times \boldsymbol{B}$ - drift) in the north (NH-dusk/$B_y < 0$) and south (SH-dawn/$B_y < 0$). The perspective is looking from the Sun towards the Earth. (North is up and Dusk is to the right). The poleward and equatorward branches of the R1 Birkeland current, connected to the outer and inner edges of the low-latitude boundary layer (LLBL), are marked C2 and R1, respectively. These Birkeland currents are connected to the magnetopause current (J_{MP}) at high latitudes via J_{LLBL} in the LLBL and to the Pedersen current (J_P) at the ionospheric level. The C1 Birkeland current is threaded by old open field lines (OOFL) and polar rain (PR) precipitation. Plasma flows in dawn-dusk asymmetric convection cells applicable to our cases are indicated: 2-cell pattern in north and 3-cells in the south. The lobe cell in the Southern Hemisphere (marked by circle) is favoured by the summer dipole tilt. The associated Birkeland currents are marked L1–L2. Current L1 is associated with polar arcs while current L2 is accompanied by a dropout of polar rain precipitation. The $\boldsymbol{E}$-field/momentum coupling from the magnetosheath ($\boldsymbol{E}_{MSH}$) to the ionosphere (FC 2) along old open field lines is indicated. Flow channels FC 1 on newly open field lines (Cusp/LLBL precipitation) are also marked.

FC 2 depending on the relevant combinations of IMF B_y polarity, hemisphere (N/S), and dawn/dusk side of the polar cap. In this study we explore the FC 2 variants in both hemispheres under IMF $B_y < 0$ conditions (NH-dusk/$B_y < 0$ and SH-dawn/$B_y < 0$) further and place them in the context of polar cap convection/precipitaton states as detected by DMSP spacecraft and SuperDARN radars.

In previous studies we have repeatedly pointed out that flow channel FC 2 may give rise to a component of the Svalgaard-Mansurov effect Svalgaard (1973) that comes in addition to (spatial extension in the antisunward direction) the ground magnetic deflection which is attributed to the effect of magnetic tension on newly open magnetic field lines. In our terminology the latter is the FC 1 – related ground deflection in the cusp/cleft region. In this study we report a detailed documentation of the ground magnetic deflection (Svalgaard-Mansurov effect) associated with channel FC 2 appearing in the NH-dusk/$B_y < 0$ variant during the Earth passage of the 20 November 2007 interplanetary (IP) magnetic cloud (MC). The temporal behaviour of flow channel FC 2 may be derived from the associated ground magnetic deflections.

The spatial structure we study involves the interhemisphere asymmetry of lobe cell convection (Crooker and Rich, 1993), associated polar arcs (Eriksson et al., 2003) and dropout of polar rain precipitation at dusk in the Southern Hemisphere (adjacent to the polar arcs) under the prevailing external magnetic field (southwest: $B_z < 0$; $B_y < 0$; $B_x = 0$) and the low ($< 1\,\mathrm{cm}^{-3}$) plasma density conditions in one MC.

We selected two intervals of B_y-negative forcing by IP magnetic clouds (Burlaga et al., 1981) passing Earth during the minimum phase of solar cycle 24. These two cloud intervals correspond to high ($10–20\,\mathrm{cm}^{-3}$) and low ($1–2\,\mathrm{cm}^{-3}$) plasma densities, respectively. The levels of solar wind forcing and IMF B_x conditions (zero versus -5 nT) were also different. This allows us to explore the influence of solar wind forcing, plasma density and IMF B_x on the polar cap convection and precipitation states. The abrupt polar rain dropout mentioned above is different from the "normal" IMF B_y dependent dawn-dusk asymmetry (smooth gradient) of polar rain precipitation (Meng et al., 1977). The different flow speeds corresponding to the FC 2 flow channels in the two cloud cases are tentatively attributed to the different levels of forcing as estimated by the Boyle et al. (1997) formula for the cross-polar cap potential (CPCP).

This paper is organised as follows. First we describe the model of solar wind-magnetosphere-ionosphere coupling which provides a conceptual framework for interpreting the observations. In the data description section we report the observations in the two case examples. This is followed by a summary of the observations and their discussion in terms of the conceptual model of ICME-magnetosphere-ionosphere coupling.

2 Model description

Figure 1 shows a schematic illustration of our conceptual model of solar wind-magnetosphere-ionosphere coupling

applicable to the conditions of the southwest-directed magnetic fields in the two ICMEs that we present in this study. The model consists of the following elements:

1. The R1 Birkeland current is split into two branches (R1 and C2) corresponding to two branches of ionospheric Pedersen current closure, the auroral zone branch and the polar cap branch (not shown). R1 is connected to field-transverse current (J_{LLBL}) at the LLBL inner edge (closed bloundary layer) while C2 is connected to the LLBL outer (open boundary layer) part (J_{LLBL}). For a discussion of this type of IMF-magnetosphere interconnection topology, LLBL substructure (and flow shear) and associated Birkeland current excitation we refer to the MHD simulations of Siscoe and Siebert (2003) (see their Fig. 3) and the boundary layer theory of Sonnerup and Siebert (2003).

2. Flow channel FC 2, threaded by "old open field lines" (OOFL) and polar rain precipitation (Fairfield and Scudder, 1985; Sotirelis et al., 1997), is observed on the opposite sides (dawn/dusk) in the two hemispheres for the prevailing negative polarity of the magnetic field B_{y} component in the ICME (NH-dusk/$B_{\mathrm{y}} < 0$ and SH-dawn/$B_{\mathrm{y}} < 0$). Areas of "newly open field lines" and flow channel FC 1 in the cusp region are also marked (inside dashed curved line). The latter indicates the projected dayside merging (reconnection) line.

3. As we shall document in this paper momentum transfer via the C1–C2 currents give rise to flow channel FC 2 (see also Sandholt and Farrugia, 2009) and its associated Hall currents gives the antisunward extension of the Svalgaard-Mansurov effect beyond the cusp/cleft region. The latter effect comes in addition to the flow-asymmetry which is due to magnetic tension on newly open field lines.

4. A lobe cell with polar arcs in its center is present in the hemisphere (south) where dipole tilt (summer) is favourable for lobe reconnection (Crooker and Rich, 1993).

5. The Birkeland currents marked L1–L2 are those which are associated with lobe cell convection (Eriksson et al., 2002).

6. The outward-directed Birkeland current (L1) in the center of the lobe cell is accompanied by flow shear arcs (Reiff et al., 1978). These polar cap arcs are accelerated polar rain precipitation in the region of a converging electric field (see Carlson and Cowley, 2005; Sandholt et al., 2006).

7. The inward-directed Birkeland current (L2) in the dusk-side part of the lobe cell is located equatorward of the regime of sunward convection. As we shall see below this region is characterized by the dropout of polar rain precipitation. The presence of polar rain (PR) in the dawn side of the polar cap in the Southern Hemisphere is marked in the figure. As mentioned earlier, the polar rain dropout discussed here in connection with a proposed downward/inward FAC is different from the normal dawn-dusk polar rain asymmetry (smooth gradient) and its IMF B_{y}-dependence (Newell et al., 2009).

The ICME-magnetosphere interconnection topology indicated in Fig. 1 implies that flow channel FC 2 is part of the low-altitude mapping of the Stern gap (Stern, 1984). FC 2 appears as a result of effective $\boldsymbol{E}$-field/momentum coupling from the magnetosheath ($\boldsymbol{E}_{\mathrm{MSH}}$) along old-open field lines. As we shall see in the cases reported below an interhemispheric asymmetry in FC 2 excitation seems to be related to the background conductivity (sunlight conditions). There are also indications that the degree of solar wind forcing is a factor for the strength of the FC 2 flow. As regards the conductivity effect we find that our result is consistent with previous studies of solar wind-magnetosphere coupling indicating that the solar wind acts like a current-limited voltage generator (see e.g. Borovsky et al., 2009).

3 Data description

3.1 Case 1: 17 December 2008

Figure 2 shows Wind plasma and magnetic field data from the SWE (Ogilvie et al., 1995) and the MFI (Lepping et al., 1995) instruments, respectively. Wind was located at (254, −28, 24) R_{E} at the center of the interval of interest (10:00 UT, 17 December). From top to bottom the panels show the proton plasma density, bulk speed, and temperature, the dynamic pressure, the magnetic field strength and the magnetic field components in GSM coordinates, the proton plasma beta and, in red, the Alfvén Mach number, and the IMF clock angle, i.e., the polar angle in the GSM (YZ) plane. The bottom panel shows the cross polar cap potential (CPCP) after Boyle et al. (1997). The latter is used as an expression for the level of solar wind forcing.

The period of low density (average $\sim$1.9 $\pm$1.0 cm^{-3}), and correspondingly low dynamic pressure (average 0.36$\pm$0.18 nPa) during the time interval 03.30–13.40 UT stands out. During this time the field executes a large and smooth rotation. This was identified by Davis et al. (2009) as the "void" region of an ICME corresponding to the dark cavity of the CME. It is a slow moving configuration, where a wide range of clock angles are realized and, with its strongly westward - pointing field ($B_{\mathrm{y}} < 0$), there is a an interval of several hours where the field's clock angle stays close to 90°.

We shall confine our analysis of magneto-spheric/ionospheric data to the interval 11:00–15:00 UT,

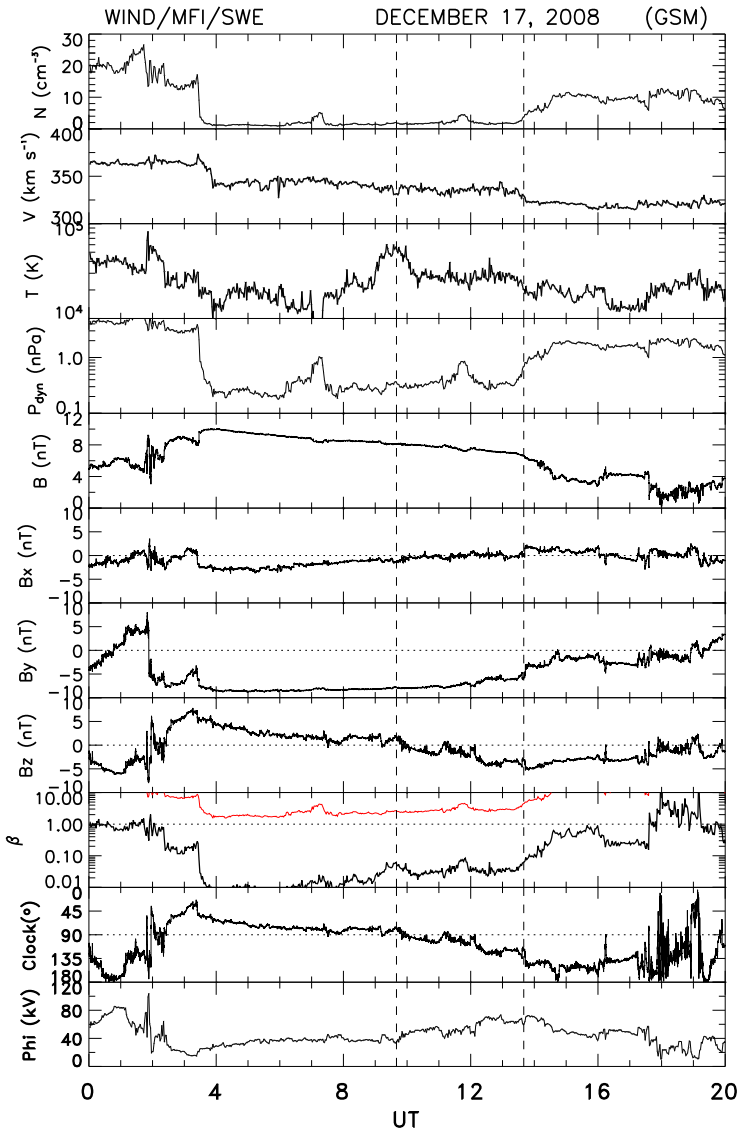

Fig. 2. Wind plot for the interval 00:00–20:00 UT, 17 December 2008. From top to bottom the panels show the proton plasma density, bulk speed, and temperature, the dynamic pressure, the magnetic field strength and the magnetic field components in GSM coordinates, the proton plasma beta and, in red, the Alfvén mach number, and the IMF clock angle, i.e., the polar angle in the GSM (YZ) plane. The interval corresponding to the low-altitude observations discussed in this paper is marked by vertical guidelines.

placed at the rear end of the ICME. With an estimate convection delay of ∼80 min, this corresponds to interplanetary conditions shown between the vertical guidelines. In this interval the ICME field goes from being B_y-dominated (clock angle=90°) to more B_z-dominated (clock angle=140°). The density is 2 cm^{-3} except for the rise at the end of the interval (13:30–14:30 UT).

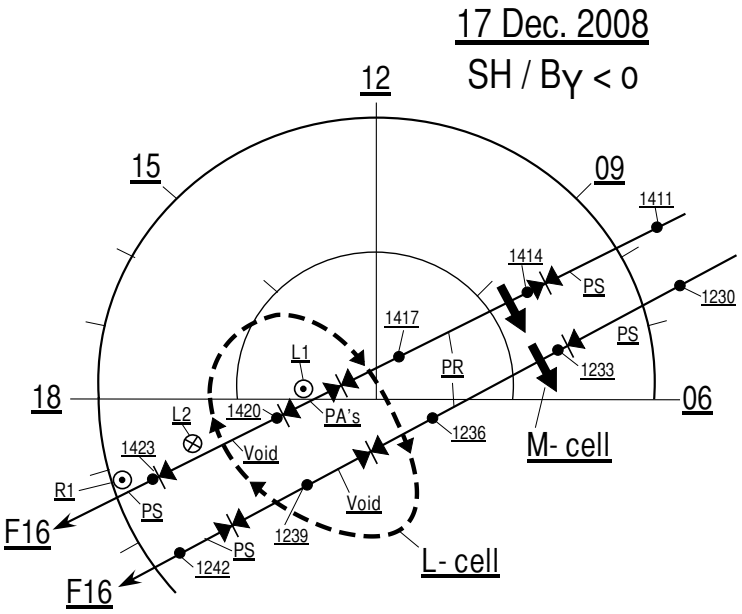

Fig. 3. Tracks of spacecraft DMSP F16 during the intervals 12:30–12:42 and 14:11–14:23 UT plotted in MLT/MLAT coordinates. Precipitation (PS; PR; PAs; void) and Birkeland current (L1; L2; R1) regimes along the tracks are indicated. Cross-track ion drifts in the merging (antisunward; dawn side) and lobe (sunward; dusk side) convection cells are also marked. A lobe cell circulation which is consistent with the satellite observations has been schematically indicated by the dashed loop.

Figure 3 shows tracks of spacecraft DMSP F16 during the intervals 12:30–12:42 and 14:11–14:23 UT. Precipitation regimes such as PS (plasma sheet), PR (polar rain), PAs (polar arcs), void and Birkeland current regimes (L1; L2; R1) along the tracks are indicated. Cross - track ion drifts in the merging (antisunward; dawn side) and lobe (sunward; dusk side) cells are also marked. A lobe cell circulation which is consistent with the satellite observations has been schematically indicated by the dashed loop. Thus the present convection configuration is the composite pattern consisting of merging and convection cells which has been predicted and simulated during intervals of B_y-dominated IMF orientations (Reiff and Burch, 1985; Crooker et al., 1998). The associated polar arcs in the lobe cell during intervals of similar IMF conditions has been documented in previous studies (Eriksson et al., 2003; Sandholt et al., 2006). For information on the L1–L2 Birkeland currents we refer to Eriksson et al. (2002).

Flow shear (gradient in cross-track ion drift) is observed in sector of polar arcs (PAs). This means that the PAs are so-called flow shear arcs (Reiff et al., 1978). Polar arcs are located where the flow shear is largest in the lobe cell. Sunward flow in the polar cap is defined as lobe cell convection. This convection feature is driven by lobe reconnection (Crooker and Rich, 1993). The "void" region marks the dropout of polar rain precipitation in the lobe cell on the dusk side of the polar arcs. This abrupt dropout is an effect which is different from the smooth dawn-dusk gradient of polar rain associated with IMF B_y. The corresponding data are shown below.

Figure 4 shows DMSP F16 data during a polar cap crossing from the dawn (07:00 MLT; −77° MLAT) to the evening (21:00 MLT; −73° MLAT) side in the Southern Hemisphere. Different convection/precipitation states are marked by vertical guidelines. We note the following features of electron precipitation (top panel) and cross-track ion drift (fourth panel):
(i) antisunward convection and polar rain (PR) precipitation on the dawn side (left) of the central polar cap, (ii) sunward convection and dropout of polar rain precipitation on the evening side of the polar cap (between the second and third vertical guidelines).

Figure 5 shows DMSP F16 data during a subsequent crossing of the polar cap from the morning (8.3 MLT; −77.2° MLAT; 14:14 UT) to the evening (19.3 MLT; −73.1° MLAT) side. We shall focus attention on the following features:
(i) polar rain (PR) precipitation and antisunward convection on the morning side of the polar cap, (ii) traversal of a regime

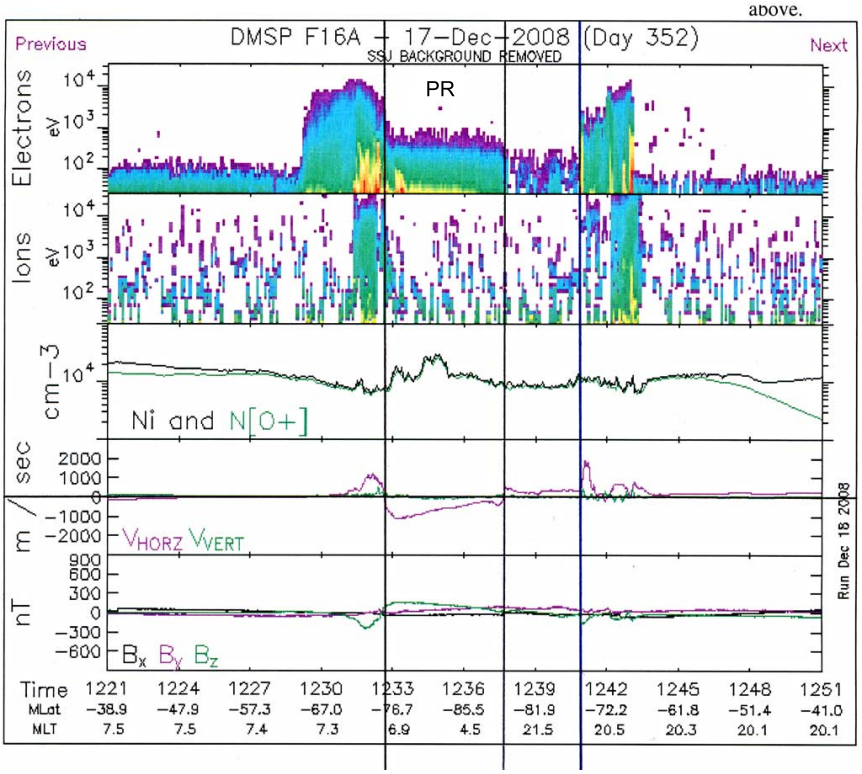

Fig. 4. DMSP F16 Southern Hemisphere data for the interval 12:21–12:51 UT on 17 December 2008. Panels from top to bottom show electron precipitation flux, ion precipitation flux, ion densities, cross track ion drifts, and magnetic deflection components B_x, B_y, and B_z. Polar rain (PR), polar arcs (PA) and dropout of polar rain on the dusk side of the arcs have been marked. Different convection/precipitation states are marked by vertical guidelines. Dropout of polar rain in the regime of sunward convection is marked by the second and third vertical guidelines.

of higher energy electrons (polar arc; PA) on the dusk side of the polar cap, (iii) dropout of polar rain precipitation in the regime of sunward convection in the evening sector of the polar cap (between the fourth and the fifth vertical guidelines).

Figure 6 shows tracks of spacecraft DMSP F13 and F17 across the polar cap from dawn to dusk in the Southern Hemisphere (SH) during the interval 13:20–13:30 UT. These F13 and F17 passes occurred between the two previously described F16 passes (Figs. 3–5). Particle precipitation and Birkeland current regimes along the tracks are marked. Flow channel FC 2 (SH-dawn/$B_y < 0$), as detected by spacecraft DMSP F17, is indicated by the hatched arrow. This flow channel appears slightly weaker in the F13 data in Fig. 8 (peak velocity 1.2 km/s versus 1.5 km/s).

The sector called "void" marks the dropout of polar rain in the regime of sunward convection (lobe cell) on the dusk side of the polar arcs (PAs) in the F13 data. The Birkeland current regimes L1 (outward in PA regime) and L2 (inward in "void" regime) are those which are also marked in Fig. 1. The corresponding data sets are shown below.

Figure 7 shows DMSP F13 data during a crossing of the polar cap in the Southern Hemisphere from the dawn (7.5 MLT; $\sim -78.3°$ MLAT) to the dusk (17.4 MLT; 80.4° MLAT) side during the interval 13:21–13:28 UT. We note the following features:
(i) dawn-dusk asymmetric antisunward convection (fourth panel) and polar rain (PR) electron precipitation (top panel) in the central polar cap, (ii) the presence of polar arcs (PAs) on the dusk side of the polar cap at high latitudes ($\sim$82–85° MLAT), (iii) sunward convection and dropout of polar rain precipitation between the polar cap arcs and auroral oval (between the second and third guidelines) on the dusk side.

Figure 8 shows DMSP F17 data for a dawn-dusk polar cap crossing in the Southern Hemisphere during the interval

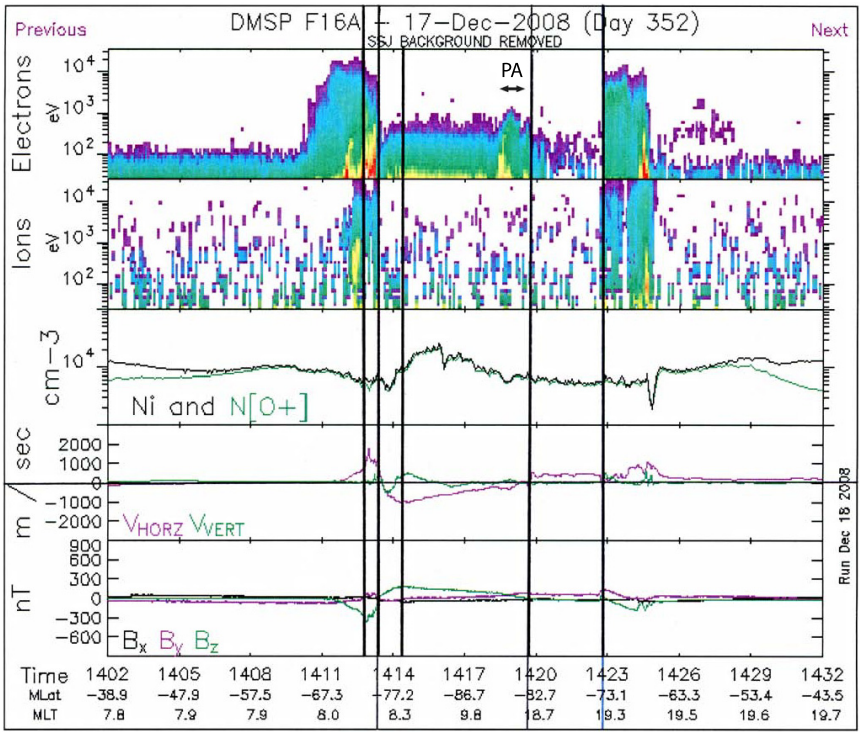

Fig. 5. DMSP F16 data representing the interval 14:02–14:32 UT on 17 December 2008. Particle precipitation, ion drift, and magnetic deflections obtained by spacecraft DMSP F 13 during a Southern Hemisphere pass during 13:10–13:40 UT on 17 December 2008. Same format as in Fig. 4.

13:10–13:40 UT. We note that this is identical to the F13 interval shown in Fig. 7. We shall focus on the interval 13:21–13:28 UT when the spacecraft crossed into the polar cap on the dawn side (∼07:00 MLT; 78° MLAT) and exited the polar cap on the dusk side (∼16:00 MLT; 80° MLAT). We notice the following features: (i) asymmetric cross-track (antisunward) ion drift with continuously decreasing speeds in the central polar cap (polar rain/PR precipitation) from the dawn to the dusk side. (ii) The dusk side of the polar cap (between vertical guidelines) is characterized by a large flow shear centered on the convection reversal and associated inverted-V type electron precipitation (polar arcs; PAs). (iii) A channel of enhanced (1.5 km/s) antisunward convection near the auroral precipitation boundary on the dawn (left) side of the polar cap. This is our flow channel FC 2. There are slightly different FC 2 signatures in the DMSP observations obtained in the close passes made by DMSP F13 (Fig. 7: 77° MLAT/7.3 MLT) and F17 (Fig. 8: 78° MLAT/7.0 MLT) at 13:21 UT. The FC 2 signature is marginally stronger in the F17 data (maximum speed 1.5 km/s) compared to the F13 data (maximum speed 1.2 km/s). This is an indication of spatial structure in the FC 2 flow channel.

Figure 9 shows a spatial plot of plasma convection in the postnoon sector for the scan at 11:12–11:14 UT on 17 December 2008 obtained by SuperDARN radars in Finland and Iceland (http://superdarn.jhuapl.edu) (Greenwald et al., 1995; Ruohoniemi and Greenwald, 2005). Dawn is to the right. We notice the presence of a rotational convection reversal in the postnoon sector with a channel of enhanced (yellow) antisunward flow on its poleward side. The latter, which we identify as our flow channel FC 2 (category NH-dusk/$B_y < 0$), is centered at 80° MLAT/15:00–18:00 MLT. We emphasize that these data are from the Northern Hemisphere and that the FC 2 flow channel is observed in a sector of dark ionosphere. Thus, the level of background ionization is low in this winter case.

Figure 10 shows the convection configuration in the postnoon/dusk sector obtained by SuperDARN radars at 14:00–14:02 UT. Dashed line marks the position of the discrete aurora, as observed by meridian scanning photometer (MSP)

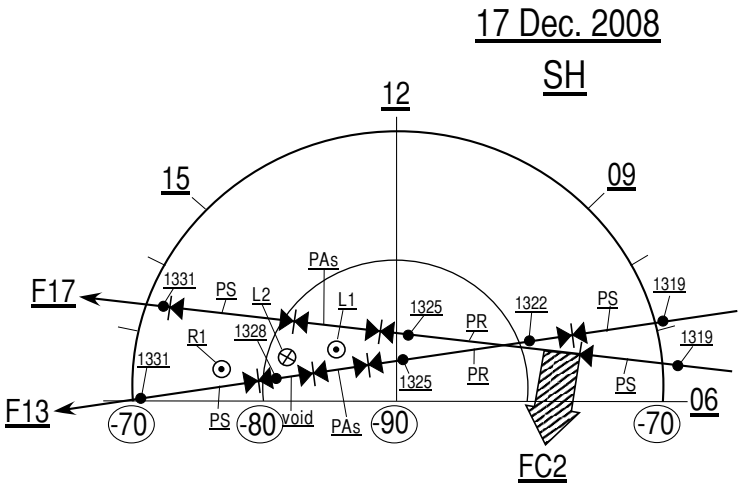

Fig. 6. Tracks of spacecraft DMSP F13 and F17 across the polar cap from dawn to dusk in the Southern Hemisphere (SH) during the interval 13:20–13:30 UT shown in MLT/MLAT coordinates. Regimes of particle precipitation (PS; PR; PAs; void), and Birkeland currents (R1; L1; L2) along the tracks are indicated. Flow channel FC 2 on the dawn side (07:00 MLT; 78° MLAT) as detected by S/C F17 is marked by hatched arrow. The sector called "void" marks the dropout of polar rain in the regime of sunward convection (lobe cell) on the dusk side of the polar arcs (PAs) in the F13 data.

in Longyearbyen, Svalbard (75° MLAT). The MSP field of view is indicated by the double-arrowed meridional line. Ground station Hornsund (HOR; 74° MLAT) is marked by dotted circle. The location of the flow channel FC 2 (NH-dusk/$B_y < 0$) on the poleward side of the discrete oval aurora is marked by the hatched arrow.

Figure 11 shows SuperDARN observations of ion drift vectors and plasma flow lines for 14:10–14:12 UT. We notice the presence of flow channels FC 1 (noonward convection in early postnoon sector) and FC 2 (antisunward convection at dusk) in the dusk-side merging convection cell. We shall focus on the convection channel FC 2 at dusk (NH-dusk/$B_y < 0$), located in the Svalbard sector. This allows us to study the association between the FC 2 flow channel activity and ground magnetic deflections. The ground magnetic deflection observed in association with the convection event at 13:55–14:10 UT, recorded at station Hornsund (HOR) on Svalbard (see Fig. 10), is shown in the next figure.

Figure 12 shows the X-component magnetic deflection recorded from station HOR (74° MLAT) on Svalbard during the interval 10:00–15:00 UT. A clear negative X-deflection appears after 13:55 UT when flow channel FC 2 had moved into a favourable position with respect to ground station HOR (Fig. 10) associated with an expansion of the polar cap during the interval 13:00–14:00 UT. The latter expansion is inferred from the auroral observations (not shown). This behaviour is consistent with the southward rotation of the IP cloud field during the interval 11:00–13:40 UT, as recorded by spacecraft Wind (see B_z panel in Fig. 2).

3.2 Case 2: 20 November 2007

We now discuss the second event, on 20 November 2007. Figure 13 now shows Wind SWE and MFI data for the 30 h interval, 14:00 UT, 19 November–20:00 UT, 20 November 2007. The format is the same as that of Fig. 2. Wind was situated at (236, 86, 16) R_E at 04:00 UT, 20 November and the convection delay is ∼1 h. The observations during the interval bear a similarity to those of 17 December 2008. A magnetic cloud is seen between ∼00:30–11:30 UT, 20 November. However, in this instance this transient is followed by a stream interaction region (Tsurutani et al., 2006) forming the leading edge of a faster stream. The interplanetary configuration is thus that of an ICME interacting with a faster stream. A shock driven by the MC is seen by Wind at ∼17:15 UT, 19 November.

A major difference with that of 17 December 2008 is the higher density and dynamic pressure. Here, during 00:00 UT–09:00 UT, 20 November, their values are (average + standard deviation): 8.89±4.55 cm^{-3} and 3.25±1.59 nPa, respectively. The magnetic field strength is also higher. Like 17 December 2008 the major component is the unipolar (westward) component. Again, an interval of clock angle ≈90° is evident (between 04:00–09:00 UT, 20 November). The qualitiative similarities between the two events are overall very marked. But the quantitative differences are important in the ionospheric response as we shall see presently.

As in the previous case our analysis of magnetospheric/ionospheric data is restricted to an interval

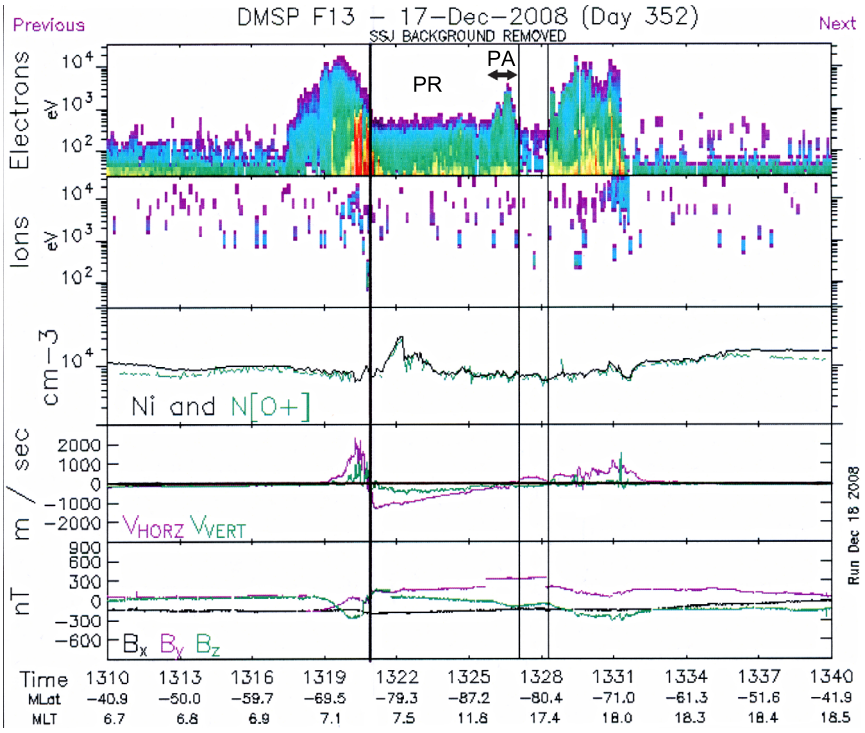

Fig. 7. Particle precipitation, ion drift, and magnetic deflections obtained by spacecraft DMSP F 13 during a Southern Hemisphere pass during 13:10–13:40 UT on 17 December 2008. Panels from top to bottom show electron precipitation flux, ion precipitation flux, ion densities, cross track ion drifts, and magnetic deflection components B_x, B_y, and B_z. Polar rain (PR), polar arcs (PA) and dropout of polar rain on the dusk side of the arcs have been marked.

(11:00–13:00 UT) placed at the rear end of the ICME (approx. 10:00–12:00 UT in the Wind plot). In the latter interval, delimited by the vertical guidelines in Fig. 13, B_y is strongly negative (B_y=−16 nT). Contrary to case 1 ($B_x = 0$) B_x is −5 nT in this case. The density is high (10–40 cm^{-3}). This is the trailing edge of the ICME, i.e., the interplanetary correspondence to the high-density core of the 3-part structure of CMEs (Illing and Hundhausen, 1985, 1986; Low, 2001).

Figure 14 shows DMSP F13 data obtained during a crossing of the polar cap from dawn (6.8 MLT; −78.3° MLAT) to evening (19.5 MLT; −70.7° MLAT) in the Southern Hemisphere. We shall focus on the following features occurring in the interval 11:29–11:39 UT:
(i) dawn-dusk asymmetric ($B_y < 0$ type) polar cap convection (panel four) and polar rain precipitation (top panel) in the central polar cap (between the third and fourth vertical guidelines). (ii) enhanced (3 km/s) antisunward convection (flow channel FC 2) on the dawn-side polar cap boundary (6.8 MLT; −78 to −80° MLAT; 11:30 UT).

Figure 15 shows DMSP F17 data obtained during a dawn to dusk crossing of the polar cap in the Southern Hemisphere. We shall focus on the following features of the observations in the interval 11:55–12:05 UT when the F17 spacecraft made a dawn-to-dusk traversal of the polar cap from (6.3 MLT; −76° MLAT) to (17.5 MLT; −73.7° MLAT):
(i) dawn-dusk asymmetric polar cap convection ($B_y < 0$ type; panel four) and polar rain electron precipitation (top panel) in the polar cap, (ii) enhanced (2.5 km/s) antisunward convection (flow channel FC 2) on the dawn side polar cap boundary.

Figure 16 shows the track of satellite DMSP F17 during the interval 11:56–12:05 UT. Flow channel FC 2 at dawn is marked. We note that the F13 satellite (data in Fig. 14) crossed the same dawn-side MLT sector 25 min earlier (11:30 UT). Similar FC 2 convection profiles (maximizing at 3 and 2.5 km/s) were identified in the two cases centered at 78° MLAT/5.8 MLT (F13 at 11:30 UT) and at 77° MLAT/6.3 MLT (F17 at 11:56 UT), respectively.

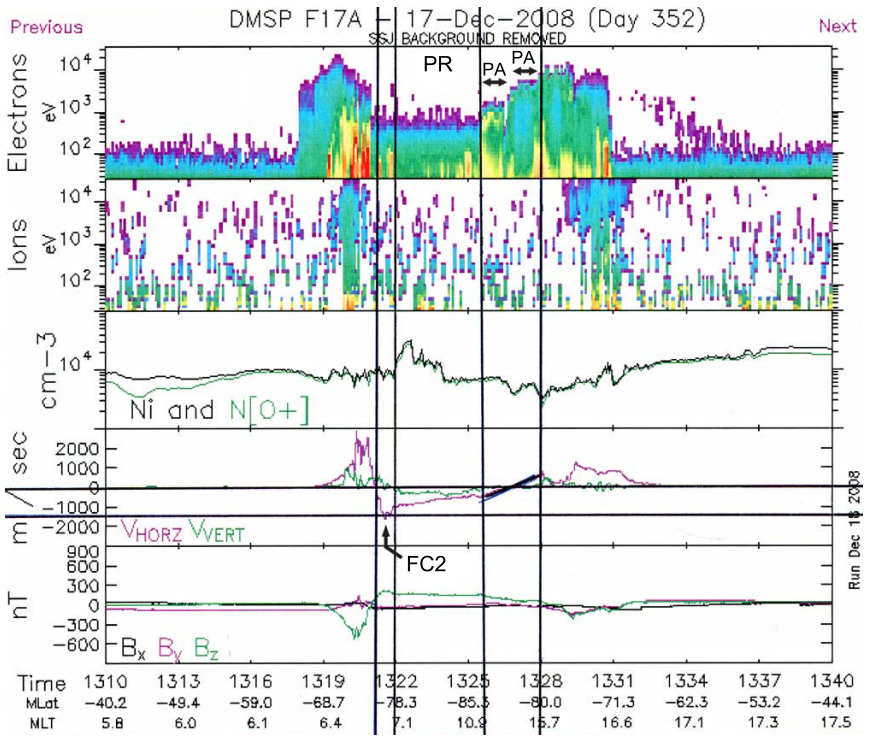

Fig. 8. DMSP F17 Southern Hemisphere data for the interval 13:10–13:40 UT on 17 December 2008. Same format as in Fig. 7. Flow channel FC 2 of category SH-dawn/$B_y < 0$ is marked. Polar arcs (PA) are located in region of flow shear (ion drift gradient) marked between the third and the fourth guidelines.

Figure 17 shows a SuperDARN spatial plot in MLT/MLAT coordinates for 11:52–11:54 UT illustrating the presence of flow channel (enhanced antisunward convection) centered at 15:00 MLT/72–73° MLAT, i.e., near the southern tip of the arctic island Svalbard. This is identified as FC 2 of category NH-dusk/$B_y < 0$. FC 2 is seen in the vicinity of the Svalbard ground station Hornsund (HOR) located at 73° MLAT, whose approximate location is indicated in the figure. In the next figure we shall report ground magnetometer readings from stations on Svalbard including HOR.

Figure 18 shows X-component deflections during the interval 10:30–13:00 UT detected at the Svalbard IMAGE stations (http://www.geo.fmi.fi/image) Ny Ålesund (NAL; 75° MLAT), Hornsund (HOR; 74° MLAT), and Bear Island (BJN; 71° MLAT). A series of six major deflection events are identified during the interval 11:00–12:40 UT when the stations swept through the ∼14:30–16:10 MLT sector. Arrows in the HOR-BJN panels mark deflection maxima at these stations (71–74° MLAT) centered at 11:05, 11:18, 11:42, 11:52, 12:12, and 12:32 UT. The event at 11:52 UT corresponds to the time of the SuperDARN convection plot shown in Fig. 17. We notice that the event duration time is 5–10 min. The deflections are weaker on the northernmost station (NAL) suggesting that this location was farther away from the center of the convection channel.

4 Summary and discussion

We reported observations of aspects of polar cap precipitation and convection states in both hemispheres during two selected intervals of the Earth passage of two ICMEs which were accompanied by different levels of external forcing of the magnetosphere. The observations in the Northern and Southern Hemispheres were obtained by SuperDARN radars (north) and DMSP spacecraft (south), respectively. The application of SuperDARN plasma convection data in the Svalbard sector allowed us to study the ground magnetic effect associated with flow channel FC 2 (NH-dusk/$B_y < 0$) located on the dusk (NH) side of the polar cap during the prevailing $B_y < 0$ conditions in the two IP clouds.

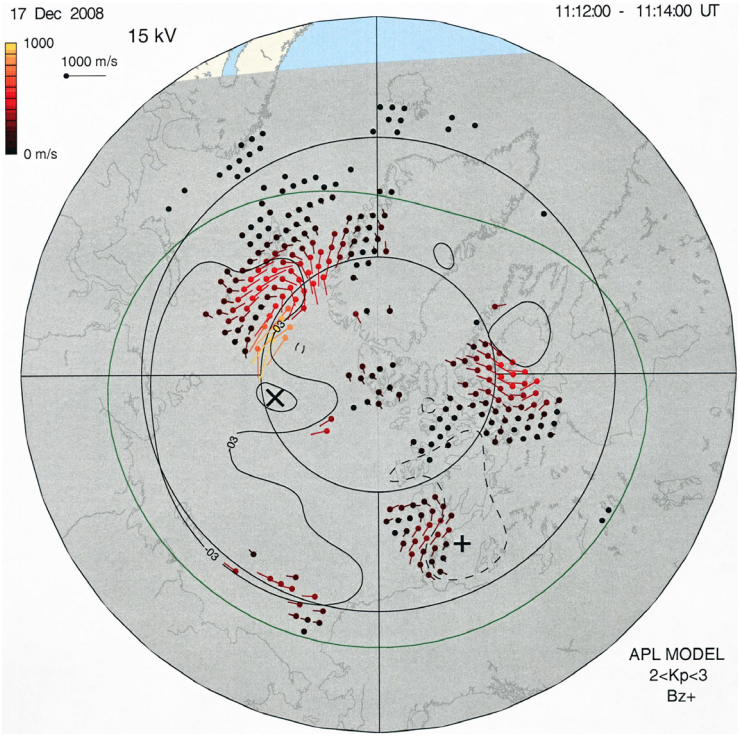

Fig. 9. SuperDARN spatial convection plot for 11:12–11:14 UT, 17 December 2008 representing flow channel FC 2 of type NH-dusk/$B_y < 0$. The coordinate system is MLAT/MLT. The Sun is at the top and dusk is to the left.

The observations may be summarized as follows:

1. We document the presence of flow channel FC 2 in both these solar minimum ICME cases. The effect (NH-dusk/$B_y < 0$ and SH-dawn/$B_y < 0$) is most pronounced in our case 2 which is characterized by strong solar wind forcing ($CPCP_{Boyle}$=120–180 kV).

2. In case 1, under moderate solar wind forcing ($CPCP_{Boyle}$=80 kV), we observe a weak or absent FC 2 flow channel in the Southern Hemisphere. FC 2 in the north is clearly present around 14:00 UT (when B_z in the IP cloud had decreased to −4 nT), as demonstrated in Fig. 11. The different FC 2 responses in the two IP cloud cases (and within one cloud interval) may reflect a dependence on the level of solar wind forcing.

3. For the first time we document the presence of a Svalgaard-Mansurov (S-M) effect associated with flow channel FC 2, this time in the form of category NH-dusk/$B_y < 0$. In our case 2 this S-M effect appears as a series of 5–10 min. long negative (50–100 nT) X-component deflections in the region of the FC 2 flow channel (71–74° MLAT; 14:30–16:00 MLT) in the winter hemisphere. From these ground deflections on 20 November 2007 we infer a series of convection/precipitation events at the polar cap boundary in the 14:30–16:10 MLT sector. From these data we may infer that flow channel FC 2 is pulsed in this particular case. A ground magnetic effect is also documented in case 1 after 13:55 UT when the FC 2 channel had moved into a favourable position with respect to ground station Hornsund (HOR).

4. A lobe cell with polar arcs is present in the Southern (summer) Hemisphere in the low-density (<1–$2\,cm^{-3}$) case 1 under the prevailing $B_x = 0$ conditions. This suggests the previous indication that dipole tilt (season) determines the inter-hemisphere asymmetry when IMF B_x is small (see Crooker and Rich, 1993). According to Crooker and Rich (1993) lobe reconnection is favoured in the summer hemisphere. In our case 2 ($B_x < 0$) lobe cell convection and polar arcs are not observed in the south despite the favoured dipole tilt. This may be due

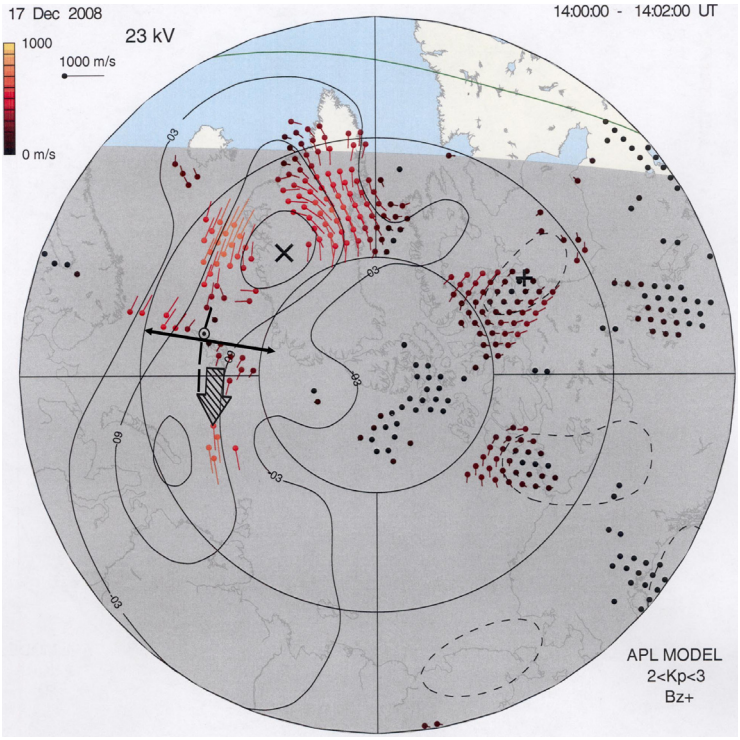

Fig. 10. SuperDARN spatial convection plot for 14:00–14:02 UT. Ground station Hornsund (HOR) on Svalbard (17 MLT; 74° MLAT), flow channel FC 2 and the approximate location of discrete aurora (poleward boundary/dashed line) as observed by meridian scanning photometer (MSP) in Longyearbyen (75° MLAT) have been marked by dotted circle, hatched arrow (in addition to the ion drift vectors in the antisunward direction), and double-arrowed meridional line, respectively. The latter is the Longyearbyen MSP field of view in the the 630.0 nm emission line.

to the negative IMF B_x which favours lobe reconnection in the Northern Hemisphere.

5. The polar arc precipitation appears as accelerated polar rain (see Carlson and Cowley, 2005) in a regime where outward-directed Birkeland current is expected in the center of the lobe cell in the Southern Hemisphere (see the L1-current in Fig. 1 which has been documented by Eriksson et al., 2002). The presence of the L1-current is confirmed by the present data (see negative B_z-gradient in Fig. 7).

6. We document the dropout of polar rain precipitation in the regime of sunward convection on the dusk side of the lobe cell polar arcs where previous study (see Eriksson et al., 2002 and the present work) documented the presence of inward-directed Birkeland current (see L2 FAC in Fig. 1 and positive B_z-gradient in Fig. 7). This may be explained by the presence of a field-aligned potential drop in the regime of inward-directed Birkeland return current (L2) which prevents the polar rain electrons from coming down into the ionosphere. Thus, this polar rain dropout may be seen as an analogy to the presence of black aurora observed in the downward-directed return current regime between multiple auroral arcs in the auroral oval (Marklund et al., 2001). This effect is different from the normal IMF B_y related dawn-dusk asymmetry of polar rain precipitation (see review by Newell et al., 2009).

7. The absence of polar arcs in case 2 (20 November 2007) may be partly due to the high plasma density density (10–20 cm^{-3}) in this ICME case. This is consistent with a previous result indicating that polar arcs under the prevailing southwest IMF conditions are favoured by low solar wind density (Frey et al., 2003). This effect comes in addition to the negative B_x component which is unfavourable for lobe reconnection to occur in the Southern Hemisphere.

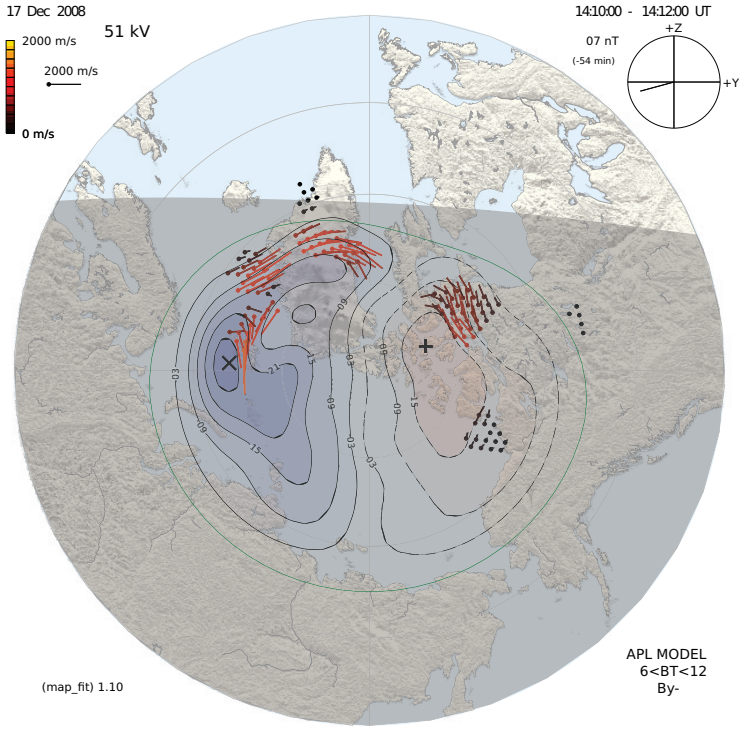

Fig. 11. SuperDARN spatial convection (ion drift) plot for 14:10–14:12 UT. A channel of enhanced antisunward convection (FC 2 of type NH-dusk/$B_y < 0$) is seen at dusk, in the Svalbard sector. The coordinate system is MLT/MLAT.

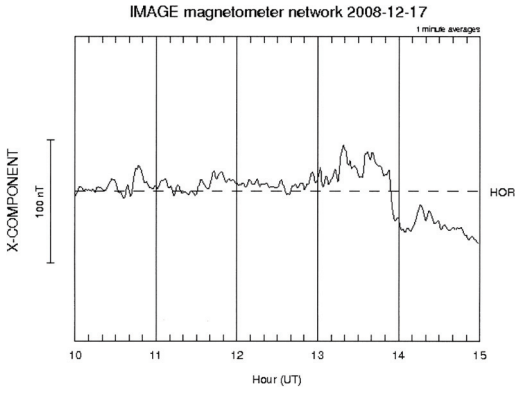

Fig. 12. X-component magnetic deflection recorded from station HOR (74° MLAT) on Svalbard. We shall focus on the negative X-deflection after 13:55 UT. This magnetic deflection reflects the Hall current associated with flow channel FC 2 (see Fig. 10.

We note that one variant of the FC 2 flow channel in the IMF $B_y < 0$ cases reported here (NH-dusk/$B_y < 0$) occur in the regime of C1 Birkeland current flowing into the ionosphere (see Fig. 1). Such enhanced **E**-fields in the regime of downward-directed Birkeland current have been observed by the Freja and FAST satellites (Marklund et al., 1997; Carlson et al., 1998) and at higher altitudes by Cluster (Karlsson et al., 2004). The latter observations are consistent with the model of the connection between Birkeland current, current closure and ionospheric cavity formation as proposed by T. Karlsson, N. Brenning, O. Marghitu, G. Marklund and S. Buchert (arXiv:0704.1610v1 [physics.space-ph], 2007). This model applies to night/wintertime conditions of low background conductivities. However, this restriction does not apply to our FC 2 flow channel. We find that generally FC 2 flows are reduced, but not necessarily absent, in the case of a sunlit ionosphere. We explain this enhanced antisunward flow as a signature of efficient momentum coupling from the solar wind along old-open field lines down to the polar cap ionosphere immediately poleward of the precipitation boundary at dawn/dusk MLTs. The interconnection topology

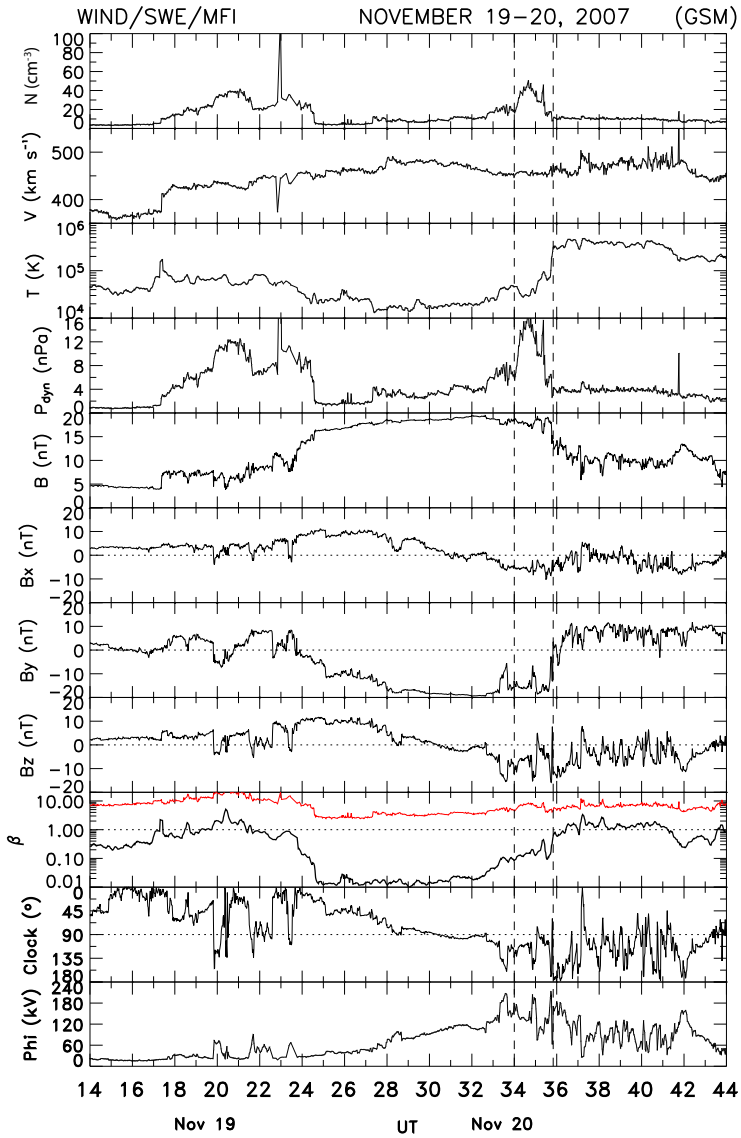

Fig. 13. Wind data for the interval 14:00 UT, 19 November–20:00 UT, 20 November 2007. The Wind interval (10:00–11:50 UT, 20 November) corresponding to the low-altitude observations discussed in this paper is marked by vertical guidelines. Same format as in Fig. 2.

is indicated in Fig. 1. We point out the DMSP F17 evidence of C2 (inward and positive B_z gradient) and C1 (outward and negative B_z gradient) in Figs. 8 and 15 (the interval 11:56–12:02 UT).

We next place the FC 2 activity in the context of convection and auroral phenomena located on newly open field lines. The flow channel on newly open field lines (LLBL/cusp precipitation) we shall refer to as FC 1. It is often observed in the form of pulsed ionospheric flows (PIFs) (also referred to as poleward moving radar auroral forms; PMRAFs) in close association with poleward moving auroral forms (PMAFs) and poleward propagating ground magnetic

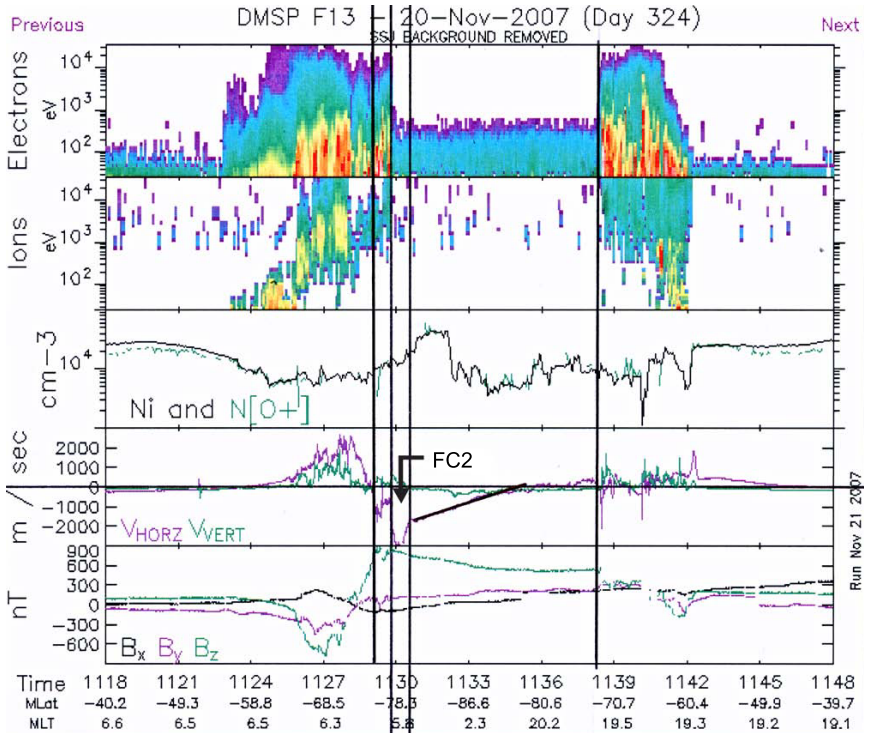

Fig. 14. DMSP data obtained by spacecraft F13 in the Southern Hemisphere during the interval 11:18–11:48 UT on 20 November 2007. Same format as in Fig. 7. Flow channel FC 2 of category SH-dawn/$B_y < 0$ is marked.

deflections (Øieroset et al., 1997; Provan et al., 1999, 2002; Wild et al., 2003).

A schematic illustration of the IMF $B_y < 0$ variant of these phenomena (Birkeland currents; auroral forms; plasma convection) is given in Fig. 19. The main focus here is on the two types of flow channels FC 1 and FC 2 and the associated auroral forms. Flow channels FC 1 are marked in the prenoon and postnoon sectors while FC 2 is marked at dusk. The illustration of the postnoon sector activities is based on observations on two different days (30 November 1997 and 21 January 2001) with similar IMF $B_y < 0$ conditions (see Sandholt and Farrugia, 2007a). The Birkeland current sheets (R2, R1, C2, C1) were obtained by the polar orbiting spacecraft FAST (Jan. 21, 2001) and DMSP F13 (15:25–15:34, 21 January 2001 and 11:24–11:32, 30 November 1997) as reported by Farrugia et al. (2004). On 21 January 2001 flow channel FC 2 was detected at approx. 13:00 MLT by the Sondrestrom radar (see Fig. 13 in Farrugia et al. (2004)) and at dusk by the DMSP F13 spacecraft. The prenoon aurora (PMAFs/prenoon) and associated plasma convection features (30 November 1997) schematically marked in the figure were reported by Thorolfsson et al. (2000).

Here we shall direct attention to contrasts between the FC 1 and FC 2 associated phenomena. FC 1 is accompanied by the following features:

1. LLBL or cusp type precipitations (mainly in the 09:00–11:00 and 13:00-15:00 MLT sectors),
2. early stages of poleward moving auroral forms (PMAFs),
3. poleward propagating pulsed ionospheric flows (PIFs),
4. poleward propagating ground magnetic deflections (DPY).

In contrast to this, flow channel FC 2 is accompanied by:

1. mantle or polar rain precipitation, mainly in the 15:00–18:00 MLT sector (NH) for the given $B_y < 0$ condition,
2. the highest-latitude stages of PMAFs/postnoon/$B_y < 0$ and PMAFs/prenoon/$B_y > 0$,
3. a series of ground magnetic deflection events in the 14:00–16:30 MLT sector (the 20 November 2007 case),

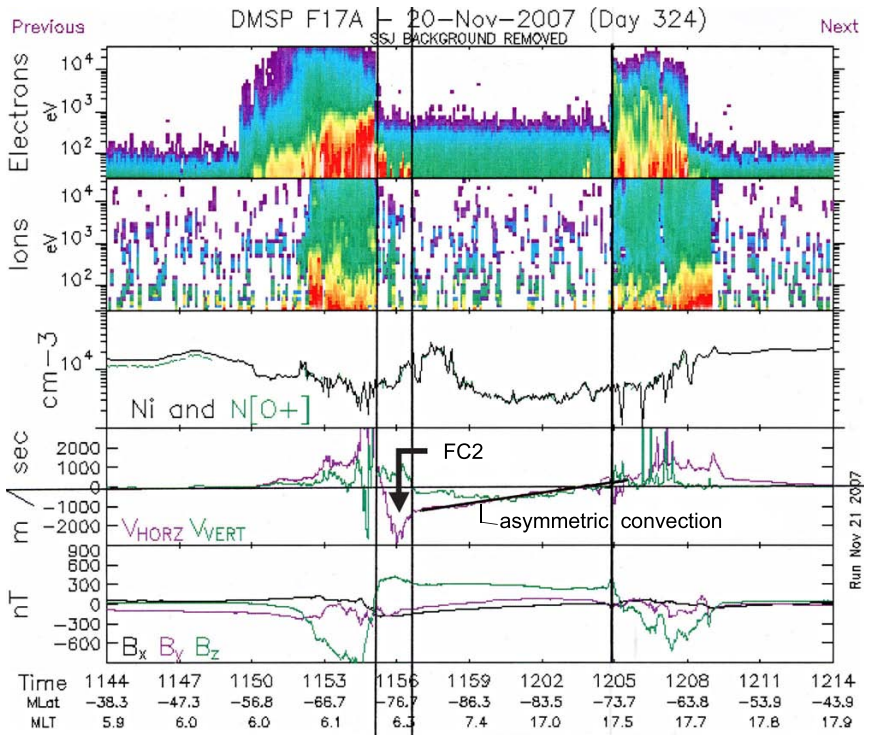

Fig. 15. DMSP data obtained by spacecraft F17 in the Southern Hemisphere during the interval 11:44–12:14 UT on 20 November 2007. Same format as in Fig. 7. Flow channel FC 2 of category SH-dawn/$B_y < 0$ and asymmetric antisunward convection in the central polar cap have been marked.

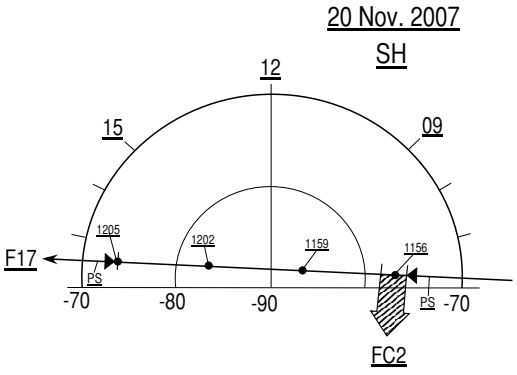

Fig. 16. Track of spacecraft DMSP F17 during the interval 11:56–12:05 UT shown in MLT/MLAT coordinates. Flow channel FC 2 at dawn is marked.

and the poleward propagation component in these events is generally absent (see Fig. 18).

The absence of the poleward propagation component in the FC 2-related events (feature (iii)) is in sharp contrast to the FC 1-related activities (Øieroset et al., 1997). The PMAFs/postnoon/$B_y < 0$ marked along the 15:00 MLT meridian in Fig. 19 refer to observations by meridian scanning photometer (MSP) and all-sky camera (field of view indicated by circle) on 30 November 1997 showing a clear poleward propagation in three stages (red forms) with the northernmost stage (weak 630.0 nm emission) corresponding to mantle-type precipitation and FC 2 (see Figs. 2, 3 and 4 in Sandholt and Farrugia, 2007a). In a previous study we documented the association between the high-latitude stage of PMAFs/prenoon/$B_y > 0$ and FC 2 (Sandholt and Farrugia, 2007b).

In summary, in the present paper (discussed in the context of previous work) we have used the strong and moderate forcing of the magnetosphere by IP magnetic clouds to establish a more comprehensive picture of the dayside and

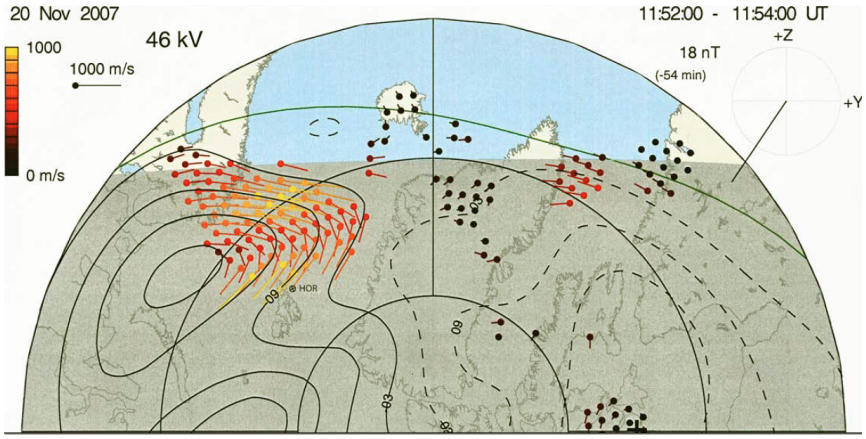

Fig. 17. SuperDARN ion drift data for 11:52–11:54 UT, 20 November 2007. Flow channel FC of category FC 2 – NH-dusk/$B_y < 0$ is seen at 15:00 MLT/72–73° MLAT. The approximate location of the magnetometer station at Hornsund (HOR) has been marked.

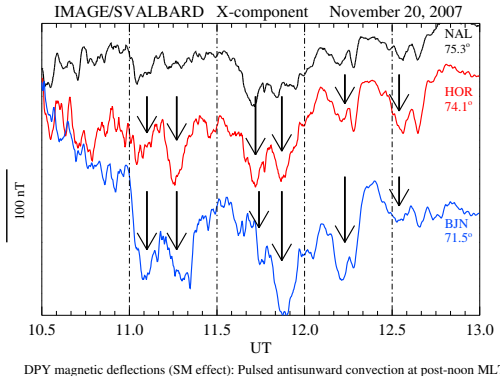

Fig. 18. IMAGE Svalbard X-component deflections at stations NAL (75° MLAT), HOR (74° MLAT), and BJN (71° MLAT) for the interval 10:00–13:00 UT, 20 November 2007. Major deflection events (negative deflection maxima) are marked by arrows in the HOR and BJN panels at 11:05, 11:18, 11:42, 11:52, and 12:12 UT.

polar cap particle precipitation morphology during southwest ($B_z < 0$; $B_y < 0$) IMF conditions and the relationship with plasma convection channels FC 1 and FC 2. In our view this represents a new and improved basis for the discussion of solar wind-magnetosphere-ionosphere coupling. Elements of the IMF $B_y < 0$ variant of this coupling during Earth passage of IP clouds are indicated in our Fig. 1.

Essential features of the precipitation morphology are:

1. "the midday gap aurora" (strongly attenuated emission intensity at noon),
2. different variants of PMAF activities appearing on both sides of "the midday gap aurora" at noon, i.e., four variants sorted by MLT sector (prenoon versus postnoon) and IMF B_y polarity,
3. polar cap arcs appearing in the two variants NH-dusk/$B_y > 0$ (see Sandholt et al., 2006) and SH-dusk/$B_y < 0$ (see DMSP Figs. 3, 4, and 6) during $B_z < 0$ conditions,
4. polar rain dropout in the SH-dusk sector of the polar cap where the Birkeland current (our L2 current) is inward-directed in the IMF $B_y < 0$ case (see the positive B_z gradient in Fig. 7).

In the present work we documented the presence of a specific ground magnetic deflection mode (a series of six 5–10 min long deflections; see Fig. 18) associated with flow channel FC 2 (NH-dusk/$B_y < 0$). The intermittent nature of the magnetic deflections on 20 November is consistent with the pulsed nature of flow channel FC 2 in this particular case. This may indicate a relationship with FTEs (see e.g. Sibeck and Lin, 2010, and references therein).

As tasks for the future investigation of flow channel FC 2 we note the following:

1. Relationship with PMAFs:
   The detailed relationship with the higher-latitude stages of PMAFs/prenoon/$B_y > 0$ and PMAFs/postnoon/$B_y < 0$ (see Fig. 19) should be investigated further.
2. Temporal structure and relationship with aurorae at dawn/dusk polar cap boundary:
   A better documentation of the temporal behaviour of flow channel FC 2 is essential. Is it typically pulsed

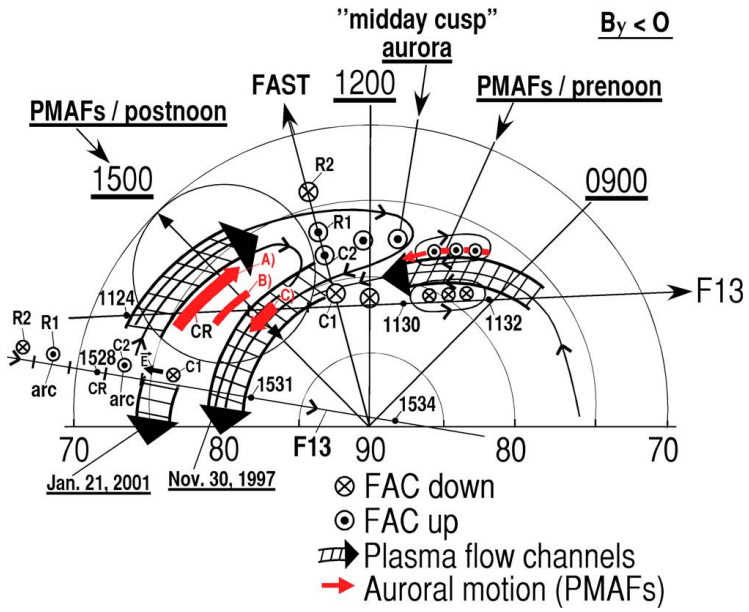

Fig. 19. Schematic illustration of plasma flow channels and aurorae located on newly open and old open field lines under IMF $B_y < 0$ conditions. Flow channels FC 1 are characterized by noonward convections in the prenoon and postnoon sectors. FC 2 shows enhanced antisunward convection at dusk. The two FC 2 channels marked at dusk refer to two different days of observations (21 January 2001 and 30 November 1997). Auroral observations in the prenoon (PMAFs/prenoon) and postnoon (PMAFs/postnoon) sectors were obtained on 30 November 1997. Tracks of spacecraft DMSP F13 from dusk to dawn refer to two intervals on different days (11:24–11:32 UT, 30 November 1997 and 15:25–15:34 UT, 21 January 2001). Relationships between latitude profiles of Birkeland currents (C1-C2-R1-R2) and poleward moving auroral forms (PMAFs; marked red) are indicated. The coordinate system is MLAT/MLT. Dusk is to the left.

or quasi-steady? Related to this we want to study the dynamics of the aurora bordering the FC 2 flow channel on its equatorward side (see the geometry in Fig. 10).

3. Spatial structure:
   The spatial structure of the FC 2 flow channel, with emphasis on the longitudinal (MLT) extent (connection to the dayside or not) of the events, needs further study.

4. IMF dependence:
   A study of the FC 2 IMF dependence is lacking. The typical situation is for FC 2 to be present either on the dawn or dusk side depending on the IMF B_y polarity. However, we need to determine the IMF clock angle range under which this normal mode of FC 2 is present. We are also curious about the possible presence of FC 2 on both sides (dusk and dawn) of the polar cap boundary during intervals of strongly southward IMF orientation (small B_y component). In one case studied so far this specific mode was present. Furthermore, we want to study the detailed FC 2 response to sharp changes in the IMF B_y polarity.

5. Contribution to the cross polar cap potential (CPCP):
   We want to document the contribution of FC 2 to the CPCP (Φ_{PC}) under various levels of solar wind forcing. A preliminary study indicates that it can contribute 20–50% to Φ_{PC} in the case of dark polar cap ionosphere and under moderate to strong solar wind forcing. This illustrates the crucial importance of flow channel FC 2 in such cases.

Acknowledgements. Access to the DMSP data base (https://swx.plh.af.mil) was kindly provided by Air Force Geophysics Research Laboratory, Hanscom, Mass. Ground magnetograms from the Svalbard IMAGE chain of ground stations were obtained from http://www.geo.fmi.fi/image. Thanks to Ari Viljanen and Truls Lynne Hansen for Svalbard magnetograms. SuperDARN convection plots were obtained from http://superdarn.jhuapl.edu. High-resolution SuperDARN data were provided by Kjellmar Oksavik. Work at University of Oslo is supported by the Norwegian Research Council (NFR). Work at UNH is supported by NASA grants NNG05GG25G and Wind grant NNX08AD11G.

Topical Editor R. Nakamura thanks S. Eriksson, T. Moretto Jorgensen, and another anonymous referee for their help in evaluating this paper.

References

Borovsky, J. E., Lavraud, B., and Kuznetsova, M. M.: Polar cap saturation, dayside reconnection, and changes to the magnetosphere, J. Geophys. Res., 114, A03224, doi:10.1029/2009JA014058, 2009.

Boyle, C. B., Reiff, P. H., and Hairston, M. R.: Empirical polar cap potentials, J. Geophys. Res., 102, 111–125, 1997.

Burlaga, L. F., Sittler, E., Mariani, F., and Schwenn, R.: Magnetic loop behind an interplanetary shock: Voyager, Helios, and IMP-8 observations, J. Geophys. Res., 86, 6673–6684, 1981.

Carlson, C. W., McFadden, J. P., Ergun, R. E., Temerin, M., Peria, W., Mozer, F. S., Klumpar, D. M., Shelley, E. G., Peterson, W. K., Mobius, E., Elphic, R., S. R., Cattell, C. A., and Pfaff, R.: Fast observations in the downward auroral current region: Energetic upgoing electron beams, parallel potential drops, and ion heating, Geophys. Res. Lett., 25, 2017–2020, 1998.

Carlson, H. C. and Cowley, S. W. H.: Accelerated polar rain electrons as the source of Sun-aligned arcs in the polar cap during northward IMF conditions, J. Geophys. Res., 110, A05302, doi:10.1029/2004JA010669, 2005.

Crooker, N. U. and Rich, F. J.: Lobe cell convection as a summer phenomenon, J. Geophys. Res., 98, 13403–13407, 1993.

Crooker, N. U., Lyon, J. G., and Fedder, J. A.: MHD model merging with IMF B_y: Lobe cells, sunward polar cap convection, and overdraped lobes, J. Geophys. Res., 103, 9143–9151, 1998.

Davis, C. J., Davies, J. A., Lockwood, M., Roillard, A. P., Eyles, C. J., and Harrison, R. A.: Stereoscopic imaging of an Earth-impacting solar coronal mass ejection: A major milestone for the STEREO mission, Geophys. Res. Lett., 36, L08102, doi:10.1029/GL038021, 2009.

Eriksson, S., Bonnell, J. W., Blomberg, L. G., Ergun, R. E., Marklund, G. T., and Carlson, C. W.: Lobe cell convection and field-aligned currents poleward of the Region 1 current system, J. Geophys. Res., 107(A8), 1185, doi:10.1029/2001JA005041, 2002.

Eriksson, S., Peria, W. J., Bonnell, J. W., Su, Y. J., Ergun, R. E., Tung, Y. K., Parks, G. K., and Carlson, C. W.: Lobe cell convection and polar cap precipitation, J. Geophys. Res., 108(A5), 1198, doi:10.1029/2002JA009725, 2003.

Fairfield, D. H. and Scudder, J. D.: Polar rain: Solar coronal electrons in the Earth's magnetosphere, J. Geophys. Res., 90, 4055–4068, 1985.

Farrugia, C. J., Sandholt, P. E., Maynard, N. C., Torbert, R. B., and Ober, D. M.: Temporal variations in a four-sheet field-aligned current system and associated aurorae as observed during a Polar-ground magnetic conjunction in the midmorning sector, J. Geophys. Res., 108(A6), 1230, doi:10.1029/2002JA009619, 2003.

Farrugia, C. J., Lund, E. J., Sandholt, P. E., Wild, J. A., Cowley, S. W. H., Balogh, A., Mouikis, C., Möbius, E., Dunlop, M. W., Bosqued, J.-M., Carlson, C. W., Parks, G. K., Cerisier, J.-C., Kelly, J. D., Sauvaud, J.-A., and Rème, H.: Pulsed flows at the high-altitude cusp poleward boundary, and associated ionospheric convection and particle signatures, during a Cluster – FAST – SuperDARN-Søndrestrøm conjunction under a southwest IMF, Ann. Geophys., 22, 2891–2905, 2004, http://www.ann-geophys.net/22/2891/2004/.

Frey, H., Immel, T. J., Lu, G., Bonnel, J., Fuselier, S. A., Mende, S. B., Hubert, B., Østgaard, N., and Le, G.: Properties of localized, high-latitude, dayside aurora, J. Geophys. Res., 108(A4), doi:10.1029/2002JA009332, 2003.

Greenwald, R. A., Baker, K., Dudeney, J. R., Pinnock, M., Thomas, E. C., Villain, J. P., Cerisier, J.-C., Senior, C., Hanuise, C., Hunsucker, R. D., Sofko, G. J., Koehler, J., Nielsen, E., Pellinen, R., Walker, A. D. M., Sato, N., and Yamagishi, H.: DARN/SUPERDARN: A Global View of the Dynamics of High-Latitude Convection, Space Sci. Rev., 71, 761–796, 1995.

Illing, R. M. E. and Hundhausen, A. J.: Observation of a coronal transient from 1.2 to 6 solar radii, J. Geophys. Res., 90, A1, doi:10.1029/JA090iA01p00275, 1985.

Illing, R. M. E. and Hundhausen, A. J.: Disruption of a coronal streamer by an eruptive prominence and coronal mass ejection, J. Geophys. Res., 91, A10, doi:10.1029/JA091iA10p10951, 1986.

Karlsson, T., Marklund, G. T., Figueiredo, S., Johansson, T., and Buchert, S.: Separating spatial and temporal variations in auroral electric and magnetic fields by Cluster multipoint measurements, Ann. Geophys., 22, 2463–2472, 2004, http://www.ann-geophys.net/22/2463/2004/.

Lepping, R. P., Acũna, M. H., Burlaga, L. F., Farrell, W. M., Slavin, J. A., Schatten, K. H., Mariani, F., Ness, N. F., Neubauer, F. M., Whang, Y. C., Byrnes, J. B., Kennon, R. S., Panetta, P. V., Scheifele, J., and Worley, E. M.: The WIND magnetic field investigation, Space Sci. Rev., 71, 207–229, 1995.

Low, B. C.: Coronal mass ejections, magnetic flux ropes, and solar magnetism, J. Geophys. Res., 106, A11, doi:10.1029/2000JA004015, 2001.

Lund, E. J., Farrugia, C. J., and Sandholt, P. E.: Momentum transfer at the high-latitude magnetopause and boundary layers, Ann. Geophys., 26, 2449–2458, 2008, http://www.ann-geophys.net/26/2449/2008/.

Marklund, G., Karlsson, T., and Clemmons, J.: On low-altitude particle acceleration and intense electric fields and their relationship to black aurora, J. Geophys. Res., 102, 17509–17522, 1997.

Marklund, G. T., Ivchenko, N., Karlsson, T., Fazakerley, A., Dunlop, M., Lindqvist, P.-A., Buchert, S., Owen, C., Taylor, M., Vaivalds, A., Carter, P., Andre, M., and Balogh, A.: Temporal evolution of the electric field accelerating electrons away from the auroral ionosphere, Nature, 414, 724–727, 2001.

Meng, C.-I., Akasofu, S.-I., and Anderson, K. A.: Dawn-dusk gradient of the precipitation of low-energy electrons over the polar cap and its relation to the interplanetary magnetic field, J. Geophys. Res., 82, 5271–5275, 1977.

Newell, P. T., Liou, K., and Wilson, G.: Polar cap particle precipitation and aurora: Review and commentary, J. Atmos. Solar-Terr. Phys., 71, 199–215, 2009.

Ogilvie, K. W., Chornay, D., Fritzenreiter, R., Hunsaker, F., Keller, J., Lobell, J., Miller, G., Scudder, J. D., Sittler Jr., E. C., Torbert, R. B., Bodet, D., Needell, G., Lazarus, A. J., Steinberg, J., T., Tappan, J. H., Mavretic, A., and Gergin, E.: SWE, a comprehensive plasma instrument for the WIND spacecraft, Space Sci. Rev., 55, 71–77, 1995.

Øieroset, M., Sandholt, P. E., Luhr, H., Denig, W., and Moretto, T.: Auroral and geomagnetic events at cusp/mantle latitudes in the prenoon sector during positive IMF B_y conditions: Signatures of pulsed magnetopause reconnection, J. Geophys. Res., 102, A4, doi:10.1029/96JA03716, 1997.

Provan, G., Yeoman, T. K., and Cowley, S. W. H.: The influence of the IMF B_y component on the location of pulsed flows in the dayside ionosphere observed by an HF radar, Geophys. Res. Lett.,

26, 4, doi:10.1029/1999GL900009, 1999.

Provan, G., Milan, S. E., Lester, M., Yeoman, T. K., and Khan, H.: Letter to the Editor: Simultaneous observations of the ionospheric footprint of flux transfer events and dispersed ion signatures, Ann. Geophys., 20, 281–287, 2002, http://www.ann-geophys.net/20/281/2002/.

Reiff, P. H. and Burch, J. L.: IMF B_y-dependent dayside plasma flow and Birkeland currents in the dayside magnetosphere, 2, A global model for northward and southward IMF, J. Geophys. Res., 90, 1595–1609, 1985.

Reiff, P. H., Burch, J. L., and Heelis, R. A.: Dayside auroral arcs and convection, Geophys. Res. Lett., 5, 391–394, 1978.

Ruohoniemi, J. M. and Greenwald, R. A.: Dependencies of high-latitude plasma convection: Consideration of interplanetary magnetic field, season, and universal time factors in statistical patterns, J. Geophys. Res., 110, A09204, doi:10.1029/2004JA010815, 2005.

Sandholt, P. E. and Farrugia, C. J.: Poleward moving auroral forms (PMAFs) revisited: responses of aurorae, plasma convection and Birkeland currents in the pre- and postnoon sectors under positive and negative IMF By conditions, Ann. Geophys., 25, 1629–1652, 2007a, http://www.ann-geophys.net/25/1629/2007/.

Sandholt, P. E. and Farrugia, C. J.: The role of poleward moving auroral forms in the dawn-dusk precipitation asymmetries induced by IMF B_y, J. Geophys. Res., 112, A04203, doi:10.1029/2006JA011952, 2007b.

Sandholt, P. E. and Farrugia, C. J.: Plasma flow channels at the dawn/dusk polar cap boundaries: momentum transfer on old open field lines and the roles of IMF B_y and conductivity gradients, Ann. Geophys., 27, 1527–1554, 2009, http://www.ann-geophys.net/27/1527/2009/.

Sandholt, P. E., Farrugia, C. J., and Denig, W. F.: Detailed dayside auroral morphology as a function of local time for south-east IMF orientation: implications for solar wind-magnetosphere coupling, Ann. Geophys., 22, 3537–3560, 2004, http://www.ann-geophys.net/22/3537/2004/.

Sandholt, P. E., Dyrland, M., and Farrugia, C. J.: Dayside aurorae and polar arcs under south-east IMF orientation, Ann. Geophys., 24, 3421–3432, 2006, http://www.ann-geophys.net/24/3421/2006/.

Sibeck, D. and Lin, R.-Q.: Concerning the motion of flux transfer events generated by component reconnection across the dayside magnetopause, J. Geophys. Res., 115, A04209, doi:10.1029/2009JA014677, 2010.

Siscoe, G. L. and Siebert, K. D.: Local boundary layer properties from non-local processes illustrated by MHD simulations, in: Earth's Low-Latitude Boundary Layer, edited by: Newell, P. T. and Onsager, T., no. 133 in AGU Monograph, pp. 377–384, American Geophysical Union, Washington, D.C., 2003.

Sonnerup, B. U. O. and Siebert, K. D.: Theory of the low-latitude boundary layer and its coupling to the ionosphere: A tutorial review, in: Earth's Low-Latitude Boundary Layer, edited by: Newell, P. T. and Onsager, T., vol. 133 of *Geophysical Monograph*, pp. 13–32, American Geophysical Union, Washington, D.C., 2003.

Sotirelis, T., Newell, P. T., and Meng, C.-I.: Polar rain as a diagnostic of recent rapid dayside merging, J. Geophys. Res., 102, A4, doi:10.1029/96JA03564, 1997.

Stern, D. P.: Magnetospheric dynamo processes, in: Magnetospheric Currents, edited by: Potemra, T. A., vol. 28 of Geophys. Monogr., pp. 200–207, AGU, Washington, D.C., 1984.

Svalgaard, L.: Polar cap magnetic variations and their relationship with the interplanetary magnetic sector structure, J. Geophys. Res., 78, 2064–2078, 1973.

Thorolfsson, A., Cerisier, J.-C., Lockwood, M., Sandholt, P. E., Senior, C., and Lester, M.: Simultaneous optical and radar signatures of poleward-moving auroral forms, Ann. Geophys., 18, 1054–1066, 2000, http://www.ann-geophys.net/18/1054/2000/.

Tsurutani, B., McPherron, R., Gonzalez, W., Lu, G., Sobral, J. H. A., and Gopalswamy, N. (Eds.): Recurrent Magnetic Storms: Corotating Solar Wind Streams, vol. 167 of Geophysical Monograph, AGU, Washington, D.C., 2006.

Wild, J. A., Milan, S. E., Cowley, S. W. H., Dunlop, M. W., Owen, C. J., Bosqued, J. M., Taylor, M. G. G. T., Davies, J. A., Lester, M., Sato, N., Yukimatu, A. S., Fazakerley, A. N., Balogh, A., and Rème, H.: Coordinated interhemispheric SuperDARN radar observations of the ionospheric response to flux transfer events observed by the Cluster spacecraft at the high-latitude magnetopause, Ann. Geophys., 21, 1807–1826, 2003, http://www.ann-geophys.net/21/1807/2003/.

II

Ann. Geophys., 29, 2189–2201, 2011
www.ann-geophys.net/29/2189/2011/
doi:10.5194/angeo-29-2189-2011

Annales Geophysicae

Dayside and nightside contributions to cross-polar cap potential variations: the 20 March 2001 ICME case

Y. L. Andalsvik[1], **P. E. Sandholt**[1], **and C. J. Farrugia**[2]

[1]Department of Physics, University of Oslo, Oslo, Norway
[2]Space Science Center, University of New Hampshire, Durham, USA

Received: 18 August 2011 – Revised: 8 November 2011 – Accepted: 12 November 2011 – Published: 29 November 2011

Abstract. We investigate the association between temporal-spatial structure of polar cap convection and auroral electrojet intensifications during a 5-h-long interval of strong forcing of the magnetosphere by an ICME/Magnetic cloud on 20 March 2001. We use data from coordinated ground-satellite observations in the 15:00–20:00 MLT sector. We take advantage of the good latitudinal coverage in the polar cap and in the auroral zone of the IMAGE chain of ground magnetometers in Svalbard – Scandinavia – Russia and the stable magnetic field conditions in ICMEs. The electrojet events are characterized by a sequence of 10 min-long AL excursions to −1000/−1500 nT followed by poleward expansions and auroral streamers. These events are superimposed on a high disturbance level when the AL index remains around −500 nT for several hours. These signatures are different from those appearing in classical substorms, most notably the absence of a complete recovery phase when AL usually reaches above −100 nT. We concentrate on polar cap convection in both hemispheres (DMSP F13 data) in relation to the ICME B_y conditions, electrojet intensifications, and the global UV auroral configuration obtained from the IMAGE spacecraft. The temporal evolution of convection properties such as the cross-polar cap potential (CPCP) drop and flow channels at the dawn/dusk polar cap (PC) boundaries around the time of the electrojet events are investigated. This approach allows us to distinguish between dayside (magnetopause reconnection) and nightside (magnetotail reconnection) sources of the PC convection events within the context of the expanding-contracting model of high-latitude convection in the Dungey cycle. Inter-hemispheric symmetries/asymmetries in the presence of newly-discovered convection channels at the dawn or dusk side PC boundaries are determined.

Correspondence to: Y. L. Andalsvik
(y.l.andalsvik@fys.uio.no)

Keywords. Ionosphere (Plasma convection) – Magnetospheric physics (Auroral phenomena; Polar cap phenomena)

1 Introduction

In this study we extend previous investigations of polar cap convection and specific polar cap (PC) flow channels appearing during intervals of strong and stable forcing of the magnetosphere associated with Earth passage of interplanetary CMEs (Burlaga et al., 1981). A PC flow channel is defined as a latitudinally restricted (few 100 km) regime of enhanced ($>1\,\mathrm{km\,s^{-1}}$) antisunward convection. Here we shall focus on the condition of strongly south directed magnetic field ($B_z = -15$ nT; $B_y = 0$) in the ICME of 20 March 2001 during a 5-h-long interval when the ICME magnetic field rotated slowly from a south-westerly ($B_z < 0$; $B_y < 0$) to a south-easterly orientation ($B_z < 0$; $B_y > 0$). This extension consists of a data-based investigation of the temporal behaviour of the cross-polar cap potential (CPCP) as the dayside and nightside sources of the plasma convection in the ionosphere vary.

Figure 1 shows a schematic illustration of a combined high-latitude (HBL) – low-latitude boundary layer (LLBL) – tail plasma sheet model of the multi-stage evolution of Dungey cell plasma convection, emphasizing the dayside and nightside sources of plasma flows in the polar cap ionosphere along the periphery of the polar cap. Basic components of the model are (i) symmetric ($B_y = 0$) ionospheric convection cells/channels, (ii) westward electrojet (WEJ) currents with (iii) the associated poleward boundary intensifications (PBIs) in the aurora at the nightside polar cap boundary, (iv) field-aligned currents (R1, R2 and polar cap FACs), (v) magnetospheric currents (cross-tail current J_{CT} and partial ring current J_{PRC}), (vi) bursty bulk flows (BBFs) in the tail plasma sheet, (vii) currents flowing in the HBL (solar wind dynamo

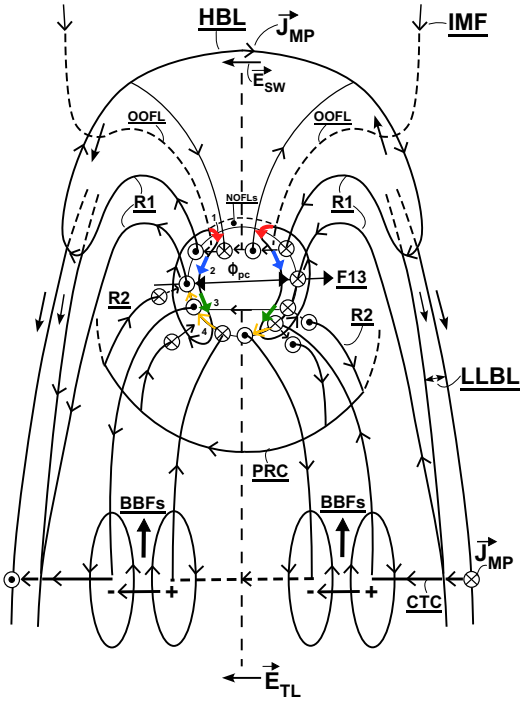

Fig. 1. Sketch of central features of multi - stage plasma convection and associated FACs of the magnetosphere-ionosphere system with emphasis on the periphery of the polar cap (see text for details). Flow channels/stages FC 1, FC 2, and FC 3, and the westward electrojet current are marked by red, blue, green, and yellow arrows, respectively.

region) and (viii) in the LLBL on the flanks of the magnetosphere.

In line with previous studies we include the temporal evolution and thus we distinguish between flow channels appearing in conjunction with newly open magnetic field lines (LLBL/cusp-type precipitation and poleward-moving auroral forms) and magnetic field lines in a later stage of evolution (old open field lines) with "feet" in polar rain precipitation (marked NOFLs and OOFLs, respectively). We refer to the ionospheric flow channels, which arise from the closure of the associated field-aligned currents via ionospheric Pedersen currents, as FC 1 and FC 2, respectively.

Related to this we note that Southwood (1987) predicted channels of pulsed flows on the flanks of the polar cap as a result of flux transfer events (FTEs) and concluded that "only near the periphery of the polar cap would the time-dependence be very evident." Such channels of pulsed antisunward flows on old open field lines (polar rain precipitation) were documented by Sandholt and Farrugia (2009) and Sandholt et al. (2010). Our aim here is to study the possible contribution of these flows to the CPCP fluctuations as measured by satellites in polar orbit or by ground-based radars. At the same time we aim at distinguishing between the dayside and nightside sources of CPCP fluctuations.

Figure 1 marks four consecutive stages in the evolution of the Dungey (1961) convection cycle. Stages 1 and 2, representing the first 20–25 min in the cycle, are accompanied by flow channels FC 1 (red) and FC 2 (blue), respectively. As noted, FC 2 is associated with the ionospheric Pedersen current closure of the dayside current system consisting of the following elements: R1 FAC – LLBL current – magnetopause current – polar cap FAC. The ionospheric Pedersen current closure gives rise to the FC 2 flow channels located near the polar cap boundary in the prenoon and/or postnoon sectors (Sandholt and Farrugia, 2009). As illustrated by the present case, flow channel FC 2 is strong on the dawn side in the Northern Hemisphere during IMF $B_y > 0$ conditions (see also Sandholt and Farrugia, 2009). For $B_y < 0$ the reverse is the case. Concerning the IMF clock angle dependence of FACs illustrated in Fig. 1 we refer to Papitashvili et al. (2002).

In Fig. 1, stage 3 of the Dungey cycle is represented by flow channel FC 3 (green) located in the pre- and postmidnight sectors (see Wang et al., 2010). As we shall argue below, channel FC 3 may be driven by processes in the tail lobe and/or tail plasma sheet. In this connection we note that the $\boldsymbol{E}$-field at the tail lobe-plasma sheet interface ($\boldsymbol{E}_{TL}$) is an important parameter for initiating plasma sheet thinning and subsequent magnetotail reconnection (Yin and Winske, 2002, and references therein). Effects of the conductivity gradient on the polar cap boundary flow channels are emphasized by Sandholt and Farrugia (2009) and Wang et al. (2010).

Stage 4 is in the dusk cell marked by southeastward convection on the equatorward side of the polar cap boundary in the Harang discontinuity region. This phenomenon we shall refer to as the streamer channel. This stage is also characterized by poleward boundary intensifications (PBIs) in the aurora, which are activated by dynamic plasma sheet processes such as magnetotail reconnection – cross-tail current disruptions (indicated by the dashed line across the mid-tail) – magnetic field dipolarizations – bursty bulk flows (BBFs) (Birn et al., 2011). Dipolarizations/BBFs may give rise to intervals of locally enhanced dawn-dusk directed electric fields ($E_Y = V_x B_z$) of ~2–5 mV m^{-1} in the few R_E wide sector of the BBFs. The dawn-dusk electric field is enhanced inside the plasma bubble due to electric polarization (Sergeev et al., 1996; Kauristie et al., 2000). The plasma bubbles are flux tubes with depleted density and plasma pressure and containing a double vortex flow pattern (see e.g. Chen and Wolf, 1993, and Kauristie et al., 2000). The convection and FACs are indicated in Fig. 1. The FACs close in the ionosphere through an azimuthal current (yellow) of Type I in Bostrom's categorization (Boström, 1964). This ionospheric current

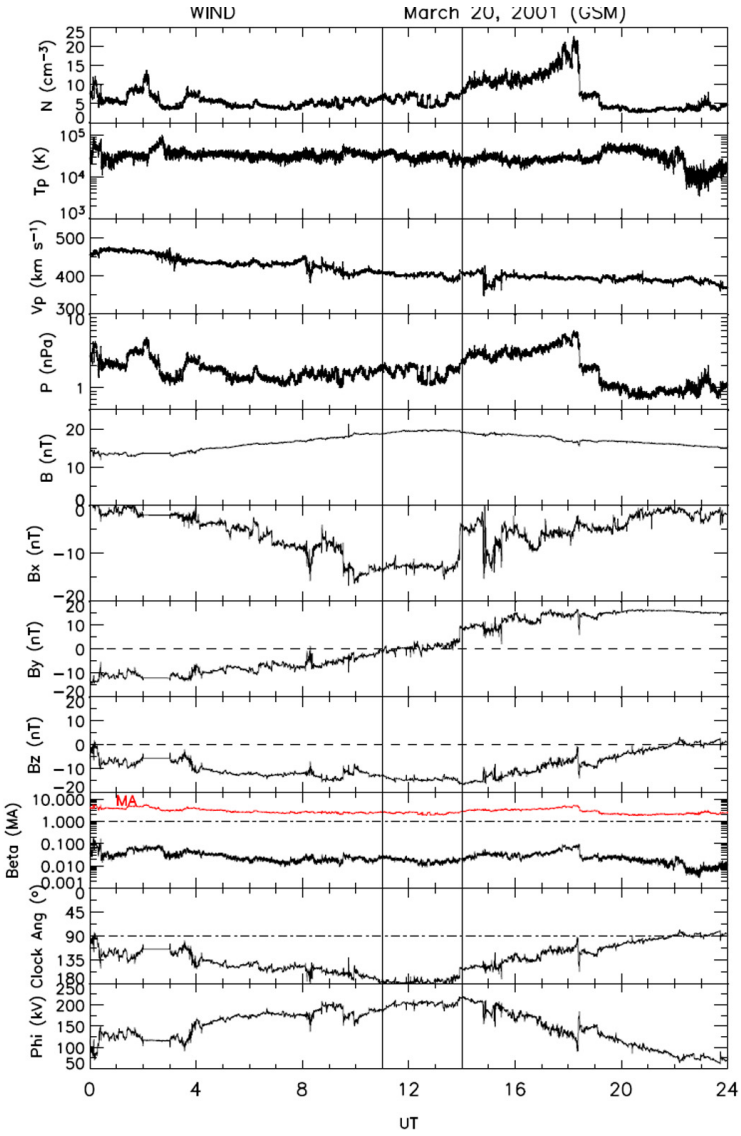

Fig. 2. Solar wind plasma and IMF observations from the spacecraft WIND for 20 March 2001. The panels show, from top to bottom, proton density, proton temperature, bulk speed, solar wind dynamic pressure, the magnetic field strength and GSM components (B_x, B_y and B_z) of the interplanetary magnetic field, the proton beta and (in red) the Alfvén Mach number, the IMF clock angle (θ) and the polar cap potential calculated by the Boyle formula. Transition between three B_y states ($B_y < 0, B_y \simeq 0, B_y > 0$) are marked by vertical lines.

closure gives rise to flow channel FC 4. The upward directed FAC component is accompanied by the phenomenon of auroral streamers (Sergeev et al., 2004). In the case we study we shall document the ground magnetic signature of the FC 4 – auroral streamer system due to the associated Hall currents (see Sandholt et al., 2002).

In the expansion-contraction model of polar cap convection (Siscoe and Huang, 1985; Cowley and Lockwood, 1992)

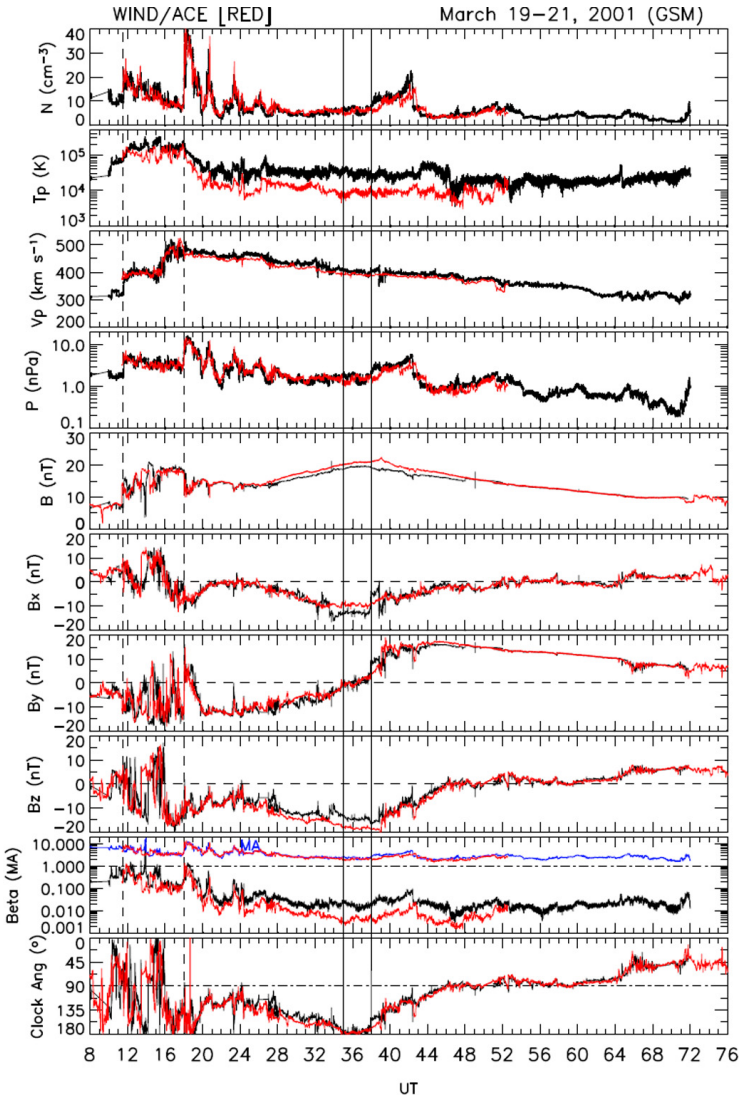

Fig. 3. WIND-ACE data overlay with ACE data shifted one hour.

it is suggested that the CPCP as measured along the 06:00–18:00 MLT meridian (by, say, low-altitude spacecraft in polar orbit) consists of a superposition of contributions from the dayside (MP reconnection: flux opening rate) and the nightside (magnetotail reconnection: lobe flux closure rate) (Milan et al., 2007, and Boudouridis et al., 2011). This gives rise to three fundamental types of plasma convection patterns, namely, (i) the unbalanced dayside type, (ii) the unbalanced nightside type, and (iii) the more or less balanced day-night type (Cowley and Lockwood, 1992; Provan et al., 2004).

With the aim of distinguishing between the dayside and nightside sources of polar cap convection as manifested in CPCP and flow channels FC 2 and FC 3 we shall investigate the association between the temporal evolution of the CPCP, obtained from DMSP F13 ion drift data along the dawn-dusk meridian, and the WEJ/streamers as monitored

by the AL-index and local magnetograms in the dusk sector obtained from the IMAGE chain of magnetometer stations in Svalbard – Scandinavia – Russia. These data are furthermore supplemented with global convection plots obtained by the SuperDARN network of ground radars (Greenwald et al., 1995).

We will here focus on the event on 20 March 2001, but several similar events have been found (see Table 1). The interval selected for this study forms part of an ICME which has been also classified as a magnetic cloud (MC) (Burlaga et al., 1981; Lepping et al., 2003). The B_y and B_z components of the cloud field lie in the ranges $[-10, 15]$ and $[-15, -5]$ nT, respectively. Initially, the B_y component of the ICME is negative and increases slowly towards zero. Then an impulsive rise to positive B_y values occurs and it remains positive after that.

2 Data description

2.1 Interplanetary data

Figure 2 shows WIND data for 20 March 2001. From top to bottom the panels show the proton density, temperature, bulk speed, dynamic pressure, total magnetic field and the x-, y- and z-components in GSM coordinates, the proton β and Alfvén Mach number (in red), the clock angle and finally the cross polar cap potential (CPCP) calculated from the Boyle formula (Boyle et al., 1997). During this time Wind was executing a distant prograde orbit, where its Y-coordinate increased to $-220\ R_E$ and its X-coordinate was $\sim$0. However, comparison with ACE near the L1 point shows exactly the same features (see Fig. 3), consistent with the long coherence lengths of plasma and field parameters in ICMEs compared to those in the normal solar wind (Farrugia et al., 2003, 2005). We shall henceforth use Wind data because of the better data coverage and higher resolution. The delay WIND-ground is estimated to be $\leq$10 min.

Our main focus here will be on the interval 12:00–17:00 UT. This ICME interval shows three consecutive stages characterized by $B_y < 0$, $B_y \sim 0$, and $B_y > 0$ nT, respectively. B_z is negative throughout.

2.2 Electrojet deflections: ground magnetometer data

Figure 4 shows the X-component of the geomagnetic field from IMAGE magnetograms for the interval 13:00–17:00 UT. The listed stations and their geomagnetic latitudes are HOR (74.1° MLAT), BJN (71.4° MLAT), SOR (67.3° MLAT), MAS (66.2° MLAT), SOD (63.9° MLAT), OUJ (61,0° MLAT), and HAN (58.7° MLAT). Local maxima of WEJ intensifications are marked by vertical dashed lines at 14:40, 15:28, and 15:58 UT. Each event onset is followed by poleward expansion and equatorward-moving current structures that are often referred to as streamers (the auroral signature). Different streamers following the three onsets are

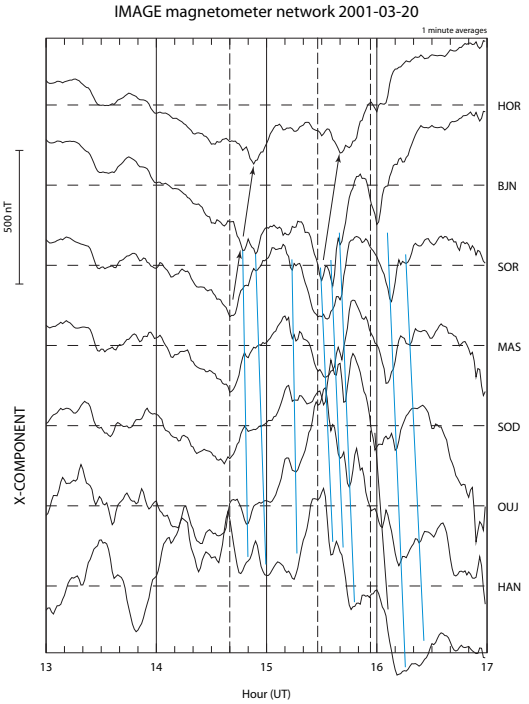

Fig. 4. IMAGE chain magnetometer data for the interval 13:00–17:00 UT. Event (WEJ) onsets, poleward expansions, and streamers are marked by vertical dashed lines, arrowed lines, and blue tilted lines, respectively.

marked by blue tilted lines in the figure. The gradual onset of the 14:40 UT WEJ event indicates a westward expansion of this intensification from a source region to the east of our stations. This interpretation is supported by the global UV aurora, as detailed below. Because of the satellite-ground conjunction at 14:40 UT we shall focus on this event. The event onset at station MAS (66.2° MLAT) is followed by a clear poleward expansion, as marked by the successive appearance of negative X-component deflections at the higher-latitude stations SOR (67.3° MLAT) – BJN (71.1° MLAT) – HOR (74.1° MLAT). The Sym-H, AU and AL indices (Fig. 5) show strong storm and substorm activities. Central to our concerns are the three major AL-deflections occurring in the interval 14:00–15:20 UT. The large negative deflection in the AL index (Tomita et al., 2011) at 14:40 UT coincides with the DMSP pass in the Northern Hemisphere (NH) shown in Fig. 6 and with the electrojet deflection signatures in the IMAGE data.

Table 1. Interplanetary and Dst conditions for four intervals of ICME passage at Earth.

Date	B_T (nT)	B_z (nT)	B_y (nT)	θ	V (km s^{-1})	n (cm^{-3})	Dst (nT)	E_{KL} (mV m^{-1})	P_{dyn} (nPa)
20 Mar 2001	19	−20	0	∼180°	400	7	−149	7.6	1.1–2.1
18 Aug 2003	17.5	−14	−10	∼150°	450	2	−148	7.4	1–3
20 Nov 2003	40–60	−20–(−50)	40–0	90°–180°	600–650	8–30	−420	26.7	4–30
30 May 2005	16	−15	−5–(−10)	140°–160°	450	10		6.3	5–8

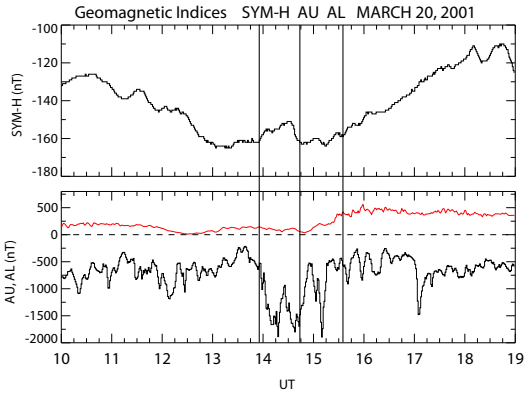

Fig. 5. Sym-H, AU and AL index data. Times of 3 F13 polar cap passes are marked by vertical guidelines.

2.3 Ionospheric flows and particle precipitation: DMSP data

Figure 6 shows DMSP F13 data during a NH dusk-dawn pass in the interval 14:30–15:00 UT. From the electron precipitation data in the top panel and the cross-track flow velocities in panel 4 (violet) we may distinguish between a southern auroral branch centered at 60° MLAT (accompanied by fast sunward convection) and a northern branch (antisunward convection) in the 66°–72° MLAT regime (17:00 MLT). The drift velocity of the antisunward convection in the polar cap (PC) increases from 0.5–1.0 km s^{-1} from the dusk to the dawn-side PC boundary, creating a dawn-dusk asymmetry of the central PC convection as expected for the prevailing IMF $B_y > 0$ conditions (after approximately 14:00 UT). A channel of enhanced (>1 km s^{-1}) antisunward flow is identified on the dawn side, in the MLAT range 70–75°.

A SH pass during the interval 13:39–14:09 UT is shown in Fig. 7. This time flow channels are present on both the dawn and dusk sides of the polar cap with peak velocities exceeding 2 km s^{-1}.

2.4 Cross polar cap ion drift: DMSP and SuperDARN data

Figure 8 shows cross-track flows during five consecutive DMSP F13 dawn-dusk passes in the Southern Hemisphere, around the time of the B_y polarity reversal (Fig. 1). Enhanced convection in PC flow channels are marked by blue arrows. We note that these five passes occurred during different stages of magnetic field orientation in the ICME (Fig. 2): (i) $B_y < 0$ during the first two passes, (ii) $B_y = 0$ during the third and fourth pass, and (iii) $B_y > 0$ during the fifth pass. Correspondingly, the PC flows shift from pre-noon to post-noon. So, this figure illustrates the following IMF-B_y dependence pattern of polar cap flow channels in the Southern Hemisphere in this case: (i) flow channel is most prominent on the dawn side in stage 1 (06:00–11:00 UT; $B_y < 0$), (ii) is present on both sides in stage 2 (11:00–14:00 UT; $B_y = 0$), and (iii) is most prominent on the dusk side in stage 3 (14:00 UT onwards; $B_y > 0$). For the third and fourth passes the dusk side flow channel ocurred at the same time as substorm activity is seen in the AL index (see Fig. 5) at 12:20 and 14:02 UT.

Figures 9 and 10 show the electrostatic potential (in kV) along the DMSP F13 tracks for two selected passes, one in the south, centered at 13:54 UT (Fig. 9) and one in the north, centered at 14:44 UT (Fig. 10). The cross-polar cap potential (CPCP) differences are naturally quite high in the south (158 kV) and in the north (174 kV) in view of the very active conditions (the ICME magnetic field). The high CPCP value for the 14:45 UT NH pass is a remarkable feature in this data interval. The 14:45 UT pass is the only one in the north for which the CPCP is higher than the Southern Hemisphere values.

The CPCP values derived for all passes (SH and NH) in the interval 09:00–17:30 UT are plotted Fig. 11. A clear trend is for the SH values (red) to be higher than the NH (blue) values. The 14:45 UT pass in the north highlights a clear exception to this general trend. At this time the NH value of the CPCP (174 kV) is 30–40 kV higher than for the closest NH passes.

Figure 12 shows the tracks of the 13:55 UT (SH; bottom panel) and 14:45 UT (NH; top) F13 passes in MLAT vs. MLT coordinates. The contributions to the CPCP from the flow channels in these cases are indicated in the figure. The

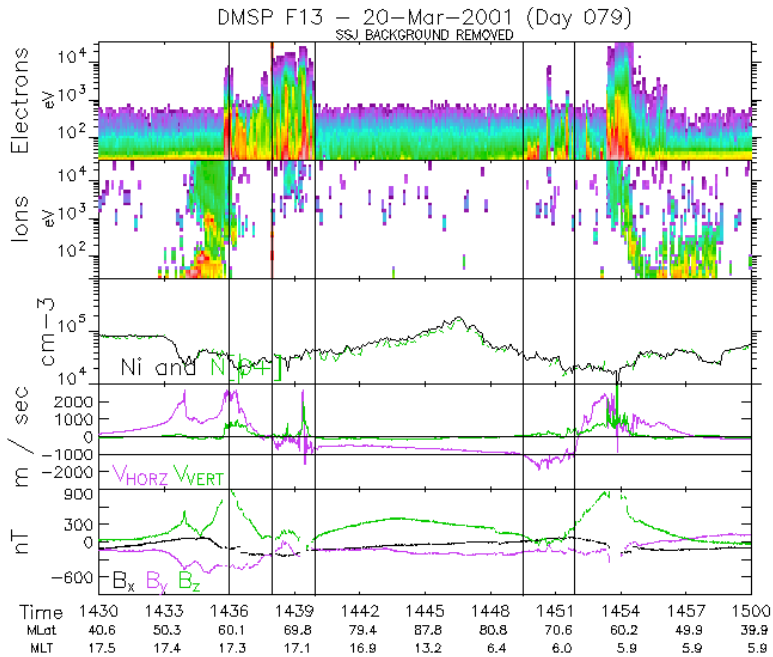

Fig. 6. DMSP F13 data from a dusk-dawn pass 14:30–15:00 UT. Panels from top to bottom show (i) spectrogram of electron and (ii) proton energy fluxes, (iii) ion densities, (iv) cross-track ion drifts (violet), and (v) magnetic deflection components B_x, B_y and B_z. Vertical guidelines mark (i) the most equatorward arc (MEA) at 60 deg. MLAT, (ii) the high-latitude auroral branch within 66–72 deg. MLAT, (iii) the polar cap, and (iv) flow channel (>1 km s^{-1} antisunward convection) within 70–75 MLAT on the dawn side.

Northern Hemisphere channel traversed at 14:50 UT represented a potential of 50 kV while the two SH channels at 13:50/14:00 UT contributed 25–30 kV each. The centers of westward (WEJ) and eastward (EEJ) electrojet currents in dusk sector of the Northern Hemisphere at the time of the satellite pass (near 14:40 UT) as derived from magnetograms recorded at the indicated local stations (Fig. 4) have been marked.

A SuperDARN convection plot (in MLT-MLAT coordinates) from the dayside part of the polar cap in Southern Hemisphere at 13:50–13:52 UT is displayed in Fig. 13. Concerning the radar technique we refer to Greenwald et al. (1995) and Ruohoniemi and Baker (1998) (see also Chisham et al., 2007). Two features in the region of good coverage above 70 deg MLAT in the prenoon to dusk sector stand out: (i) a clockwise flow vortex in the post-noon-dusk sector of the polar cap and (ii) relatively homogeneous antisunward convection in the central polar cap. These flow features, including flow channel FC 2 (yellow arrows in 14:00–16:00 MLT/70 MLAT sector), are very relevant to our study. This plot, representing the time before the major substorm activity started, resembles a flow pattern one expects for intervals of unbalanced dayside reconnection (see e.g. Provan et al., 2004). We shall return to this topic in the Discussion section.

2.5 Global UV aurora: IMAGE data

Here we shall document the central morphological features of the global UV aurora configuration obtained from spacecraft IMAGE (Mende et al., 2000): the presence of double branch oval aurora (Elphinstone et al., 1995) in the 17:00–21:00 MLT sector with auroral streamers extending from the northern branch (characterized by poleward boundary intensifications; PBIs) to the southern branch. This auroral configuration is consistent with the local ground magnetograms indicating streamer activity in the Scandinavian sector (Fig. 4). The previously documented association between auroral streamers and magnetotail bursty bulk flows (BBFs) (see Sergeev et al., 2004) furthermore confirms that BBFs are present in the magnetotail in this interval of ICME passage. We have indicated this in the magnetospheric sketch (Fig. 1).

Six selected UV images illustrating central morphological features of the global UV auroral configuration at six representative times during the interval of interest are shown in Fig. 14: (i) 13:00 UT: expanded polar cap, (ii) 13:59 UT:

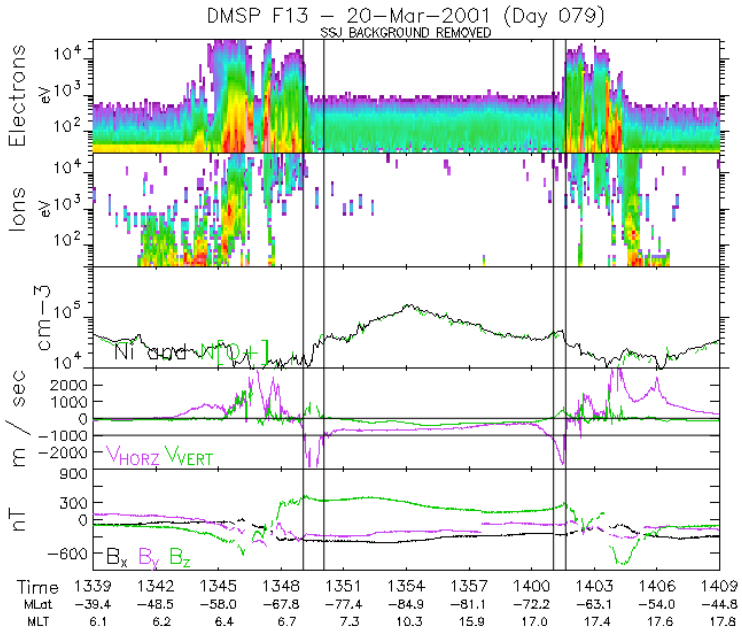

Fig. 7. DMSP F13 data from a dawn-dusk pass in the SH during the interval 13:39–14:09 UT. Same format as in Fig. 6. Vertical guidelines mark flow channels ($>1\,\mathrm{km\,s^{-1}}$ antisunward convection) on the dawn and dusk sides of the polar cap.

poleward expansion of nighside aurora when the enhanced electrojet activity started, (iii) 14:40 UT: streamer event (north-south oriented aurora) at dusk at the time of local electrojet intensification and DMSP F13 satellite pass, (iv) 14:58–15:43–15:54 UT: the presence of double oval UV aurora (see Elphinstone et al., 1995) in the 17:00–21:00 MLT sector with auroral streamers extending from the northern branch (PBIs) to the southern branch. The local ground magnetic signatures of the auroral streamers in the Scandinavian sector have been marked in Fig. 4. In previous studies we have documented the association between auroral streamers and their ground magnetic signatures (Sandholt et al., 2002).

3 Summary and discussion

In this case study we have documented an interesting spatial-temporal structure of polar cap convection during an interval of strong forcing of the magnetosphere when the interplanetary electric field (Kan and Lee, 1979) $E_{KL} > 5\,\mathrm{mV\,m^{-1}}$ at the time of an ICME passage at Earth. We want to follow the temporal evolution of the CPCP and flow channels appearing at the dawn/dusk sides of the polar cap. We aim at distinguishing between the dayside and nightside sources of these convection phenomena. DMSP ion drift profiles and associated electrostatic potentials across the polar cap were inferred from DMSP F13 data. This information is combined with selected SuperDARN convection plots and ground magnetograms from the Scandinavian sector located at dusk. The latter data in combination with the AL-index are used to monitor the local and global electrojet activities. We are particularly interested in the temporal evolution of polar cap convection associated with the enhanced AL-deflections observed during the interval 14:00–17:00 UT. Global images of the UV aurora from spacecraft IMAGE are used to infer the auroral morphology in the different stages during the interval 13:00–16:00 UT of our case study.

In previous studies we distinguished between two successive stages in the evolution of open field lines within the Dungey convection cycle for southward-directed IMF, i.e. "newly open" (time elapsed since reconnection <10 min) and "old open" (time since reconnection $\sim$10–30 min) field lines. Central features of plasma flow in these two stages are the flow channels we refer to as FC 1 (newly open) and FC 2 (old open). Recently two more stages have been added (Fig. 1). While flow channels FC 1 and 2 are driven by dayside reconnection, FC 3 is driven by closure of lobe flux associated with magnetotail reconnection (Fig. 1). In a given hemisphere the flow channel FC 2, characterized by enhanced ($>1\,\mathrm{km\,s^{-1}}$) antisunward flow in a restricted latitudinal range at the prenoon/postnoon polar cap boundary,

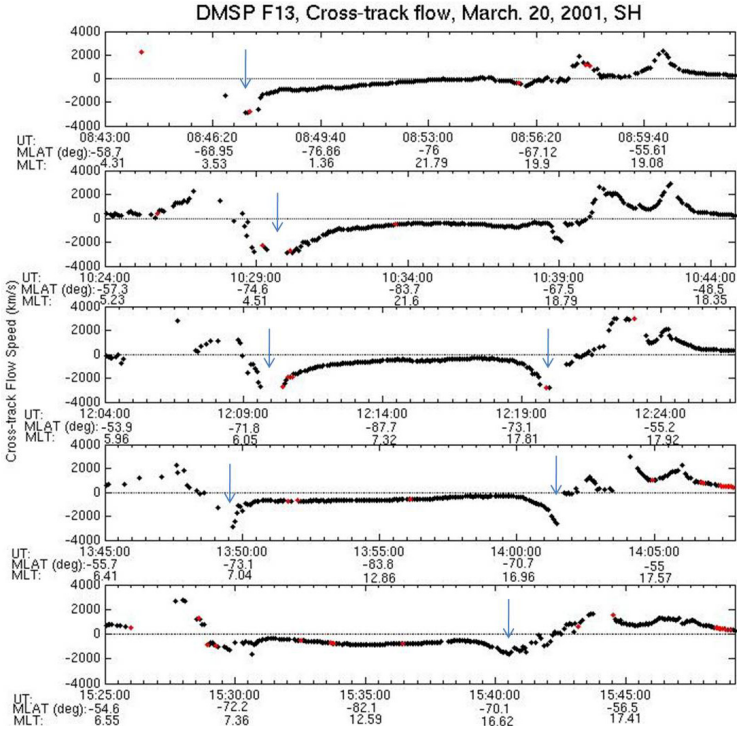

Fig. 8. Cross track flows during five consecutive DMSP F13 dawn-dusk passes in the Southern Hemisphere. Polar cap flow channels on the dawn and/or dusk sides of the PC are marked by blue arrows.

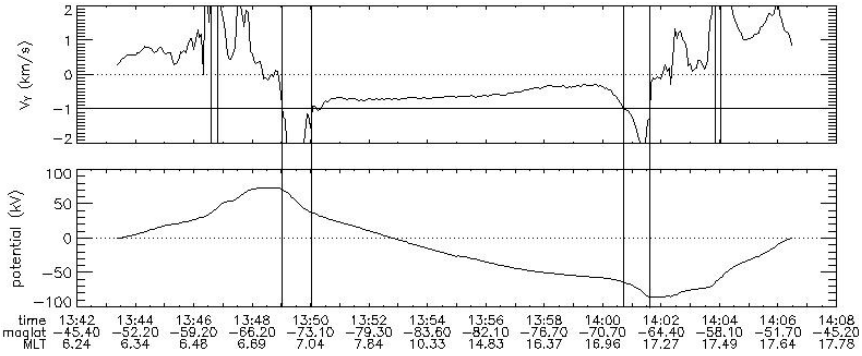

Fig. 9. DMSP F13 pass in the SH for 13:42–14:08 UT. The top panel showing cross track drift and the bottom panel showing electrostatic potential distribution. The vertical lines mark the borders of flow channels to better visualize the potential drop over these channels.

is found at opposite sides of noon corresponding to the two different IMF B_y polarities. Thus, in the case of IMF B_y-dominated IMF orientation the FC 2 flow channel contributes to enhancing the IMF B_y-related dawn-dusk convection asymmetry beyond the cusp region in the antisunward direction. A B_y-polarity dependence is confirmed by the present study (see Fig. 8). We here document the presence of flow channels on both the dawn and dusk sides of

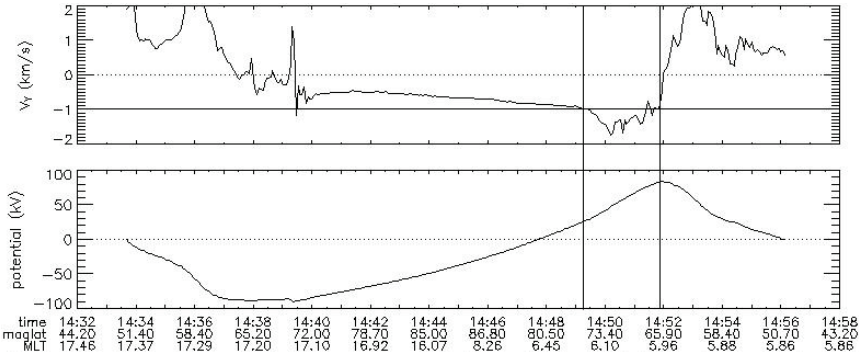

Fig. 10. DMSP F13 pass in the NH for 14:32–14:58 UT. The top panel shows cross track drift and the bottom panel shows the electrostatic potential distribution. The vertical lines mark the borders of a flow channel to better visualize the potential drop over this channel.

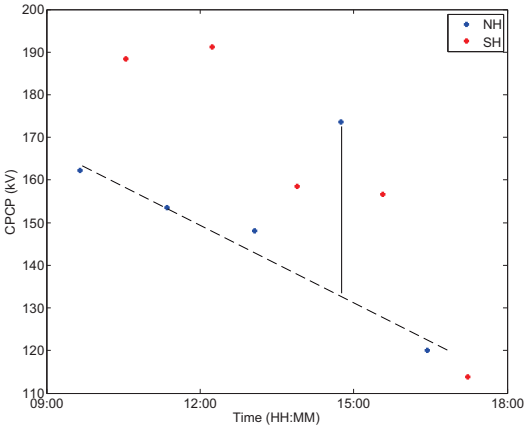

Fig. 11. CPCP estimates for the NH (blue) and SH (red) obtained from DMSP F13 passes.

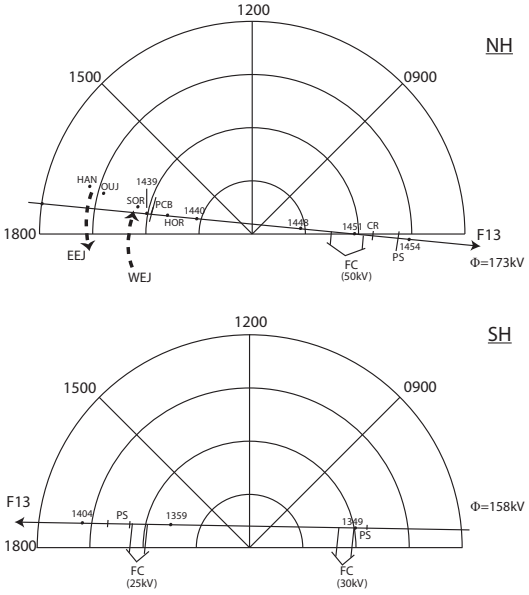

Fig. 12. Sketch of DMSP trajectories in the SH and NH in MLAT/MLT coordinates.

the polar cap during the interval 11:00–14:00 UT when the ICME field is B_z-dominated ($B_y = 0$). This new observation is consistent with the general "rule" that the convection state for B_z-dominated IMF orientation consists of a superposition of $B_y < 0$ and $B_y > 0$ states.

The two flow channels of the SH DMSP pass centered at 13:55 UT contributed 55 kV to a total CPCP of 158 kV, i.e. 35 percent. This is attributed to the magnetopause source, i.e. our flow channel FC 2. This interpretation is supported by the SuperDARN convection plot at 13:50 UT (Fig. 13) which resembles a pattern caused by unbalanced dayside reconnection (see e.g. Provan et al. (2004)). We also note that this DMSP pass occurred just before enhanced substorm activity started (see Fig. 5).

We now return to the NH F13 pass centered at 14:45 UT, i.e. in the interval of enhanced substorm activity. A significant increase (30–40 kV) in the CPCP-NH (173 kV) is observed at this time. We hypothesize that this enhancement is due to an active magnetotail source of polar cap convection (see also Provan et al., 2004; Lockwood et al., 2009; Kullen et al., 2010). This interpretation is supported by the local magnetograms in the dusk sector showing a considerable poleward expansion of the westward electrojet in the

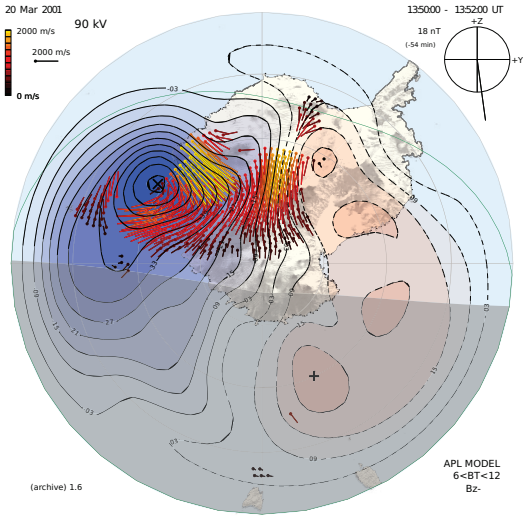

Fig. 13. Southern Hemisphere SuperDARN convection scan for 13:50–13:52 UT. The coordinate system is MLAT/MLT. The Sun is at the top and dusk is to the left.

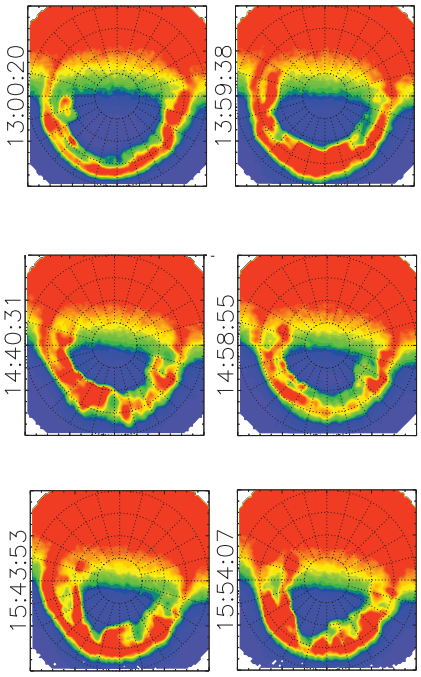

Fig. 14. UV aurora obtained from spacecraft IMAGE.

interval 14:40–14:50 UT (Fig. 4). This is consistent with polar cap contraction and excitation of flow channel FC 3. At this time (14:50 UT) the dawn-side flow channel (FC 3) contributed approximately 50 kV of the CPCP-NH (Fig. 10).

The CPCP is saturated in our case, as is normal when $E_{\mathrm{kl}} > 5\,\mathrm{mV\,m^{-1}}$ (the non-linear regime; see Burke et al. (2007) and references therein). This is demonstrated by the fact that $\Phi_{\mathrm{Boyle}} = 200\,\mathrm{kV}$ (unsaturated potential), while our CPCP estimates lie in the range 150–190 kV. We observe CPCP-SH > CPCP-NH throughout the interval. This interhemispheric asymmetry could be due to conductivity (solar zenith angle) differences in the two hemispheres (see Kan et al., 2010; Peng et al., 2009).

The flow scenario discussed above is consistent with central features of the dynamical changes of the global UV aurora: (1) expanded polar cap before the interval of enhanced substorm activity started at 13:55 UT, and (2) nightside oval contractions (poleward expansions at midnight) accompanied by auroral streamers in the 17:00–21:00 MLT sector in the interval from 13:50 UT onwards.

The previously documented association between auroral streamers and bursty bulk flows (BBFs; see Sergeev et al., 2004) confirms that BBFs are present in association with the substorm activity during this ICME passage which we have marked in the magnetospheric sketch in Fig. 1.

Finally, in Fig. 15 we summarize the essential findings of this study, i.e. the documentation of the association between the following phenomena: (i) WEJ intensifications, followed by poleward expansions, polar cap contractions and auroral streamers emanating from the polar cap boundary, as observed in the dusk-premidnight sector, (ii) activation of polar cap flow channel FC 3 (marked in Fig. 15), and (iii) CPCP enhancements as a result of this increased flow.

On the association of streamers – convection – FACs we also refer to Sergeev et al. (2004) and Pitkänen et al. (2011). The convection associated with streamers, which may be referred to as the streamer channel, is marked as stage 4 in Figs. 1 and 15. Polar cap convection jets in the pre-midnight sector (our FC 3) have also been reported by Wang et al. (2010). They find that FC 3 occurs in intervals of enhanced E_{KL}.

The dusk side flow channels in the SH DMSP passes at 12:20 and 14:02 UT (Fig. 8) are associated with electrojet intensifications (Fig. 5) and therefore belong to category FC 3. By this data set we have demonstrated the nightside source of polar cap convection in the form of localized flow channels at the dawn/dusk PC boundaries and CPCP enhancements. The implication is that flow channel FC 3 is driven by an enhanced rate of magnetotail reconnection and that this flow channel contributes significantly to the observed CPCP enhancement. This association will be investigated further in future studies.

This study emphasizes the role of magnetotail reconnection for CPCP fluctuations during intervals of strong forcing

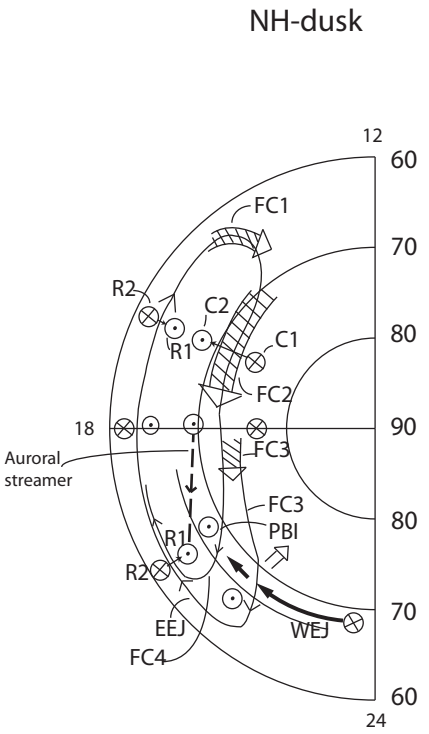

Fig. 15. Schematic illustration of plasma convection, FAC, and electrojet configurations applicable to our case. Flow channels and auroral features (PBI and streamers) in the dusk-premidnight sector are marked. Noon is at the top and dusk is to the left.

of the magnetosphere, when the dayside source had reached a level of saturation. Our scenario of multi-stage/multi-channel Dungey cell polar cap convection is placed in the context of substorm activity with auroral streamers and bursty bulk flows.

A comment on the plasma flows in the central polar cap versus that along the periphery may be appropriate at this point. In the center of the polar cap the dayside source of polar cap convection seems to saturate at speeds of 0.8–1.0 km s^{-1} which is consistent with the results of Troshichev et al. (2000). The moderate speeds of the antisunward convection in the near pole region is contrary to the much higher (1–2 km s^{-1}) speeds that are observed along the periphery of the polar cap, on the dawn (NH; $B_y > 0$ cases) and dusk (NH; $B_y < 0$ cases) sides. The traditional IMF B_y-related dawn-dusk convection asymmetry is often present in the central polar cap (see Fig. 6).

Acknowledgements. Access to the DMSP data base (https://swx.plh.af.mil) was kindly provided by Air Force Geophysics Research Laboratory, Hanscom, Mass through Gordon Wilson. Ground magnetograms from the Svalbard IMAGE chain of ground stations were obtained from http://www.geo.fmi.fi/image. Thanks to Ari Viljanen and Truls Lynne Hansen for Svalbard magnetograms. We thank M. Ruohoniemi and the SuperDARN team for the convection plots. Thanks to S. E. Milan for providing us with IMAGE UV images (PI: S. B. Mende). Work at University of Oslo is supported by the Norwegian Research Council (NFR). Work at UNH is supported by NASA grant NNX10AQ29G.

Topical Editor I. A. Daglis thanks W. Denig and another anonymous referee for their help in evaluating this paper.

References

Birn, J., Nakamura, R., Panov, E. V., and Hesse, M.: Bursty bulk flows and dipolarization in MHD simulations of magnetotail reconnection, J. Geophys. Res., 116, A01210, doi:10.1029/2010JA016083, 2011.

Boström, R.: A Model of the Auroral Electrojets, J. Geophys. Res., 69, 4983–4999, doi:10.1029/JZ069i023p04983, 1964.

Boudouridis, A., Lyons, L. R., Zesta, E., Weygand, J. M., Ribeiro, A. J., and Ruohoniemi, J. M.: Statistical study of the effect of solar wind dynamic pressure fronts on the dayside and nightside ionospheric convection, J. Geophys. Res., 116, A10233, doi:10.1029/2011JA016582, 2011.

Boyle, C. B., Reiff, P. H., and Hairston, M. R.: Empirical polar cap potentials, J. Geophys. Res., 102, 111–125, doi:10.1029/96JA01742, 1997.

Burke, W. J., Gentile, L. C., and Huang, C. Y.: Penetration electric fields driving main phase Dst, J. Geophys. Res., 112, A07208, doi:10.1029/2006JA011783, 2007.

Burlaga, L., Sittler, E., Mariani, F., and Schwenn, R.: Magnetic loop behind an interplanetary shock: Voyager, Helios, and IMP-8 observations, J. Geophys. Res., 86, 6673–6684, 1981.

Chen, C. X. and Wolf, R. A.: Interpretation of high-speed flows in the plasma sheet, J. Geophys. Res., 98, 21409–21419, doi:10.1029/93JA02080, 1993.

Chisham, G., Lester, M., Milan, S. E., Freeman, M. P., Bristow, W. A., Grocott, A., McWilliams, K. A., Ruohoniemi, J. M., Yeoman, T. K., Dyson, P. L., Greenwald, R. A., Kikuchi, T., Pinnock, M., Rash, J. P. S., Sato, N., Sofko, G. J., Villain, J.-P., and Walker, A. D. M.: A decade of the Super Dual Auroral Radar Network (SuperDARN): scientific achievements, new techniques and future directions, Surv. Geophys., 28, 33–109, doi:10.1007/s10712-007-9017-8, 2007.

Cowley, S. W. H. and Lockwood, M.: Excitation and decay of solar wind driven flows in the magnetosphere-ionosphere system, Ann. Geophys., 10, 103–115, 1992.

Dungey, J. W.: Interplanetary Magnetic Field and the Auroral Zones, Phys. Rev. Lett., 6, 47–48, doi:10.1103/PhysRevLett.6.47, 1961.

Elphinstone, R. D., Murphree, J. S., and Hearn, D. J., Cogger, L. L., Sandahl, I., Newell, P. T., Klumpar, D. M., Ohtani, S., Sauvaud, J. A., Potemra, T. A., Mursula, K., Wright, A., and Shapshak, M.: The Double Oval UV Auroral Distribution, 1. Implications for the Mapping of Auroral Arcs, J. Geophys. Res., 100, 12075–12092, 1995.

Farrugia, C. J., Matsui, H., and Torbert, R. B.: Coherence Lengths of the interplanetary electric field: Solar Cycle maximum condi-

tions, SOLAR WIND 10, 679, 766–769, doi:10.1063/1.1618705, 2003.

Farrugia, C. J., Matsui, H., Torbert, R. B., Smith, C. W., Jordanova, V. K., Ogilvie, K. W., Lepping, R. P., Berdichevsky, D. B., Terasawa, T., Kasper, J., Mukai, T., Saito, Y., and Skoug, R.: ICME and Ambient IMF correlations during the Sun-Earth Connection Events of October–November, 2003,, J. Geophys. Res., 110, A09S13, doi:10.1029/2004JA010968, 2005.

Greenwald, R. A., Baker, K., Dudeney, J. R., Pinnock, M., Thomas, E. C., Villain, J. P., Cerisier, J.-C., Senior, C., Hanuise, C., Hunsucker, R. D., Sofko, G. J., Koehler, J., Nielsen, E., Pellinen, R., Walker, A. D. M., Sato, N., and Yamagishi, H.: DARN/SuperDARN: A global view of high-latitude convection, Space Sci. Rev., 71, 763–796, 1995.

Kan, J. R. and Lee, L. C.: Energy coupling function and solar wind-magnetosphere dynamo, Geophys. Res. Lett., 6, 577–580, 1979.

Kan, J. R., Li, H., Wang, C., Tang, B. B., and Hu, Y. Q.: Saturation of polar cap potential: Nonlinearity in quasi-steady SW-M-I coupling, J. Geophys. Res., 115, A08226, doi:10.1029/2009JA014389, 2010.

Kauristie, K., Sergeev, V., Kubyshkina, M., Pulkkinen, T., Angelopoulos, V., Phan, T., Lin, R., and Slavin, J.: Ionospheric current signatures of transient plasma sheet flows, J. Geophys. Res., 105, 10677–10690, doi:10.1029/1999JA900487, 2000.

Kullen, A., Karlsson, T., Cumnock, J. A., and Sundberg., T.: Occurrence and properties of substorms associated with pseudobreakups, J. Geophys. Res., 115, A12310, doi:10.1029/2010JA015866, 2010.

Lepping, R. P., Berdichevsky, D. B., and Wu, C. C.: Sun-Earth electrodynamics: The solar wind connection, Recent Res. Devel. Astrophys., 1, 139–171, 2003.

Lockwood, M., Hairston, M., Finch, I., and Roillard, A.: Transpolar voltage and polar cap flux during the substorm cycle, J. Geophys. Res., 114, A01210, doi:10.1029/2008JA013697, 2009.

Mende, S. B., Heetderks, H., Frey, H. U., Lampton, M., Geller, S. P., Abiad, R., Siegmund, O. W., Tremsin, A. S., Spann, J., Dougani, H., Fuselier, S. A., Magoncelli, A. L., Bumala, M. B., S.Murphree, and Trondsen, T.: Far ultraviolet imaging from the IMAGE spacecraft. 2. Wideband FUV imaging, Space Sci. Rev., 91, 271–285, 2000.

Milan, S. E., Provan, G., and Hubert, B.: Magnetic flux transport in the Dungey cycle: A survey of dayside and nightside reconnection rates, J. Geophys. Res., 112, A01209, doi:10.1029/2006JA011642, 2007.

Papitashvili, V. O., Christiansen, F., and Neubert, T.: A new model of field aligned currents derived from high-precision satellite magnetic field data, Geophys. Res. Lett., 29, A2, doi:10.1029/2001JA900104, 2002.

Peng, Z., Lai, H. R., and Hu, Y. Q.: Transpolar potential and reconnection voltage of the Earth from global MHD simulations, J. Geophys. Res., 114, A04203, doi:10.1029/2008JA013604, 2009.

Pitkänen, T., Aikio, A. T., Amm, O., Kauristie, K., Nilsson, H., and Kaila, K. U.: EISCAT-Cluster observations of quiet-time near-Earth magnetotail fast flows and their signatures in the ionosphere, Ann. Geophys., 29, 299–319, doi:10.5194/angeo-29-299-2011, 2011.

Provan, G., Lester, M., Mende, S. B., and Milan, S. E.: Statistical study of high-latitude plasma flow during magnetospheric substorms, Ann. Geophys., 22, 3607–3624, doi:10.5194/angeo-22-3607-2004, 2004.

Ruohoniemi, J. M. and Baker, K. B.: Large-scale imaging of high-latitude convection with Super Dual Auroral Radar Network HF radar observations, J. Geophys. Res., 103, 20797–20811, 1998.

Sandholt, P. E. and Farrugia, C. J.: Plasma flow channels at the dawn/dusk polar cap boundaries: momentum transfer on old open field lines and the roles of IMF B_y and conductivity gradients, Ann. Geophys., 27, 1527–1554, doi:10.5194/angeo-27-1527-2009, 2009.

Sandholt, P. E., Farrugia, C. J., Lester, M., Cowley, S., Milan, S., Denig, W. F., Lybekk, B., Trondsen, E., and Vorobjev, V.: Multistage substorm expansion: Auroral dynamics in relation to plasma sheet particle injection, precipitation, and plasma convection, J. Geophys. Res., 107, A11, doi:10.1029/2001JA900116, 2002.

Sandholt, P. E., Andalsvik, Y., and Farrugia, C. J.: Polar cap convection/precipitation states during Earth passage of two ICMEs at solar minimum, Ann. Geophys., 28, 1023–1042, doi:10.5194/angeo-28-1023-2010, 2010.

Sergeev, V., Angelopoulos, V., Gosling, J., Cattell, C., and Russell, C.: Detection of localized, plasma-depleted flux tubes or bubbles in the midtail plasma sheet, J. Geophys. Res., 101, 10817–10826, doi:10.1029/96JA00460, 1996.

Sergeev, V. A., Liou, K., Newell, P. T., Ohtani, S.-I., Hairston, M. R., and Rich, F.: Auroral streamers: characteristics of associated precipitation,convection and field-aligned currents, Ann. Geophys., 22, 537–548, doi:10.5194/angeo-22-537-2004, 2004.

Siscoe, G. and Huang, T.: Polar Cap Inflation and Deflation, J. Geophys. Res., 90, 543–547, doi:10.1029/JA090iA01p00543, 1985.

Southwood, D.: The Ionospheric Signature of Flux Transfer Events, J. Geophys. Res., 92, 3207–3213, 1987.

Tomita, S., Nosé, M., Iyemori, T., Toh, H., Takeda, M., Matzka, J., Bjornsson, G., Saemundsson, T., Janzhura, A., Troshichev, O., and Schwarz, G.: Magnetic local time dependence of geomagnetic disturbances contributing to the AU and AL indices, Ann. Geophys., 29, 673–678, doi:10.5194/angeo-29-673-2011, 2011.

Troshichev, O. A., Lukianova, R. Y., Papitashvili, V. O., Rich, F. J., and Rasmussen, O.: Polar cap index (PC) as a proxy for ionospheric electric field in the near-pole region, Geophys. Res. Lett., 27, 23, doi:10.1029/2000GL003756, 2000.

Wang, H., Lühr, H., and Ridley, A. J.: Plasma convection jets near the poleward boundary of the nightside auroral oval and their relation to Pedersen conductivity gradients, Ann. Geophys., 28, 969–976, doi:10.5194/angeo-28-969-2010, 2010.

Yin, L. and Winske, D.: Simulations of current sheet thinning and reconnection, J. Geophys. Res., 2002, 1485, doi:10.1029/2002JA009507, 2002.

III

Ann. Geophys., 30, 67–80, 2012
www.ann-geophys.net/30/67/2012/
doi:10.5194/angeo-30-67-2012

Annales Geophysicae

Substorms and polar cap convection: the 10 January 2004 interplanetary CME case

Y. Andalsvik[1], P. E. Sandholt[1], and C. J. Farrugia[2]

[1]Department of Physics, University of Oslo, Oslo, Norway
[2]Space Science Center, University of New Hampshire, Durham, USA

Correspondence to: Y. Andalsvik (y.l.andalsvik@fys.uio.no)

Received: 19 October 2011 – Revised: 14 December 2011 – Accepted: 24 December 2011 – Published: 6 January 2012

Abstract. The expansion-contraction model of Dungey cell plasma convection has two different convection sources, i.e. reconnections at the magnetopause and in the magnetotail. The spatial-temporal structure of the nightside source is not yet well understood. In this study we shall identify temporal variations in the winter polar cap convection structure during substorm activity under steady interplanetary conditions. Substorm activity (electrojets and particle precipitations) is monitored by excellent ground-satellite DMSP F15 conjunctions in the dusk-premidnight sector. We take advantage of the wide latitudinal coverage of the IMAGE chain of ground magnetometers in Svalbard – Scandinavia – Russia for the purpose of monitoring magnetic deflections associated with polar cap convection and substorm electrojets. These are augmented by direct observations of polar cap convection derived from SuperDARN radars and cross-track ion drift observations during traversals of polar cap along the dusk-dawn meridian by spacecraft DMSP F13. The interval we study is characterized by moderate, stable forcing of the magnetosphere-ionosphere system (E_{KL} = 4.0–4.5 mV m^{-1}; cross polar cap potential (CPCP), Φ (Boyle) = 115 kV) during Earth passage of an interplanetary CME (ICME), choosing an 4-h interval where the magnetic field pointed continuously south-west ($B_z < 0$; $B_y < 0$). The combination of continuous monitoring of ground magnetic deflections and the F13 cross-track ion drift observations in the polar cap allows us to infer the temporal CPCP structure on time scales less than the ∼10 min duration of F13 polar cap transits. We arrived at the following estimates of the dayside and nightside contributions to the CPCP (CPCP = CPCP/day + CPCP/night) under two intervals of substorm activity: CPCP/day ∼110 kV; CPCP/night ∼50 kV (45 % CPCP increase during substorms). The temporal CPCP structure during one of the substorm cases resulted in a dawn-dusk convection asymmetry measured by DMSP F13 which is opposite to that expected from the prevailing negative B_y polarity of the ICME magnetic field, a clear indication of a nightside source.

Keywords. Ionosphere (Plasma convection) – Magnetospheric physics (Solar wind-magnetosphere interactions; Storms and substorms)

1 Introduction

The temporal structure in polar cap convection and the associated cross polar cap potential (CPCP) has been the subject of much study over the years. The presence of an underlying temporal structure was indicated by the large scatter appearing in plots of CPCP, as measured by low-altitude spacecraft, versus the geoeffective interplanetary electric field, E_{KL} (Kan and Lee, 1979) (see Cowley, 1984, his Fig. 3). An interpretation of this scatter in terms of the influence from the closure of open flux during substorm activity, i.e. satellite polar cap traversals under different substorm phases, was given by e.g. Lockwood and Cowley (1992). This is a natural consequence of the expansion-contraction model of polar cap convection (Siscoe and Huang, 1985; Cowley and Lockwood, 1992).

The same conclusion was reached on the basis of observations from SuperDARN radars by Shepherd et al. (2002). They found a highly variable CPCP for any given value of E_{KL}. Thus they concluded that upstream parameters alone are not enough to describe the instantaneous CPCP value. Processes internal to the magnetosphere-ionosphere system must be included as well.

In a case study Grocott et al. (2002) documented the excitation of new voltage during the substorm expansion phase. The total transpolar voltage typically increased by a factor of 2 (100 %) during the expansion phase. Milan et al. (2003) found that the polar cap contraction characteristic of the expansion phase continues throughout the recovery phase and can last as long as 100 min after substorm onset. Provan et al. (2005) observed by ground radars a 70 % CPCP increase (40 kV) during the 12 min interval following substorm onset.

In a recent study by Lockwood et al. (2009) it was found that the nightside source (magnetotail reconnection) of the CPCP dominates in the substorm expansion and recovery phases. The dayside source (MP reconnection) is the most important contributor to the CPCP in the growth phase only. An increase in the CPCP by a factor of 2 from growth to expansion phase was derived.

The MHD simulation study of Gordeev et al. (2011) shows a rapid response of the CPCP to substorm onset, but they find that the nightside contribution to the CPCP is generally less in magnitude than the dayside source. In their study, the CPCP typically increased by 25 % after substorm onset.

From these examples we conclude that there is no consensus on the relative contributions to the total CPCP from CPCP/day and CPCP/night. According to Gordeev et al. (2011) "a direct quantitative evaluation of the efficiency of the nightside reconnection in contributing to the polar cap potential still awaits to be done." A reason for this might be that direct measurements of the CPCP temporal structure by ground radars are difficult to make because of limited coverage of these radars at the high polar cap latitudes. A widely used method to determine the CPCP is to integrate the $\boldsymbol{E}$-field component along the satellite track across the polar cap (Hairston et al., 1998). The temporal resolution of CPCP values derived from such cross-track ion drift observations during dawn-dusk traversals of the polar cap by low-altitude satellites is limited. As we shall see, the polar cap transit time of approx. 10 min may introduce deviations from the instantaneous CPCP value during intervals of transient convection sources. The presence of non-ideal satellite trajectories (deviations from dawn-dusk meridian) may also be a problem with this technique.

Indirect measurements in the form of ground magnetic deflections (the PC index) are widely used as an indicator of polar cap convection (Troshichev et al., 2011). Responses in polar cap ground magnetic deflections to the dayside and nightside convection sources has been distinguished by Kullen et al. (2010).

Our approach is to combine direct and indirect observations in order to derive a finer temporal structure in the CPCP. In this article we shall use this approach to focus on the magnetotail source of CPCP temporal structure, i.e. that related to substorm activity, by applying an appropriate combination of ground and satellite data as described next.

We shall combine continuous observations of (i) high latitude (Svalbard) magnetic deflections and (ii) cross-track ion drift observations during dusk-dawn passes by satellite DMSP F13. The continuous monitoring of the ground signature allows us to identify the temporal structure of polar cap convection on time scales shorter than the approx. 10 min-long traversal time of DMSP F13 across the polar cap. As noted above, the latter is a widely used technique to derive CPCP values.

The magnetotail source is monitored by its associated substorm electrojet activity. For the latter purpose we use ground-satellite DMSP F15 conjunctions in the dusk-premidnight sector, and the AL auroral index.

The case we study occurred during an interval of ICME passage at Earth on 10 January 2004. We focus on a 4-h long interval when the stable ICME B_z component meaured by ACE lies within -5 to -7 nT after a rapid southward turning. The B_y component was negative throughout the whole interval. The corresponding geoeffective interplanetary electric field (E_{KL} (Kan and Lee, 1979)) lies within 4.0–4.5 mV m^{-1}.

The combination of the present data sets also allow us to document a non-traditional dawn-dusk convection asymmetry, as measured during a DMSP F13 polar cap transit, which may appear during intervals of substorm activity. Expectations on dawn-dusk convection asymmetries are based on the effect of IMF B_y on dayside convection (Jørgensen et al., 1972; Cowley et al., 1991). We hypothesize that the reversed asymmetry we observe is further evidence of a nightside contribution.

2 Data description

We shall study the evolution of plasma convection features and the associated CPCP during a 4-h-long interval of steady southwestly ICME magnetic field which contains two intervals of substorm activity. The interplanetary conditions associated with this interval of ICME passage, as recorded from ACE, are given in Fig. 1.

After describing the interplanetary data, we illustrate the observation geometry for this case study. Then we describe two ground-satellite conjunction studies which took place during the substorm intervals 15:50–16:40 UT and 17:40–18:30 UT in more detail.

2.1 Interplanetary conditions: ICME

The interplanetary data from the MAG (Smith et al., 1998) and SWEPAM (McComas et al., 1998) instruments on ACE are shown (Fig. 1) for the interval 13:00–18:00 UT. From top to bottom, the panels show the proton density, bulk speed and temperature (in red: the expected temperature of the normal solar wind after Lopez, 1987), the α particle-to-proton number density ratio, the dynamic pressure, the GSM components of the magnetic field and the total field strength,

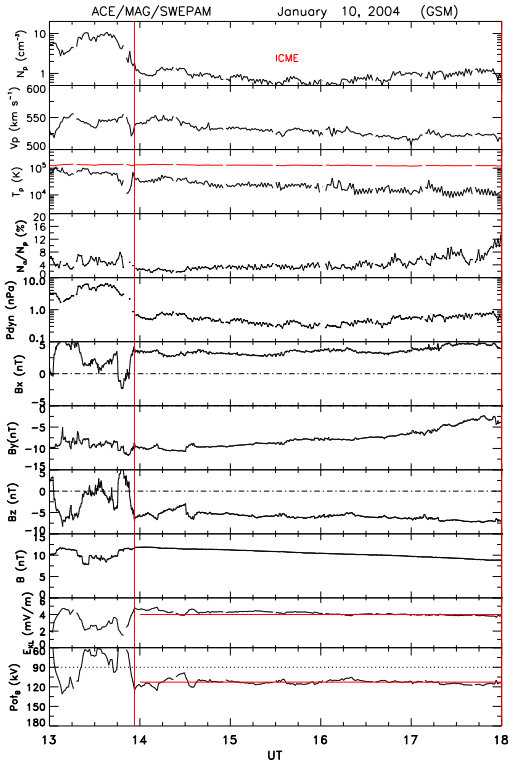

Fig. 1. Interplanetary parameters obtained from ACE during the interval 13:00–18:00 UT. Panels from top to bottom shows: (i) proton density, (ii) bulk speed, (iii) proton temperature, (iv) the alfa/proton density ratio), (v) dynamic pressure, (vi)–(ix) magnetic field components B_X, B_y, B_z, and the total field, (x) the geoeffective interplanetary electric field, E_{KL}, and (xi) the Boyle potential. The ICME front boundary is marked by vertical guideline.

the interplanetary electic field in the formulation of Kan and Lee (1979) and the Boyle potential (see Boyle et al., 1997). The quantity E_{KL} is defined as $V_p\sqrt{(B_y^2+B_z^2)}\sin^2(\text{clock}/2)$, where θ is the clock angle.

The interval we study, 14:00–18:00 UT, is characterized by an exceptionally slow and smooth rotation of the ICME magnetic field. The clock angle (not shown) increases slowly from ∼120° to 160°. B_z lies within −5 to −7 nT, while B_y is increasing from −10 to −3 nT. The total field strength B decreases slowly from 12 to 8 nT. The bulk speed is decreasing from 550 to 520 km s^{-1} while the dynamic pressure lies below 1 nPa throughout. The latter is lower than typical. The electric field, E_{KL}, is very stable within 4–4.5 mV m^{-1}. This is slightly smaller than values needed to saturate the CPCP (e.g. Muhlbachler et al., 2005, and references therein), so that a linear response of the CPCP to interplanetary driving is expected. As a corollary, formulae for CPCP assuming linearity (e.g. Boyle et al., 1997) may be employed. An estimate of the evolution of the CPCP/day during this interval, based on the Boyle formula (∼115 kV), is given in the bottom panel of Fig. 1. A propagation delay of approx. 50 min from ACE to Earth should be added when comparing ACE data with the low-altitude data reported below (see Sandholt et al., 2010).

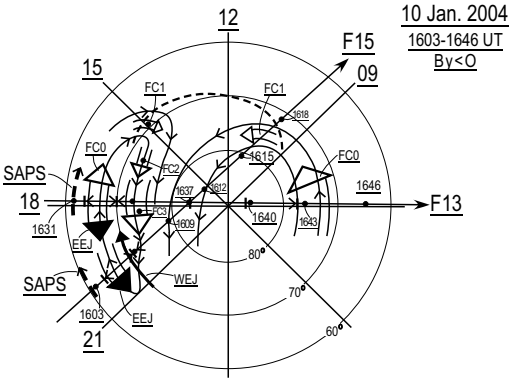

Fig. 2. Observation geometry placed in the context of global plasma convection as derived from DMSP F13 and F15 data.

2.2 Observation geometry and global convection context

Figure 2 is a sketch containing the main elements of the first of these conjunctions where the DMSP F13 and F15 passes are indicated. The coordinate system is MLAT vs. MLT, with dawn on the right and noon at the top. The features of polar cap convection appearing along the dusk-dawn meridian (F13 data and ground magnetograms) and the substorm activity in the dusk-premidnight sector (F15 data and ground magnetograms) we shall focus on are placed in the context of the global convection pattern as estimated on the basis of the F15 ion drift and precipitation data on the dayside.

The indicated convection geometry with emphasis on spatial structure, i.e. flow channels along the periphery of the polar cap, calls for a short comment. First of all, the two asymmetric convection cells are as expected for the prevailing ICME B_y negative conditions in our case. An outstanding feature is the traditional IMF B_y-related dawn-dusk convection asymmetry (Jørgensen et al., 1972; Cowley et al., 1991; Weimer, 1995; Ruohoniemi and Greenwald, 2005).

Flow channel 1 (FC 1) represents a restricted flow channel associated with newly open field lines (LLBL, cusp, precipitation) in the prenoon and postnoon sectors. It is accompanied by poleward moving auroral forms (PMAFs; see e.g. Lockwood et al., 1989) located on either side of noon and which are separated by a sector of strongly attenuated auroral emission near noon, the "midday gap aurora" (see

e.g. Sandholt and Farrugia, 2007). The approximate location of the open-closed field line boundary is marked by dashed curved line.

The spatial structure on the dusk side of the polar cap, which we refer to as FC 2 and FC 3, is related to the dayside and nightside sources of plasma convection, respectively. These regimes of enhanced ($>1\,\mathrm{km\,s^{-1}}$) antisunward convection are accompanied by polar rain precipitation. FC 2 is a result of the persistence of open flux tubes previously opened by bursts of reconnection (flux transfer events; FTEs) along the flanks of the polar cap, as predicted by Southwood (1987). The presence of these flows has been documented by Sandholt et al. (2010). The IMF B_y dependence and the role of conductivity gradients at the polar cap boundary for the formation of these flow channels have been discussed by Sandholt and Farrugia (2009).

The presence of flow channel FC 3 on the nightside of the polar cap we attribute to the nightside source (magnetotail reconnection). The role of the conductivity gradients for the presence of flow channels in this MLT sector (beyond approx. 18:00 MLT) has been described by Wang et al. (2010) who point out their relationship to enhanced geoeffective interplanetary electric field (E_{KL}, Kan and Lee, 1979) and that it is mainly a winter phenomenon.

The westward and eastward-directed electrojet (WEJ and EEJ) currents in auroral oval in the Harang discontinuity region are essential elements of substorm activity in the dusk-premidnight sector. An important substructure of the convection pattern appearing in association with auroral streamers (see e.g. Sergeev et al., 2004) in the substorm expansion phase is not included in this sketch.

Below we shall give a more detailed description of the observations of the ground-satellite conjunction indicated in the sketch.

1. F13 dusk-to-dawn pass across auroral oval segments and the polar cap during 16:31–16:46 UT. The following regimes are marked along the track: subauroral latitudes with subauroral polarization streams (SAPS); duskside auroral oval with flow channel FC 0 (return flow) and EEJ; polar cap with flow channel FC 3 (nightside old open field lines) at the duskside boundary; dawnside oval with FC 0.

2. F15 pass from evening to pre-noon MLTs during 16:03–16:18 UT. The following regimes are marked along the track: SAPS; EEJ; WEJ; polar cap; FC 1 (flow channel associated with LLBL/cusp/mantle precipitation - poleward moving auroral forms; PMAFs).

3. Flow channels FC 1 and FC 2 are indicated on the basis of F15 data in this case and previous studies (FC 2). This flow pattern is consistent with complementary statistical studies of field-aligned current patterns inferred from Iridium data (Anderson et al., 2008) (see their Fig. 5). Flow channel FC 3 is documented by SuperDARN plot at 15:56 UT, in the second F15 conjunction at 17:47 UT, and in F13 data at 18:14 UT (see below).

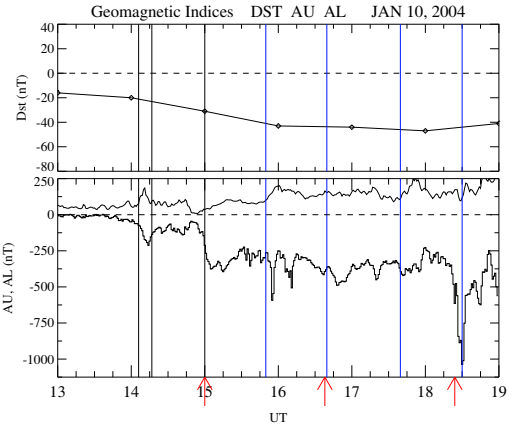

Fig. 3. Geomagnetic indices for the interval 13:00–19:00 UT: Dst (upper), AU and AL (bottom). Vertical guidelines mark (i) southward turning responses at 14:00 and 15:00 UT, (ii) substorm interval 1: 15:50–16:40 UT, and (iii) substorm interval 2: 17:40–18:30 UT. Three DMSP F13 passes in the central polar cap are marked by red arrows.

In the sequel emphasis will be laid on the variability of polar cap convection in relation to substorm activity. This represents a CPCP temporal fine-structure giving rise to non-traditional polar cap flow patterns which may deviate from those expected from the actual IMF B_y conditions, i.e. the well-known IMF B_y-related dawn-dusk asymmetry of polar cap convection with flow strengths in the PC increasing toward dusk (i.e. those which consider solely the dayside source). A good example on this non-traditional dawn-dusk asymmetry is the second case of F13 observations (18:14–18:25 UT) we study below, showing increasing antisunward convection towards the dawn side of the NH polar cap during the prevailing $B_y < 0$ ICME conditions.

2.3 Global substorm activity: AL-index on 10 January 2004

Figure 3 shows the Dst (hour averages) and the AL and AU indices for the interval 13:00–19:00 UT. A moderate storm is underway during this interval. Focusing now on the AL-index (Tomita et al., 2011) for the interval 13:00–19:00 UT the following features may be noted (marked by vertical guidelines):

1. DP2 events (enhanced E_{KL} and associated plasma convection) at 14:00 and 15:00 UT, which are activated by southward turnings of the ICME magnetic field. DP2 is

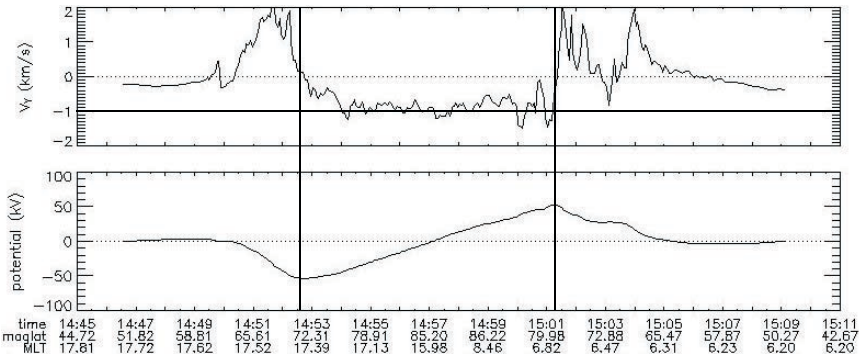

Fig. 4. DMSP F13 data showing cross-track ion drift (V_y) and electrostatic potential (bottom) for the interval 14:45–15:11 UT. Polar cap dusk- and dawn-side boundaries are marked by vertical guidelines.

defined as polar magnetic disturbances which are unrelated to substorms and controlled by the geoeffective interplanetary electric field, E_{KL} (Troshichev et al., 2011). So, these events are due to enhanced E_{KL} and associated excitation of plasma convection.

2. The two substorm intervals we study: 15:50–16:40 and 17:40–18:30 UT. Blue vertical guidelines mark the two intervals of substorm activity which is clearly manifest in the local IMAGE chain magnetic deflections in the dusk-premidnight sector, as we shall show shortly. In the figure we marked by bold arrows the three DMSP F13 passes through the central polar cap (15:00, 16:38, and 17:24 UT) which we use for CPCP estimates.

2.4 Pre-substorm conditions

Figure 4 shows DMSP F13 cross track ion drifts (V_y) and the electrostatic potential obtained during the interval 14:45–15:11 UT. We shall focus on the interval of polar cap crossing from dusk (17.39 MLT/72.3 MLAT) to dawn (6.82 MLT/80 MLAT) during the interval 14:52:50–15:01:00 UT, delimited by vertical guidelines. For this interval we derive a dawn-dusk potential drop of 107 kV. This method of deriving the CPCP is the same as that used by e.g. Hairston et al. (1998) (see their Fig. 1) Note that the pass reached high enough MLATs to sample the whole CPCP.

The interval of this CPCP measurement (14:53–15:01 UT) represents the conditions of enhanced plasma flow after the southward turning of the ICME magnetic field recorded by ACE about 1 h earlier, i.e. at 13:50 UT and well before the first substorm interval 15:50–16:40 UT. The excitation of FC 1–FC 2 flows (see Fig. 2) during the interval 14:50–15:00 UT on this day can be seen in the IMAGE magnetometer data reported by Sandholt et al. (2010) (see their Fig. 3). On the rapid convection enhancement during the first 10–15 min after a southward turning of IMF we also refer to Greenwald et al. (1999).

2.5 Ground-satellite conjunctions in substorm interval 1: 15:50–16:40 UT

Figure 5 shows X-component magnetic deflections from IMAGE stations in Svalbard – Scandinavia – Russia. We notice the following features of the activity:

(i) a quiet interval from 15:00–15:50 UT is followed by electrojet activity lasting from 15:50 to 16:40 UT, (ii) positive X-deflection (EEJ) maximizing at stations LOZ-PEL (63–64° MLAT) near 16:00 UT, is followed by (iii) WEJ and EEJ intensifications appearing at stations BJN (71° MLAT) and SOR (67° MLAT), respectively, at 16:09 UT, and (iv) electrojet and polar cap (NAL-HOR: 75–71° MLAT) magnetic deflection event at 16:37–16:40 UT, which occur at the same time when satellite F13 traversed the central polar cap (see Fig. 2).

Feature (iii) appeared just after satellite F15 crossed the oval poleward boundary (71° MLAT) at 16:06 UT.

Figure 6 shows the observation geometry for the ground-satellite conjunction in the 18:00–21:00 MLT sector during the interval 16:00–16:10 UT. In order of increasing latitude the satellite intersected (i) SAPS, (ii) EEJ, (iii) WEJ and discrete aurora, and (iv) polar cap.

As we saw from the ground data, the satellite intersected the EEJ (16:03–16:04 UT) and WEJ (16:05–16:06 UT) at the time of a local convection/electrojet enhancement, and entered the polar cap at 71° MLAT, just before the larger WEJ intensification occurred at this latitude (71° MLAT) at 16:08 UT. The hatched arrow centered at 76° MLAT/18:00 MLT marks the polar cap flow channel detected by SuperDARN radars at 15:56 UT (data shown below).

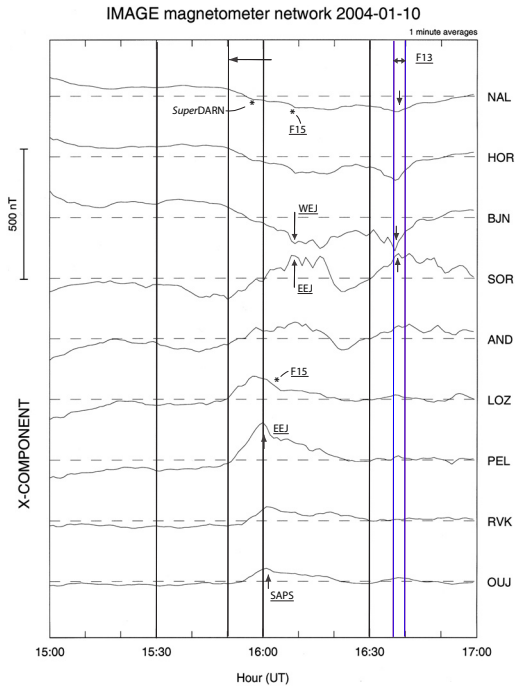

Fig. 5. The X-component of the geomagnetic field for the interval 15:00–17:00 UT from ground stations of the IMAGE chain in Svalbard – Scandinavia – Russia. The station acronyms are marked on the right side. Deflection maxima relating to EEJ (16:00, 16:09 and 16:38 UT) and WEJ (16:09, 16:37 UT) activities are indicated by arrows. Near perfect conjunctions of satellite F15 and ground stations LOZ (16:04 UT) and NAL (16:08 UT) have been marked by starred symbols along the respective traces. The interval of enhanced antisunward flow in the polar cap detected by F13 in the interval 16:37–16:40 UT is marked by vertical lines.

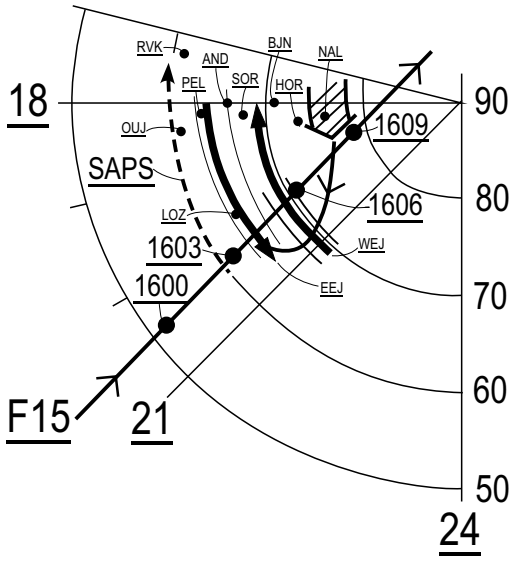

Fig. 6. Overview of ground-satellite F15 conjunction in the 18:00–21:00 MLT sector during the interval 16:00–16:10 UT. The coordinate system is MLT versus MLAT. The three latitudinal regimes of (i) SAPS (westward ion drift (V_w) $>0.5\,km\,s^{-1}$ centered at $\sim 60°$ MLAT), (ii) plasma sheet precipitation and the eastward electrojet (EEJ) current within 64–66° MLAT, and (iii) arcs near the poleward boundary accompanied by westward electrojet (WEJ) current within 68–71° MLAT have been marked along the track and in the MLT sector of the magnetometer stations. The locations of nine ground magnetometer stations in the IMAGE network (mainly along the 18:00 MLT meridian) are marked by solid dots. Solid curved lines mark the centers of the westward (WEJ) and eastward (EEJ) electrojet activities as estimated from the ground magnetograms and the satellite observations of cross-track ion drift/precipitation. The center of the westward-directed ion drift at subauroral latitudes (SAPS), as inferred from the satellite ion drift data, is marked by the westward-directed dashed curved arrow. Polar cap flow channel FC 3 (enhanced antisunward convection) above Svalbard detected by SuperDARN at 15:56 UT is marked by the wide, hatched arrow in the Svalbard region.

As indicated in the figure there is very good coverage of ground magnetometer stations along the 18:00 MLT meridian in this case.

Figure 7 shows the spatial plot of plasma convection (ion drift vectors and streamlines; see Ruohoniemi and Baker, 1998) in the Northern Hemisphere obtained by SuperDARN radars at 15:56 UT. We notice the presence of crescent-shaped dusk-side cell as appropriate for the prevailing $B_y < 0$ conditions in the interplanetary CME and the presence of a polar cap flow channel over Svalbard, centered at 76–80° MLAT/18:00 MLT.

Figure 8 shows particle precipitation, ionospheric ion drift and magnetic deflections detected by satellite DMSP F15 during the pass from pre-midnight (20:00 MLT) to pre-noon (10:00 MLT) during the interval 16:03–16:20 UT. The track is indicated in Fig. 6. We shall concentrate on the ion and electron precipitation spectra in panels 3 and 4, the cross-track ion drift in panel 5, and the eastward magnetic deflection (the B_z trace) in the bottom panel. We note the following features traversed along the track: (i) westward-directed subauroral ion drift in the form of polarization streams (SAPS) and inward-directed Birkeland current within 55–61° MLAT; (ii) auroral oval precipitation and outward-directed Birkeland currents within 64–70° MLAT ("most equatorward arc" at 64–66° MLAT), (iii) sharp poleward boundary of aurora at 70.6° MLAT, (iv) polar rain precipitation in the polar cap; and (v) enhanced noonward ion drift (flow channel FC 1)

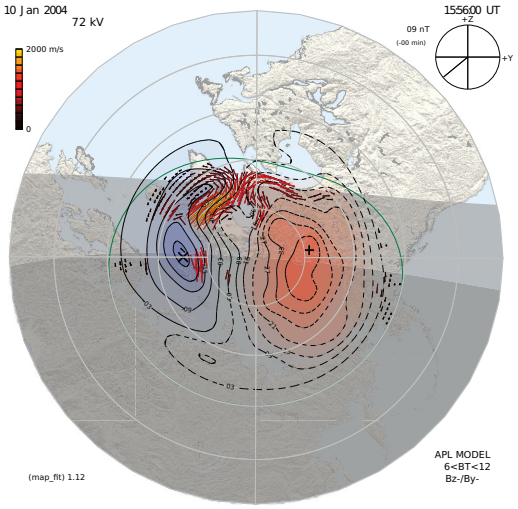

Fig. 7. SuperDARN spatial convection plot for 15:56 UT. We notice the presence of crescent-shaped dusk-side convection cell and flow channel FC 2 over Svalbard (76–80° MLAT/18:00 MLT).

within ∼73–78° MLAT in the prenoon sector (see schematic Fig. 2) with electron precipitation structures extending to 1 keV energy on its equatorward boundary. FACs directed in (R0/mantle current) and out (dayside R1) on the poleward and equatorward FC 1 boundaries, respectively, are marked in the figure.

The electron precipitation feature on the prenoon side (10:00 MLT), associated with flow channel FC 1, corresponds to the auroral phenomenon we refer to as PMAFs/prenoon/$B_y < 0$, as documented in Sandholt and Farrugia (2007) (see their Figs. 7 and 8).

The satellite crossed the poleward boundary of the aurora (70.6° MLAT/20:00 MLT) at 16:06 UT, just before the 16:08 UT WEJ intensification at this latitude (see the BJN magnetogram in Fig. 5).

Figure 9 shows cross-track ion drift (V_y) and the electrostatic potential curve obtained during the dusk to dawn pass of DMSP F13 during the interval 16:27–16:51 UT. The satellite track is indicated in Fig. 2.

We shall focus on the interval of polar cap traversal from the dusk-side (17.87 MLT/67.9 MLAT) to the dawnside (6.18 MLT/74.87 MLAT) polar cap boundary during the interval 16:33–16:43 UT. Enhanced antisunward convection ($V_y = 1.6\,\mathrm{km\,s^{-1}}$) over a $1\,\mathrm{km\,s^{-1}}$ background is observed in the central polar cap during 16:37–16:40 UT. This interval is marked in Fig. 2. The CPCP value derived for this pass is 160 kV.

2.6 Ground-satellite conjunctions in substorm interval 2: 17:40–18:30 UT

Figure 10 shows eight X-component magnetograms from the IMAGE chain of stations in Svalbard – Scandinavia – Russia for the interval 17:00–19:00 UT. The magnetograms are shown in order of decreasing latitude, from the highest (top: SOR at 67.3° MLAT) to the lowest (KAR at 56° MLAT) latitude. The following features are important: (i) the quiet conditions prevailing from 17:00 to 17:40 UT are followed by, (ii) sudden onset of enhanced westward electrojet (negative X-deflection) at 17:41 UT (see AND trace in the second panel), (iii) maximum of westward (−400 nT at AND; 66.5°) and eastward (300 nT at RVK; 62.2° MLAT) electrojet deflections reached at 17:45–17:48 UT, (iv) 50–100 nT positive X-deflections at subauroral latitudes (DOB-NUR-KAR representing the latitude range 59.3–56.4° MLAT) maximizing at 17:48–17:52 UT (see arrows at the DOB and KAR traces), (v) a second WEJ intensification ocurring at station SOR (67° MLAT) at 18:05 UT was followed by streamer events (see the blue tilted lines) in the interval 18:10–18:30 UT.

Interval of enhanced polar cap convection detected by F13 in the polar cap is delimited by the blue vertical guidelines. The station locations are given in Fig. 11.

Figure 11 shows the track of satellite DMSP F15 during the interval 17:40–17:52 UT. The traversals of latitude segments of (i) enhanced ($>0.5\,\mathrm{km\,s^{-1}}$) westward-directed ion drift at subauroral latitudes (SAPS within 58–62° MLAT), (ii) EEJ current within 62–64° MLAT and (iii) auroral oval discrete arcs (accelerated electrons) within 64–66.5° MLAT with the westward electrojet current centered at ∼66° MLAT have been marked.

We note that the satellite reached the latitude of auroral oval poleward boundary at 17:46 UT, i.e. just in the maximum phase of the local WEJ intensification recorded at station AND (66° MLAT). The position of eight magnetometer stations in the IMAGE chain which are central in this study (see the X-component deflections reported above) are marked by solid dots. These stations are representative of the three latitude regimes we study, i.e. (i) KAR, NUR and DOB lie within the SAPS regime, (ii) RVK and OUJ lie within the EEJ, and (iii) SOR, AND and LOZ lie within the latitude regime of the WEJ. We note that AND and LOZ stay within the WEJ during the whole 17:42–17:50 UT event while stations RVK and OUJ are within the EEJ regime only initially (17:42–17:47). After 17:47 (OUJ) and 17:50 UT (RVK) the OUJ and RVK magnetometers are sensitive to WEJ activity. This is consistent with the equatorward expansion of the Harang discontinuity during the event.

Figure 12 shows particle precipitation, ionospheric ion drift and magnetic deflections detected by satellite DMSP F15 during the pass illustrated in Fig. 11. F15 crossed the local segment (20.5 MLT) of the oval (confined to the latitude range 64–66.5° MLAT) during the interval 07:45–07:46:30 UT. Thus, F15 crossed the auroral oval poleward

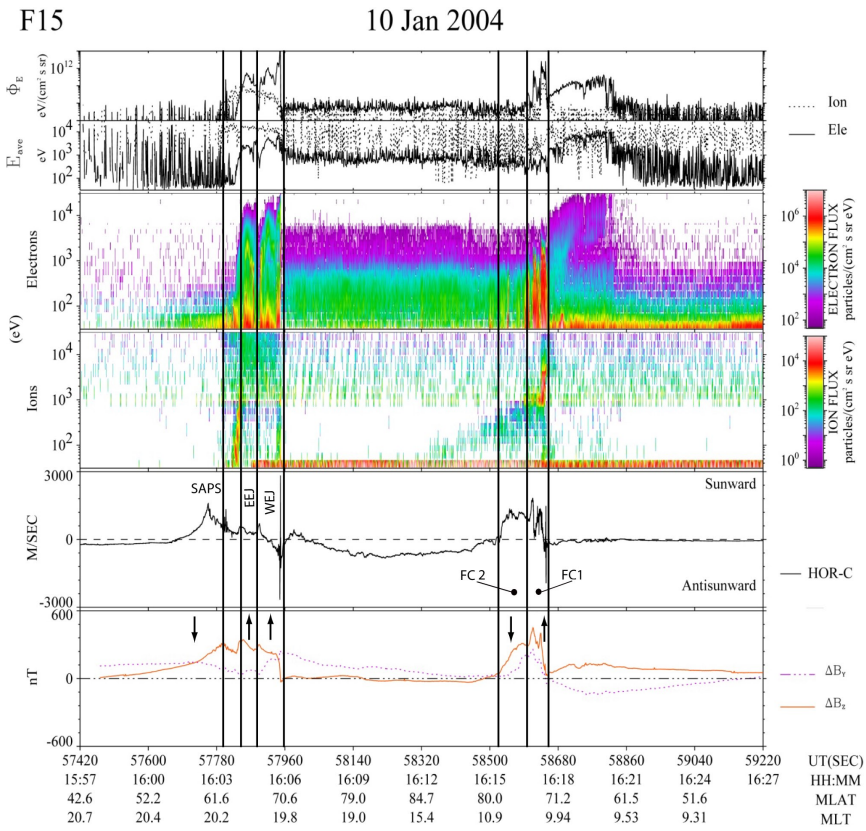

Fig. 8. DMSP F15 data obtained during the interval 15:57–16:27 UT along the track shown in Fig. 6. Panels from top to bottom shows ion (electron) precipitation energy flux, average energy, electron and ion spectrograms, cross-track ion drift, and magnetic deflection components across (ΔB_Z) and along the track. The following latitude regimes along the 20:00 MLT meridian are marked: (i) 58–62° MLAT: enhanced subauroral ion drift/SAPS, (ii) 64–66° MLAT: plasma sheet precipitation (most equatorward arc) and moderate westward ion drift (the EEJ regime), and (iii) 66–70.6° MLAT: auroral arc at oval poleward boundary and westward electrojet (WEJ). Field-aligned current directions (in and out) are marked at the B_Z-trace in the bottom panel. The vertical guidelines on the right side (prenoon sector) mark the traversal of flow channel FC 1 and electron precipitation structures extending to 1 keV energy on its equatorward side.

boundary (centered at 66° MLAT) just at the maximum of its brightening phase (17:46 UT).

We note the following features of the ion drift and magnetic field data: (i) positive B_Z-gradient (inward-directed R2 FAC) and enhanced westward ion drift V_W ($>0.5\,\mathrm{km\,s^{-1}}$) in SAPS within ~58–62° MLAT traversed during the interval 17:43–17:44:30 UT, (ii) negative B_Z-gradient (outward-directed R1 FAC) and auroral oval precipitation (boundary plasma sheet) within the MLAT range 63.5–66.5° MLAT traversed during the interval 17:45–17:46:30 UT, (iii) enhanced westward ion drift (northward-directed $\boldsymbol{E}$-field) immediately equatorward of the "high-energy arc", and (iv) eastward ion drift (southward-directed $\boldsymbol{E}$-field) within the regime of discrete auroral precipitation ("high-energy arc"). The latter corresponds to the latitude regime of the westward electrojet (WEJ).

The latitude regimes of the westward and eastward electrojets (WEJ and EEJ) as inferred from the ground magnetic deflections are indicated in the figure. The presence of flow channel FC 3 immediately poleward of the polar cap boundary may be seen in the ion drift data.

Figure 13 shows cross-track ion drifts (V_y) and electrostatic potential curves for the interval 18:08–18:32 UT. This interval includes a dusk (18.19 MLT/67.73° MLAT) to dawn (6.34 MLT/73.47° MLAT) crossing of the polar cap during the interval 18:14–18:24 UT. Two features are worthy of

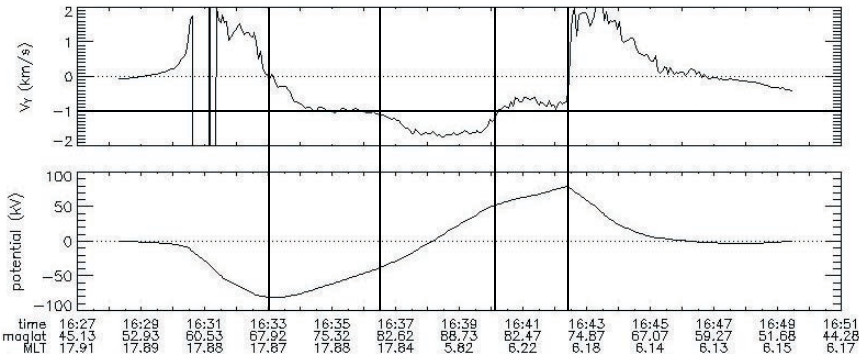

Fig. 9. DMSP F13 cross-track ion drift (V_y) and potential curves during the interval 16:27–16:51 UT. Polar cap dawn- and dusk-side boundaries and sector of enhanced antisunward flow in the central polar cap (16:37–16:40 UT) are marked by vertical guidelines. Same format as in Fig. 4. The satellite track is indicated in Fig. 2.

notice: (i) a latitudinally restricted (200 km wide) region of enhanced (1 km s^{-1}) antisunward flow near the dusk side polar cap boundary (our FC 3 flow channel), bracketed by the first two vertical guidelines, and (ii) an antisunward convection increase towards the dawn side of the polar cap, with V_y exceeding 2 km s^{-1} on occasion on the dawn side (6.31 MLT/81.37° MLAT) of the polar cap.

The CPCP value derived from these data is 153 kV. We note that the V_y-profile showing increasing antisunward convection on the dawn side of the polar cap. As we shall argue below this non-traditional dawn-dusk asymmetry is a temporal effect (rather than spatial structure) which is related to the prevailing substorm activity (see Fig. 10).

3 Summary and discussion

3.1 CPCP fluctuations on 10 January 2004

We reported cases of polar cap convection enhancements associated with two intervals of substorm activity (15:50–16:40 UT and 17:40–18:30 UT) during a 4-h long interval of very steady interplanetary conditions on 10 January 2004 (15:00–19:00 UT). The steady external conditions are perfect for our purpose of determining the contribution to the polar cap potential from magnetotail reconnection.

The substantial increases in the CPCP of ∼50 kV during the two substorm intervals are clearly demonstrated in Fig. 14. A stable background level of 110 kV is observed outside the two substorm intervals.

As stated above we aim at discriminating between the dayside and nightside sources of plasma convection in this case of moderate forcing of the magnetosphere by an ICME. The dayside (magnetopause) and nightside (magnetotail) contributions to CPCP we refer to as CPCP/day and CPCP/night, respectively. The prevailing geoeffective interplanetary electric field (E_{KL}) of 4–4.5 mV m^{-1} in our case means that we are in the upper part of the linear regime of CPCP/day variations in response to E_{KL} (see e.g. Muhlbachler et al., 2005, and Burke et al., 2007). Applying a previously derived empirical relation between IMF B_z and CPCP/day (CPCP/B_z = −20) (Yeoman et al., 2002; Milan et al., 2003) we get 120 kV for our case ($B_z = -6$ nT).

Three dusk-dawn NH passes of DMSP F13 in this interval are used to derive CPCP values. The second and third F13 passes (16:37–16:40 and 18:14–18:24 UT) ocurred within the two intervals characterized by substorm electrojet intensifications (AL = −300 to −400 nT). They may therefore be used to estimate CPCP/night.

Since the first F13 pass (14:53–15:01 UT) ocurred before substorm activity started, and just after a southward turning of the ICME field (ground magnetic signature of FC 1 is seen at 14:45–14:50 UT), this pass may be used as an estimate of the dayside (magnetopause) contribution to the CPCP in our case. From this F13 pass we get CPCP/day = 107 kV. This CPCP/day value is close to the above given estimate on the basis of the prevailing ICME B_z value and the CPCP value derived from the Boyle formula (Boyle et al., 1997) (see below).

In the two substorm intervals we observed polar cap ion drift events in the form of enhanced (>1 km s^{-1}) antisunward convection. The first convection event (16:37–16:40 UT) is short-lived (3 min), occurring when F13 was in central polar cap (marked along the F13 track in Fig. 9), while the second event (18:14–18:24 UT) lasted longer than the 10 min period of the F13 polar cap transit. In the latter case the cross-track ion drift (antisunward flow) increased continuously during the pass from the dusk to the dawn side of the polar cap when a substorm was in progress. The result is a dawn-dusk asymmetric convection profile in the Northern Hemisphere which is totally unexpected, being in the opposite sense to

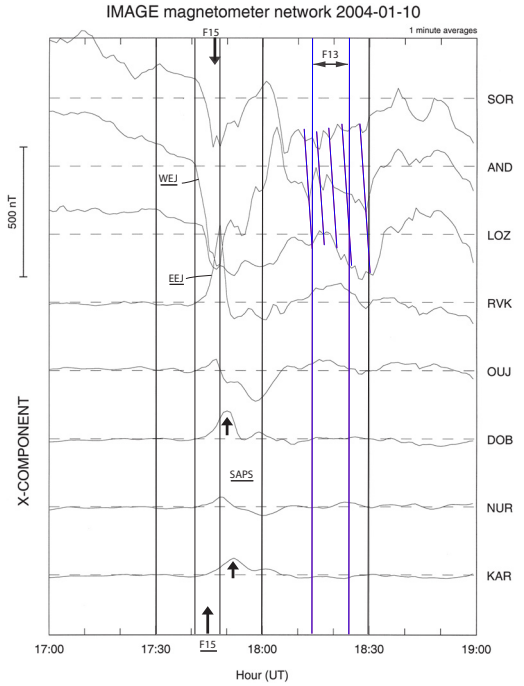

Fig. 10. X-component magnetograms from eight selected stations in the IMAGE chain of stations in Svalbard – Scandinavia – Russia for the interval 17:00–19:00 UT. The station acronyms are marked on the right side. The onset of electrojet activity (WEJ at station AND) at 17:41 UT and the maximum phase of the westward (−400 nT at AND; 66.4° MLAT) and eastward (300 nT at RVK; 62° MLAT) electrojet deflections at 17:48 UT are marked by vertical guidelines. A series of auroral streamers in the interval 18:10–18:30 UT are shown by the blue tilted lines. Interval of F13 dusk-dawn crossing of the polar cap is marked by blue vertical lines.

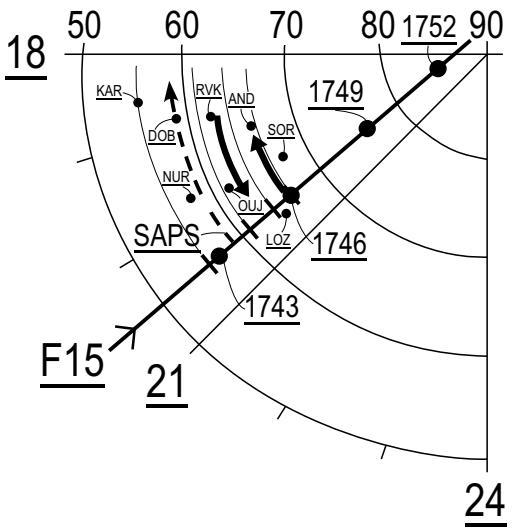

Fig. 11. Observation geometry of ground-satellite conjunction in the 19:00–21:00 MLT sector with track of satellite DMSP F15 marked during the interval 17:43–17:52 UT. The three latitudinal regimes of (i) subauroral polarization streams (SAPS; westward ion drift (V_W) $>0.5\,km\,s^{-1}$ within ∼58–62° MLAT), (ii) central plasma sheet precipitation and the eastward electrojet (EEJ) current within 62–64° MLAT, and (iii) auroral oval (AO) arcs within 64–66.5° MLAT and the westward electrojet (WEJ) centered at ∼66° MLAT have been marked along the track and in the MLT sector of the magnetometer stations. The coordinate system is MLT versus MLAT. The locations of eight stations of ground magnetometers in the IMAGE chain are marked by solid dots. Solid curved lines mark the centers of the westward (WEJ) and eastward (EEJ) electrojet activities as estimated from the ground magnetograms and the satellite observations of cross-track ion drift. The center of the westward-directed ion drift at subauroral latitudes (SAPS) which is marked by the dashed curved arrow is inferred from the satellite data.

that expected in view of the prevailing $B_y < 0$ ICME conditions. This is an interval of substorm electrojet activity and the presence of auroral streamers (see e.g. Sandholt et al., 2002, and Sergeev et al., 2004) emanating from the polar cap boundary (see Fig. 10).

Both these polar cap traversals are characterized by a convection structure subject to temporal variability, as can be derived from the continuous monitoring of the associated ground magnetic deflections in the polar cap and in the nightside oval with its auroral electrojet activity.

Various techniques may be applied to distinguish between the dayside and nightside sources of the CPCP as estimated from the F13 data in our cases.

If we assume that CPCP/day is approximately constant in our case, as indicated by the DMSP observations in Fig. 14, and the constant E_{KL}, we may use the first polar cap pass (14:53–15:01 UT) as an estimate of CPCP/day (107 kV). This is also consistent with the CPCP value derived from the Boyle formula (Boyle et al., 1997) in our case: 112.8 ± 3.7 kV (see Fig. 1).

The two values of the total CPCP we derived for the intervals 16:33–16:43 and 18:14–18:24 UT are 160 and 153 kV, respectively. If we subtract the CPCP/day value we got from the first F13 pass (107 kV), under quiet substorm conditions, we find that CPCP/night is 53 and 46 kV in these two cases. From this estimate we find that the actual substorm activities caused a 50 % increase in the total CPCP we measure.

A more direct method to extract CPCP/day from the second pass, which includes the 16:37–16:40 UT short-lived event, may be to use the potential curves in Fig. 9 to extrapolate the pre-event drift velocity ($V_y = 1\,km\,s^{-1}$) across

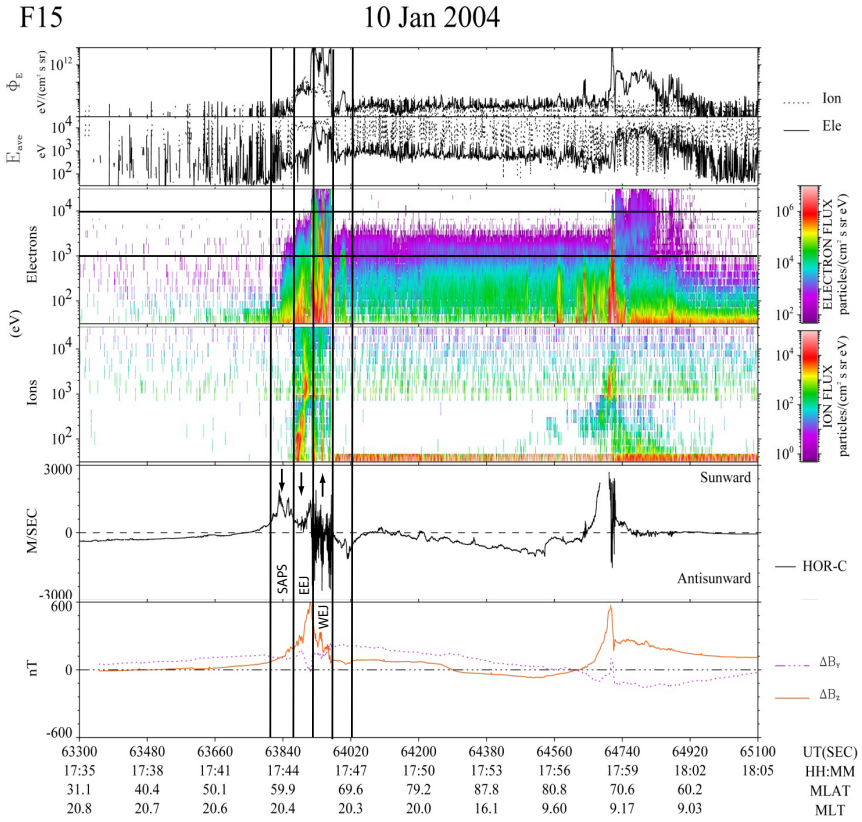

Fig. 12. DMSP F15 data obtained during the interval 17:35–18:05 UT. Same format as in Fig. 8. Latitude regimes corresponding to subauroral polarization stream (SAPS), and the eastward and westward electrojets (EEJ and WEJ) have been delimited by vertical guidelines. Field-aligned current directions (R2 in: positive B_Z gradient; and R1 out: negative B_Z gradient) are marked in the ion drift panel.

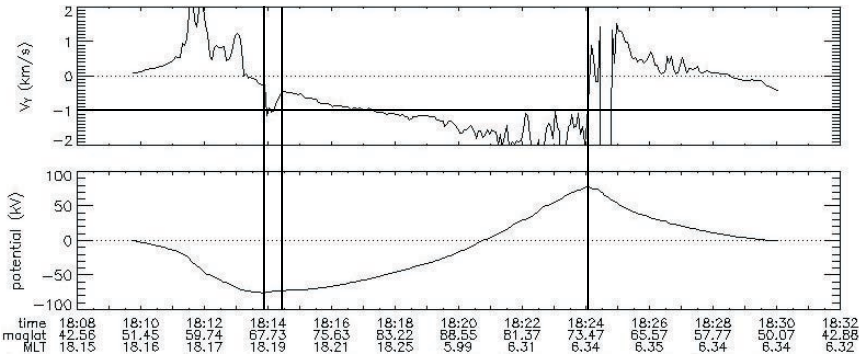

Fig. 13. DMSP F13 cross-track ion drift (V_y) and electrostatic potential curves for the interval 18:08–18:32 UT. Flow channel FC 3 at the dusk side polar cap boundary is marked by the two first guidelines. The third guideline marks the polar cap boundary on the dawn side.

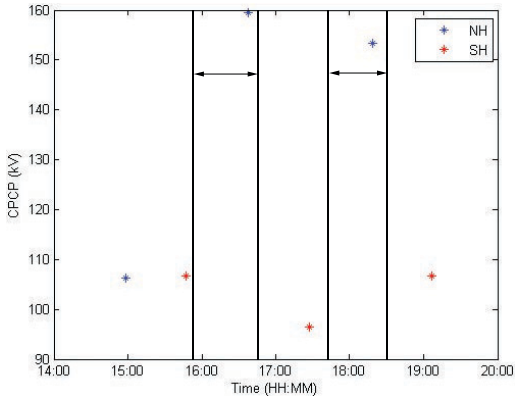

Fig. 14. CPCP estimates derived from F13 cross-track ion drift observations across the polar cap in both hemispheres. Two intervals of enhanced substorm activity are marked by vertical guidelines.

the whole polar cap to obtain CPCP/day. This gives CPCP (pre-event) = 120 kV, which is slightly higher that the result of the first method. The corresponding CPCP/B_z ratio is 20, which is exactly the same value as derived by Yeoman et al. (2002). If this method is used, the consequence is that CPCP/night = 40 kV (33 % increase) in this case.

A questionable point in the last approach is that the pre-event value of CPCP may contain a contribution from CPCP/night since the pre-event conditions (15:50–16:37 UT) are not void of substorm activity which prevails during the interval 15:50–16:40 UT (see Fig. 5).

3.2 On the relative strengths of CPCP/day and CPCP/night

Some studies of the relative contributions of CPCP/day and CPCP/night to the total CPCP (CPCP = CPCP/day + CPCP/night), as measured along the dawn-dusk meridian, have been reported over the last 10 years. Some of these results are summarized below. Grocott et al. (2002) found 100 % CPCP increase associated with an isolated substorm. The CPCP increase occurred during a 15 min interval of the expansion phase, and then decayed to the pre-onset level over ∼10 min during recovery. A similar effect is documented in Provan et al. (2004).

Lockwood et al. (2009) found that CPCP/night makes the larger contribution during the expansion and recovery phases but not in the growth phase when CPCP/day dominates. In his cases the substorm expansion phase typically gave rise to 100 % CPCP increase.

In the statistical study of Kullen et al. (2010) the average substorm response (CPCP/night) represents approx. 40–50 % instantaneous increase of the CPCP at substorm onset. A smaller substorm effect is obtained by Gordeev et al. (2011). In their MHD simulations, substorm onset gives rise to a CPCP increase of approx. 25 %.

Comparing with these previous calculations our estimates of approx. 50 % CPCP increase associated with the substorm activity is comparable to the results of Kullen et al. (2010). Thus, we find that the CPCP/night contribution to CPCP/total during substorms is significantly higher than the estimates of Gordeev et al. (2011), but less than the values obtained by Lockwood et al. (2009).

3.3 Non-traditional dawn-dusk convection asymmetry

The non-traditional dawn-dusk convection asymmetry we find during intervals of substorm activity (see Fig. 13) illustrates that substorms significantly disturb the polar cap convection pattern imposed by the IMF B_y-related magnetopause reconnection geometry (see e.g. Moore et al., 2002) and confirms that magnetopsheric convection is driven by two independent sources. We demonstrate that a substorm-related distortion of the convection pattern is strongly present in our satellite measurements along the dawn-dusk meridian during the interval 18:14–18:24 UT. In this case the dawn-dusk convection asymmetry (enhanced antisunward convection on the dawn side of the polar cap) is opposite to the traditonal B_y negative pattern indicated in Fig. 2. But this is in our view due to a temporal evolution of polar cap convection occurring during the DMSP F13 traversal of the polar cap when the substorm is in progress (see Figs. 13 and 3).

Our result on this point is consistent with the previously published radar observations by Grocott et al. (2010). They found "a lack of IMF B_y-control in the nightside auroral zone. On the dayside each pattern exhibits the expected B_y asymmetry, yet on the nightside the asymmetry is exactly the opposite to that associated with IMF B_y in the absence of substorms."

3.4 Spatial-temporal convection structure: flow channels at the polar cap boundary

The temporal nature of polar cap antisunward flow events is well illustrated by the F13 event at 16:37–16:40 UT (Fig. 9). The correlation with the temporal evolution of the auroral electrojet is demonstrated in Fig. 5.

On the other hand, spatial structure, in the form of enhanced flow near the dawn/dusk side boundaries of the polar cap, is also seen in our data set: (i) dusk-side flow channel in substorm interval 1 (15:55 UT SuperDARN plot in Fig. 7), (ii) dusk-side flow channel in substorm interval 2 (F13 ion drift data at 18:14 UT; Fig. 13), and (iii) dawn-side flow channel in substorm interval 2 (F13 ion drift data during 18:35–18:40 UT when the WEJ intensification was in progress).

Previous studies of flow channels at the nightside polar cap boundary (Wang et al., 2010) reveal relationships with (i) conductivity gradient at the polar cap boundary, (ii) the

degree of solar wind forcing (high E_{KL}), and (iii) solar ionization state ("winter phenomenon").

All these three factors are favourable for flow channel formation in our case. In addition we would like to add one parameter which seems to be favorable too: substorm activity.

Finally, we would like to point out one difference between flow channels FC 2 and FC 3, in addition to the different momentum source in the solar wind-magnetosphere-ionosphere system. The relationship with the FAC configuration may be different. FC 2 is related to ionospheric Pedersen current closure of FACs located poleward of the R1-R2 system, generated in the magnetospheric boundary layers (coupled HBL/LLBL dynamo system) (Sandholt and Farrugia, 2009). In the model of Wang et al. (2010) the FC 3 channel is located immediately poleward of the nightside oval FACs (see Wang et al., 2010, their Figs. 1 and 8). This is also confirmed by our DMSP observations reported in Fig. 12. The F15 ion drift data shows an FC 3 flow channel immediately poleward of the polar cap boundary at 17:46–17:48 UT (centered at 68° MLAT/20 MLT), when the WEJ maximizes at stations AND and SOR (66–67° MLAT). On the latitude profiles of conductivity and E-field (ion drift) at the polar cap boundary during substorms we also refer to Kamide and Kokubun (1996) (see their Fig. 4).

Acknowledgements. Access to the DMSP data base (https://swx.plh.af.mil) was kindly provided by Air Force Geophysics Research Laboratory, Hanscom, Mass through Gordon Wilson. Ground magnetograms from the Svalbard IMAGE chain of ground stations were obtained from http://www.geo.fmi.fi/image. We thank Ari Viljanen and Truls Lynne Hansen for IMAGE chain magnetograms and W. Denig for providing high-quality DMSP F15 data used in Figs. 8 and 12. We thank M. Ruohoniemi and the SuperDARN team for the convection plots. Work at University of Oslo is supported by the Norwegian Research Council (NFR). Work at UNH is supported by NASA grant NNX10AQ29G.

Topical Editor I. A. Daglis thanks W. Denig and another anonymous referee for their help in evaluating this paper.

References

Anderson, B. J., Korth, H., Waters, C. L., Green, D. L., and Stauning, P.: Statistical Birkeland current distributions from magnetic field observations by the Iridium constellation, Ann. Geophys., 26, 671–687, doi:10.5194/angeo-26-671-2008, 2008.

Boyle, C. B., Reiff, P. H., and Hairston, M. R.: Empirical polar cap potentials, J. Geophys. Res., 102, 111–125, 1997.

Burke, W. J., Gentile, L. C., and Huang, C. Y.: Penetration electric fields driving main phase Dst, J. Geophys. Res., 112, A07206, doi:10.1029/2006JA012137, 2007.

Cowley, S. W. H.: Solar wind control of magnetospheric convection, in: Achievements of the International Magnetospheric Study, no. 217 in ESA SP, pp. 483–494, 1984.

Cowley, S. W. H. and Lockwood, M.: Excitation and decay of solar wind-driven flows in the magnetosphere-ionosphere system, Ann. Geophys., 10, 103–115, 1992.

Cowley, S. W. H., Morelli, J. P., and Lockwood, M.: Dependence of convective flows and particle precipitation in the high-latitude dayside ionosphere on the X and Y components of the interplanetary magnetic field, J. Geophys. Res., 96, 5557–5564, 1991.

Gordeev, E. I., Sergeev, V., Pulkkinen, T. I., and Palmroth, M.: Contribution of magnetotail reconnection to the cross-polar cap electric potential drop, J. Geophys. Res., 116, A08219, doi:10.1029/2011JA016609, 2011.

Greenwald, R. A., Ruohoniemi, J. M., Baker, K., Bristow, W. A., Sofko, G. J., Villain, J. P., Lester, M., and Slavin, J.: Convective response to a transient increase in dayside reconnection, J. Geophys. Res., 104, 10007–10015, 1999.

Grocott, A., Cowley, S. W. H., Sigwarth, J. B., Watermann, J. F., and Yeoman, T. K.: Excitation of twin-vortex flow in the nightside high-latitude ionosphere during an isolated substorm, Ann. Geophys., 20, 1577–1601, doi:10.5194/angeo-20-1577-2002, 2002.

Grocott, A., Milan, S. E., and Yeoman, T. K.: Superposed epoch analysis of the ionospheric convection evolution during substorms: IMF B_y dependence, J. Geophys. Res., 115, A00I04, doi:10.1029/2010JA015663, 2010.

Hairston, M. R., Heelis, R. A., and Rich, F. J.: Analysis of the ionospheric cross polar cap potential using DMSP data during the National Space Weather Program study period, J. Geophys. Res., 103, 26337–26347, 1998.

Jørgensen, T. S., Friis-Christensen, E., and Wilhjelm, J.: Interplanetary magnetic field direction and high-latitude ionospheric currents, J. Geophys. Res., 77, 1976–1977, 1972.

Kamide, Y. and Kokubun, S.: Two-component auroral electrojet: importance for substorm studies, J. Geophys. Res., 101, doi:10.1029/96JA00142, 1996.

Kan, J. R. and Lee, L. C.: Energy coupling function and solar wind-magnetosphere dynamo, Geophys. Res. Lett., 6, 577–580, 1979.

Kullen, A., Karlsson, T., Cumnock, J. A., and Sundberg, T.: Occurrence and properties of substorms associated with pseudobreakups, J. Geophys. Res., 115, A12310, doi:10.1029/2010JA015866, 2010.

Lockwood, M. and Cowley, S. W. H.: Ionospheric convection and the convection cycle, in: SUBSORMS 1, no. 335 in ESA - SP, pp. 99–109, 1992.

Lockwood, M., Sandholt, P. E., and Cowley, S. W. H.: Dayside auroral activity and magnetic flux transfer from the solar wind, Geophys. Res. Lett., 16, 33–36, 1989.

Lockwood, M., Hairston, M., Finch, I., and Roillard, A.: Transpolar voltage and polar cap flux during the substorm cycle, J. Geophys. Res., 114, A0120, doi:10.1029/2008JA013697, 2009.

Lopez, R. E.: Solar cycle invariance in solar wind proton temperature relationships, J. Geophys. Res., 92, 11189–11194, 1987.

McComas, D. J., Bame, S. J., Barker, P., Feldman, W. C., Phillips, J. L., Riley, P., and Griffee, J. W.: Solar wind electron proton alpha monitor (SWEPAM) for the Advanced Compostion Explorer, Space Sci. Rev., 86, 563–612, 1998.

Milan, S. E., Lester, M., Cowley, S. W. H., Oksavik, K., Brittnacher, M., Greenwald, R. A., Sofko, G., and Villain, J.-P.: Variations in the polar cap area during two substorm cycles, Ann. Geophys., 21, 1121–1140, doi:10.5194/angeo-21-1121-2003, 2003.

Moore, T. E., Fok, M.-C., and Chandler, M. O.: The dayside reconnection X line, J. Geophys. Res., 107, 1332, doi:10.1029/2002JA009381, 2002.

Muhlbachler, S., Farrugia, C. J., Raeder, J., Biernat, H. K., and Tor-

bert, R.: A statistical investigation of dayside magnetosphere erosion showing saturation of response, J. Geophys. Res., 110, A11207, doi:10.1029/2005JA011177, 2005.

Provan, G., Lester, M., Mende, S. B., and Milan, S. E.: Statistical study of high-latitude plasma flow during magnetospheric substorms, Ann. Geophys., 22, 3607–3624, doi:10.5194/angeo-22-3607-2004, 2004.

Provan, G., Lester, M., Grocott, A., and Cowley, S. W. H.: Pulsed flows observed during an interval of prolonged northward IMF, Ann. Geophys., 23, 1207–1225, doi:10.5194/angeo-23-1207-2005, 2005.

Ruohoniemi, J. M. and Baker, K. B.: Large-scale imaging of high-latitude convection with Super Dual Auroral Radar Network HF radar observations, J. Geophys. Res., 103, 20797–20811, 1998.

Ruohoniemi, J. M. and Greenwald, R. A.: Dependencies of high-latitude plasma convection: Consideration of interplanetary magnetic field, season, and universal time factors in statistical patterns, J. Geophys. Res., 110, A09204, doi:10.1029/2004JA010815, 2005.

Sandholt, P. E. and Farrugia, C. J.: Poleward moving auroral forms (PMAFs) revisited: responses of aurorae, plasma convection and Birkeland currents in the pre- and postnoon sectors under positive and negative IMF B_y conditions, Ann. Geophys., 25, 1629–1652, doi:10.5194/angeo-25-1629-2007, 2007.

Sandholt, P. E. and Farrugia, C. J.: Plasma flow channels at the dawn/dusk polar cap boundaries: momentum transfer on old open field lines and the roles of IMF B_y and conductivity gradients, Ann. Geophys., 27, 1527–1554, doi:10.5194/angeo-27-1527-2009, 2009.

Sandholt, P. E., Farrugia, C. J., Lester, M., Cowley, S. W. H., Milan, S., Denig, W. F., Lybekk, B., Trondsen, E., and Vorobjev, V.: Multistage substorm expansion: Auroral dynamics in relation to plasma sheet particle injection, precipitation, and plasma convection, J. Geophys. Res., 107, 1342, doi:10.1029/2001JA900116, 2002.

Sandholt, P. E., Andalsvik, Y., and Farrugia, C. J.: Polar cap flow channel events: spontaneous and driven responses, Ann. Geophys., 28, 2015–2025, doi:10.5194/angeo-28-2015-2010, 2010.

Sergeev, V. A., Liou, K., Newell, P. T., Ohtani, S.-I., Hairston, M. R., and Rich, F.: Auroral streamers: characteristics of associated precipitation, convection and field-aligned currents, Ann. Geophys., 22, 537–548, doi:10.5194/angeo-22-537-2004, 2004.

Shepherd, S. G., Greenwald, R. A., and Ruohoniemi, J. M.: Cross polar cap potentials measured with Super Dual Auroral Radar Network during quasi-steady solar wind and interplanetary magnetic field conditions, J. Geophys. Res., 107, 1094, doi:10.1029/2001JA000152, 2002.

Siscoe, G. L. and Huang, T. S.: Polar cap inflation and deflation, J. Geophys. Res., 90, 543–547, 1985.

Smith, C. W., L'Heureux, J., Ness, N. F., Acuna, M. H., Burlaga, L. F., and Scheifele, J.: The ACE magnetic fields experiment, Space Sci. Rev., 86, 613–632, 1998.

Southwood, D. J.: The ionospheric signature of flux transfer events, J. Geophys. Res., 92, 3207–3213, 1987.

Tomita, S., Nosé, M., Iyemori, T., Toh, H., Takeda, M., Matzka, J., Bjornsson, G., Saemundsson, T., Janzhura, A., Troshichev, O., and Schwarz, G.: Magnetic local time dependence of geomagnetic disturbances contributing to the AU and AL indices, Ann. Geophys., 29, 673–678, doi:10.5194/angeo-29-673-2011, 2011.

Troshichev, O. A., Podorozhkina, N. A., and Janzhura, A. S.: Invariability of relationship between the polar cap magnetic activity and geoeffective interplanetary electric field, Ann. Geophys., 29, 1479–1489, doi:10.5194/angeo-29-1479-2011, 2011.

Wang, H., Lühr, H., and Ridley, A. J.: Plasma convection jets near the poleward boundary of the nightside auroral oval and their relation to Pedersen conductivity gradients, Ann. Geophys., 28, 969–976, doi:10.5194/angeo-28-969-2010, 2010.

Weimer, D. R.: Models of high-latitude electric potentials derived with a least error fit of spherical harmonic coefficients, J. Geophys. Res., 100, 19595–19608, 1995.

Yeoman, T. K., Hanlon, P. G., and McWilliams, K. A.: Letter to the Editor: A statistical study of the location and motion of the HF radar cusp, Ann. Geophys., 20, 275–280, doi:10.5194/angeo-20-275-2002, 2002.

IV

Ann. Geophys., 30, 1539–1553, 2012
www.ann-geophys.net/30/1539/2012/
doi:10.5194/angeo-30-1539-2012

Annales Geophysicae

The pulsed nature of the nightside contribution to polar cap convection: repetitive substorm activity under steady interplanetary driving

P. E. Sandholt[1], **Y. L. Andalsvik**[1], **and C. J. Farrugia**[2]

[1]Department of Physics, University of Oslo, Oslo, Norway
[2]Space Science Center, University of New Hampshire, Durham, USA

Correspondence to: P. E. Sandholt (p.e.sandholt@fys.uio.no)

Received: 30 March 2012 – Revised: 14 August 2012 – Accepted: 15 September 2012 – Published: 12 October 2012

Abstract. The aim of this study is to investigate the relative contributions of dayside and nightside processes to the spatial and temporal structure of polar cap plasma convection. The central parameter is the cross-polar cap potential (CPCP). Selecting a 10-h-long interval of stable interplanetary driving by an interplanetary CME (ICME), we are able to distinguish between the dayside and nightside sources of the convection. The event was initiated by an abrupt enhancement of the magnetopause (MP) reconnection rate triggered by a southward turning of the ICME magnetic field. This was followed by a long interval (10 h) of steady and strong driving. Under the latter condition a long series of electrojet intensifications was observed which recurred at 50 min intervals. The detailed temporal structure of polar cap convection in relation to polar cap contraction events is obtained by combining continuous ground observations of convection-related magnetic deflections (including polar cap magnetic indices in the Northern and Southern Hemispheres, PCN and PCS) and the more direct, but lower-resolution ion drift data obtained from a satellite (DMSP F13) in polar orbit. The observed PCN enhancements combined with DMSP satellite observations (F13 and F15 data) of polar cap contractions during the evolution of selected substorm expansions allowed us to estimate the CPCP enhancements (25 %) associated with individual events in the series. Ground-satellite conjunctions are further used to investigate the spatial structure of polar cap convection, i.e., the homogeneous plasma flow in the centre ($V_i \leq 1\,\mathrm{km\,s^{-1}}$) versus channels of enhanced antisunward flows ($V_i \geq 1\,\mathrm{km\,s^{-1}}$) along the periphery of the polar cap. We emphasise the temporal structure of these polar cap flow phenomena in relation to the prevailing solar wind forcing and the repetitive substorm activity.

Keywords. Ionosphere (Plasma convection) – Magnetospheric physics (Polar cap phenomena; Solar wind-magnetosphere interactions)

1 Introduction

The two-source nature of polar cap convection is a basic feature of the expansion–contraction model of magnetospheric plasma convection (Siscoe and Huang, 1985; Lockwood et al., 1990; Cowley and Lockwood, 1992). The relative contributions to the cross-polar cap potential (CPCP) from the dayside (CPCP/day) and nightside (CPCP/night) sources during intervals of substorm activity have been studied in recent years, applying different observational techniques (Bristow et al., 2004; Lockwood et al., 2009; Kullen et al., 2010; Gordeev et al., 2011; Andalsvik et al., 2011, 2012).

Fox et al. (1999), Grocott et al. (2002) and Provan et al. (2004) estimated the convection response to isolated substorms by continuous observations, applying a ground-based radar technique. Grocott et al. (2010) studied the convection responses in the dayside and nightside sectors of the polar cap to substorms occurring during intervals of positive and negative interplanetary magnetic field (IMF) B_y polarity, applying a superposed epoch analysis.

Bristow et al. (2004) documented CPCP fluctuations of 20 kV amplitude, as obtained from DMSP satellite ion drift measurements during intervals of steady interplanetary conditions. In the MHD simulation study of Gordeev et al.

(2011) substorm onsets gave rise to rapid, moderate (25 %) CPCP increases in intervals of steady southward-directed IMF. Lockwood et al. (2009) reported a statistical study of CPCP variability in the context of substorm phases. They found that the nightside contribution (CPCP/night) is larger than the dayside source (CPCP/day) in all substorm phases except for the growth phase.

A documentation of polar cap convection in the context of (i) repetitive substorms and (ii) the detailed substructure of substorm evolution, from the pre-breakup arc through breakup and poleward expansion, poleward boundary intensifications (PBIs) and auroral streamers, is lacking at present. A relevant approach to shed light on these issues by direct observations is to select intervals of clearly defined substorms occurring during conditions of quasi-steady solar wind forcing, as measured by the geoeffective interplanetary electric field (E_{KL}; see Kan and Lee, 1979). (E_{KL} is defined as $V B_{\mathrm{T}} \sin^2(\theta/2)$) where $B_{\mathrm{T}} = (B_{\mathrm{y}}^2 + B_z^2)^{1/2}$ in GSM coordinates and θ is the IMF clock angle.) Quasi-steady driving can be observed during Earth passage of interplanetary CMEs (ICMEs), an approach that was first suggested by Farrugia et al. (1993). One can then take advantage of the well-organised behaviour of the magnetic fields in ICMEs (Burlaga et al., 1981; Andalsvik et al., 2012). An increase of the CPCP of about 33 % (from 120 to 160 kV) during the evolution of a substorm, under extremely steady interplanetary CME conditions, was observed by Andalsvik et al. (2012).

The polar cap (PC) index is a measure of equivalent ionospheric convection in the center of the polar cap which is considered to be linearly related to E_{KL} (Troshichev et al., 2000). The general, statistical response of the PC index (in both winter and summer hemispheres) to substorm activity, as measured by the AE/AL-index, has been studied by Janzhura et al. (2007), Kullen et al. (2010) and Gao et al. (2012). In the detailed case study of Kullen et al. (2009) 10 (mostly weak substorms) tail dipolarisations is compared with AE index, PC indices and solar wind parameters. It shows that clear correlations between AE and PC index exist only for substorms with peak AE clearly above 200 nT. Janzhura et al. (2007) found that in the growth phase of substorms the PC index in summer polar cap rises faster and reaches a higher value than in the winter hemisphere. In expansion phase development of substorms the response is strongest in the winter hemisphere. The winter PC index always reflects better the AL-events, independent on whether the winter PC index is measured in the same hemisphere or not. This is a most relevant background for our case study of repetitive substorm activity where we aim at distinguishing between the dayside and nightside sources of the PC index (summer and winter hemispheres) and the CPCP. In this context we also refer to the results of Kullen et al. (2010) who were able to separate the dayside and nightside contributions to the CPCP (CPCP/day and CPCP/night), (see their Fig. 7). We shall get back to these earlier results when discussing our main findings.

A critical point in such studies is to monitor the temporal evolution of polar cap convection and the CPCP with high temporal resolution. The two currently available techniques of direct CPCP measurements, i.e., via satellite ion drift data (Hairston et al., 1998) and ground-based radars (Greenwald et al., 1999; Grocott et al., 2002; Provan et al., 2004), are both incomplete. This is due to the limited temporal resolution of the satellite measurements, on one hand, and the missing spatial coverage at high latitudes of the present radars, on the other. In this study, we shall, therefore, use the polar cap index obtained for the Northern (summer) and Southern (winter) Hemispheres (PCN and PCS) as a proxy for antisunward convection in the near-pole region (Troshichev et al., 2000). For a sub-interval of four hours, including four major AL-excursions, we combine the DMSP F13 ion drift data from the three best polar cap passes, i.e., successive passes that all reach high latitudes, and the PCN-index, in order to to derive a detailed temporal evolution of the CPCP. The result is compared with the Hill-Siscoe formula for the CPCP which is applicable to the prevailing high level of solar wind forcing (see Eq. 1 in Hairston et al., 2003).

Another aim of this study is to follow the detailed evolution of one substorm using very good ground–satellite conjunctions in the dusk to pre-midnight sector. In this approach we apply the combination of passes by satellites DMSP F13 and F15, occurring in different stages of the evolution of this particular substorm. Latitudinal profiles of precipitation, ion drift, and Birkeland currents were obtained in the 18:00–20:00 MLT sector. This information is combined with the evolution of auroral electrojet activity inferred from ground magnetograms. Here we shall take advantage of the wide latitudinal coverage of the ground magnetometer chain (IMAGE) in Svalbard – Scandinavia – Finland (Tomita et al., 2011) in the monitoring of the geomagnetic activity from the polar cap across the auroral oval to mid-latitudes as these stations moved from noon to dusk under similar interplanetary conditions. We shall, thereby, be able to investigate the evolution of the PC indices in the context of the following three latitude regimes of geomagnetic deflection: (i) polar cap convection bays, (ii) westward electrojet (WEJ) deflections (AL-index), and (iii) mid-latitude convection bays.

This dataset allows us to study the detailed evolution of plasma convection in the central polar cap as substorm activity progresses from pre-breakup via the expansion phase, with its series of PBIs and streamers, through recovery (see e.g., Sandholt et al., 2002). From the known association between PBIs/streamers, bursty bulk flows (BBFs) and transient magnetotail reconnection (see e.g., Sergeev et al., 2004; Shi et al., 2012, and Lyons et al., 2012) the expected effect on polar cap convection from such reconnection events can be investigated on the basis of ground data alone. An initial observation of this kind of relationship between substorm evolution and polar cap convection has been recently reported by Andalsvik et al. (2012). Here we follow up with a more detailed analysis of an interval of ICME passage at Earth,

characterised by a long-lasting (10 h), southwest-directed ($B_z < 0$; $B_y < 0$) magnetic field of large amplitude (15 to 17 nT), with the IMF clock angle (polar angle in GSM Y-Z plane) varying around an average value of ∼145°, with corresponding moderate E_{KL} variations within 5.5–7 mV m^{-1}, on 30 May 2005. In this interval a series of electrojet intensifications (AL-excursions to between −1000 and −2000 nT), recurring at 40–120 min intervals, were superimposed on a continuously high disturbance level (AL ≤ −500 nT). From these data we infer that the repetitive substorms gave rise to a pulsed mode of polar cap convection. The pulsing reflects the episodic contribution from the repetitive sequence of substorms.

Concerning the second aspect of our study, i.e., the spatial structure of polar cap convection appearing in the form of flow channels (convection jets) at the boundary of the polar cap in the night sector, these flows are considered to be preferentially a winter phenomenon and associated with conductivity gradients at the polar cap boundary during intervals of high solar wind forcing, as measured by E_{KL} (Wang et al., 2010). Their results are confirmed by the present case study. We observed a strong flow channel with the flow speed reaching 2 km s^{-1} at the polar cap boundary in the Southern (winter) Hemisphere (−74° MLAT/20 MLT). We point out that this flow event is observed at the time of PBI/streamer activity in the same MLT sector in the Northern (summer) Hemisphere. This is an interesting observation which is consistent with the ideas and observations of Andalsvik et al. (2011, 2012), but the relationship between these polar cap flow channel events and substorm activity (substorm onset, PBIs, streamers, and BBFs) is still uncertain and needs further documentation (see e.g., Lyons et al., 2012).

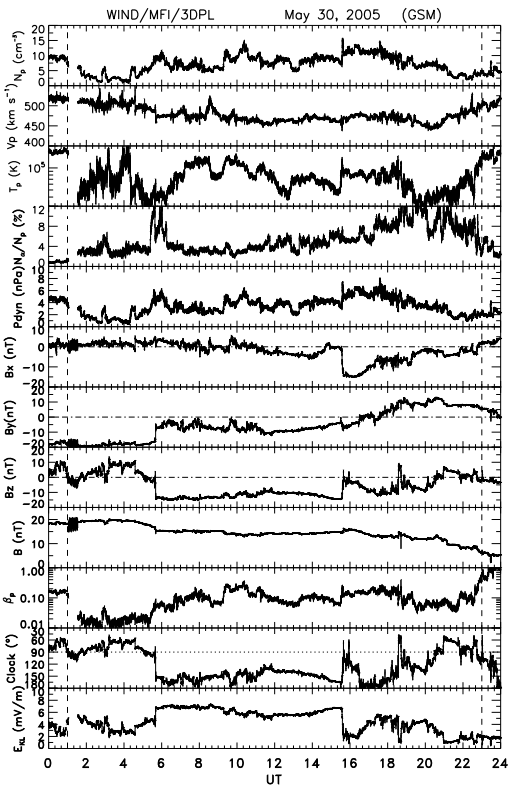

Fig. 1. Interplanetary data from spacecraft Wind on 30 May 2005. Panels from top to bottom shows proton density, bulk speed, proton temperature, alpha/proton number density ratio, dynamic pressure, magnetic field components B_x, B_y, and B_Z (GSM coordinates), the total field, plasma beta, clock angle of the $\boldsymbol{B}$-field, and the reconnection electric field E_{KL}. The ICME interval from 01:00 to 23:00 UT is delimited by the vertical dashed guidelines.

2 Data description

2.1 Wind interplanetary data

Figure 1 shows interplanetary (IP) data from spacecraft Wind during passage of an ICME on 30 May 2005. The ICME extends from 01:00–23:00 UT (Richardson and Cane, 2010). Features of the ICME are (i) strong magnetic fields, (ii) high α particle-to-proton number density ratios, and a low proton β. In the middle of the interval we study (12:00 UT) Wind was located at (225.4, 99.8, 8.0) R_E (GSE coordinates). A clear directional discontinuity (DD) occur at 05:45 UT, when the $\boldsymbol{B}$-field changed orientation from being B_y-dominated to B_z-dominated. This type of DD is often referred to as a southward turning. It is associated with a sharp increase in the α/p density ratio. At this time the geoeffective IP $\boldsymbol{E}$-field, E_{KL}, increased sharply from 4 to 7 mV m^{-1} (see bottom panel). The new south-west orientation is exceptionally stable during the 10-h long interval from 05:40–15:40 UT when E_{KL} stays between 5.5–7 mV m^{-1}. The clock angle of the $\boldsymbol{B}$-field in the GSM Y-Z plane fluctuates between 135–165°.

Among the other relevant IP parameters of this ICME we mention: (i) proton density between 5–10 cm^{-3}, (ii) bulk speed around 475 km s^{-1}, (iii) dynamic pressure between 2–6 nPa, (iv) strong magnetic field (15–20 nT), and (v) low proton beta (β_p).

We shall study the magnetosphere-ionosphere response to (i) the initial southward turning and (ii) the long interval of steady and strong forcing of the magnetosphere following this southward turning, with emphasis on temporal-spatial structure of polar cap convection in relation to substorm activity. The interval selected is particularly interesting for our purpose of investigating the relative contributions of the dayside and nightside magnetospheric sources of spatial-temporal structure of polar cap convection. The dayside source as measured by geoeffective interplanetary

electric field, E_{KL}, increased rapidly at 06:40 UT, taking into account the DD propagation delay (60 min) from Wind to Earth, and then stayed at a relatively constant level (5.5–7 mV m^{-1}) for 10 h. In such a case, it is easy to separate the dayside (magnetopause reconnection) and nightside (magnetotail reconnection) sources of polar cap convection. The level of interplanetary driving from 06:40 UT onwards is at such a high value (5.5–7 mV m^{-1}) that its contribution to dayside magnetic flux erosion and the cross-polar cap potential (CPCP) is expected to approach a level of saturation (Siscoe et al., 2002; Muhlbachler et al., 2005) after the initial phase of R1 field-aligned current build-up (see Siscoe et al., 2011). The magnetosphere-ionosphere response to the enhanced level of magnetopause reconnection rate, with emphasis on ground magnetic deflections in the cusp region and polar cap convection in the near-pole region, as measured by the PC-indices, is a central topic of this study.

2.2 Observation geometry

Figure 2 shows a schematic illustration of the observation geometry with emphasis on the substorm interval 14:40–15:25 UT, which includes passes of spacecraft DMSP F15 (pre-midnight to pre-noon) and F13 (dusk-to-dawn) during the intervals 14:37–14:58 and 15:09–15:24, respectively. The track of spacecraft F15 from pre-noon to pre-midnight in the Southern Hemisphere during the interval 15:32–15:53 UT is marked by the blue dashed arrowed line.

Based on the combined ground-satellite data we have drawn an approximate pattern of large-scale convection (streamlines) as well as electrojet currents and precipitation features observed along the satellite tracks: (i) auroral oval crossing marked by double-arrowed lines, (ii) ion isotropy boundary (arrows), (iii) westward electrojets (WEJ; red) and associated outward-directed FACs in two phases (14:42 and 15:13 UT) of the substorm, (iv) polar cap boundary/boundary intensification (PBI; 15:13 UT)), and (v) flow channel at the polar cap boundary in the south (marked FC 3; blue).

The convection state indicated in the figure was initiated by the rapid southward turning of the ICME magnetic field affecting the Earth's magnetosphere from 06:40 UT onwards. We shall follow the ground magnetic responses to the indicated convection features, as well as the substorm electrojet currents, within the MLAT range 57–75°, as the ground stations in Svalbard – Scandinavia – Finland moved with the Earth from ~10:00 to 19:00 MLT within the interval 06:40–16:30 UT, during the continuous, strong and stable forcing of the magnetosphere by the presence of the large amplitude, south-west directed magnetic field of the ICME.

We selected the interval 14:40–16:10 UT for a detailed study of substorm evolution since (i) this interval is representative for the long interval of repetitive substorms (07:00–20:00 UT), and (ii) in this interval we have a very good coverage of ground-satellite data in the different substorm phases. Recall that we want to study the evolution of polar cap convection (CPCP) in relation to the different substorm phases and substructures (PBIs/streamers).

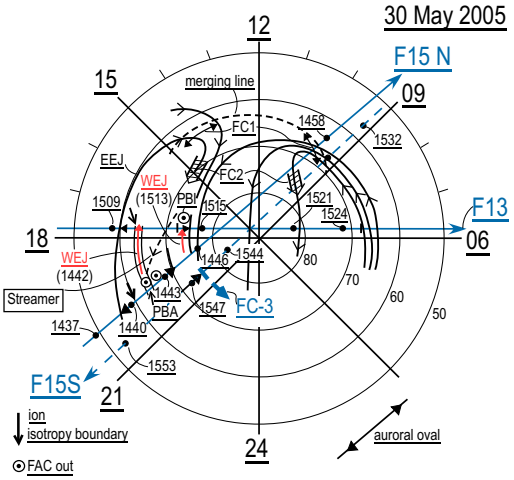

Fig. 2. Illustration of observation geometry on 30 May 2005 with schematic convection pattern and flow channels along the polar cap boundary superimposed. Three satellite passes occurring during different phases of substorm evolution are marked: (i) DMSP F15 (pre-midnight to pre-noon) and DMSP F13 (dusk to dawn) during the intervals 14:37–14:58 and 15:09–15:24 UT, respectively, in the Northern Hemisphere and (ii) one F15 pass in the south (blue dashed line) from pre-noon to pre-midnight during the interval 15:32–15:53 UT. Approximate convection pattern (streamlines) and merging line (dashed curved line) are shown as well as eastward (EEJ) and westward (WEJ; 14:42 and 15:13 UT; red arrows) electrojets and precipitation features at dusk/pre-midnight (isotropy boundary, pre-breakup arc (PBA; 14:43 UT), poleward boundary intensification (PBI; 15:13 UT) observed along the satellite tracks in the north and south (see text for details). FC 3 marks a nightside flow channel ($V_i > 2$ km s^{-1}) at the the polar cap boundary in the south traversed by spacecraft F15 just before 15:47 UT (see data below). Flow channels along the polar cap boundary on the dayside are marked FC 1 (newly open field lines) and FC 2 (old open field lines). The coordinate system is MLAT versus MLT.

The three satellite passes marked in the figure occurred in different stages of substorm evolution in this interval (14:40–16:10 UT): (i) F15 crossed the evening sector oval in the pre-breakup phase (14:40–14:44 UT) and flow channel FC 1 (14:57 UT) at ~10:00 MLT; (ii) F13 crossed the oval at dusk with a poleward boundary arc in the expansion phase (15:09–15:15 UT), and polar cap during 15:15–15:25 UT; and (iii) F15 crossed a flow channel at the polar cap boundary in the pre-midnight sector of the Southern Hemisphere (blue arrow marked FC 3; 15:46 UT) during the late expansion phase.

We remark that flow channels FC 1 and FC 2 represent flows in different stages of the evolution of open field lines

in the Dungey (1961) convection cycle. FC 1 is located on newly open field lines and is accompanied by poleward moving auroral forms (PMAFs) appearing on either side of noon, as documented during winter conditions (Sandholt and Farrugia, 2007). FC 2 is a few 100 km wide channel of enhanced ($>1\,\mathrm{km\,s^{-1}}$) antisunward convection on old open field lines (embedded in polar rain precipitation) along the periphery of the dayside polar cap. This represents the flow excited during an intermediate interval occurring approximately from 10–20 min after magnetopause reconnection, when the open field lines are connected to the solar wind, before these field lines sink into the tail lobes. The fastest flows in this channel are expected to be associated with the large conductivity gradient appearing at the polar cap boundary in the winter hemisphere (Sandholt and Farrugia, 2009). The spatial structure (the $\boldsymbol{E}$-field gradient) in these flows is expected to be less prominent in the summer hemisphere, but the temporal structure, attributed to flux transfer event (FTE) flux tubes moving along the periphery of the polar cap, as first predicted by Southwood (1987), is still prominent even during the summer conditions.

2.3 Ground magnetometer data

Figure 3 shows the geoeffective interplanetary electric field (E_{KL}), the geomagnetic indices PCN (north; summer), PCS (south; winter) and the AL-index. E_{KL} is based on the Wind data given in Fig. 1. Here we added 1 h to the Wind measurements in order to take into account the Wind-to-Earth propagation delay.

The PC-index (in both hemispheres) is a measure of equivalent convection in the near-pole region (Troshichev et al., 2000). It is derived from ground magnetic deflection due to the ionospheric Hall-current associated with plasma convection. Because of the two-source nature of polar cap convection the PC-index is shown to be linearly related to E_{KL} and the AL-index (Gao et al., 2012). It is expressed in the unit of $\mathrm{mV\,m^{-1}}$.

We note the following features: (i) abrupt increase of E_{KL} from 4–7 $\mathrm{mV\,m^{-1}}$ at 06:40 UT, associated with southward turning of the ICME magnetic field; (ii) stable, high level of E_{KL} (5–7 $\mathrm{mV\,m^{-1}}$) during the subsequent 10 h; (iii) initial phase of increasing PC-index from 06:40–07:10 UT; (iv) a series of PCN/PCS enhancements during the interval 07:10–20:00 UT; and (v) a long series of negative AL-excursions (westward electrojet enhancements) during the same interval (07:10–20:00 UT).

The two sources of the PC-index, i.e., E_{KL} and the AL-index, (see Gao et al., 2012), are clearly manifest in this case, i.e., the initial response to the E_{KL} enhancement and the response to the repetitive substorm activity (AL-excursions). The sensitivity to the AL-excursions is observed to be highest in the PCS (winter)-index. A particularly high sensitivity of PCS to AL-events (PCS/night) is observed from 14:40 UT onwards (PCS reaching $\sim$15 $\mathrm{mV\,m^{-1}}$). This seasonal dependence of the AL-response is in good agreement with previous work (Janzhura et al., 2007).

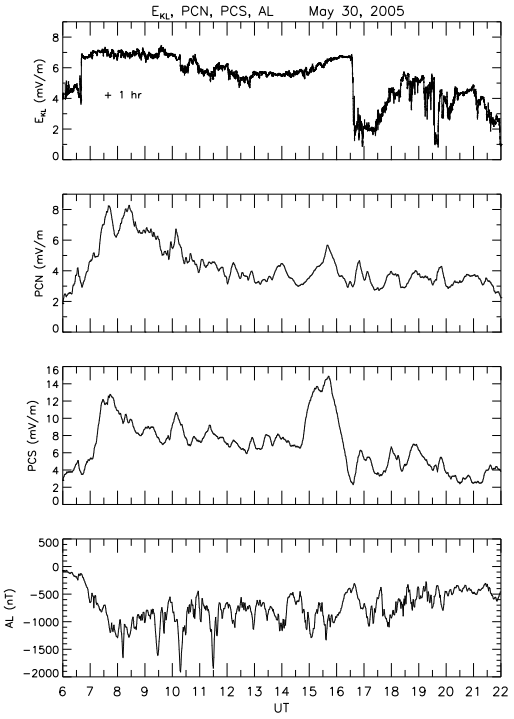

Fig. 3. Panels from top to bottom shows E_{KL} based on observations from spacecraft Wind, the polar cap indices in the Northern (PCN) and Southern (PCS) Hemispheres, and the AL-index (bottom panel) for the interval 06:00–22:00 UT (30 May 2005).

Since the dayside source of polar cap convection, as measured by E_{KL}, is relatively constant after the southward turning, this case is particularly suitable for separating the dayside and nightside sources of polar cap convection. We start by distinguishing between the dayside and nightside sources of the PC index, which we shall refer to as PC/day and PC/night, respectively. PC/night is the component which is related to substorm activity, as measured by the AL-index. The PC/day component may be inferred from the background (inter-substorm) trend that is obtained by subtracting the short-lived, AL-related enhancements in the PC-index traces.

Based on the above reasoning on the two sources of the PC-index and the observed PCN trace we may infer from Fig. 3 a three-stage evolution of the PCN-index: (i) an initial transient phase of PC enhancement with contributions from both dayside (polar cap expansion phase) and nightside sources, (ii) an intermediate phase with decreasing PCN/day component, and (iii) a long interval of relatively constant

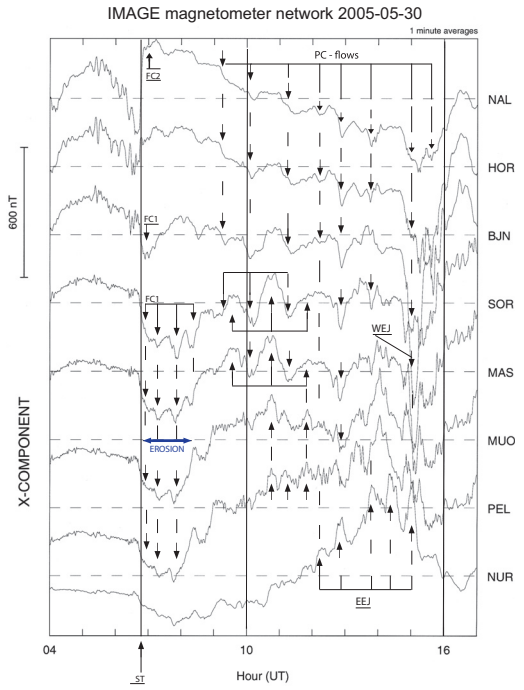

Fig. 4. X-component magnetic deflections from ground stations in Svalbard – Scandinavia – Finland during the interval 04:00–17:00 UT (30 May 2005), ordered by decreasing latitude: NAL (75.2° MLAT), HOR (74.1° MLAT), BJN (71.4° MLAT), SOR (67.3° MLAT), MAS (66.2° MLAT), MUO (64.7° MLAT), PEL (63.6° MLAT), and NUR (56.9° MLAT). Magnetic effects related to specific flow features and electrojet currents have been marked. See text for details.

PCN/day (= 3) with a series of PCN/night events (recurring at 50 min intervals) superimposed from 12:00 UT onwards.

Figure 4 shows X-component magnetic deflections from ground stations in Svalbard – Scandinavia – Finland during the interval 04:00–17:00 UT. We shall point out the following magnetic deflection features, corresponding to different spatial (MLT/MLAT) plasma flow regimes: (i) FC 2 flows in the prenoon polar cap (06:40–08:20 UT/71–75° MLAT), (ii) FC 1 flows at lower latitudes in the cusp region (06:40–08:20 UT/64–67° MLAT), (iii) flows associated with polar cap boundary motions (ground stations being alternatively in positive and negative X-component regimes) in postnoon sector (09:00–12:00 UT; 66–67° MLAT), (iv) substorm-related polar cap flow events (09:00–15:00 UT), and (v) electrojet events in the postnoon-dusk sector from 12:00 UT onwards (polar cap – auroral oval (WEJ) – mid-latitudes (EEJ)).

From the measurements shown in Fig. 4, we may distinguish between magnetic deflection events associated with the dayside magnetopause source of plasma convection (events in the interval 06:40–08:20 UT marked FC 1/FC 2), and events relating to the nightside (magnetotail) source. From the top and bottom panels we infer that the IMAGE chain of stations are increasingly sensitive to the nightside source during the interval 09:00–15:00 UT. The three major AL-deflections in the interval 09:00–12:00 UT (Fig. 3) are well correlated with the oscillating negative/positive X-component deflections appearing in the SOR–MAS (66–67° MLAT) traces in the same interval. This behaviour is indicative of PC boundary motions in the close vicinity of these stations.

The magnetic deflections in the interval 06:40–08:20 UT represent the response to the rapid southward turning of the ICME magnetic field recorded by spacecraft Wind at 05:45 UT whose arrival at Earth is shown by the first vertical guideline. This response consists of (i) large negative X-deflections with the centre expanding equatorward in the MLAT range from 71–65° MLAT (BJN-MUO) and (ii) positive X-deflections expanding equatorward from NAL to BJN (75–71° MLAT). These magnetic effects at ∼10:00 MLT can be explained by the establishment of a convection pattern as shown in Fig. 2 and the corresponding ionospheric Hall currents.

Feature (i) is related to the noonward flow marked FC 1, while the positive X-deflection at NAL (75° MLAT) is related to the antisunward convection near this latitude, marked FC 2 (prenoon) in the NAL magnetogram. From these magnetograms we infer that the convection reversal between the FC 1 and FC 2 flows descended in latitude from that of NAL (75° MLAT) to that of BJN (71° MLAT) during the interval 06:40–07:20 UT. From 07:20 to 08:20 UT station BJN is sensitive to the FC 2 (prenoon) flow regime. After 08:20 UT BJN is increasingly sensitive to FC 3 (substorm-related) events. This is seen in the series of negative X-deflections during the interval 08:20–15:00 UT, as marked in Fig. 4. From the present data, we may infer that the centre of the FC 1/prenoon flows expanded equatorward from ∼71° MLAT (station BJN) to ∼65° MLAT (MAS–MUO) in response to the southward turning.

The observed change in the deflection pattern from 06:40 UT onwards reflects the erosion event and associated polar cap expansion triggered by the rapid southward turning of the ICME magnetic field as it reached Earth. Just before 06:40 UT the polar cap is in a relatively contracted state. This convection state, corresponding to B_y-dominant ICME magnetic field (clock angle of approx. 90°), probably consists of a composite pattern of merging and lobe cells (see e.g., Crooker et al., 1998). The lobe cell is expected to disappear on arrival of the southward turning.

The interval 06:40–08:20 UT is characterised by strong Hall currents (FC 1 flows) maximising at stations MAS–MUO. The corresponding X-component negative bay (centred at ∼65° MLAT, as observed in the 10:00–11:30 MLT sector) is marked "EROSION" in Fig. 4. The convection

pattern shown in the schematic overview figure represents the state of expanded polar cap after the initial erosion event.

Later in the interval of south-west directed ICME magnetic field (09:00 UT onwards), ground deflections associated with the following features (see Fig. 2) can be identified in Fig. 4: (i) mid-latitude positive bays reflecting the eastward electrojet (EEJ) activity from ∼12:00 UT (15:00 MLT) onwards, (ii) the westward electrojet (WEJ) from ∼14:40 UT onwards, and (iii) polar cap flow events (see negative convection bays in NAL and HOR magnetograms) from 09:00 UT (12:00 MLT) onwards, with the nightside source (see the AL-index) dominating.

Concerning the spatial distributions of the different regimes of convection and electrojet currents for the present high disturbance level, we also refer to Feldstein et al. (2006) (see their Fig. 15e). We note that our stations become sensitive to the westward electrojet (WEJ) after 14:40 UT. Next we shall, therefore, focus on the evolution of substorm activity appearing at dusk in the interval 14:40–16:10 UT.

Figure 5 shows X-component ground magnetic records from the same stations in Svalbard – Scandinavia – Finland. Here we place focus on the shorter interval 12:00–17:00 UT and we shall emphasise the substorm evolution during the interval 14:40–16:10 UT which contains the following elements: (i) pre-breakup event (pre-breakup arc/PBA identified in satellite data; see below) at the latitudes of MUO–PEL at 14:43 UT, (ii) poleward boundary intensifications (PBIs; see satellite data below) at HOR – BJN – SOR followed by (iii) streamers (blue tilted lines) during the interval 14:55–16:10 UT. This substorm activity is placed in the context of polar cap flow events as marked in the top panel. These polar cap flow enhancements are inferred from the PCN index (see Fig. 3).

On the association between auroral streamers (equatorward moving auroral forms emanating from poleward boundary intensifications; PBIs) and their ground magnetic signatures we refer to Sandholt et al. (2002). The phenomenon of auroral streamers is a distinct substructure of the substorm process. It is the auroral signature of bursty bulk flows (BBFs) in the magnetotail (see e.g., Sergeev et al., 2004). In Fig. 5 we document the magnetic signature of auroral streamers and their associated convection channels (streamer channels).

Passages of satellite DMSP F15 across the auroral oval poleward boundary in the pre-midnight sector in the north (pre-breakup phase) and in the Southern Hemisphere during the late expansion phase have been marked at the top of the figure.

2.4 DMSP F13 and F15 data

Here we shall report satellite data from two Northern Hemisphere passages and one Southern Hemisphere pass of the auroral oval/polar cap in different stages of substorm evolution.

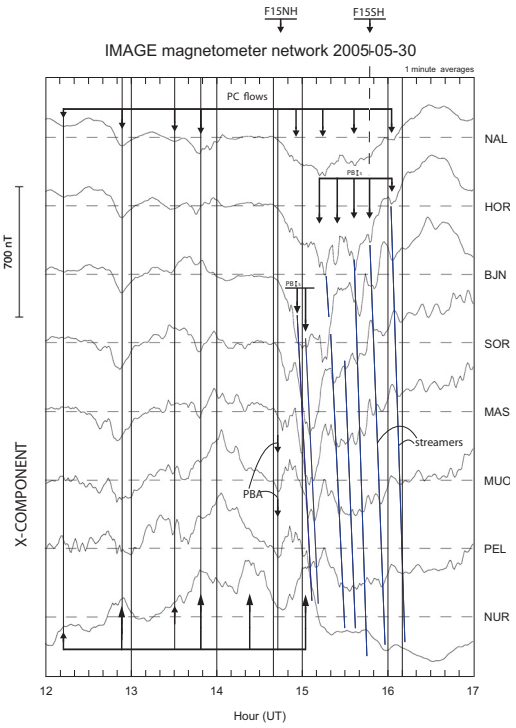

Fig. 5. X-component magnetic deflections from ground stations in Svalbard – Scandinavia – Finland, ordered by decreasing latitude, during the interval 12:00–17:00 UT on 30 May 2005. Various features are marked in the figure: (i) polar cap flow enhancements (upper panel), (ii) poleward boundary intensifications (PBIs) (second and third panels), (iii) auroral streamers (blue tilted lines), (iv) PBA at 14:43 UT and EEJ enhancements (bottom panel). Passes of satellites F15 across the pre-midnight auroral oval in the Northern (NH) and Southern (SH) Hemispheres are marked at the top.

Figure 6 shows DMSP F15 data obtained during the pass from pre-midnight to pre-noon in the interval 14:34–15:04 UT. The track is marked in Fig. 2. The crossing of the oval in the pre-midnight sector occurred in the pre-breakup phase. We draw attention to the following features: (i) ion isotropy boundary (Newell et al., 1996) identified at 60° MLAT (equatorward boundary of zone of homogeneous and isotropic ion precipitation; marked by first vertical guideline), (ii) pre-breakup arc (Sergeev et al., 2012) located at 63° MLAT (14:42 UT), (iii) crossing from oval into the polar cap at 71° MLAT (14:44 UT), and (iv) flow channel at 67–69° MLAT/10 MLT.

Feature (ii) is also marked in Fig. 5. The crossing of this arc marks a perfect ground-satellite conjunction (see magnetograms from stations MUO–PEL in Fig. 5). This arc is located at the flow reversal boundary between the eastward

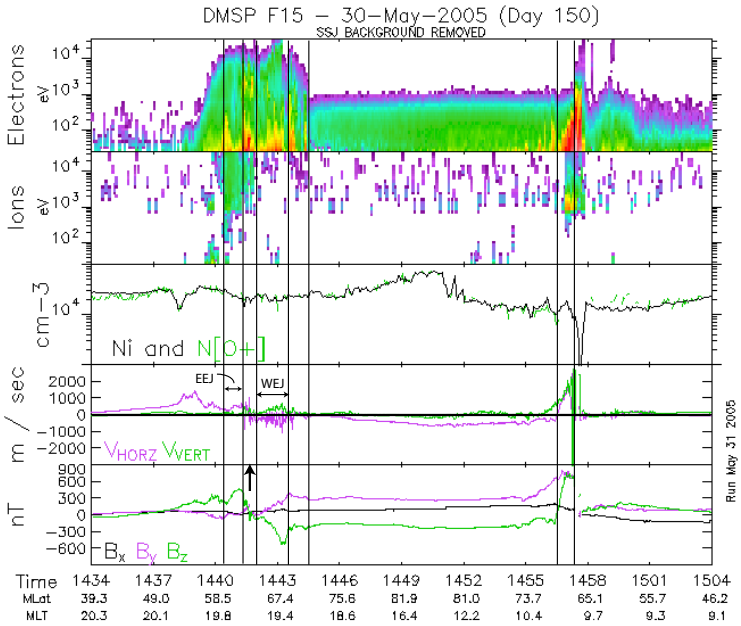

Fig. 6. DMSP F15 data obtained during the pass from pre-midnight to pre-noon in the interval 14:34–15:04 UT. Panels from top to bottom show electron and ion energy spectrograms, ion density, cross-track ion drift (horizontal component in violet), and magnetic deflection components B_X, B_Y, and B_Z (B_Z is the east-west component shown in green). Ion isotropy boundary, pre-breakup arc (PBA), polar cap boundary and flow channel at 67–69° MLAT/10 MLT are marked by vertical guidelines. Latitude regimes of auroral electrojets (EEJ and WEJ) are indicated.

and westward electrojets. According to Sergeev et al. (2012) the pre-breakup arc maps to a magnetospheric location which is close to the earthward-most edge of the thin cross-tail current sheet. The latter magnetotail location maps to the ion isotropy boundary (Newell et al., 1996).

Immediately after 14:42 UT, the AL-index goes negative (Fig. 3; electrojet enhancement) and the PCN index starts the increase from 3 to 4.3 during the interval 14:43–15:15 UT. The latter is an indication of enhanced antisunward convection (Troshichev et al., 2000).

Figure 7 shows DMSP F13 data obtained during the pass from dusk to dawn in the interval 15:03–15:33 UT. The track is marked in Fig. 2.

We note the following: (i) ion isotropy boundary at 63.8° MLAT, (ii) poleward boundary arc at 72–74° MLAT traversed at 15:13 UT (at the time of auroral streamer signatures in the local magnetograms), and (iii) strong homogeneous antisunward convection (1 km s^{-1}) across the central polar cap.

The poleward boundary arc (15:13 UT; 72–74° MLAT) is accompanied by outward-directed Birkeland current as inferred from the negative B_Z-gradient in the bottom panel of Fig. 7. The Birkeland current and the westward electrojet associated with this poleward boundary intensification (PBI; see negative X-deflections at stations HOR and BJN) have been marked in Fig. 2.

Figure 8 shows F15 data obtained during the Southern Hemisphere pass from pre-noon to pre-midnight in the interval 15:26–15:56 UT. The track is marked in Fig. 2. We notice the presence of an FC 3 flow channel (flow speed approaching 2 km s^{-1}) at the polar cap boundary traversed at 15:46 UT. This flow channel, which is marked in Fig. 2, occurred during the substorm phase characterised by auroral streamer activity (see Fig. 5).

2.5 The cross-polar cap potential

Figure 9 shows successive DMSP F13 tracks in the north and south and cross-track ion drifts for the interval 13:30–18:00 UT. These passes are the most suitable for CPCP estimates on this day since they reach such high latitudes that relevant CPCP values may be derived (see criteria in Hairston et al., 1998). We notice the contrast between the relatively homogeneous antisunward convection at 1 km s^{-1} in the summer hemisphere and the more inhomogeneous flows in the winter hemisphere, characterised by channels of enhanced (1–2 km s^{-1}) flows along the periphery of the

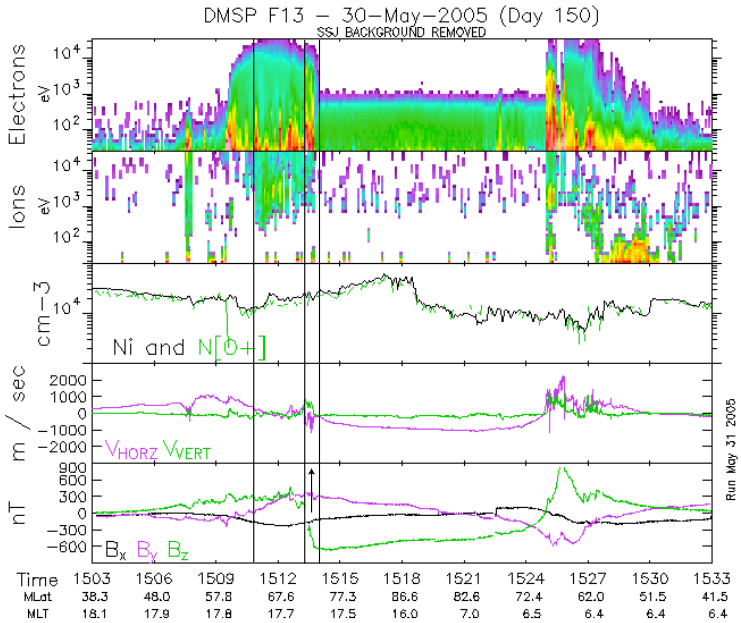

Fig. 7. DMSP F13 data obtained during the pass from dusk to dawn in the interval 15:03–15:33 UT on 30 May 2005. Same format as in Fig. 6.

polar cap. The CPCP values derived for the three NH passes are: 159 (13:37 UT), 127 (15:18 UT) and 147 kV (16:59 UT). These values are plotted in the next figure where we shall use the PCN index to interpolate between the three DMSP F13 data points for the purpose of obtaining an estimate of the more detailed temporal variability of the CPCP in this interval.

Figure 10 shows an estimate of the CPCP development during the interval 13:00–17:00 UT. This is based on ion drift data (circled crosses) from the three best Northern Hemisphere passes of satellite DMSP F13 in our interval of study (see Fig. 9). The F13 data points at 13:37, 15:18, and 16:59 UT refer to the centre times of polar cap crossings. PCN index values shown at selected times (dots) illustrate the trend in the variation of the polar cap convection in this interval.

The CPCP estimates in Fig. 10 are based on the following assumptions (approximations): (i) homogeneous polar cap convection (see Fig. 9), (ii) the approximate empirical relationship between CPCP and PCN applicable to the interval from 12:00 UT onwards (persistent phase of solar wind-magnetosphere coupling): CPCP (V) = 10 PCN (mV m^{-1}) × L_{PC} (km), where L_{PC} is the cross-polar cap distance in the dawn-dusk direction, and (iii) fluctuations of L_{PC} from ∼3000 to 4000 km (see Fig. 9).

The observed PCN-fluctuations (3–6 mV m^{-1}) and the estimated CPCP fluctuations (120–180 kV) during the interval 13:00–16:30 UT occurred at the time of relatively steady interplanetary driving, as given by E_{KL} (slowly increasing from 5.5 to 7 mV m^{-1}). We notice that all three CPCP maxima are associated with negative AL-excursions (westward electrojet events). AL-recoveries during the intervals 14:10–14:40 and 15:50–16:40 UT are accompanied by significant PCN (and PCS) decreases.

The L_{PC} scale on the right-side axis of Fig. 10 gives the L_{PC} values which corresponds to the CPCP values marked on the left side axis if we apply the empirical relationship given in point (ii) above. The CPCP variability can then be expressed as: $\Delta CPCP/CPCP = \Delta PCN/PCN + \Delta L_{PC}/L_{PC}$, for the prevailing conditions of steady solar wind forcing. According to the expansion–contraction model, PCN and L_{PC} are expected to vary in counter-phase, i.e., PCN enhancements are accompanied by polar cap contractions. This association is confirmed in our case. The estimated range of CPCP variations in Fig. 10 (120–180 kV) are consistent with PCN and L_{PC} variations between 3–6 mV m^{-1} and 4000–3200 km, respectively. Related to this we note that the latitudes of the dusk-side polar cap boundary crossings of satellites DMSP F15 and F13 at 14:44 and 15:14 UT correspond to different stages of substorm evolution. The two boundary crossings occurred at 71° MLAT in the breakup phase (F13

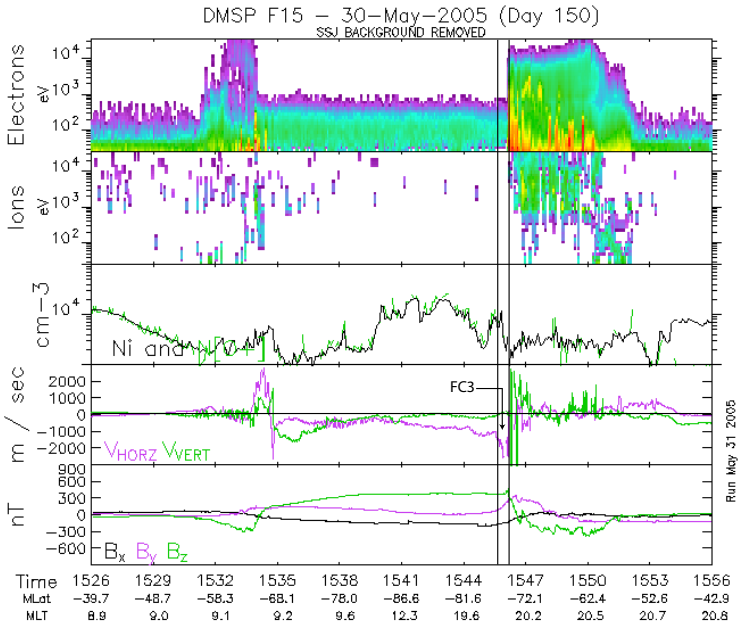

Fig. 8. DMSP F15 data obtained during the Southern Hemisphere pass from pre-noon to pre-midnight in the interval 15:26–15:56 UT on 30 May 2005. Same format as in Fig. 6.

at 14:44 UT) and 74° MLAT, well into the expansion phase (F13 at 15:14 UT), respectively, and they where close in MLT (see the geometry in Fig. 2). From this observation we infer that the interval between these two crossings is characterised by a significant polar cap contraction, as expected during the substorm expansion phase.

From the above considerations we obtain the following estimates of CPCP average increases occurring during the individual events in the series of PCN-enhancements (substorm expansions) from 3 to 4.5 mV m^{-1} (with corresponding L_{PC} decreases) in our case (see the interval from 12:00 UT onwards in Fig. 1): 120–150 kV.

In Fig. 11 we plot E_{KL} and the Hill-Siscoe cross-polar cap potential ($\Phi_{H\text{-}S}$) for our case. Both expressions are based on interplanetary parameters given in Fig. 1. Quantity $\Phi_{H\text{-}S}$ depends on E_{KL}, the conductance (Σ_P), and the solar wind dynamic pressure. The curves in the middle and bottom panels of the figure show results for ionospheric conductance values $\Sigma_P = 5$ and 10 mhos, respectively. $\Phi_{H\text{-}S}$ is taken from Eq. (1) in Hairston et al. (2003) and it takes into account the possible CPCP saturation appearing at high levels of interplanetary driving ($E_{KL} > 5$ mV m^{-1}). In the interval we study in detail (13:00–17:00 UT) $\Phi_{H\text{-}S}$ increases slightly from 110–115 (150–170) kV, when applying $\Sigma_P = 10$ (5) mhos, before the abrupt decrease associated with the northward turning of the ICME magnetic field affecting Earth from ~16:40 UT onwards.

The three CPCP values measured by DMSP F13 in the interval 13:00–17:00 UT were 159, 127, and 147 kV. These values typically lie between the $\Phi_{H\text{-}S}$ ($\Sigma_P = 10$ mho) and $\Phi_{H\text{-}S}$ ($\Sigma_P = 5$ mho) curves. One exception is the CPCP value derived from the F13 ion drift measurements centred at 16:59 UT, which did not reflect the E_{KL} drop estimated to occur at 16:40 UT. The convection response to the abrupt E_{KL} decrease is seen in the PCS (winter) index but not in PCN (summer). Reduced polar cap convection velocities are also seen in the Southern Hemisphere data at 17:47 UT (see the bottom right panel in Fig. 9).

We note that the Hill-Siscoe potential shows smooth and small variations which are closely related to the corresponding smooth and small changes of the interplanetary parameters (E_{KL}). $\Phi_{H\text{-}S}$ ($\Sigma_P = 10$ mho) represents a good estimate of the background inter-substorm level of polar cap convection in the persistent phase of our case.

3 Discussion

Contrary to most previous studies of the convection response to magnetospheric substorms, emphasising intervals of isolated substorms (see Introduction), we focus here on the phenomenon of repetitive substorm expansions. In a

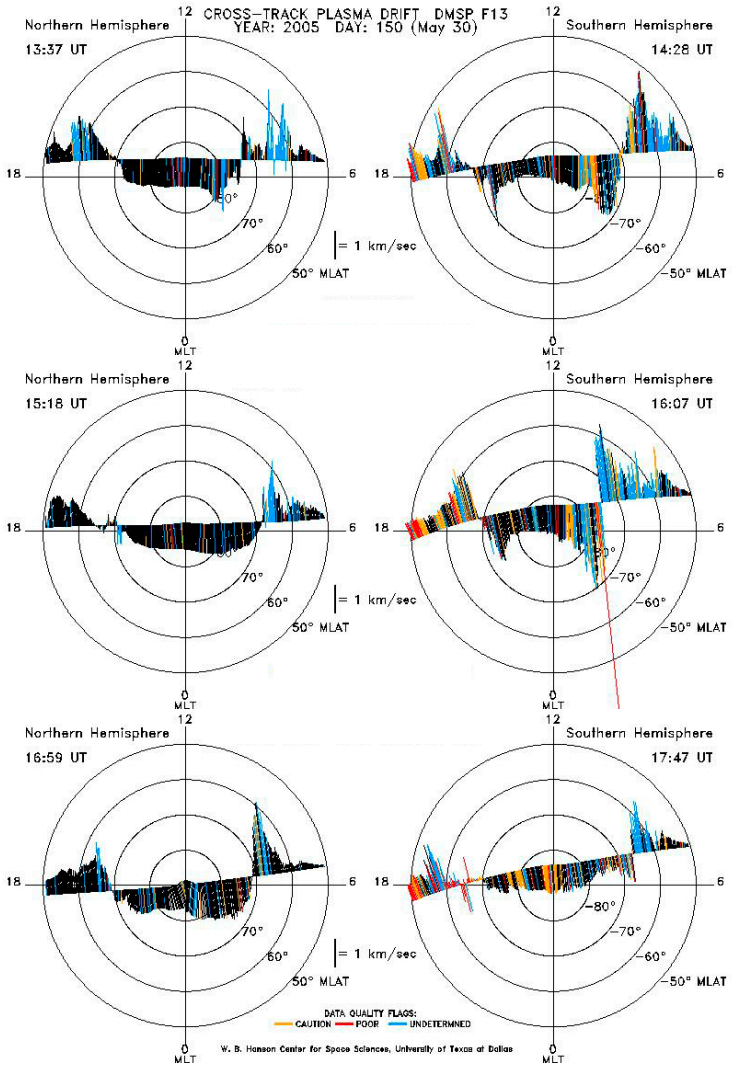

Fig. 9. DMSP F13 cross-track ion drifts on 30 May 2005 obtained during consecutive passes of the polar cap in the Northern (summer; left panels) and in the Southern (winter; right panels) Hemispheres during the interval 13:30–18:00 UT. The centre times of each polar cap crossing are given. The coordinate system is MLAT/MLT.

ground-satellite conjunction study we documented a mode of 50 min period pulsed polar cap convection (PC-index fluctuations) driven by the repetitive substorm activity characterised by ∼15-min-long, major electrojet intensifications. We apply the 1 min resolution PC-index as a continuous monitor of the detailed temporal evolution of polar cap convection (Troshichev et al., 2000). This indirect information (equivalent convection) from the central polar cap is combined with the more direct, but at lower resolution, ion drift data obtained from satellites in polar orbit. This combination of different datasets is used to estimate the CPCP temporal variability for a selected time interval of the several hours long repetitive substorm activity. Our estimate of a 30 kV CPCP enhancement (25 %) during the individual substorm expansions in this case study compares well with the MHD simulation results of Gordeev et al. (2011).

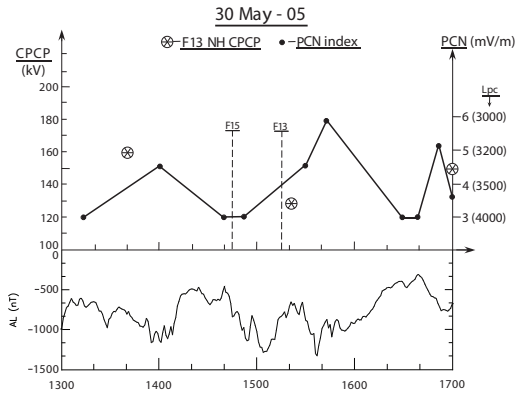

Fig. 10. The top panel shows CPCP estimates during the interval 13:00–17:00 UT on 30 May 2005 as derived from DMSP F13 cross-track ion drifts (circled crosses at 13:37, 15:18, and 16:59 UT) and the trend of the PCN-index (dots) taken from Fig. 3. The AL-index is shown in the bottom panel. Crossings of the dusk-side polar cap boundary by satellites F15 at 14:44 UT (71° MLAT) and F13 at 15:14 UT (74° MLAT) are indicated.

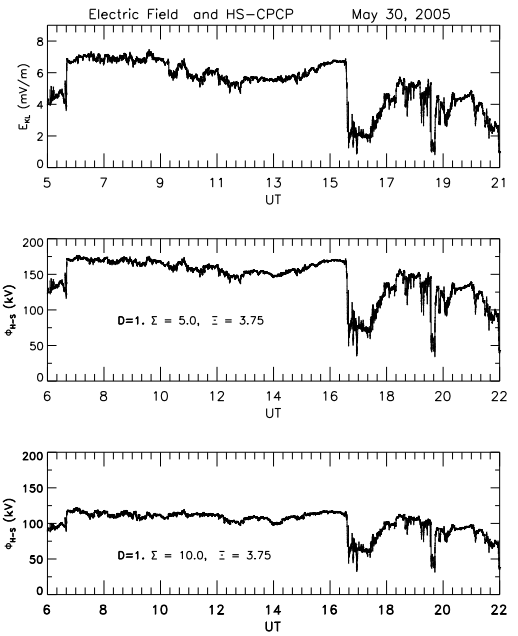

Fig. 11. The geoeffective interplanetary $\boldsymbol{E}$-field (E_{KL}) and Hill-Siscoe CPCPs ($\Phi_{H\text{-}S}$) during the interval 06:00–22:00 UT on 30 May 2005. $\Phi_{H\text{-}S}$ is taken from Eq. (1) in Hairston et al. (2003). Hill-Siscoe potentials are calculated for the two ionospheric conductance values $\Sigma_P = 5$ mho (second panel) and 10 mho (bottom).

This interval was initiated by an abrupt enhancement of E_{KL} from 4 to 7 mV m^{-1} associated with the southward turning of the ICME magnetic field recorded by Wind at 05:40 UT. The general response to abrupt E_{KL}-enhancements are divided into two phases, as suggested by Siscoe et al. (2011): (i) an initial transient phase of dayside magnetic flux erosion and the build-up of the dayside R1 current system with associated plasma convection enhancement, and (ii) a long persistent phase characterised by repetitive substorm activity accompanied by convection events. From the PCN trace in our case we may distinguish between three phases: (i) initial transient phase (PCN/day increase), (ii) intermediate phase (PCN/day decreasing from 6 to 3), and (iii) persistent phase with steady PCN/day component (PCN/day = 3) and repetitive PCN/night enhancements from 12:00 UT onwards.

The case of repetitive substorm activity occurred during a 10-h-long interval of continuously high solar wind forcing associated with the ICME Earth passage on 30 May 2005. The series of PC-index enhancements occurring on time scales of the electrojet intensifications is attributed to the nightside source of polar cap convection. Our separation of the PC index into a component driven by the dayside convection source (PC/day) and another component driven by the nightside source (PC/night) is consistent with the results of Kullen et al. (2010) on the separation of the dayside and nightside contributions to the CPCP, CPCP/day and CPCP/night (see their Fig. 7).

The response of the PC-index (fluctuations) to substorm activity (AL-events) is even larger in the winter (PCS-index) than in the summer hemisphere, consistent with the results of Janzhura et al. (2007) and Troshichev and Janzhura (2009). Like us, Troshichev and Janzhura (2009) reported a study of the PC-index where they included intervals of repetitive substorm activity appearing when E_{KL} reached 5–6 mV m^{-1}. We emphasise the role of the nightside source of polar cap convection, as predicted by the expansion–contraction model of polar cap convection (Siscoe and Huang, 1985; Cowley and Lockwood, 1992). The latter perspective is lacking in Troshichev and Janzhura (2009).

The AL-events we study show some characteristics in common with the so-called sawtooth events (SEs) (Henderson et al., 2006), i.e., their quasi-periodicity and occurrence during intervals of continuously moderate-to-strong interplanetary forcing. The ∼50 min average recurrence period observed in our case, is, however, different from the 2–4 h periods of recurring SEs that has been reported in the literature (see e.g., Henderson et al., 2006, and Huang, 2011). The short recurrence period in our case may be due to the short or absent growth phase as has been pointed out in relation to similar cases documented by Troshichev and Janzhura (2009). According to Huang (2011) substorms may be triggered by moderate solar wind dynamic pressure pulses if the

magnetotail lobe flux lies at a critical level of 1 GWb. We notice the presence of repetitive pressure pulses in our case (see Fig. 1).

We selected the sub-interval 14:40–16:30 UT for a detailed study of polar cap convection during the evolution of the substorm, since (i) this interval is representative for the long interval of repetitive substorm activity, and (ii) there is very good coverage of ground-satellite data in the different substorm phases. This allowed us to document the detailed association between polar cap contraction and convection enhancement during the substorm expansion phase. The amplitude of the fluctuations in the estimated CPCP (∼120–180 kV) we obtained during the slowly increasing IP driving ($E_{KL} = 5.5$–$7\,mV\,m^{-1}$) in the interval 13:00–16:30 UT is larger than observed in previous studies that are restricted to lower levels of external forcing ($E_{KL} \leq 3\,mV\,m^{-1}$; see Bristow et al., 2004). The estimated 25 % CPCP enhancements in response to individual substorm expansions in our case are not captured by the Hill-Siscoe formula (Hairston et al., 2003) which is based on interplanetary parameters and ionospheric conductivity.

During winter conditions, when large conductivity gradients are present at the polar cap boundary, the condition of enhanced antisunward convection in the night sector of the polar cap is expected to give rise to flow channel FC 3 (see Andalsvik et al., 2011, their Fig. 1). This is exactly what we observed by spacecraft DMSP F15 when it traversed the nightside polar cap boundary in the Southern Hemisphere at 15:46 UT, in the late expansion phase, in our case (see Fig. 8). This observation confirms the previous results of Wang et al. (2010), demonstrating that these events occur in intervals of enhanced E_{KL} in winter. Furthermore, we postulate that these flows at the nightside polar cap boundary are also enhanced by substorm activity. This is a natural consequence of the two-source nature of polar cap convection. The two sources are dayside (magnetopause) and nightside (magnetotail) reconnection processes. The FC 3 flow channel observation at 15:46 UT occurred at the time of auroral streamer activity as inferred from the magnetograms in Fig. 5. On the association between auroral and magnetic signatures of streamers we refer to Sandholt et al. (2002).

Auroral streamers have been demonstrated to be an ionospheric signature of localised magnetotail magnetic field dipolarizations and bursty bulk flows (BBFs) (Sergeev et al., 2004; Lyons et al., 2012). It is likely that such smaller scale dipolarizations (compared to substorm onset events) also give rise to enhanced $\boldsymbol{E}$-fields in the tail lobe, such as observed by Sauvaud et al. (2012) at substorm onsets. The role of Earthward-propagating dipolarisation front flow bursts within $X = -20$ to $-10\,R_E$ as a basic element (substructure) in the substorm process in the magnetotail is emphasized by Lyons et al. (2012). On the association between dipolarization of flux tubes, inward transport of flux from the tail, and the generation of twin-cell flow in the ionosphere we refer to the review paper by Cowley (2000) and the recent simulation results of Yang et al. (2012).

Our study of the substructure of one substorm interval documented the presence of auroral streamer activity, as inferred from the ground magnetograms (series of equatorward-moving X-component deflections), and a polar cap flow channel (F13/F15 ion drift data) in the winter hemisphere. These observations may indicate a relationship between Earthward-moving magnetotail dipolarisation fronts/BBFs (Lyons et al., 2012) and the activation of ionospheric convection channel events along the nightside polar cap boundary (our FC 3; marked in Fig. 2).

4 Summary

In a case study, we documented interesting spatial and temporal structure of polar cap convection during a long interval of strong and steady interplanetary driving. This was characterised by a series of substorm expansions – polar cap contractions recurring at ∼50 min intervals. The temporal structure consists of quasi-periodic enhancements of antisunward convection associated with the repetitive substorm expansions. The convection response to these substorms is observed in both the summer and winter hemispheres, but it is larger in the winter hemisphere (ΔPCS/PCS > ΔPCN/PCN). The observed behaviour of polar cap contraction and convection enhancement can be explained by the two-component expansion–contraction model of plasma convection. A combination of ground and satellite observations allowed us to estimate typical (average) CPCP enhancements of ∼30 kV (25 %) occurring in the Northern (summer) Hemisphere (PCN-enhancements from 3 to $4.5\,mV\,m^{-1}$) associated with the individual polar cap contraction events in the series of substorm expansions in the persistent phase of solar wind-magnetosphere coupling. The spatial convection structure we emphasize consists of flow channels along the nightside polar cap boundary which is restricted to the winter hemisphere in this case. Plasma flows in these channels are possibly enhanced during the intervals of substorm expansion.

Acknowledgements. We thank the World Data Center in Kyoto, Japan for providing PCN index and O. Troshichev for providing us with PCS data. Access to the DMSP data base was kindly provided by Kevin Martin of Boston College (https://dmsp.isr.bc.edu). Ground magnetograms from the Svalbard IMAGE chain of ground stations were obtained from http://www.geo.fmi.fi/image. We thank Truls Lynne Hansen and Ari Viljanen for operating the IMAGE chain magnetometers. We thank both referees for constructive criticism. Work at University of Oslo is supported by the Norwegian Research Council (NFR). Work at UNH is supported by NASA grant NNX10AQ29G.

Topical Editor R. Nakamura thanks A. Kullen and one anonymous referee for their help in evaluating this paper.

References

Andalsvik, Y. L., Sandholt, P. E., and Farrugia, C. J.: Dayside and nightside contributions to cross-polar cap potential variations: the 20 March 2001 ICME case, Ann. Geophys., 29, 2189–2201, doi:10.5194/angeo-29-2189-2011, 2011.

Andalsvik, Y., Sandholt, P. E., and Farrugia, C. J.: Substorms and polar cap convection: the 10 January 2004 interplanetary CME case, Ann. Geophys., 30, 67–80, doi:10.5194/angeo-30-67-2012, 2012.

Bristow, W. A., Greenwald, R. A., Shepherd, S. G., and Hughes, J. M.: On the observed variability of the cross-polar cap potential, J. Geophys. Res., 109, A02203, doi:10.1029/2003JA010206, 2004.

Burlaga, L. F., Sittler, E., Mariani, F., and Schwenn, R.: Magnetic loop behind an interplanetary shock: Voyager, Helios, and IMP-8 observations, J. Geophys. Res., 86, 6673–6684, 1981.

Cowley, S. W. H.: Magnetosphere-ionosphere interactions: A tutorial review, in: Magnetospheric Current Systems, Geophysical Monograph Series, vol. 118, pp. 91–106, AGU (American Geophysical Union), Washington D.C., USA, 2000.

Cowley, S. W. H. and Lockwood, M.: Excitation and decay of solar wind-driven flows in the magnetosphere-ionosphere system, Ann. Geophys., 10, 103–115, 1992.

Crooker, N. U., Lyon, J. G., and Fedder, J. A.: MHD model merging with IMF B_y: Lobe cells, sunward polar cap convection, and overdraped lobes, J. Geophys. Res., 103, 9143–9151, 1998.

Dungey, J. W.: Interplanetary magnetic field and the auroral zones, Phys. Rev. Lett., 6, 47–48, 1961.

Farrugia, C. J., Freeman, M. P., Burlaga, L. F., Lepping, R. P., and Takahashi, K.: The Earth's magnetosphere under continued forcing: Substorm activity during the passage of an interplanetary magnetic cloud, J. Geophys. Res., 98, 7657–7671, 1993.

Feldstein, Y. I., Popov, V. A., Cumnock, J. A., Prigancova, A., Blomberg, L. G., Kozyra, J. U., Tsurutani, B. T., Gromova, L. I., and Levitin, A. E.: Auroral electrojets and boundaries of plasma domains in the magnetosphere during magnetically disturbed intervals, Ann. Geophys., 24, 2243–2276, doi:10.5194/angeo-24-2243-2006, 2006.

Fox, N. J., Cowley, S. W. H., Davda, V. N., Enno, G., Friis-Christensen, E., Greenwald, R. A., Hairston, M. R., Lester, M., Lockwood, M., Lühr, H., Milling, D. K., Murphree, J. S., Pinnock, M., and Reeves, G. D.: A multipoint study of a substorm occurring on 7 December, 1992, and its theoretical implications, Ann. Geophys., 17, 1369–1384, doi:10.1007/s00585-999-1369-6, 1999.

Gao, Y., Kivelson, M. G., Walker, R. J., and Weygand, J. M.: Long-term variation of driven and unloading effects on polar cap dynamics, J. Geophys. Res., 117, A02203, doi:10.1029/2011JA017149, 2012.

Gordeev, E. I., Sergeev, V., Pulkkinen, T. I., and Palmroth, M.: Contribution of magnetotail reconnection to the cross-polar cap electric potential drop, J. Geophys. Res., 116, A08219, doi:10.1029/2011JA016609, 2011.

Greenwald, R. A., Ruohoniemi, J. M., Baker, K., Bristow, W. A., Sofko, G. J., Villain, J. P., Lester, M., and Slavin, J.: Convective response to a transient increase in dayside reconnection, J. Geophys. Res., 104, 10007–10015, 1999.

Grocott, A., Cowley, S. W. H., Sigwarth, J. B., Watermann, J. F., and Yeoman, T. K.: Excitation of twin-vortex flow in the nightside high-latitude ionosphere during an isolated substorm, Ann. Geophys., 20, 1577–1601, doi:10.5194/angeo-20-1577-2002, 2002.

Grocott, A., Milan, S. E., and Yeoman, T. K.: Superposed epoch analysis of the ionospheric convection evolution during substorms: IMF B_y dependence, J. Geophys. Res., 115, A00I04, doi:10.1029/2010JA015663, 2010.

Hairston, M. R., Heelis, R. A., and Rich, F. J.: Analysis of the ionospheric cross polar cap potential using DMSP data during the National Space Weather Program study period, J. Geophys. Res., 103, 26337–26347, 1998.

Hairston, M. R., Hill, T. W., and Heelis, R. A.: Observed saturation of the ionospheric polar cap potential during the 31 March 2001 storm, Geophys. Res. Lett., 30, 1325, doi:10.1029/2002GL015894, 2003.

Henderson, M. G., Skoug, R., Donovan, E., Thomsen, M. F., Reeves, G. D., Denton, M. H., Singer, H. J., McPherron, R. L., Mende, S., Immel, T. J., Sigwarth, J. B., and Frank, L. A.: Substorms during the 10–11 August 2000 sawtooth event, J. Geophys. Res., 111, A06206, doi:10.1029/2005JA011366, 2006.

Huang, C.-S.: Relation between magnetotail magnetic flux and changes in the solar wind during sawtooth events: Towards resolving the controversy of whether all substorms are externally triggered, J. Geophys. Res., 116, A04202, doi:10.1029/2010JA016371, 2011.

Janzhura, A., Troshichev, O., and Stauning, P.: Unified PC indices: Relation to isolated magnetic substorms, J. Geophys. Res., 112, A09207, doi:10.1029/2006JA012132, 2007.

Kan, J. R. and Lee, L. C.: Energy coupling function and solar wind-magnetosphere dynamo, Geophys. Res. Lett., 6, 577–580, 1979.

Kullen, A., Ohtani, S., and Karlsson, T.: Geomagnetic signatures of auroral substorms preceded by pseudobreakups, J. Geophys. Res., 114, A04201, doi:10.1029/2008JA013712, 2009.

Kullen, A., Karlsson, T., Cumnock, J. A., and Sundberg, T.: Occurrence and properties of substorms associated with pseudobreakups, J. Geophys. Res., 115, A12310, doi:10.1029/2010JA015866, 2010.

Lockwood, M., Cowley, S. W. H., and Freeman, M. P.: The excitation of plasma convection in the high-latitude ionosphere, J. Geophys. Res., 95, 7961–7972, 1990.

Lockwood, M., Hairston, M., Finch, I., and Roillard, A.: Transpolar voltage and polar cap flux during the substorm cycle, J. Geophys. Res., 114, A0120, doi:10.1029/2008JA013697, 2009.

Lyons, R. L., Nishimura, Y., Xing, X., Runov, A., Angelopoulos, V., Donovan, E., and Kikuchi, T.: Coupling of dipolarisation front flow bursts to substorm expansion phase phenomena within the magnetosphere, J. Geophys. Res., 117, A02212, doi:10.1029/2011JA017265, 2012.

Muhlbachler, S., Farrugia, C. J., Raeder, J., Biernat, H. K., and Torbert, R.: A statistical investigation of dayside magnetosphere erosion showing saturation of response, J. Geophys. Res., 110, A11207, doi:10.1029/2005JA011177, 2005.

Newell, P. T., Feldstein, Y. I., Y., and Meng, C.-I.: Morphology of nightside precipitation, J. Geophys. Res., 101, 10737–10748, 1996.

Provan, G., Lester, M., Mende, S. B., and Milan, S. E.: Statistical study of high-latitude plasma flow during magnetospheric substorms, Ann. Geophys., 22, 3607–3624, doi:10.5194/angeo-22-3607-2004, 2004.

Richardson, I. G. and Cane, H. V., Near-Earth interplanetary coronal mass ejections during solar cycle 23 (1996–2009): Catalog and summary of properties, Solar Phys., 264, 189–237, 2010.

Sandholt, P. E. and Farrugia, C. J.: Poleward moving auroral forms (PMAFs) revisited: responses of aurorae, plasma convection and Birkeland currents in the pre- and postnoon sectors under positive and negative IMF B_y conditions, Ann. Geophys., 25, 1629–1652, doi:10.5194/angeo-25-1629-2007, 2007.

Sandholt, P. E. and Farrugia, C. J.: Plasma flow channels at the dawn/dusk polar cap boundaries: momentum transfer on old open field lines and the roles of IMF B_y and conductivity gradients, Ann. Geophys., 27, 1527–1554, doi:10.5194/angeo-27-1527-2009, 2009.

Sandholt, P. E., Farrugia, C. J., Lester, M., Cowley, S. W. H., Milan, S., Denig, W. F., Lybekk, B., Trondsen, E., and Vorobjev, V.: Multistage substorm expansion: Auroral dynamics in relation to plasma sheet particle injection, precipitation, and plasma convection, J. Geophys. Res., 107, 1342, doi:10.1029/2001JA900116, 2002.

Sauvaud, J.-A., Jacquey, C., Oka, M., Palin, L., Fruit, G., Kistler, L. M., Balough, A., Cao, J. B., Reeves, G., Mukai, T., Shinohara, I., and Grigorenko, E.: A study of the near-Earth plasma sheet and lobe driven by multiple substorms: Comparisons with a full particle simulation of reconnection, J. Geophys. Res., 117, AO1221, doi:10.1029/2011JA017033, 2012.

Sergeev, V. A., Liou, K., Newell, P. T., Ohtani, S.-I., Hairston, M. R., and Rich, F.: Auroral streamers: characteristics of associated precipitation,convection and field-aligned currents, Ann. Geophys., 22, 537–548, doi:10.5194/angeo-22-537-2004, 2004.

Sergeev, V., Nishimura, Y., Kubyshkina, M., Nakamura, R., and Singer, H.: Magnetospheric location of the equatorward prebreakup arc, J. Geophys. Res., 117, A01212, doi:10.1029/2011JA017154, 2012.

Shi, Y., Zesta, E., Lyons, L., Boudouridis, A., Ge, Y. S., Ruohoniemi, J. M., and Mende, S.: Two-dimensional ionospheric flow pattern associated with auroral streamers, J. Geophys. Res., 117, A02208, doi:10.1029/2011JA017110, 2012.

Siscoe, G. L. and Huang, T. S.: Polar cap inflation and deflation, J. Geophys. Res., 90, 543–547, 1985.

Siscoe, G. L., Erickson, G. M., Sonnerup, B. U. O., Maynard, N. C., Schoendorf, J. A., Siebert, K. D., Weimer, D. R., White, W. W., and Wilson, G. R.: Hill model of transpolar potential saturation: Comparison with MHD simulations, J. Geophys. Res., 107, 1085, doi:10.1029/2001JA000109, 2002.

Siscoe, G. L., Farrugia, C. J., and Sandholt, P. E.: Comparison between the two basic modes of magnetospheric convection, J. Geophys. Res., 116, A05210, doi:10.1029/2010JA015842, 2011.

Southwood, D. J.: The ionospheric signature of flux transfer events, J. Geophys. Res., 92, 3207–3213, 1987.

Tomita, S., Nosé, M., Iyemori, T., Toh, H., Takeda, M., Matzka, J., Bjornsson, G., Saemundsson, T., Janzhura, A., Troshichev, O., and Schwarz, G.: Magnetic local time dependence of geomagnetic disturbances contributing to the AU and AL indices, Ann. Geophys., 29, 673–678, doi:10.5194/angeo-29-673-2011, 2011.

Troshichev, O. and Janzhura, A.: Relationship between the PC and AL indices during repetitive bay-like magnetic disturbances in the auroral zone, J. Atmos. Sol. Terr. Phys., 71, 1340–1352, 2009.

Troshichev, O. A., Lukianova, R. Y., Papitashvili, V. O., Rich, F. J., and Rasmussen, O.: Polar cap index (PC) as a proxy for ionospheric electric field in the near-pole region, Geophys. Res. Lett., 27, 23, doi:10.1029/2000GL003756, 2000.

Wang, H., Lühr, H., and Ridley, A. J.: Plasma convection jets near the poleward boundary of the nightside auroral oval and their relation to Pedersen conductivity gradients, Ann. Geophys., 28, 969–976, doi:10.5194/angeo-28-969-2010, 2010.

Yang, J., Toffoletto, F. R., Wolf, R. A., Sazykin, S., Ontiveros, P. A., and Weygand, J. M.: Large-scale current systems and ground magnetic disturbance during deep substorm injections, J. Geophys. Res., 117, A04223, doi:10.1029/2011JA017415, 2012.